

**NITROGEN- AND PHOSPHINE-DONOR RUTHENIUM(II/III) AND  
PALLADIUM(II) COMPLEXES: SYNTHESIS AND CATALYTIC  
HYDROGENATION OF KETONES, ALKENES AND ALKYNES**

by

**ALOICE OMONDI OGWENO**

**Submitted in fulfilment of the academic requirements for the degree of Doctor of  
Philosophy in Chemistry in the College of Agriculture, Engineering and Science,  
University of KwaZulu-Natal  
Pietermaritzburg**

**Supervisor: Dr Stephen Ojwach**

May 2015

## PREFACE

The role of transition metal complexes in catalytic syntheses of organic compounds has tremendously developed over the past century. Specifically, platinum group metals have been widely used both in academia and in industries for the hydrogenation of unsaturated substrates such as ketones, alkenes and alkynes to produce petrochemical, agrochemical, fine chemical and pharmaceutical products. However, the quest for effective catalytic systems is ongoing and researchers are continuously exploring different chemical properties of these complexes in order to obtain effective catalysts for these reactions. The main areas of interest are catalyst activity, selectivity and stability in hydrogenation reactions. In attempts to achieve a balance between catalyst activity, stability and selectivity we investigated some mixed nitrogen- and phosphine-donor ruthenium and palladium complexes in catalytic hydrogenation reactions. This thesis is made up of six chapters. In **Chapter 1**, an introduction to catalytic hydrogenation of ketones, alkenes and alkynes is presented. The chapter also discusses the role of metal catalysts in the hydrogenation process and briefly highlights some of the domestic and industrial applications of the ketones, alkenes and alkynes hydrogenation products. Finally, the importance of catalyst design in improving catalytic efficiency is also presented.

**Chapter 2** of the thesis reviews the relevant literature on catalytic transfer and high pressure hydrogenation of ketones, alkenes and alkynes. It presents a review on ruthenium complexes as transfer hydrogenation catalysts and homogeneous palladium and ruthenium complexes as high pressure hydrogenation catalysts.

Towards the end of the chapter, a review on biphasic high pressure hydrogenation of unsaturated hydrocarbons is presented, with the focus mainly on water soluble ruthenium complexes. The chapter ends by presenting the rationale and highlights the main objectives of the whole study.

**Chapter 3** describes the synthesis, characterization and catalytic activity of new (pyridyl)benzoazoleruthenium(II) and ruthenium(III) complexes in the transfer hydrogenation of ketones. The study focused on the role of heteroatom and ancillary phosphine ligands in transfer hydrogenation reactions. To further understand the reactivity trend of these complexes, density functional theory (DFT) studies using Gaussian5.0 were conducted on three of the six complexes. The findings of this chapter have been published in *Dalton Trans.* **43** (2014) 1228-1237.

In **Chapter 4**, the synthesis, characterization and catalytic application in high pressure hydrogenation of alkenes and alkynes using benzoazole and pyrazolyl palladium(II) complexes are discussed. This work involved the use of molecular hydrogen under high pressure together with palladium (II) complexes as catalysts. The study further compared the reactivity of the rigid benzoazole versus flexible pyrazolyl ligands. The effects of cationic versus neutral complexes are also discussed. Density functional theory (DFT) studies using Gaussian5.0 was used to explain the reactivity trends of the two sets of palladium complexes.

**Chapter 5** describes the synthesis and characterization of water soluble cationic pyridyl(benzoazole)ruthenium(II) complexes. It further discusses the results of their application as catalysts in high pressure homogeneous and biphasic hydrogenation reactions of alkenes and alkynes. This is an improvement of **Chapter 4** aimed at bridging the gap between the homogeneous and heterogeneous catalysis.

It focuses on facilitating the ease of separation of the catalytic products from the reaction mixture and recycling the catalysts. The results and findings of this chapter have been published in *Appl. Catal. A: Gen.* **486** (2014) 250-258. Finally, general conclusions on the key findings of this study and the future prospects are presented in **Chapter 6**.

## DECLARATION

I, **Aloice Omondi Ogweno** declare that;

1. The research reported in this thesis, “NITROGEN- AND PHOSPHINE-DONOR RUTHENIUM(II/III) AND PALLADIUM(II) COMPLEXES: SYNTHESIS AND CATALYTIC HYDROGENATION OF KETONES, ALKENES AND ALKYNES” except where otherwise indicated, is my original research.
2. This thesis has not been submitted for any degree or examination at any other university.
3. This thesis does not contain other persons’ data, pictures, graphs or other information, unless specifically acknowledged as being sourced from other persons.
4. This thesis does not contain other persons' writing, unless specifically acknowledged as being sourced from other researchers. Where other written sources have been quoted, then:
  - a. Their words have been re-written but the general information attributed to them has been referenced.
  - b. Where their exact words have been used, then their writing has been placed in italics and inside quotation marks and referenced.
5. This thesis does not contain text, graphics or tables copied and pasted from the Internet, unless specifically acknowledged, and the source being detailed in the thesis and in the References sections.

Signed: .....

As the candidate’s supervisor I have/have not approved this thesis/dissertation for submission.

Signed:..... Name:..... Date:.....

## DECLARATION – PUBLICATIONS AND OUTPUTS

This thesis is based on the following original publications and conference presentations;

### Publications:

1. (Pyridyl)benzoazoleruthenium(II) and ruthenium(III) complexes: Role of heteroatom and ancillary phosphine ligand in the transfer hydrogenation of ketones, **Aloice O. Ogwen**, Stephen O. Ojwach and Matthew P. Akerman, *Dalton Trans.* **43** (2014) 1228-1237.
2. Cationic pyridyl(benzoazole)ruthenium(II) complexes: Efficient and recyclable catalysts in biphasic hydrogenation of alkenes and alkynes, **Aloice O. Ogwen**, Stephen O. Ojwach, Matthew P. Akerman, *Applied Catalysis A: Gen.* **486** (2014) 250-258.
3. New cationic (pyridyl)benzoazolepalladium(II) complexes and their application in high pressure hydrogenation of alkenes and alkynes, **Aloice O. Ogwen**, Stephen O. Ojwach, Matthew P. Akerman, *J. Catal.-Manuscript in preparation.*
4. (Pyrazo-1-lylmethyl)pyridinepalladium(II) complexes: Syntheses and kinetic studies in high pressure hydrogenation of alkenes and alkynes, **Aloice O. Ogwen**, Stephen O. Ojwach, Matthew P. Akerman, *J. Mol. Catal. A: Chem.-Manuscript in preparation.*

### Conference Presentations:

1. *New (pyridyl)benzoazoleruthenium complexes: Highly active Catalysts for Transfer hydrogenation of ketones*, A.O. Ogwen, S. O. Ojwach. INORG2013 Conference held at Southern Sun Elageni, Durban, KwaZulu-Natal South Africa, 30<sup>th</sup> June-4<sup>th</sup> July 2013.
2. *(Pyridyl)benzoazoleruthenium(II) and ruthenium(III) Complexes: Role of Heteroatom in the Transfer Hydrogenation of Ketones*, A.O. Ogwen, S. O. Ojwach, M. P. Akerman, 41<sup>st</sup> International Conference on Coordination Chemistry held at Suntec Singapore Convention and Exhibition Centre, Singapore, 21<sup>st</sup>-25<sup>th</sup> July 2014.
3. *(Pyridyl)BenzoazolePalladium(II) Complexes: Structure and Catalytic Hydrogenation of Alkenes and Alkynes*, A.O. Ogwen, S. O. Ojwach, M. P. Akerman, College Research Open Day held at UKZN-Westville Campus, Durban, KwaZulu-Natal South Africa, 27<sup>th</sup> October 2014.

Signed:.....

## ABSTRACT

The ligands, 2-(2-pyridyl)benzimidazole (**L1**), 2-(2-pyridyl)benzothiazole (**L2**), and 2-(2-pyridyl)benzoxazole (**L3**) were prepared from *o*-phenylenediamine, *o*-aminothiophenol and 2-aminophenol, respectively, following literature procedures. While alkylation of **L1** using bromopropane gave ligand 1-propyl-2-(pyridin-2-yl)-1H-benzoimidazole (**L4**). Ligands, 2,6-bis(3,5-dimethylpyrazolylmethyl)pyridine (**L5**) and 2,6-bis(3,5-diphenylpyrazolylmethyl)pyridine (**L6**) were prepared by phase transfer alkylation of 2,6-bis(chloromethyl)pyridine with one mole equivalents of the appropriate pyrazole.

Reactions of ligands **L1-L4** with  $\text{RuCl}_3 \cdot 3\text{H}_2\text{O}$  produced the corresponding compounds  $[\text{RuCl}_3(\text{L1})]$  (**1**),  $[\text{RuCl}_3(\text{L2})]$  (**2**),  $[\text{RuCl}_3(\text{L3})]$  (**3**) and  $[\text{RuCl}_3(\text{L4})]$  (**7**), respectively. Likewise, reaction of ligands **L1-L3** with  $\text{RuCl}_2(\text{PPh}_3)_3$  gave  $[\text{RuL1}(\text{PPh}_3)_2\text{Cl}_2]$  (**4**),  $[\text{RuL2}(\text{PPh}_3)_2\text{Cl}_2]$  (**5**) and  $[\text{RuL3}(\text{PPh}_3)_2\text{Cl}_2]$  (**6**). Complexes **1-7** were characterized by mass spectrometry, elemental analysis,  $^1\text{H}$ ,  $^{13}\text{C}$  and  $^{31}\text{P}$  NMR spectroscopy and single X-ray analyses. They were then evaluated as catalysts for the transfer hydrogenation of ketones. The catalytic activity of the ruthenium(III) complexes, **1-3** and **7** is believed to be a result of their coordinative unsaturation while the high lability of the coordinated  $\text{PPh}_3$  ligands are responsible for the catalytic activity of ruthenium(II) complexes, **4-6**, in the transfer hydrogenation of ketones. Ruthenium(II) catalysts bearing  $\text{PPh}_3$  ancillary ligands formed more active systems than the corresponding ruthenium(III) trichloride counterparts. Complexes bearing benzimidazole ligand **L1** were more active than those of the respective benzothiazole (**L2**) and benzoxazole (**L3**). DFT studies show that the catalytic activities of the complexes depend on the dipole moment of the resultant catalysts.



The benzoazole complexes [PdCl<sub>2</sub>(L1)] (8), [PdCl<sub>2</sub>(L2)] (9), [PdCl<sub>2</sub>(L3)] (10) and [PdClMe(L1)] (11) were prepared by reacting the corresponding ligands L1-L3 with either [PdCl<sub>2</sub>(NCMe)<sub>2</sub>] or [PdClMe(COD)]. Treatment of complex 8 with one molar equivalent of PPh<sub>3</sub> and PPh<sub>3</sub>/NaBAR<sub>4</sub> produced the cationic complexes, [Pd(L1)ClPPh<sub>3</sub>]Cl (12) and [Pd(L1)ClPPh<sub>3</sub>]BAR<sub>4</sub> (13), respectively. Similarly, neutral pyrazolyl palladium complexes, [PdCl<sub>2</sub>(L5)] (14), [PdCl<sub>2</sub>(L6)] (15) and [PdClMe(L5)] (16) were prepared by reaction of ligands L5 and L6 with [PdCl<sub>2</sub>(NCMe)<sub>2</sub>] or [PdClMe(COD)]. The corresponding cationic complexes [Pd(L5)ClPPh<sub>3</sub>]Cl (17) and [Pd(L5)ClPPh<sub>3</sub>]BAR<sub>4</sub> (18) were prepared by reaction of complex 14 with equimolar amounts of PPh<sub>3</sub> and PPh<sub>3</sub>/NaBAR<sub>4</sub>, respectively. The synthesized compounds were characterized by a combination of <sup>1</sup>H, <sup>13</sup>C and <sup>31</sup>P-NMR spectroscopy, microanalyses and single X-Ray analyses for complexes 13 and 18. Ligands L1 and L5 bind to the Pd metal centre in a bidentate mode as confirmed by the molecular structures of complexes 13 and 18. Complexes 8-18 were applied as catalysts in the high pressure hydrogenation of alkenes and alkynes.

The catalytic activities of complexes 8-18 were controlled by complex structure, catalyst concentration, hydrogen pressure, time and type of substrate. While the cationic benzoazole complexes [Pd(L1)PPh<sub>3</sub>Cl]Cl (12) and [Pd(L1)PPh<sub>3</sub>Me]BAR<sub>4</sub> (13) were generally less active compared to the neutral Pd(II) complexes, the cationic pyrazolyl palladium complexes [Pd(L5)ClPPh<sub>3</sub>]Cl (17) and [Pd(L5)ClPPh<sub>3</sub>]BAR<sub>4</sub> were relatively more active than the corresponding neutral complexes. Generally, the benzoazole complexes 8-13 were more active compared to the pyrazolyl complexes, 14-18.

Conjugated substrates were more reactive than non-conjugated substrates. The hydrogenation of aliphatic alkenes and alkynes were accompanied by isomerization reactions and higher activities were reported in the hydrogenation of alkynes compared to the corresponding alkenes. A mercury poisoning test on the complexes established that the catalytic systems were heterogeneous in nature. Further TEM analyses revealed that indeed the Pd(II) complexes **8-18** formed nanoparticles to produce heterogeneous hydrogenation systems. The kinetic of hydrogenation reactions indicated that the reactions are *pseudo* first order with respect to the catalyst and substrate. Catalyst loading, hydrogen pressure and temperature also influenced the activity of the catalysts. DFT studies further showed that the activity trend of complexes **8-18** depended on the average  $\{(N_{\text{Py}} + N_{\text{bz/pz}})/2\}$  bond lengths and the HOMO-LUMO energy gaps. The activities generally decreased with the increase in  $\{(N_{\text{Py}} + N_{\text{bz/pz}})/2\}$  bond lengths and decrease in the HOMO-LUMO energy gap.

To bridge the gap between homogeneous and heterogeneous catalysis, water soluble ruthenium(II) complexes were synthesized and used in biphasic olefin hydrogenation reactions. Reactions of ligands **L1-L3** with  $[\eta^6\text{-(2-phenoxyethanol)RuCl}_2]_2$  dimer afforded the respective cationic 2-(2-pyridyl)benzoazole)ruthenium(II) complexes:  $[\eta^6\text{-(2-phenoxyethanol)RuCl(L1)Cl}]^+$  (**19**),  $[\eta^6\text{-(2-phenoxyethanol)RuCl(L2)Cl}]^+$  (**20**) and  $[\eta^6\text{-(2-phenoxyethanol)RuCl(L3)Cl}]^+$  (**21**) in high yields. The complexes were characterized by a combination of  $^1\text{H}$  and  $^{13}\text{C}$ -NMR spectroscopy, microanalyses and X-ray crystallography for complexes **19-21**.

Solid state structures of complexes **19-21** confirmed the bidentate coordination modes of ligands **L1-L3** and the formation of cationic species through displacement of one chloride ligand from the Ru(II) coordination sphere. Complexes **19-21** were found to form active catalysts for the high pressure hydrogenation of alkenes and alkynes in toluene and biphasic media. Hydrogenation of alkynes produced a mixture of alkanes and alkenes. The complexes were recyclable and retained significant catalytic activities after six cycles. Reaction parameters such as substrate/catalyst ratio, temperature, and aqueous/organic ratio affected the catalytic trends.

## **ACKNOWLEDGEMENTS**

First and foremost, I would like to thank God Almighty for His mercies and grace which has made it possible for me to come this far. Secondly, I wish to express my deep and sincere gratitude to my supervisor, Dr. Stephen O. Ojwach. His enthusiasm, advice, inspiration, guidance and efforts led me to the completion of these studies. Without his support, this dissertation would not have been possible. I am also grateful to Dr. Matthew P. Akerman for his great assistance in molecular structure solution and refinement. This great assistance is sincerely acknowledged.

I am grateful to the technical and administrative staff in the School of Physics and Chemistry, University of KwaZulu-Natal, for their great support that saw the project run to completion. I wish to thank all my colleagues in the catalysis research group, Pietermaritzburg campus. The chemistry post graduate community in PMB is also acknowledged for each and every little support they accorded me while I was carrying out this study. Irresistible gratitude goes to my cousins; Dalin, Alice, Joane, and Alfred and my family for all the support they gave me. You have always wished me well while away; your timeless words of encouragements have finally paid off. May God bless you all. Lastly, I wish to express my sincere gratitude to the University of KwaZulu-Natal for financial support and a bursary for this project. Without this support, nothing would have been possible.

## LIST OF FIGURES

Page

Figure 1.1: Intermolecular bonding between carbonyl groups .....	3
Figure 1.2: Examples of natural ketones and their applications .....	4
Figure 1.3: Various ketone derivatives .....	5
Figure 1.4: Natural alkenes and alkynes and their applications.....	12
Figure 1.5: Reactions of (a) alkenes and (b) alkynes.....	14
Figure 1.6: Structures of Wilkinson and Vaska homogeneous catalysts .....	16
Figure 2.1: Effect of the electronic factor on catalytic activity of ruthenium(II) complexes towards transfer hydrogenation.....	22
Figure 2.2: <i>Pseudo</i> - N <sub>3</sub> , ruthenium(II) complexes .....	23
Figure 2.3: (a) $\beta$ -Aminophosphine and (b) diminophosphine ruthenium(II) complexes.....	24
Figure 2.4: (a) Tetradentate diphosphine/diamine and (b) diphosphine/dimine Ru(II) complexes.....	24
Figure 2.5: Chiral (a) TsDPEN, (b) tethered TsDPEN (DPEN = 1,2- diphenylethylenediamine) and (c) terdentate Ru(II) complexes.....	25
Figure 2.6: Chemical structure of carbapenem antibiotic.....	26
Figure 2.7: Pincer ruthenium(II) complexes.....	26
Figure 2.8: Structures of (a) phosphine Pd(II) and (b) dinuclear phosphine Pd(0) complexes for homogeneous hydrogenation reactions .....	33
Figure 2.9: Bidentate nitrogen-donor Pd(0) complexes for partial homogeneous hydrogenation of alkynes.....	34
Figure 2.10: Water soluble bidentate nitrogen-donor Pd(0) complexes for the homogeneous hydrogenation of olefins .....	34

Figure 2.11: Tridentate hydrozonic Pd(II) complexes for homogeneous hydrogenation of unsaturated carbon-carbon bonds.....	35
Figure 2.12: N-Heterocyclic carbene palladium complexes for semi hydrogenation of 1-phenyl-1-propyne.....	36
Figure 2.13: Neutral ruthenium complexes for high pressure hydrogenation .....	38
Figure 2.14: Cationic N-heterocyclic ruthenium(II) complexes for homogeneous hydrogenation.....	40
Figure 2.15: Cationic water-soluble transition metal complexes for hydrogenation reactions ....	41
Figure 2.16: Water-soluble transition metal complexes for hydrogenation reactions .....	41
Figure 3.1: $^1\text{H}$ NMR spectrum of ligand 1-propyl-2-(pyridin-2-yl)-1H-benzo[ <i>d</i> ]imidazole (L4). .....	53
Figure 3.2: HR-MS spectrum of complex <b>1</b> .....	55
Figure 3.3: $^{31}\text{P}\{^1\text{H}\}$ NMR spectra of complex $[\text{Ru}(\text{L1})\text{PPh}_3)_2\text{Cl}_2](\mathbf{4})$ in DMSO. The signal at -6.72 ppm is assigned to free $\text{PPh}_3$ and points to the dissociation of coordinated $\text{PPh}_3$ . .....	56
Figure 3.4: $^{31}\text{P}\{^1\text{H}\}$ NMR spectra for complex <b>6</b> (a) $\text{DMSO-}d_6$ , signal at 6.56 ppm reveals the generation of free $\text{PPh}_3$ (b) in $\text{CDCl}_3$ , one signal at 29.93 ppm indicates that the two <i>trans</i> - $\text{PPh}_3$ ligands are chemically equivalent. ....	58
Figure 3.5: Molecular structure of complex <b>1</b> containing coordinated acetonitrile solvent drawn with 50% probability ellipsoids. ....	59
Figure 3.6: Molecular structure of complex <b>2</b> containing coordinated acetonitrile solvent drawn with 50% probability ellipsoids. ....	59

Figure 3.7: ORTEP view of complex <b>6</b> showing the atom labelling drawn at 50% probability ellipsoids (the structure could not be satisfactorily refined due to desolvation and the data obtained are not suitable for publication and discussion of bond parameters). Hydrogen atoms are omitted for clarity. ....	62
Figure 3.8: Typical $^1\text{H}$ NMR spectrum of the 2-phenylethanol product obtained from the transfer hydrogenation reactions confirming the identity and purity of the product. ....	64
Figure 3.9: Time-dependence of transfer hydrogenation of acetophenone by complexes <b>1</b> , <b>2</b> and <b>4</b> showing a shorter induction period for <b>4</b> . ....	66
Figure 3.10: $^{31}\text{P}\{^1\text{H}\}$ NMR spectra showing evidence of displacement of $\text{PPh}_3$ in $i\text{PrOH/KOH}$ solution to form metal-alkoxide <b>6-I</b> from complex <b>6</b> . The signal at -5.29 ppm reveals the generation of free $\text{PPh}_3$ (inset; $^{31}\text{P}$ NMR spectrum of complex <b>6</b> in $\text{CDCl}_3$ , the signal at 29.83 ppm indicates that the two trans- $\text{PPh}_3$ ligands are chemically equivalent).....	72
Figure 3.11: Frontier molecular orbitals of ruthenium(II) complexes $[\text{RuCl}_2(\text{L1})]$ ( <b>1a</b> ) $[\text{RuCl}_2(\text{L2})]$ ( <b>2a</b> ) and $[\text{RuCl}_2(\text{L3})]$ ( <b>3a</b> ) as determined by Density Functional theory using B3LYP level of theory and LANL2DZ basis set (isovalue 0.02). ....	74
Figure 4.1a: $^1\text{H}$ NMR spectrum for complex <b>11</b> showing coordinated Me ligand. ....	86
Figure 4.1b: $^1\text{H}$ NMR spectrum for complex <b>18</b> .....	86
Figure 4.2a: $^{31}\text{P}\{^1\text{H}\}$ NMR spectrum for complex <b>12</b> showing a peak for coordinated $\text{PPh}_3$ .....	87
Figure 4.2b: $^{31}\text{P}\{^1\text{H}\}$ NMR spectrum for complex <b>18</b> showing a peak for coordinated $\text{PPh}_3$ .....	87
Figure 4.3: HR-MS showing a $m/z$ peak of complex <b>9</b> fragment. ....	88
Figure 4.4: HR-MS of complex <b>11</b> showing the fragmentation pattern. ....	89

Figure 4.5: ESI mass spectrum showing $m/z$ peak of molecular cation of complex <b>12</b> .	89
Figure 4.6: HR-MS of complex <b>16</b> showing $m/z$ peak of $[\text{Pd}(\text{L5})\text{Me}]^+$ fragment.	90
Figure 4.7: Molecular structures of complexes <b>13</b> and <b>18</b> drawn with 50% probability ellipsoids.	91
Figure 4.8: Time-dependence of high pressure hydrogenation of styrene by (a) benzoazole Pd(II) complexes <b>8-13</b> and (b) pyrazoly Pd(II) complexes <b>14-18</b> .	94
Figure 4.9: Plot of $\ln[\text{Sty}]_0/[\text{Sty}]_t$ vs time for styrene hydrogenation with (a) <b>8-13</b> and (b) <b>14-18</b> .	100
Figure 4.10: Effect of catalyst loading in hydrogenation of styrene using complexes (a) <b>8</b> and (b) <b>15</b> . Styrene, 8.00 mmol; pressure, 5 bar; temperature, 30 °C; solvent, toluene (50 mL); stirring speed, 600 rpm.	101
Figure 4.11: Plot of observed rate constants ( $k_{\text{obs}}$ ) versus catalyst concentration for complexes (a) <b>8</b> and (b) <b>15</b> .	102
Figure 4.12: Effect of hydrogen pressure on hydrogenation of styrene using (a) complex <b>8</b> and (b) complex <b>15</b> . Styrene, 8.00 mmol. Pressure, 5 bar; temperature: 30 °C; solvent: toluene (50 mL); stirring speed, 600 rpm.	103
Figure 4.13: Plot of observed rate constants ( $k_{\text{obs}}$ ) versus hydrogen pressure (a) <b>8</b> and (b) <b>15</b> .	103
Figure 4.14: Effect of temperature on the kinetic of hydrogenation of styrene using complex <b>8</b> : Substrate (8.00 mmol); Pressure: 5 bar; Solvent; toluene (50 mL); Stirring speed; 600 rpm.	104



Figure 4.15: Effect of substrate on the kinetic of hydrogenation of alkenes and alkynes using complex <b>8</b> (a) and complex <b>15</b> (b). Substrate, 8.00 mmol; pressure, 5 bar; temperature, 30 °C; solvent, toluene (50 mL); stirring speed, 600 rpm. ....	106
Figure 4.16: GC spectra showing isomerization of (a) 1-hexene and (b) 1-hexyne .....	107
Figure 4.17a: Hydrogenation and isomerization of (a) 1-hexene and 1-hexyne; (b) 1-octene and 1-octyne using catalyst <b>8</b> . H <sub>2</sub> pressure; 5 bar; temperature; 30 °C; Solvent; toluene (50 mL); stirring speed; 600 rpm; time; 45 min.....	108
Figure 4.17b: Hydrogenation and isomerization of (a) 1-hexene and 1-hexyne; (b) 1-octene and 1-octyne using catalyst <b>15</b> . H <sub>2</sub> pressure; 5 bar; temperature; 30 °C; Solvent; toluene (50 mL); stirring speed; 600 rpm; time; 45 min.....	108
Figure 4.18: Conversion/ selectivity vs. time profile for hydrogenation of 1-hexene using catalysts (a) <b>8</b> and (b) <b>15</b> H <sub>2</sub> pressure, 5 bar, temperature, 30 °C; solvent, toluene (50 mL); stirring speed, 600 rpm; time, 2 h. ....	109
Figure 4.19: Conversion/ selectivity vs. time profile for hydrogenation of phenylacetylene using (a) <b>8</b> and (b) <b>15</b> . H <sub>2</sub> pressure: 5 bar; temperature, 30 °C; solvent, toluene (50 mL); stirring speed, 600 rpm; time, 2 h. ....	111
Figure 4.20: TEM image of complexes (a) <b>11</b> and (b) <b>12</b> isolated after catalytic reactions.....	115
Figure 4.21a: Frontier molecular orbitals of benzoazole Pd(II) complexes, <b>8-13</b> (as determined by density functional theory using B3LYP level of theory and LANL2DZ basis set (isovalue 0.02). ....	117
Figure 4.21b: Frontier molecular orbitals of benzoazole Pd(II) complexes, <b>14-17</b> (as determined by Density Functional theory using B3LYP level of theory and LANL2DZ basis set (isovalue 0.02). ....	120

Figure 5.1: An overlay of $^1\text{H}$ NMR spectra for ligand, <b>L1</b> , and complex <b>19</b> . .....	131
Figure 5.2: ES-MS spectrum of complex <b>19</b> showing $m/z$ signal at 470.02 (100%) corresponding to the molecular ion, $\text{M}^+-\text{Cl}$ of <b>19</b> . .....	132
Figure 5.3: An overlay of $^1\text{H}$ NMR spectra for complex <b>19</b> and $[\eta^6$ -(2- phenoxyethanol) $\text{RuCl}_2$ ] $_2$ dimer. ....	133
Figure 5.4: Thermal ellipsoid plots (50% probability surfaces) showing the atom numbering schemes of complexes (a) <b>19</b> , (b) <b>20</b> and (c) <b>21</b> . Hydrogen atoms have been rendered as spheres of arbitrary radius. ....	134
Figure 5.5: [a] Partial space-filling model illustrating the solvent and anion-filled channels of complex <b>20</b> . The channels are co-linear with the $a$ -axis. [b] Hydrogen bonding interactions between the hydroxyl groups of the cations, the water molecules and the chloride anions of complex <b>20</b> (viewed down the $a$ -axis). These interactions lock the solvent molecules and chloride anions in the channels.....	137
Figure 5.6: Effect of substrate/catalyst molar ratio on (a) conversion (b) TOF of complex <b>20</b> on hydrogenation of styrene.....	144
Figure 5.7: Catalytic activity and selectivity of complex <b>21</b> in the hydrogenation of various substrates. Reaction conditions: substrate, 4.9 mmol; catalyst; 0.01 mmol (0.2 mol%); 10 bar; MeOH (50 mL), temperature, 25 °C; time, 1 h. ....	146
Figure 5.8: Conversion of styrene as a function of cycles by complexes <b>19-21</b> . Reaction conditions: styrene, 4.9 mmol; catalyst; 0.01 mmol (0.2 mol%); 10 bar; $\text{H}_2\text{O}$ :Toluene (1:1, total volume, 50 mL), temperature, 25 °C, time, 1 h. ....	148

Figure 5.9: Influence of aqueous: organic volume ratio and temperature on catalyst regeneration using complex <b>21</b> .....	151
Figure 6. 1: General structures of the proposed N <sup>^</sup> P (a) and monohydride N <sup>^</sup> N ruthenium(II) complexes (b) .....	156
Figure 6.2: General structure of the proposed hemilabile palladium(II) complexes .....	157
Figure 6.3: Possible structures of anchored cationic benzazole Ru(II) complexes .....	157
Figure 6.4: Proposed structure of asymmetric Ru(II) complexes .....	158

<b>LIST OF SCHEMES</b>	<b>Page</b>
Scheme 1.1: Methods of ketone synthesis .....	3
Scheme 1.2: Nucleophilic attack on ketone substrate in reductive hydrogenation reaction under acidic conditions .....	6
Scheme 1.3: A general scheme of electrophilic attack on ketone in reductive hydrogenation .....	6
Scheme 1.4: MPV reduction of ketone .....	7
Scheme 1.5: MPV reduction and Oppenauer oxidation of ketone.....	8
Scheme 1.6: Transfer hydrogenation reaction using hydrogen donor molecules .....	9
Scheme 1.7: <i>Wittig</i> reaction .....	10
Scheme 1.8: Catalytic hydrogenation of benzene using a Raney Ni catalyst.....	15
Scheme 1.9: Partial hydrogenation of an alkyne using a Lindlar catalyst .....	15
Scheme 1.10: Monsanto's industrial synthesis of L-3,4-dihydroxyphenylalanine (L-DOPA) using a modified Wilkinson catalyst.....	17
Scheme 2.1: Direct hydrogen transfer route for Meerwein-Ponndorf-Verley (MPV) reduction reaction.....	28
Scheme 2.2: Two different pathways for the 'hydridic route' .....	29
Scheme 2.3: Metal monohydride mechanisms of transfer hydrogenation; (a) inner-sphere and (b) outer-sphere .....	30
Scheme 2.4: Transfer hydrogenation mechanism using homogeneous ruthenium complex.....	31
Scheme 2.5: Mechanism of semi-hydrogenation of 4-octyne .....	37
Scheme 2.6: Substitution reactions of neutral ruthenium(II) complexes.....	39
Scheme 3.1: Synthetic protocol for ruthenium(II) and ruthenium(III) compounds.....	54
Scheme 3.2: Catalytic transfer hydrogenation of acetophenone by complexes <b>1-6</b> . .....	63

Scheme 3.3: Proposed catalytic cycle for the transfer hydrogenation of ketone by complex <b>6</b> in the presence of isopropanol and KOH.....	71
Scheme 4.1a: Synthesis of benzoazole palladium(II) complexes, <b>8-13</b> .....	84
Scheme 4.2: Catalytic hydrogenation of styrene using Pd(II) complexes, <b>8-18</b> .....	94
Scheme 4.3: Oxidative–addition of H <sub>2</sub> on a metal complex.....	112
Scheme 4.4: Proposed mechanism for high pressure hydrogenation of styrene by complex <b>8</b> .....	114

**LIST OF TABLES****Page**

Table 3.1: Crystal data collection and structural refinement parameters for complexes <b>1</b> and <b>2</b> .....	60
Table 3.2: Selected bond lengths [ $\text{\AA}$ ] and bond angles [ $^\circ$ ] for complexes <b>1</b> and <b>2</b> .....	61
Table 3.3: Summary of transfer hydrogenation of acetophenone of complexes <b>1-6</b> .....	65
Table 3.4: Transfer hydrogenation of different ketones and bases using complex <b>4</b> .....	69
Table 3.5: Summary of the data obtained from DFT calculations of the Ru(II) complexes .....	74
Table 4.1: Data collection and structural refinement parameters of complexes <b>13</b> and <b>18</b> .....	92
Table 4.2: Selected bond lengths ( $\text{\AA}$ ) and bond angles ( $^\circ$ ) for complexes <b>13</b> and <b>18</b> .....	93
Table 4.3a: Effect of reaction parameters on the hydrogenation of styrene by benzoazole complexes <b>8-13</b> .....	97
Table 4.3b: Effect of reaction parameters on the hydrogenation of styrene by benzoazole complexes <b>14-18</b> .....	97
Table 4.4: Rate constants ( $k_{\text{obs}}$ ) dependence on the average Pd-N bond length and HOMO- LUMO gap for complexes <b>8-17</b> .....	119
Table 5.1: Crystal data and structure refinement details for complexes <b>19-21</b> .....	135
Table 5.2: Selected bond lengths ( $\text{\AA}$ ) and bond angles ( $^\circ$ ) for complexes <b>19</b> , <b>20</b> and <b>21</b> .....	136
Table 5.3: Summary of hydrogen bond lengths ( $\text{\AA}$ ) and bond angles ( $^\circ$ ) of complexes <b>19</b> - <b>21</b> .....	138
Table 5.4: Effect of reaction parameters on the hydrogenation of styrene to ethylbenzene by complexes <b>19-21</b> .....	140
Table 5.5: Comparison of the TOFs catalysts <b>19-21</b> in the first and sixth cycle experiments ...	150

## ABBREVIATIONS

Å	angstrom
bz <sub>im</sub>	benzoimidazole
bz <sub>thio</sub>	benzothiazole
bz <sub>ox</sub>	benzoxazole
CDCl <sub>3</sub>	deuterated chloroform
COD	1,5-cyclooctadiene
d	doublet
DCM	dichloromethane
ESI	electron spray ionization
g	gram(s)
GC	gas chromatography
h	hour
Hz	hertz
<i>J</i>	coupling constant
L	ligand
m	multiplet
Me	methyl
MeCN	acetonitrile
MeOH	methanol
MHz	megahertz
min	minutes
mL	millilitres

mmol	millimoles
MS	mass spectrometry
NMR	nuclear magnetic resonance
Ph	phenyl
ppm	parts per million
py	pyridine
pz	pyrazole
r.t.	room temperature
s	singlet
t	triplet
TOF	turnover frequency
w	weak
$\alpha$	alpha
$\beta$	beta
$\delta$	chemical shift



<b>TABLE OF CONTENTS</b>	<b>Page</b>
PREFACE.....	ii
DECLARATION.....	v
DECLARATION – PUBLICATIONS AND OUTPUTS.....	vi
ABSTRACT.....	viii
ACKNOWLEDGEMENTS.....	xii
LIST OF FIGURES.....	xiii
LIST OF SCHEMES.....	xx
LIST OF TABLES.....	xxii
ABBREVIATIONS.....	xxiii
TABLE OF CONTENTS.....	xxv
CHAPTER 1.....	1
Catalytic hydrogenation of ketones, alkenes and alkynes: Industrial significance and the role of transition metal catalysts.....	1
1.1 Introductory remarks.....	1
1.2 Ketones.....	2
1.2.1 <i>Industrial applications of ketones</i> .....	4

1.2.2	<i>Reactions of ketones</i>	5
1.2.2.1	<i>Traditional methods of hydrogenation of ketones to alcohols</i>	7
1.2.2.2	<i>Transfer hydrogenation of ketones using transition metal catalysts</i>	9
1.3	<i>Alkenes and Alkynes</i>	10
1.3.1	<i>Industrial applications of alkenes and alkynes</i>	11
1.3.2	<i>High pressure hydrogenation</i>	13
1.3.2.1	<i>Heterogeneous catalytic hydrogenation of alkene and alkynes</i>	13
1.3.2.2	<i>Homogeneous catalytic hydrogenation of alkene and alkynes</i>	16
1.4	<i>Rationale of catalyst design</i>	18
CHAPTER 2		20
Literature review of catalytic hydrogenation reactions using ruthenium and palladium metal complexes		20
2.1	<i>Introduction to transfer and high pressure hydrogenation</i>	20
2.2	<i>Transition metal catalysed transfer hydrogenation of ketones</i>	20
2.2.1	<i>Ruthenium catalysed transfer hydrogenation of ketones</i>	21
2.2.1.1	<i>Phosphine donor ruthenium complexes</i>	21
2.2.1.2	<i>Nitrogen-donor ruthenium complexes</i>	22

2.2.1.3	<i>Asymmetric mixed phosphine-nitrogen donor ruthenium complexes</i> .....	23
2.2.1.4	<i>N-heterocyclic carbene ruthenium complexes</i> .....	26
2.2.2	<i>Mechanisms of transfer hydrogenation of ketones with ruthenium complexes</i> .....	27
2.2.2.1	<i>'Direct hydrogen transfer' versus 'hydridic route'</i> .....	27
2.2.2.2	<i>'Inner sphere' vs 'outer sphere' mechanism</i> .....	29
2.3	<i>Transition metal catalysed high pressure hydrogenation of alkenes and alkynes</i> .....	31
2.3.1	<i>High pressure hydrogenation of alkenes and alkynes using palladium complexes</i> .....	32
2.3.1.1	<i>Phosphine-donor palladium complexes</i> .....	32
2.3.1.2	<i>Nitrogen-donor palladium complexes</i> .....	33
2.3.1.3	<i>Mixed nitrogen-phosphine donor palladium complexes</i> .....	35
2.3.2	<i>Mechanisms of high pressure semi-hydrogenation of alkynes with Pd(II) complexes</i> .....	36
2.3.3	<i>High pressure hydrogenation of alkenes and alkynes using ruthenium complexes</i> .....	37
2.3.3.1	<i>Homogeneous phosphine ruthenium complexes</i> .....	37
2.3.3.2	<i>Cationic ruthenium complexes for homogeneous hydrogenation of alkenes and alkynes</i> .....	39
2.4	<i>Biphasic catalytic hydrogenation of unsaturated hydrocarbons</i> .....	40
2.5	<i>Rationale of study</i> .....	42

2.6	Objectives .....	44
CHAPTER 3	.....	45
(Pyridyl)benzoazoleruthenium(II) and ruthenium(III) complexes: Role of heteroatom and ancillary phosphine ligands in the transfer hydrogenation of ketones .....		45
3.1	Introduction .....	45
3.2	Experimental section .....	46
3.2.1	<i>General methods and instrumentation</i> .....	46
3.2.1.1	<i>Synthesis of 1-propyl-2-(pyridin-2-yl)-1H-benzo[d]imidazole (L4)</i> .....	47
3.2.1.2	<i>Synthesis of [<math>\{2-(2\text{-pyridyl})\text{benzimidazole}\}\text{RuCl}_3</math>] (1)</i> .....	47
3.2.1.3	<i>Synthesis of [<math>\{2-(2\text{-pyridyl})\text{benzothiazole}\}\text{RuCl}_3</math>] (2)</i> .....	48
3.2.1.4	<i>Synthesis of [<math>\{2-(2\text{-pyridyl})\text{benzoxazole}\}\text{RuCl}_3</math>] (3)</i> .....	48
3.2.1.5	<i>Synthesis of [<math>\{2-(2\text{-pyridyl})\text{benzimidazole}\}\text{RuCl}_2(\text{PPh}_3)_2</math>] (4)</i> .....	48
3.2.1.6	<i>Synthesis of [<math>\{2-(2\text{-pyridyl})\text{benzothiazole}\}\text{RuCl}_2(\text{PPh}_3)_2</math>] (5)</i> .....	49
3.2.1.7	<i>Synthesis of [<math>\{2-(2\text{-pyridyl})\text{benzoxazoles}\}\text{RuCl}_2(\text{PPh}_3)_2</math>] (6)</i> .....	50
3.2.1.8	<i>Synthesis of [<math>\{1\text{-propyl-2-(pyridin-2-yl)-1H-benzo[d]imidazole}\}\text{RuCl}_3</math>] (7) .....</i>	50
3.2.2	<i>Transfer hydrogenation of ketones</i> .....	51
3.2.3	<i>Density functional theory (DFT) modelling</i> .....	51

3.2.4 X-ray crystallographic analyses.....	51
3.3 Results and discussion.....	52
3.3.1 Synthesis of 1-propyl-2-(pyridin-2-yl)-1H-benzo[d]imidazole ( <b>L4</b> ).....	52
3.3.2 Synthesis of ruthenium complexes.....	53
3.3.3 Molecular structures of complexes <b>1</b> and <b>2</b> .....	58
3.3.4 Transfer hydrogenation of ketones catalysed by complexes <b>1-6</b> .....	63
3.3.5 Proposed transfer hydrogenation reaction mechanism.....	70
3.3.6 DFT calculations.....	73
3.3.7 Conclusions.....	75
CHAPTER 4.....	76
Cationic (pyridyl)benzoazole and (pyrazo-1-lylmethyl)pyridinepalladium(II) complexes: Syntheses, characterization and kinetic studies in high pressure hydrogenation of alkenes and alkynes.....	76
4.1 Introduction.....	76
4.2 Experimental Section.....	78
4.2.1 Materials and instrumentation.....	78
4.2.2 Synthesis of cationic palladium(II) complexes.....	79
4.2.2.1 Synthesis of [ $\{2-(2\text{-pyridyl})\text{benzimidazole}\}\text{PdPPh}_3\text{Cl}\}\text{Cl}$ ( <b>12</b> ).....	79

4.2.2.2	Synthesis of [ <i>{2-(2-pyridyl)benzimidazole}PdMePPh<sub>3</sub>]</i> BAR <sub>4</sub> ( <b>13</b> ).....	79
4.2.2.3	Synthesis of [ <i>{2-(3,5-dimethylpyrazol-1-ylmethyl)pyridine}PdPPh<sub>3</sub>Cl]</i> Cl ( <b>17</b> ).....	80
4.2.2.4	Synthesis of [ <i>{2-(3,5-dimethylpyrazol-1-ylmethyl)pyridine}PdClPPh<sub>3</sub>]</i> BAR <sub>4</sub> ( <b>18</b> ).....	80
4.2.3	Density functional theory (DFT) modelling of <b>8-18</b> .....	81
4.2.4	X-ray crystallography.....	81
4.2.5	High pressure hydrogenation reactions of alkenes and alkynes.....	82
4.2.6	TEM analyses.....	83
4.3	Results and discussion.....	83
4.3.1	Synthesis and structural characterization of benzoazole and pyrazolyl Pd(II) complexes.....	83
4.3.2	Molecular structures of complexes <b>13</b> and <b>18</b> .....	90
4.3.3	Catalytic high pressure hydrogenation reactions of alkenes and alkynes.....	93
4.3.4	Kinetic of hydrogenation reactions.....	95
4.3.4.1	Effect of catalyst structure on the hydrogenation of styrene.....	95
4.3.4.1.1	(Pyridyl)benzoazolepalladium(II) complexes <b>8-13</b> .....	95
4.3.4.1.2	(Pyrazolyl)pyridinepalladium(II) complexes <b>14-18</b> .....	98

4.3.4.2	<i>Effect of catalyst concentration on the kinetic of reaction</i> .....	100
4.3.4.3	<i>Effect of hydrogen pressure on the kinetic of reactions</i> .....	102
4.3.4.4	<i>Effect of temperature on hydrogenation of styrene</i> .....	104
4.3.4.5	<i>Effects of substrates on the kinetic of hydrogenation</i> .....	105
4.3.5	<i>Chemo- and regio-selectivity of hydrogenation reactions</i> .....	106
4.3.5.1	<i>Isomerization of terminal alkenes and alkynes</i> .....	106
4.3.5.2	<i>Effect of time on chemo-selectivity of hydrogenation of 1-hexene</i> .....	109
4.3.6	<i>Proposed mechanism of styrene hydrogenation</i> .....	112
4.3.7	<i>TEM analysis</i> .....	114
4.3.8	<i>DFT studies</i> .....	116
4.4	<b>Conclusions</b> .....	121
CHAPTER 5	.....	123
	Cationic Pyridyl(benzoazole)ruthenium(II) complexes: Efficient and recyclable catalysts in biphasic hydrogenation of alkenes and alkynes.....	123
5.1	<b>Introduction</b> .....	123
5.2	<b>Experimental</b> .....	125
5.2.1	<i>Materials and instrumentation</i> .....	125

5.2.2	<i>Syntheses of cationic Ru(II) complexes</i> .....	126
5.2.2.1	<i>Synthesis of <math>[\eta^6\text{-}(2\text{-phenoxyethanol})\text{RuClL1}]\text{Cl}</math> (<b>19</b>)</i> .....	126
5.2.2.2	<i>Synthesis of <math>[\eta^6\text{-}(2\text{-phenoxyethanol})\text{RuClL2}]\text{Cl}</math> (<b>20</b>)</i> .....	126
5.2.2.3	<i>Synthesis of <math>[\eta^6\text{-}(2\text{-phenoxyethanol})\text{RuClL3}]\text{Cl}</math> (<b>21</b>)</i> .....	127
5.2.3	<i>X-ray crystallography analyses of complexes <b>19-21</b></i> .....	127
5.2.4	<i>Hydrogenation reactions</i> .....	128
5.2.4.1	<i>Homogenous experiments</i> .....	128
5.2.4.2	<i>Biphasic hydrogenation experiments</i> .....	129
5.3	<i>Results and discussion</i> .....	130
5.3.1	<i>Synthesis of cationic ruthenium(II) complexes</i> .....	130
5.3.2	<i>Molecular structures of complexes <b>19-21</b></i> .....	133
5.3.3	<i>High pressure catalytic hydrogenation of olefins</i> .....	138
5.3.3.1	<i>Effect of catalyst structure on hydrogenation of styrene</i> .....	138
5.3.3.2	<i>Proposed mechanism for hydrogenation of styrene</i> .....	141
5.3.3.3	<i>Optimization of hydrogenation reaction conditions</i> .....	143
5.3.3.4	<i>Substrate scope</i> .....	145
5.3.3.5	<i>Biphasic catalysis and catalyst recycling</i> .....	147



5.4	Conclusions .....	152
CHAPTER 6 .....		153
General concluding remarks and future prospects.....		153
6.1	General conclusions.....	153
6.2	Future prospects.....	155
References.....		159

## CHAPTER 1

### **Catalytic hydrogenation of ketones, alkenes and alkynes: Industrial significance and the role of transition metal catalysts**

#### *1.1 Introductory remarks*

There is rapid growth in transition metal chemistry, especially in the syntheses and applications of transition metal complexes as catalysts in various organic transformations.<sup>1</sup> The critical roles played by these metal complexes in various catalytic reactions, for example, in transforming organic compounds to industrially valuable products, remains one of the main reasons for the concerted efforts aimed at developing new catalytic systems. Moreover, catalysts are major players in the manufacturing and processing industries accounting for about 85% of all industrial products.<sup>2</sup> Research endeavours have always sought to improve the efficiencies of the existing catalytic systems, besides developing new ones. The key areas of concern in catalysts development include but are not limited to activity, selectivity, stability, cost and most important the ultimate industrial applications.<sup>3</sup>

Transition metal complexes have been extensively used in catalytic transformations of organic compounds in the past century and are still receiving great attention mainly because of their significance in laboratory and industrial processes.<sup>4,5</sup> One of the significant chemical reactions where transition metal complexes are successfully being applied is catalytic hydrogenation. Catalytic hydrogenation is a process of adding hydrogen atoms across unsaturated bonds of organic compounds using catalysts. Catalytic hydrogenation of ketones and other unsaturated hydrocarbons such as alkenes and alkynes are some of the important reactions where various

transition metal complexes have been significantly applied.<sup>6</sup> It is reported that about 75% of industrially manufactured molecular organic compounds pass through either catalytic hydrogenation or oxidation processes.<sup>7</sup>

Catalytic hydrogenation is divided into different types based on the source of hydrogen: transfer hydrogenation, high pressure hydrogenation and hydrosilation among others. This first chapter highlights some important industrial applications of ketones, alkenes, alkynes and their derivatives.<sup>8,9</sup> It also briefly introduces transfer hydrogenation and high pressure hydrogenation processes and further discusses how catalyst design greatly influences the efficiency of transition metal catalysts.

## **1.2 Ketones**

Ketones are a group of organic compounds bearing a carbonyl (C=O) moiety sandwiched between either alkyl or aryl groups. They are unsaturated and the most common organic substrates used in industrial catalysis. They are polar, containing dipoles along the carbon-oxygen double bond creating weak attractive forces between the ketone molecules (Figure 1.1). Their intermolecular attractive forces are not as strong as hydrogen bonding interactions exhibited by alcohols and water. Ketones can also form hydrogen bonding with polar solvents such as H<sub>2</sub>O through the interaction of the partially charged carbonyl oxygen atom and the partially charged hydrogen atoms of the polar solvents. Ketones are synthesized from other organic compounds through reactions such as Friedel-Craft acylation of alkanoyl chlorides, ozonolysis of alkenes and dehydration of carboxylic acids (Scheme 1.1).

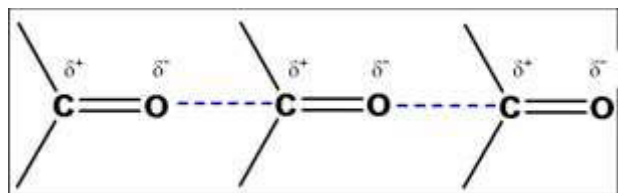
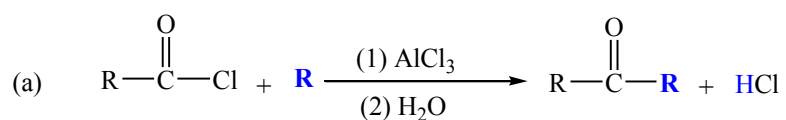
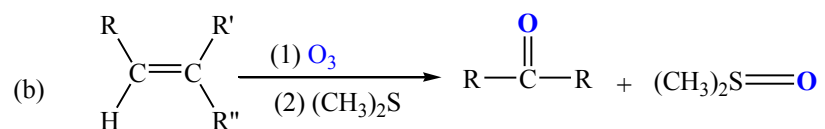


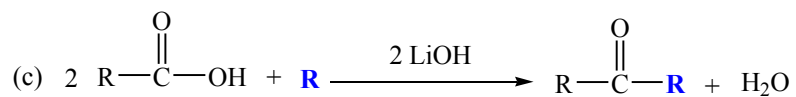
Figure 1.1: Intermolecular bonding between carbonyl groups



Friedel-Crafts Acylation



Ozonolysis of alkene



Dehydration of carboxylic acids

R = alkyl, aryl

Scheme 1.1: Methods of ketone synthesis

### 1.2.1 Industrial applications of ketones

Generally, ketones are widely used as reagents and solvents, for example, acetone is mainly used as an industrial solvent because of its ability to dissolve several organic compounds. Acetone is also used in chemical products such as paints, varnishes, resins, coatings, and nail-polish removers because of its low boiling point (56 °C).

Other ketones are used as starting materials for the manufacture of other final products such as plastics,<sup>10</sup> perfumes,<sup>11</sup> flavouring agents,<sup>12</sup> dyes<sup>13</sup> and precursors for the pharmaceutical,<sup>14</sup> agrochemical<sup>15</sup> and fine chemical industries.<sup>16</sup> For example, acetophenone, is a chemical component of pistachio nuts which are used for making ice creams; camphor is an active component of liniments and inhalants; carvone is used for making candies and toothpastes and muscone for perfumes (Figure 1.2)<sup>17</sup>

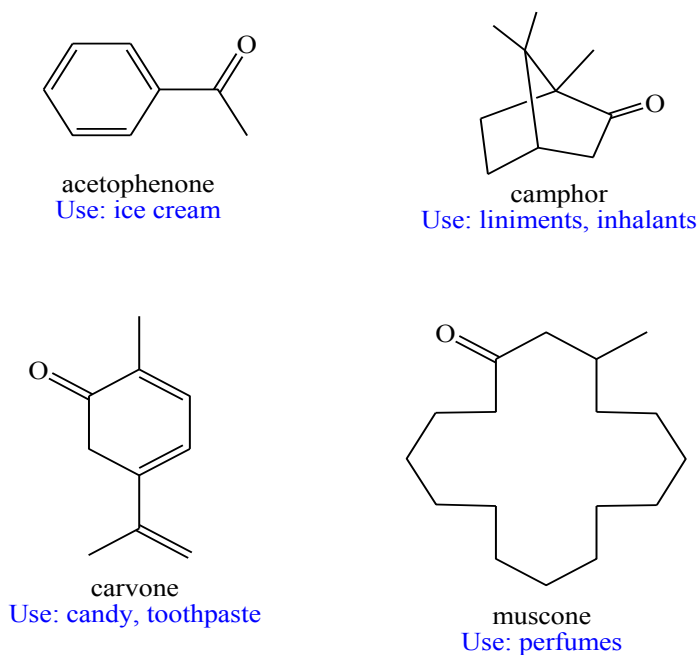


Figure 1.2: Examples of natural ketones and their applications<sup>17</sup>

### 1.2.2 Reactions of ketones

Ketones are susceptible to nucleophilic or electrophilic attack due to the polar nature of their carbonyl, C=O, group and are used as starting materials to synthesize alcohols, alkenes, imines, amines, acetals and oximes among other valuable organic compounds (Figure 1.3).<sup>17,18</sup>

Alcohols are one of the main compounds derived from ketones and the process is a nucleophilic addition reaction, very much dependent on the reaction conditions, as shown by the general Schemes 1.2 and 1.3. For example, in basic conditions, the process is initiated by a nucleophilic attack on the partially positive carbonyl (C=O) carbon breaking the carbonyl bond and forming a C-H bond.

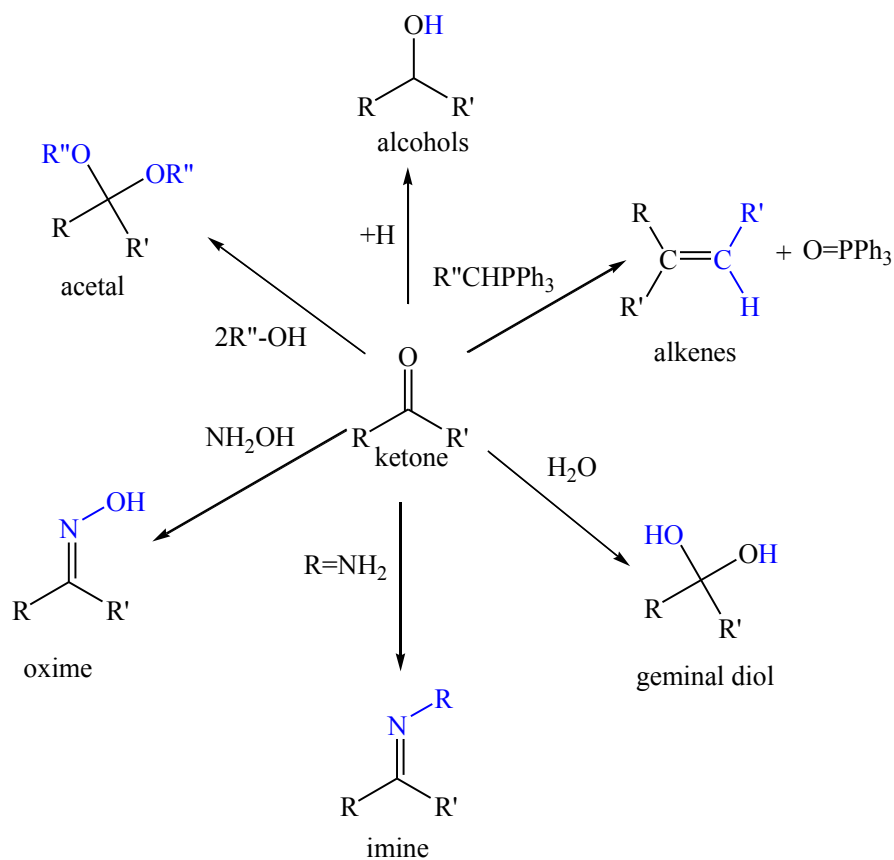
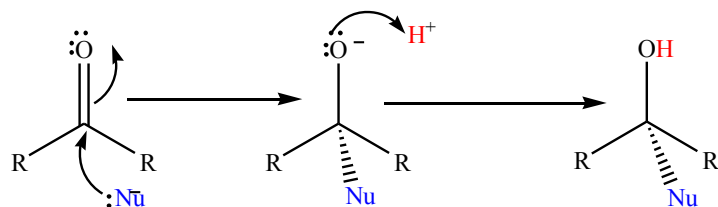
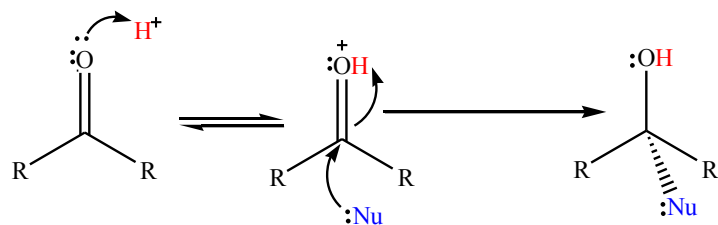


Figure 1.3: Various ketone derivatives



Scheme 1.2: Nucleophilic attack on ketone substrate in reductive hydrogenation reaction under acidic conditions

This makes the oxygen atom more susceptible to protonation resulting to the formation of alcohol (Scheme 1.2). In acidic conditions, the process is initiated by an electrophilic attack by the proton ( $H^+$ ) on the carbonyl oxygen making the system more electrophilic. A subsequent nucleophilic attack on the carbonyl carbon results to the breaking of the  $C=O$  double bond to form the corresponding alcohol (Scheme 1.3).



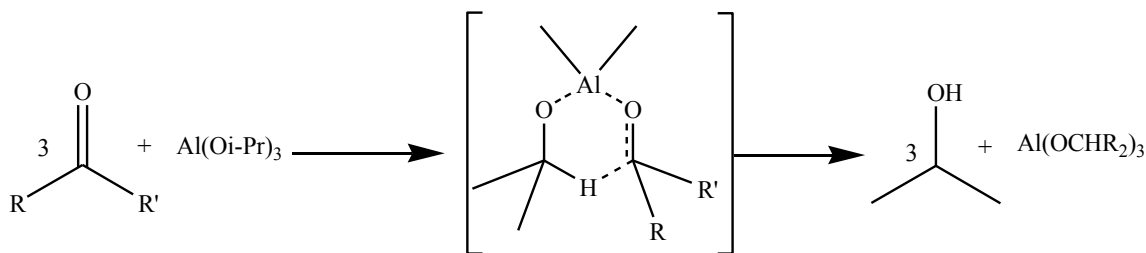
Scheme 1.3: A general scheme of electrophilic attack on ketone in reductive hydrogenation

Ketone hydrogenation to alcohols has been carried out through different methods, for example, by molecular hydrogen in the presence of a catalyst, using main group metal hydride complexes and transfer hydrogenation. Molecular hydrogen and main group metal hydrogenation of ketones are considered traditional methods. In the next section, a brief discussion on traditional and transfer hydrogenation of ketones is presented.

### 1.2.2.1 Traditional methods of hydrogenation of ketones to alcohols

Traditional hydrogenation of ketones to alcohols is mainly carried out in the presence of metal hydride complexes or by molecular hydrogen using heterogeneous catalysts.<sup>19</sup> Lithium aluminum hydride ( $\text{LiAlH}_4$ ) and sodium borohydride ( $\text{NaBH}_4$ ) have been traditionally used to reduce ketones to alcohols.<sup>20</sup> Though effective, these metal hydrides have some disadvantages which limit their applications. The metal hydrides are pyrophoric and lead to the production of stoichiometric amounts of metal salts.<sup>21-23</sup> Besides, they cannot be applied in the asymmetric synthesis to afford optically active alcohol products.<sup>24</sup>

On the other hand, catalytic hydrogenation using molecular hydrogen poses high risks especially when highly flammable reagents are used. Moreover, the reactions are carried at high temperatures and pressures and special equipment are required.<sup>21a, 25</sup> For these reasons subsequent attempts to find suitable catalytic systems were carried. In 1925, Meerwein and co-workers reported the successful use of aluminum isopropoxide, ( $\text{Al}(\text{O}i\text{-Pr})_3$ ) and isopropanol to reduce ketones to alcohols and subsequently named the newly discovered reaction the Meerwein-Ponndorf-Verley (MPV) process (Scheme 1.4).<sup>26</sup>

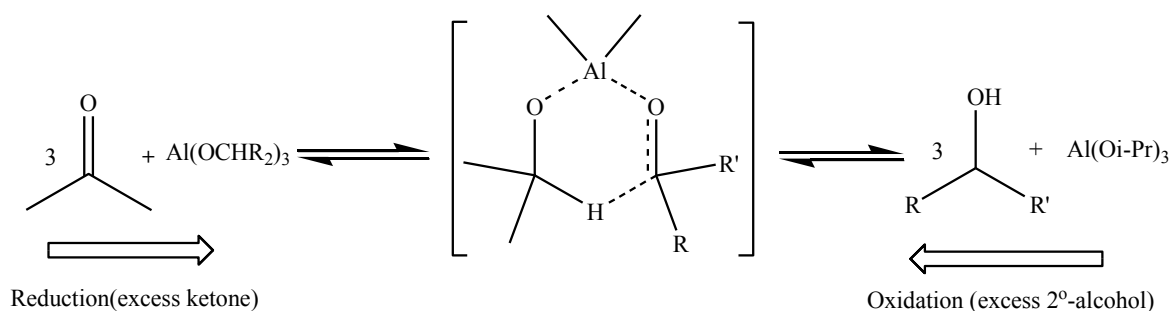


Scheme 1.4: MPV reduction of ketone<sup>26</sup>



The MPV reduction reaction is a catalysed process which involves hydrogen transfer from isopropanol to the ketone to give an alcohol and acetone as the by-product. It has several advantages over traditional methods of hydrogenation; it is highly selective, cheap and uses environmentally friendly metal catalysts.<sup>27</sup> One of the major challenges of MPV reduction is solvolysis which significantly lowers the yields.<sup>28</sup>

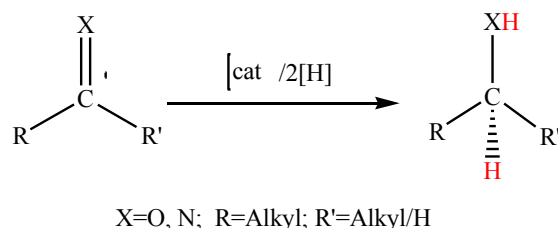
The reverse reaction (oxidation) was discovered by Oppenauer (Scheme 1.5) when he observed that secondary alcohols could be easily oxidized to the corresponding ketones using aluminum isopropoxide.<sup>29</sup> Oppenauer oxidation is one of the notable challenges of transfer hydrogenation of ketones. It has been partially solved by the use of formic acid mainly because CO<sub>2</sub> and H<sub>2</sub>, the by-products, cannot initiate the reverse reaction. For these reasons, consistent efforts are being spent to develop catalytic systems that eliminate the challenges faced by traditional and MPV hydrogenation reactions.<sup>21a,b</sup> Catalytic hydrogenation in the presence of transition metal complexes was later discovered and became a preferred choice for transfer hydrogenation over MPV aluminum isopropoxide.



Scheme 1.5: MPV reduction and Oppenauer oxidation of ketone<sup>29</sup>

### 1.2.2.2 Transfer hydrogenation of ketones using transition metal catalysts

Transition metal transfer hydrogenation is a mild and effective way of reducing multiple bonds in organic compounds using hydrogen donor molecules other than molecular hydrogen in the presence of a catalyst.<sup>30</sup> It has been extensively used to reduce ketones, aldehydes and imines to their corresponding alcohols and amines, respectively (Scheme 1.6). The process has also been extended to the reduction of alkenes and alkynes, though with limited success.<sup>31-33</sup> However, it has several advantages over other forms of hydrogenation such as; high selectivity, simplicity and ability to operate under mild conditions.<sup>34-36</sup>

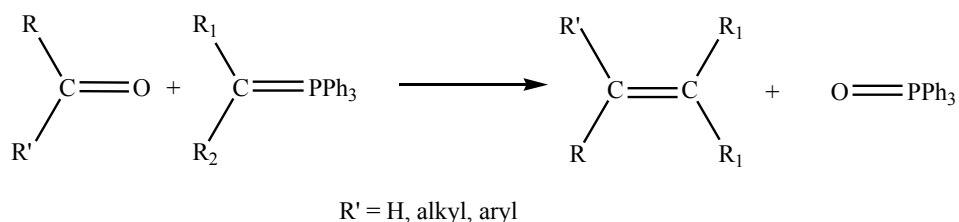


Scheme 1.6: Transfer hydrogenation reaction using hydrogen donor molecules<sup>33b</sup>

The hydrogen atoms are transferred from hydrogen sources such as isopropanol, formic acid, 1,4-cyclohexadiene, hydrazine, phosphinic acid, sodium hypophosphite, ammonium formate and trimethylamine among others.<sup>37</sup> Isopropanol is preferred because of its stability, ease of handling, cost, environmental friendliness and its moderate boiling point (82 °C).<sup>38</sup> In addition, the acetone by-product is easily removed from the product mixture due to its low boiling point.<sup>16,25,39</sup>

### 1.3 Alkenes and Alkynes

Alkenes are hydrocarbons containing one or more carbon-carbon double bond in the backbone of the compounds. They occur naturally in petroleum, plants and animal tissues, for example, camphene, limonene, isoprene, ethylene and pinene. They can also be prepared from other organic compounds by partial hydrogenation of alkynes and from ketones and aldehydes by the *Wittig reaction* (Scheme 1.7). Alkenes are chemically reactive due to their unsaturation. Hence, they are commonly used as starting materials for the synthesis of other important domestic and industrial products.<sup>40,41</sup>



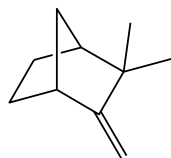
Scheme 1.7: *Wittig* reaction

On the other hand, alkynes contain at least one C≡C triple bond on the hydrocarbon backbone. They also occur naturally in plants and animals tissues, for example, thiarubrine A, capillin, parsalmide and norethynodrel.<sup>42</sup> Alkynes can be prepared by dehydrohalogenation of vicinal or vinyl dihalides. They are more reactive compared to their corresponding alkenes.

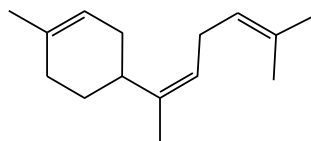
### ***1.3.1 Industrial applications of alkenes and alkynes***

Some of the naturally occurring alkenes and alkynes are used as natural medication while others are used as starting materials to prepare organic derivatives (Figure 1.4). Alkenes can be transformed to other organic compounds such as alkanes, alcohols, ketones, aldehydes, carboxylic acids, organo-halides, epoxides, esters, polymers and halohydrins (Figure. 1.5 (a)). Likewise, alkynes can be transformed to organic acids,<sup>43</sup> alcohols, alkyl halides, diones, and alkenes<sup>44</sup> among other organic compounds (Figure 1.5 (b)). These alkene and alkyne derivatives are significant raw materials for the syntheses of a wide range of industrial and domestic products.<sup>45-48</sup>

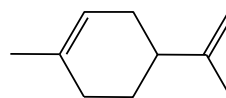
The most common derivatives of carbon-carbon multiple bond hydrocarbons are the corresponding saturated alkanes produced via hydrogenation reactions. Their applications range from industrial to domestic products. For example, lower alkanes ( $C_3$  to  $C_4$ ) are used as fuel in gas burners and propellants in aerosols sprays. ( $C_5$  to  $C_8$ ) alkanes are commonly used as fuels in internal combustion engines while ( $C_9$  to  $C_{16}$ ) alkanes are used in diesel and aviation fuel. High molecular weight alkanes, ( $C_{17}$  to  $C_{35}$ ), are mainly used as lubricating oils, for making candles and as anti-corrosive agents.



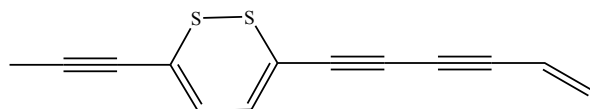
camphene  
Use: fragrance



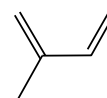
zingiberine  
Use: kitchen spice



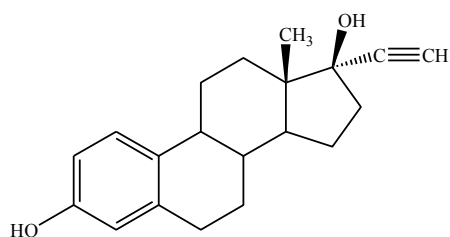
limonene  
Use: cosmetic, fragrance



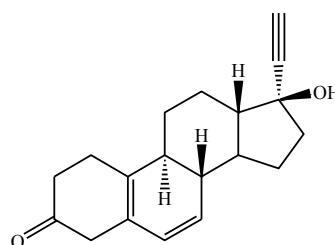
thiarubrine A  
Use: antiviral



isoprene  
Use: rubber



17-ethinylestradiol  
Use: anticancer



norethynodrel  
Use: contraceptive

Figure 1.4: Natural alkenes and alkynes and their applications

### ***1.3.2 High pressure hydrogenation***

High pressure hydrogenation reactions are carried out in special reactors and studies are highly motivated by the drive for clean technology, atom efficiency, the abundance and relative low cost of hydrogen gas.<sup>49</sup> The reactions have been known and studied for several decades since its inception in 1869<sup>50</sup> and later leading to the award of Nobel Prize in chemistry in 1912 to Paul Sabatier and Victor Grignard.<sup>51</sup> However, new discoveries and approaches in high pressure hydrogenation continue to stimulate research interest to date.<sup>52</sup>

Transition metal complexes of ruthenium, rhenium, iridium, rhodium, palladium, platinum and nickel are commonly used as hydrogenation catalysts. They are generally preferred because of their high catalytic activity owing to the presence of empty *d*-orbitals which can accept electrons from substrates thereby activating them for reduction.<sup>53,54</sup> The reactions are carried out using either heterogeneous or homogeneous systems. The following sections discuss heterogeneous and homogeneous catalytic systems for high pressure hydrogenation of alkenes and alkynes.

#### ***1.3.2.1 Heterogeneous catalytic hydrogenation of alkene and alkynes***

Heterogeneous catalysts have been used for hydrogenation reactions for many years mainly due to the ease of separation of products and catalysts in the reaction mixture and because the catalysts can often be recycled. They have been widely used in industrial syntheses of several fine chemicals.<sup>55</sup> Examples of well-known heterogeneous hydrogenation catalysts are Raney nickel and Lindlar catalysts.<sup>56</sup> Raney nickel catalyst is a fine solid: an alloy of nickel and aluminium prepared by adding nickel to molten aluminium before being quenched by a promoter.<sup>57</sup> The alloy is then activated by adding sodium hydroxide solution to a suspension of the alloy in water.<sup>58</sup>

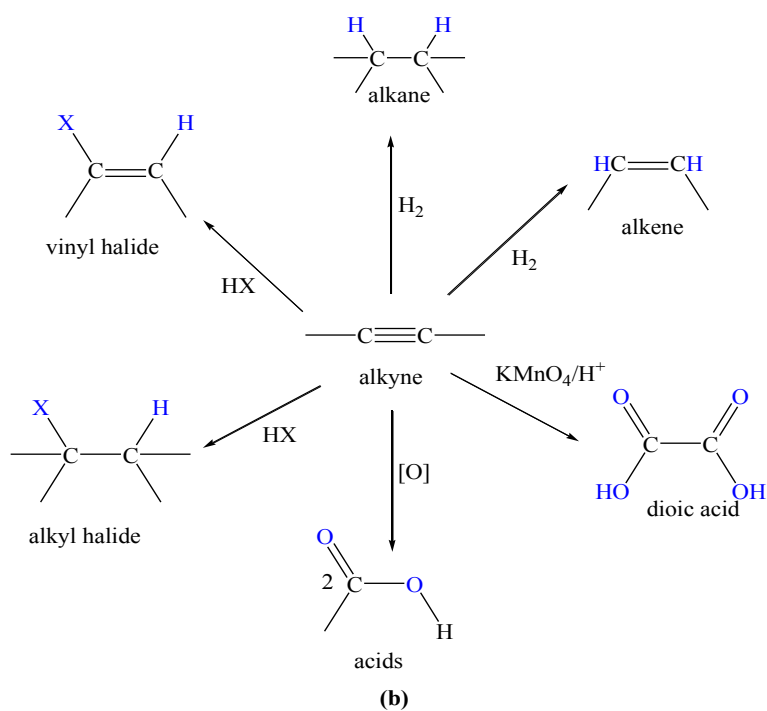
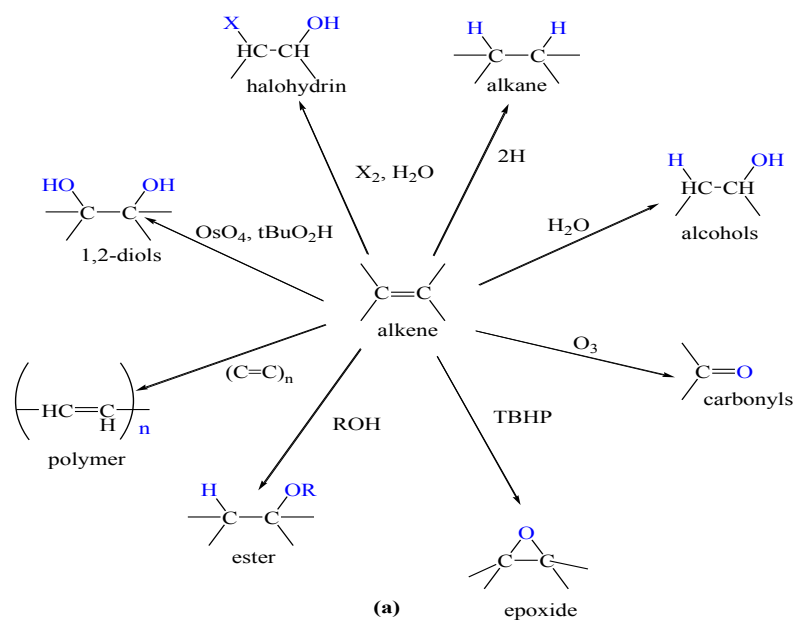
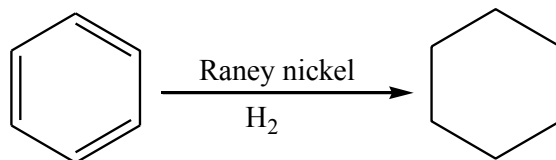


Figure 1.5: Reactions of (a) alkenes and (b) alkynes

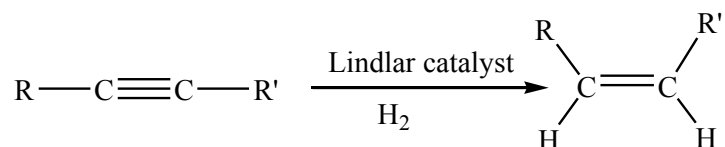
The Raney nickel catalyst was discovered in 1926 by Murray Raney<sup>59</sup> and was previously used for the hydrogenation of vegetable oils. However, its application has since been extended to the

hydrogenation of many other organic compounds, for example, in the hydrogenation of benzene to cyclohexane (Scheme 1.8), alkynes, aldehydes, ketones and nitro compounds.<sup>60</sup>



Scheme 1.8: Catalytic hydrogenation of benzene using a Raney Ni catalyst

Another heterogeneous hydrogenation catalyst with wide industrial application is the Lindlar catalyst.<sup>61</sup> It is prepared by depositing calcium carbonate on palladium metal and eventually adding lead compounds such as lead acetate and lead oxide to regulate its activity.<sup>62</sup> To improve the selectivity of the Lindlar catalyst, further deactivation can be carried out by addition of quinoline.<sup>63</sup> It has been traditionally used to partially reduce alkynes to *Z*-disubstituted alkenes in the presence of H<sub>2</sub> (Scheme 1.9).<sup>64</sup>



Scheme 1.9: Partial hydrogenation of an alkyne using a Lindlar catalyst

Other examples of heterogeneous hydrogenation catalysts include; supported Pd(0) nanoparticles,<sup>65</sup> poly(N-vinyl-2-pyrrolidone) stabilized Pt nanoparticles,<sup>66</sup> and ruthenium-tin clusters.<sup>67</sup> Despite the wide application of heterogeneous catalysts in hydrogenation, they still suffer from lack of selectivity, relatively high temperatures, and to some extent leaching of the active catalysts from the support rendering them less effective with time. For these reasons, homogeneous catalytic systems are being considered as suitable alternatives.



### 1.3.2.2 Homogeneous catalytic hydrogenation of alkene and alkynes

Homogeneous catalytic systems are still commonly used in the transformation of several organic compounds. Their preferential use is motivated by several properties, namely, high selectivity, mild reaction conditions (low reaction temperatures and pressure), ease of establishing reaction mechanisms and ease of tuning reaction sites.<sup>68</sup> However, homogeneous catalytic systems suffer from the challenge of separating products and catalyst from the reaction mixture.<sup>69</sup> Homogeneous hydrogenation reactions are generally performed with Rh, Pd, Ru, and Ir based catalysts.

Some of the most successful homogeneous hydrogenation catalysts reported are Wilkinson catalyst,  $(\text{RhCl}(\text{PPh}_3)_3)$ <sup>70</sup> and Vaska catalyst  $(\text{IrCl}(\text{CO})(\text{PPh}_3)_2)$  (Figure 1.6).<sup>71</sup> Wilkinson catalyst was discovered in 1965 and reported as the most active homogeneous catalyst, working at 25 °C and 1 atmosphere of hydrogen gas pressure.<sup>70</sup> Their activities are attributed to the oxidative unsaturation of the catalyst, (16e-), making them able to activate molecular hydrogen by oxidative addition.<sup>72</sup>

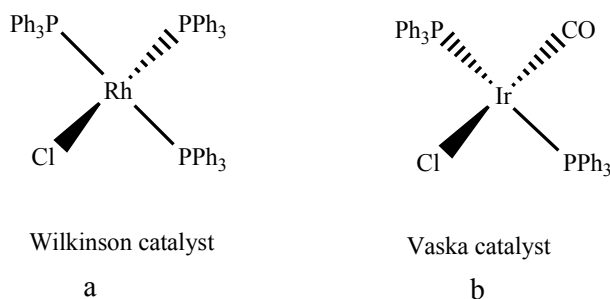
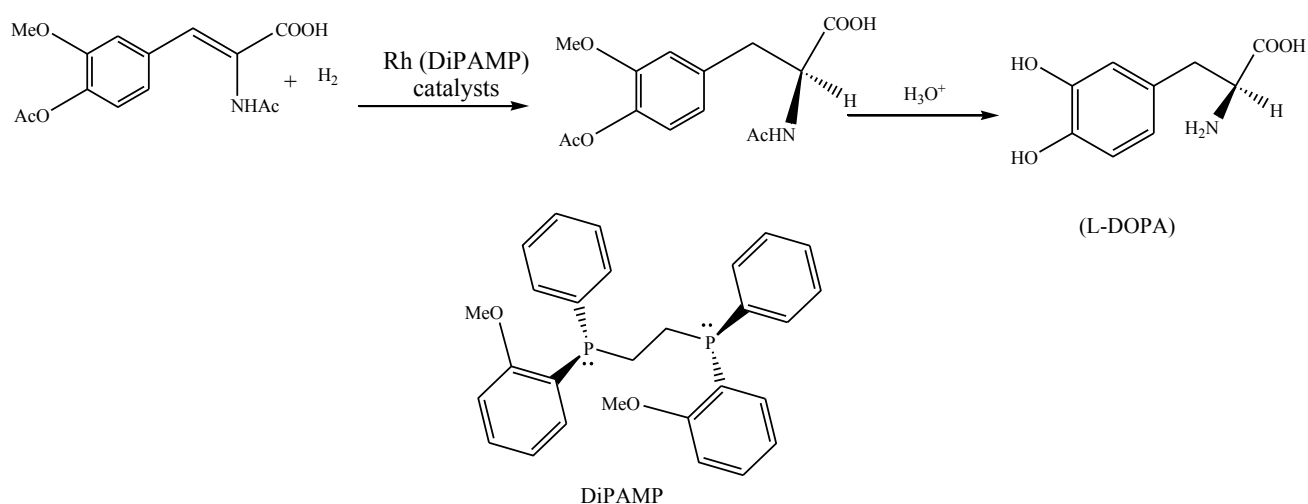


Figure 1.6: Structures of (a) Wilkinson and (b) Vaska homogeneous catalysts

Wilkinson catalyst has since been modified by introduction of chiral phosphine ligands for asymmetric hydrogenation.<sup>73</sup> Its modification facilitated the development of the first industrial process for the synthesis of L-3,4-dihydroxyphenylalanine (L-DOPA) (Scheme 1.10), a drug that has been used for the treatment of people suffering from Parkinson's disease, leading to the award of a Nobel prize in chemistry in 2001.<sup>74</sup> Other complexes used as homogeneous hydrogenation catalysts include cationic Ru and Pd complexes.<sup>75,76</sup>



Scheme 1.10: Monsanto's industrial synthesis of L-3,4-dihydroxyphenylalanine (L-DOPA) using a modified Wilkinson catalyst<sup>73</sup>

One of the challenges in the catalytic hydrogenation of alkenes and alkynes with molecular hydrogen is to achieve maximum selectivity.<sup>77</sup> For example, selectivity in the partial hydrogenation of alkynes to alkenes has been extensively used to synthesize various biologically active and natural compounds.<sup>78</sup> However, in most cases the reactions proceed to completely reduce C≡C bonds to the corresponding alkanes instead of partial hydrogenation to alkenes. Besides, alkenes and alkynes are susceptible to isomerization leading to internal alkenes.

Isomerization affects the conversions of the alkenes and alkynes to alkanes since the resulting internal alkenes are relatively less reactive towards hydrogenation.

The first step in improving catalytic hydrogenation is to understand the effects of ligands and other reaction parameters in catalytic hydrogenation. This knowledge and that of other aspects are important in designing new and more effective catalysts for the hydrogenation reactions. The following section will briefly highlight some significant effects of catalysts' design on catalytic activities on hydrogenation reactions.

#### ***1.4 Rationale of catalyst design***

To obtain a desired efficiency and selectivity for any particular catalytic reaction, optimization and adjustment of the catalyst that will carry out the intended reaction is necessary.<sup>79</sup> This optimization and adjustment can be accomplished by appropriate choice of a ligand.<sup>14</sup> Ligands are known to play a critical role in controlling the electronic and steric environment around the metal centre in complexes.<sup>80</sup> This has the overall effect of determining the selectivity, solubility and activity of the resultant catalysts.

Despite the enormous progress made in designing effective ligands for any particular catalytic reaction, the process still remains more of a prediction which involves a combination of experience, trial and error, and in most cases, a chance.<sup>3,6</sup> In this study we set out to use bidentate nitrogen-donor and phosphine-donor ligands. The bidentate nitrogen-donor ligands make the complexes stable and the heterocycle improves their solubility in organic solvents.<sup>77,81,82</sup> On the other hand, phosphine-donor ligands have made a great impact on developing homogeneous catalytic systems including for the late transition metal catalysed organic transformations.<sup>83</sup>

The presence of phosphorous moieties in the ligands also provides ease for synthetic modulation and control of both electronic and steric properties of the ligands and the complexes. This in turn leads to the ability to regulate the catalytic properties of a given metal centre. In Chapter Two, a review of previous research carried out on transfer hydrogenation (TH) of ketones and high pressure hydrogenation of carbon-carbon unsaturated bonds using ruthenium and palladium complexes is discussed.

## CHAPTER 2

### **Literature review of catalytic hydrogenation reactions using ruthenium and palladium metal complexes**

#### **2.1 Introduction to transfer and high pressure hydrogenation**

Transition metal catalysed transfer and high pressure hydrogenation reactions have been extensively employed to transform unsaturated organic compounds into various useful domestic and industrial products. This chapter presents a literature review on the use of transition metal catalysts in these reactions. The chapter covers two main areas; transfer hydrogenation of ketones using ruthenium complexes and high pressure hydrogenation of alkenes and alkynes catalysed by palladium and ruthenium catalysts. The review is extended to include biphasic catalytic hydrogenation in aqueous media in an attempt to bridge the gap between homogeneous and heterogeneous catalysis.

#### **2.2 Transition metal catalysed transfer hydrogenation of ketones**

To date, several transition metal complexes have been extensively studied and applied as transfer hydrogenation catalysts.<sup>84</sup> The first transition metal catalysed hydrogen transfer was reported by Trocha-Grimshaw and Henbest in the 1960s using the iridium hydride complex  $[\text{HIrCl}_2(\text{Me}_2\text{SO})_3]$  in the reduction of unsaturated ketones.<sup>85</sup>

After this pioneering work, many transition metal catalysts of Rh,<sup>86</sup> Ru,<sup>87</sup> Ir,<sup>88</sup> and Fe<sup>89</sup> have been studied for transfer hydrogenation of different ketones and found to display varied catalytic activities.<sup>90</sup> Ruthenium metal complexes have been established as effective and selective,

catalysts that can catalyse TH of a wide range of ketones.<sup>16b,21,91</sup> The next section reviews the development of ruthenium complexes as catalyst in the transfer hydrogenation of ketones.

## **2.2.1 Ruthenium catalysed transfer hydrogenation of ketones**

### **2.2.1.1 Phosphine donor ruthenium complexes**

The first ruthenium complex,  $[\text{RuCl}_2(\text{PPh}_3)_3]$  used in transfer hydrogenation of ketones was reported by Sasson and Blum.<sup>22,92</sup> This complex catalyses the hydrogenation of  $\alpha,\beta$ -unsaturated carbonyl compounds to the corresponding alcohols under homogeneous conditions obtaining yields as high as 96%. One major drawback of this catalyst is its thermal instability at elevated temperatures (150-200 °C).<sup>93,94</sup>

By adding 2.4 mol% of sodium hydroxide into a catalytic mixture of  $[\text{RuCl}_2(\text{PPh}_3)_3]$  and cyclohexanone in propan-2-ol, the conversion to cyclohexanol was rapidly enhanced achieving 89% in 1 h compared to <1% conversion observed after 6 h when the reaction was conducted without the base.<sup>93</sup> This discovery highlighted the key role of the base in transfer hydrogenation reactions and has been the most reliable method of producing organic alcohols from ketones. Besides, phosphine-donor ligands offer a range of steric and electronic properties and stabilize the ruthenium complexes in low oxidation states, controlling both enantio-selectivity and reactivities of the complexes towards the hydrogenation of ketones.<sup>115,95,96</sup>

Incorporation of electron withdrawing groups in the ligand architecture result in enhanced catalytic activities of the corresponding complexes towards transfer hydrogenation reactions. For example, Wang *et al.* observed that there was electronic effect induced by the ligands on the catalytic activities of ruthenium(II) complexes,  $[\text{RuCl}_2(\eta^6\text{-C}_6\text{H}_6)(\text{L})]$ , (where L = phosphorous-

donor ligand). They found that the complex bearing tri(*p*-trifloromethylphenyl)phosphine) ligand (Figure. 2.1a) is more active towards transfer of hydrogenation of ketones compared to similar systems shown in Figures 2.1 (b) and (c) respectively.<sup>97</sup>

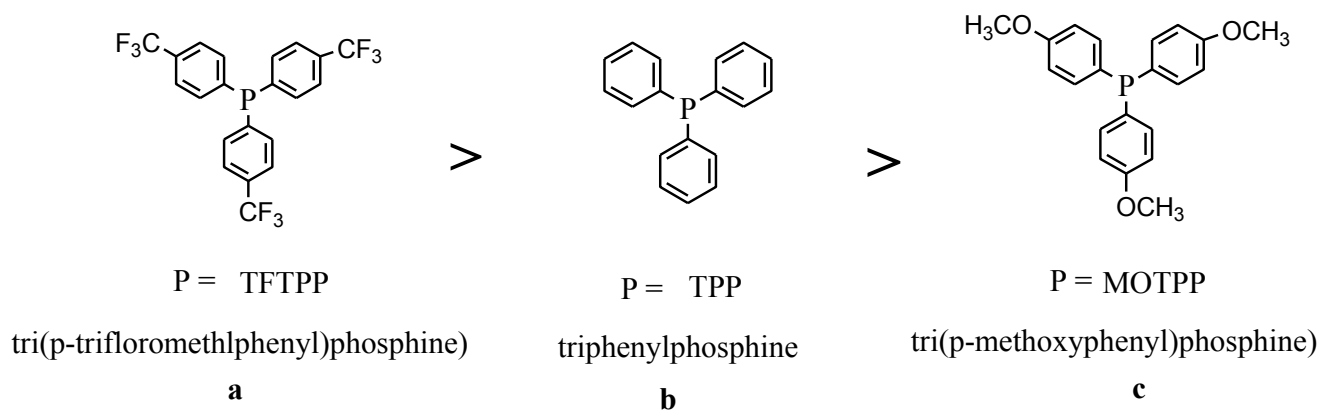


Figure 2.1: Effect of the electronic factor on catalytic activity of ruthenium(II) complexes towards transfer hydrogenation.

### 2.2.1.2 Nitrogen-donor ruthenium complexes

Nitrogen-donor ruthenium complexes have also been studied in transfer hydrogenation of ketones. Recently, several nitrogen-donor Ru(II) complexes bearing different functional groups on the ligand backbone have been developed and evaluated for transfer hydrogenation reactions.<sup>98-100</sup> For example, Yu *et al.* reported some N-heterocyclic ruthenium(II) complexes bearing tridentate nitrogen donor ligands, RuCl<sub>2</sub>(PPh<sub>3</sub>)(Me<sub>4</sub>-BPPy) (Figure 2.2a) and RuCl<sub>2</sub>(PPh<sub>3</sub>)(*i*Bu-BTP) (Figure 2.2b), in transfer hydrogenation reactions. The catalytic activities of these complexes are dependent on their structural and electronic properties.

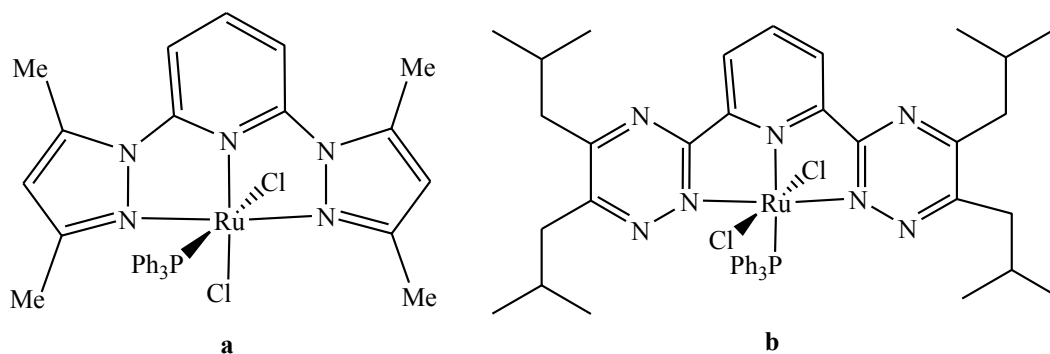


Figure 2.2: *Pseudo- N<sub>3</sub>*, ruthenium(II) complexes<sup>98</sup>

The catalyst precursor, Figure 2.2(a), achieved a turnover frequency (TOF) of 6000 h<sup>-1</sup>, while the precursor Figure. 2.2(b) achieved 1080 h<sup>-1</sup>. The huge difference in the TOFs of the two complexes is attributed to the orientation of PPh<sub>3</sub> ligand and the different substituents on the heterocyclic rings or the ligands.<sup>99</sup> In general, nitrogen donor ligands are widely used to regulate the steric and electronic properties of the complexes as well as to increase the reactivity of the complexes<sup>99,101,102</sup> The other advantage of nitrogen-donor ligand is that their complexes are also synthesized under mild conditions and in most cases do not require an inert atmosphere.<sup>103,104</sup> However, regulation of the steric and electronic properties of transition metal catalysts can also be achieved by preparing the complexes from mixed multi-donor ligands, for example, mixed phosphine- and nitrogen donor ligands.

### 2.2.1.3 *Asymmetric mixed phosphine-nitrogen donor ruthenium complexes*

Mixed phosphine-nitrogen-donor ruthenium complexes have been extensively used in the transfer hydrogenation of ketones. The great interest in phosphine-nitrogen ruthenium complexes has been motivated by the demand for chiral organic alcohols as raw materials for fine chemical and pharmaceutical industries leading to the focus on asymmetric transfer hydrogenation of



ketones.<sup>105</sup> Most notable chiral transfer hydrogenation catalysts are those reported by Noyori and co-workers of the type Ru(II)-TsDPEN (TsDPE= N-(p-toluenesulfonyl)-1,2-diphenylenediamine) (Figure 2.3) for asymmetric catalysis.<sup>106</sup>

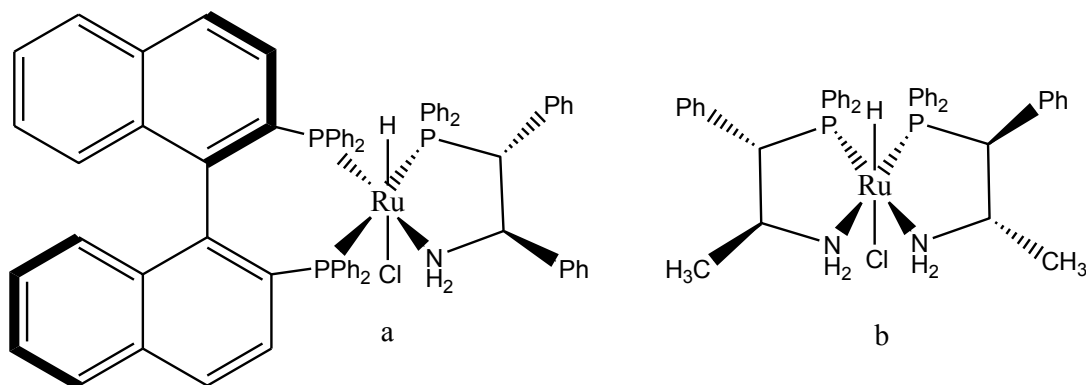


Figure 2.3: (a)  $\beta$ -Aminophosphine and (b) diminophosphine ruthenium(II) complexes<sup>107</sup>

Chiral systems such as tetradentate diphosphine/diamine and diphosphine/diimine ruthenium(II) complexes (Figure 2.4 (a) and (b)), cyclometalated terdentate species developed by Barrata *et al.*<sup>108</sup> and “reverse tethered” complexes by Morris *et al.* (Figure. 2.5) have also been reported.<sup>109</sup>

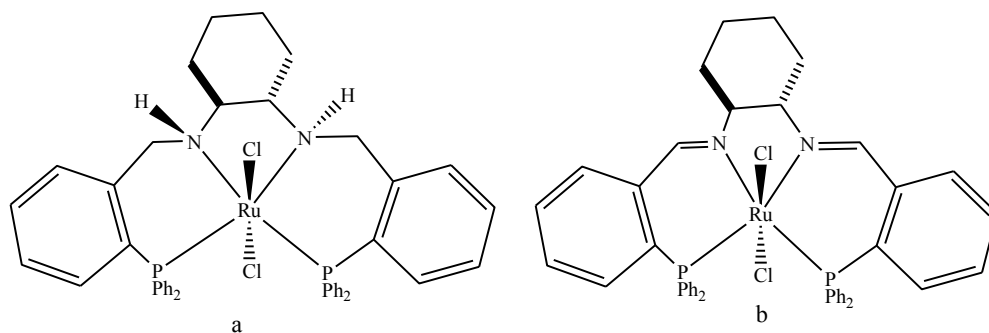


Figure 2.4: (a) Tetradentate diphosphine/diamine and (b) diphosphine/diimine Ru(II) complexes<sup>108</sup>

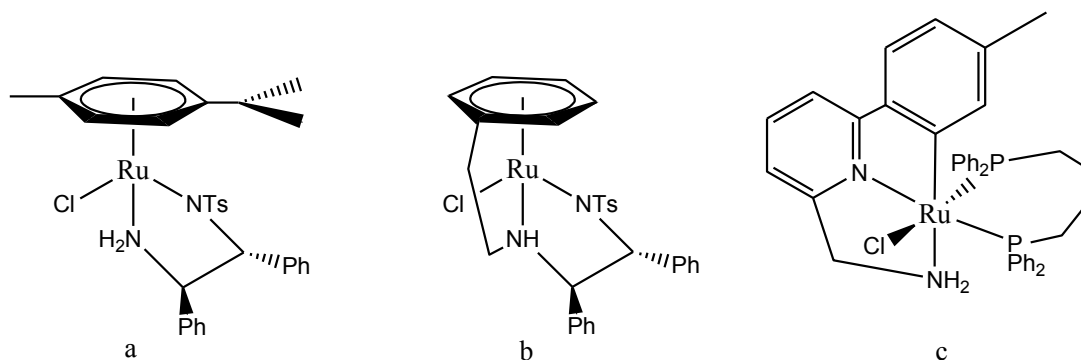


Figure 2.5: Chiral (a) TsDPEN, (b) tethered TsDPEN (DPEN = 1,2-diphenylethylenediamine) and (c) terdentate Ru(II) complexes<sup>109</sup>

These ruthenium complexes containing chiral N, P and N-P donor ligands are stable, highly active, selective and effectively produce optically active alcohol products.<sup>90c,110,111</sup> For example, the  $\beta$ -aminophosphineruthenium(II) complexes (Figure 2.3) are able to give high TOFs of up to  $6700 \text{ h}^{-1}$  at relatively low temperature of  $28 \text{ }^\circ\text{C}$ . Interestingly, significant activities can also be recorded at lower temperatures, as low as  $-20 \text{ }^\circ\text{C}$ .<sup>16c,112</sup> These improvements in activity and selectivity of the aminophosphine ruthenium complexes are attributed to the presence of the  $\alpha$ -amine moieties on the ligands which are proposed to assist in the catalytic process through a metal-ligand bi-functional mechanism.<sup>113,114</sup> Application of some of these chiral ruthenium complexes have since gone commercial e.g. in the production of chiral intermediates by Takasago International Co. for the synthesis of carbapenem antibiotics (Figure 2.6) and other organic alcohols.<sup>115</sup>

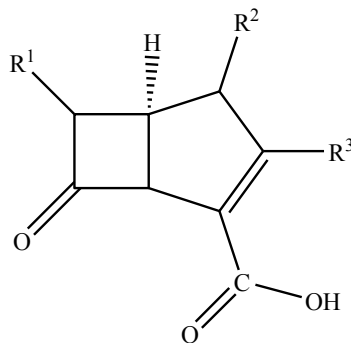


Figure 2.6: Chemical structure of carbapenem antibiotic<sup>115</sup>

#### 2.2.1.4 *N*-heterocyclic carbene ruthenium complexes

To design an effective transfer hydrogenation catalyst, it is important to predict the anticipated effects of the ligands on the resulting complexes. These may include the effects on stability, solubility, electronic and steric properties.

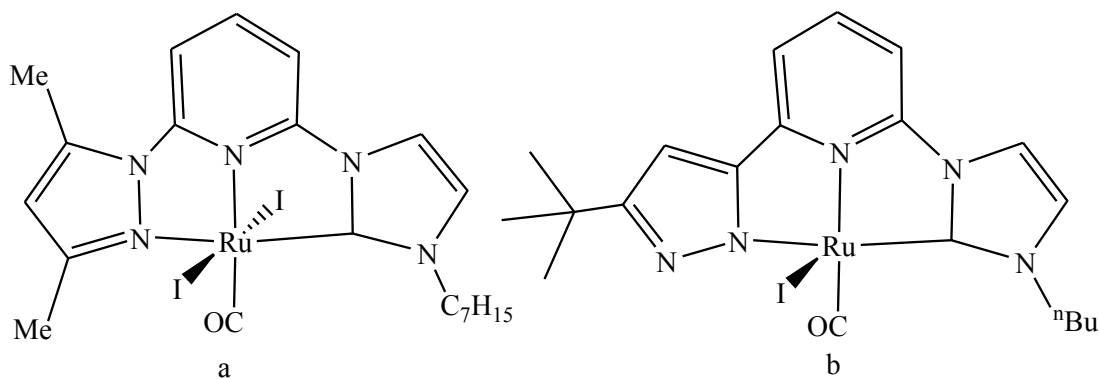


Figure 2.7: Pincer ruthenium(II) complexes<sup>98</sup>

In 2008, Zeng and Yu developed pincer NNC ruthenium complexes (Figure 2.7) and were able to regulate the physical and chemical properties of the complexes by adding different functional groups on the ligand backbone.<sup>98</sup> Besides, these complexes are effective catalysts for transfer hydrogenation of aliphatic and aromatic ketones in the absence of phosphine.

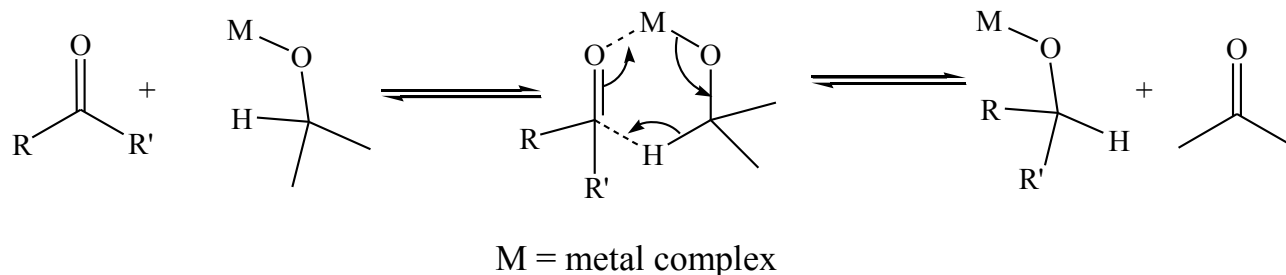
This has been attributed to the coordinative unsaturation of the Ru(II) metal centres.<sup>98</sup> Proper regulation of electronic and steric properties and understanding the transfer hydrogenation reaction mechanism is therefore important for the design of effective catalysts. The following section discusses the reaction mechanism of transfer hydrogenation using ruthenium complexes.

### ***2.2.2 Mechanisms of transfer hydrogenation of ketones with ruthenium complexes***

Transfer hydrogenation by metal complexes has been proposed to occur through two main routes: ‘direct hydrogen transfer’ and ‘hydridic’ routes.<sup>116</sup> While ‘direct hydrogen transfer’ is exhibited by main group metals, transition metals are proposed to operate through the ‘hydridic’ route. The subsequent sections highlight the fundamental differences between the different routes of transfer hydrogenation. The main focus is in the ‘hydridic’ route and the subsequent pathways exhibited by ruthenium metal complexes.

#### ***2.2.2.1 ‘Direct hydrogen transfer’ versus ‘hydridic route’***

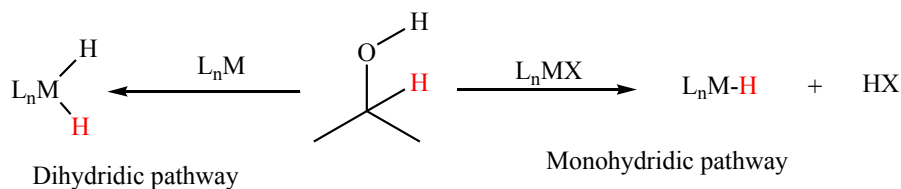
‘Direct hydrogen transfer’ is named after the process involved in moving hydrogen atoms from the donors to the substrate during hydrogenation. The process involves oxidation of the hydrogen donor and transferring the hydrogen to the ketone.<sup>21a,c, 91b,d</sup> It proceeds through a six member transition state initiated by coordination of both the ketone and the proton donor to the metal centre at close proximity (Scheme 2.1). The substrate is activated by the metal making it susceptible to attack by the hydrogen donor. This step is followed by the simultaneous transfer of the hydrogen to the propoxide and the breaking of the C=O double bond leading to the formation of metal alkoxide and acetone.<sup>21c</sup>



Scheme 2.1: Direct hydrogen transfer route for Meerwein-Ponndorf-Verley (MPV) reduction reaction<sup>117</sup>

A further addition of hydrogen to the alkoxide leads to formation and subsequent elimination of the alcohol product. Ruthenium complexes catalyse the transfer of hydrogen from isopropanol (hydrogen donor) to the ketones through the hydridic route. The ‘hydridic route’ is a stepwise process involving the formation of metal hydrides intermediates facilitated by an inorganic base.<sup>118</sup> The formation of a hydride intermediate is preceded by formation of a metal alkoxide.<sup>22</sup>

The ‘hydridic route’ is further divided into two pathways: monohydridic and dihydridic routes, based on the number of hydrides formed on the metal centre.<sup>116</sup> A monohydridic pathway is characterized by the formation of a monohydride intermediate (Scheme 2.2). The intermediate product maintains the identities of the transferred hydrogen *i.e.* the hydrogen atom (C-H) from isopropanol is the only hydrogen transferred to the metal surface to form the metal monohydride. The same hydride is subsequently transferred to the carbonyl carbon of the ketone substrate. The OH proton remains on the isopropanol and is only transferred directly to the ketone carbonyl oxygen from the hydrogen donor. This results in the transferred protons retaining their identical positions in the alcohol product.

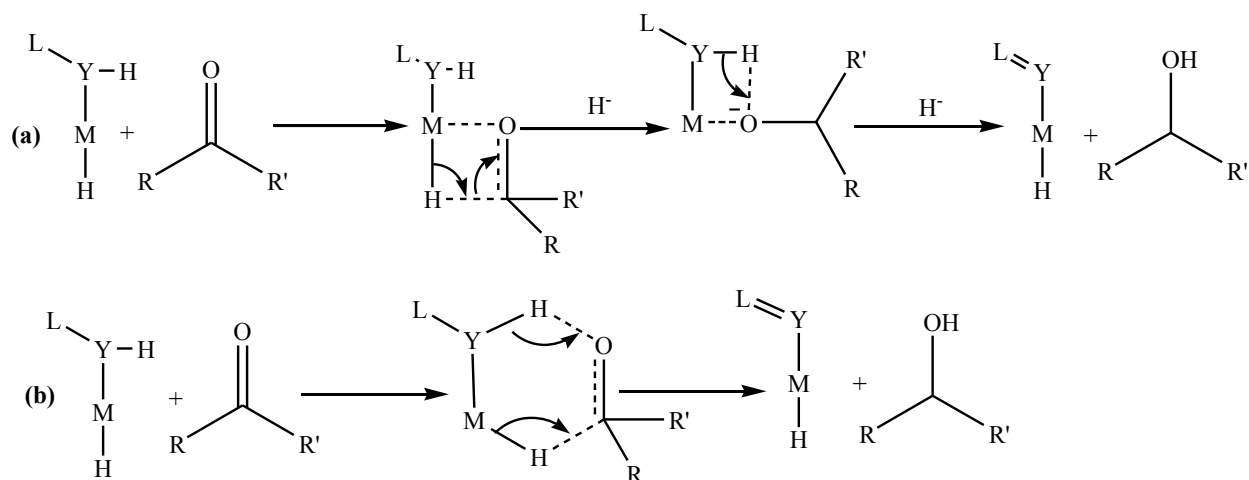


Scheme 2.2: Two different pathways for the ‘hydridic route’

On the other hand, a dihydride pathway is characterized by formation of a metal dihydride intermediate from the hydrogen of both the carbonyl carbon and OH of the isopropanol (Scheme 2.2).<sup>116</sup> The dihydridic pathway is different in the sense that any of the hydride ligands can be added to the substrate’s carbonyl carbon (C=O). Thus, retention of the identities of the protons is not guaranteed.

#### 2.2.2.2 ‘Inner sphere’ vs ‘outer sphere’ mechanism

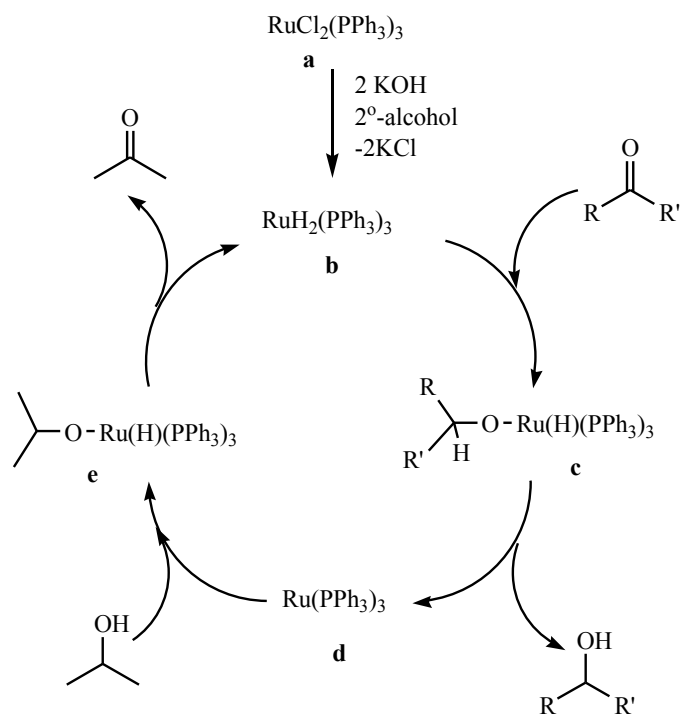
The monohydride pathway is further categorized into inner- and outer-sphere mechanisms. In an inner-sphere mechanism a metal alkoxide forms before the generation of a metal hydride. The substrate then binds to the metal centre with the assistance of the hydride ligand (Scheme 2.3a). On the other hand, an outer-sphere mechanism involves the transfer of hydrogen via a six membered transition state. In this mechanism the substrate does not coordinate to the metal but is activated by coordinating to the acidic “LY-H” (where L = ligand; Y = N,O atoms) moiety of the ligand in a process known as “metal-ligand bifunctional catalysis” (Scheme 2.3b).<sup>91c,119</sup> A detailed mechanism of transfer hydrogenation of ketones through a dihydridic pathway was proposed by Backvall (Scheme 2.4). Starting from dichlorotris(triphenylphosphine)ruthenium, RuCl<sub>2</sub>(PPh<sub>3</sub>)<sub>3</sub>, the role of the inorganic base in the reaction was highlighted.



M = transition metal, L = ligand, Y = N or O

Scheme 2.3: Metal monohydride mechanisms of transfer hydrogenation; (a) inner-sphere and (b) outer-sphere<sup>120</sup>

The process is initiated by the inorganic base, in this case KOH, which assisted in reduction of the dichloride Ru(II) complex, **a**, to form a ruthenium dihydride intermediate, **b**.<sup>116, 121</sup> The dihydride intermediate formation is a process which involves the interaction of the metal complex and the hydrogen donor, isopropanol. It leads to the formation of a metal alkoxide intermediate which is subsequently oxidized to acetone.<sup>21c,121,122</sup> The metal dihydride formed is more reactive to ketones, resulting in the alkoxide intermediate, **c**. A further transfer of hydride ligand to the alkoxide results in the formation of the corresponding alcohol and **d**. The intermediate, **d**, is unstable and in the presence of isopropanol forms the monohydride ruthenium alkoxide, **e**. The coordinated alkoxide in **e** is released as acetone to form the ruthenium dihydride complex, **b** and the catalytic cycle is repeated.<sup>21,22</sup> The rate at which the dihydride intermediate, **b**, is formed largely depends on the strength of the base used.<sup>123</sup> Strong inorganic bases such as KOH, NaOH and potassium *tert*-butoxide are therefore preferred.



Scheme 2.4: Transfer hydrogenation mechanism using homogeneous ruthenium complex<sup>22</sup>

### 2.3 Transition metal catalysed high pressure hydrogenation of alkenes and alkynes

The application of metal complexes as catalysts for the hydrogenation of carbon-carbon multiple bonds has been carried out using several transition metals. Platinum group metal complexes such as those of Fe,<sup>124</sup> Ru,<sup>125</sup> Ir,<sup>126</sup> Ni,<sup>127</sup> Pd<sup>128</sup> and Pt<sup>129</sup> have been investigated for high pressure catalytic hydrogenation of alkenes with molecular hydrogen. The significant properties of these metals that make them suitable for catalytic hydrogenation reactions is the empty *d*-orbitals which can accept electrons from substrates leading to change of oxidation states.<sup>54,130</sup> The ability to change oxidation states make them exhibit high catalytic activities under mild reaction conditions.<sup>131</sup>



Among the reported transition metal catalysts, palladium and ruthenium complexes are considered the most effective. Palladium complexes have the unique ability to selectively hydrogenate alkynes to give a mixture of alkanes and alkenes in heterogeneous and homogeneous systems.<sup>132</sup> Likewise, ruthenium complexes have been extensively applied in homogeneous hydrogenation of different unsaturated organic compounds.<sup>133</sup> The subsequent sections highlight the existing research done on high pressure catalytic hydrogenation of carbon-carbon multiple bonds using Pd and Ru metal complexes.

### ***2.3.1 High pressure hydrogenation of alkenes and alkynes using palladium complexes***

Few transition metal complexes have been known as homogeneous catalysts for a wide range of substrates with good selectivities. However, palladium metal complexes are some of the most active catalysts known in hydrogenation reactions.<sup>134,135</sup> In addition, they have been reported to be selective towards hydrogenation of alkenes and alkynes.<sup>136</sup>

The interest in modern homogeneous catalysis is motivated by the quest for efficiency and selectivity in carrying out catalytic organic transformations. The following sections discuss some of the palladium complexes bearing phosphine, nitrogen and mixed nitrogen and phosphine donor ligands which have been reported as effective homogeneous catalysts in the hydrogenation of alkenes and alkynes.

#### ***2.3.1.1 Phosphine-donor palladium complexes***

Monodentate and multidentate phosphine ligands are widely used in homogeneous catalysis in hydroformylation and hydrogenation reactions.<sup>137</sup> In the last decades, homogeneous phosphine Pd(II) complexes have been reported for the catalytic hydrogenation of olefins.

For instance, Drago and Pregosin reported bidentate (2,5-dimethylphospholano)benzene palladium(II) complexes (Figure 2.8a) for the hydrogenation of 3-methyl-2-cyclohexenone. The complexes were able to give 40% conversion of 3-methyl-2-cyclohexenone after 24 h.<sup>138</sup> Others complexes include; dinuclear palladium(0) complexes bearing 1,1-bis(diphenylphosphino)methane ligands reported by Stern and Maples (Figure 2.8b)

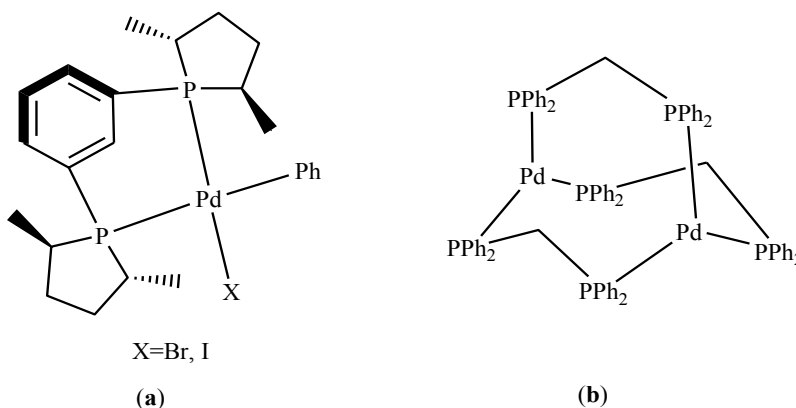


Figure 2.8: Structures of (a) phosphine Pd(II) and (b) dinuclear phosphine Pd(0) complexes for homogeneous hydrogenation reactions<sup>138</sup>

### 2.3.1.2 Nitrogen-donor palladium complexes

Nitrogen-donor palladium catalysts have also been investigated for the homogeneous hydrogenation of unsaturated organic compounds with molecular hydrogen. Examples of the nitrogen-donor catalysts include; bis(arylimino)acenaphthenepalladium(0) (Figure 2.9a)<sup>61</sup> and pyridine-2-carbaldiminepalladium(0) complexes (Figure 2.9b)<sup>139</sup>

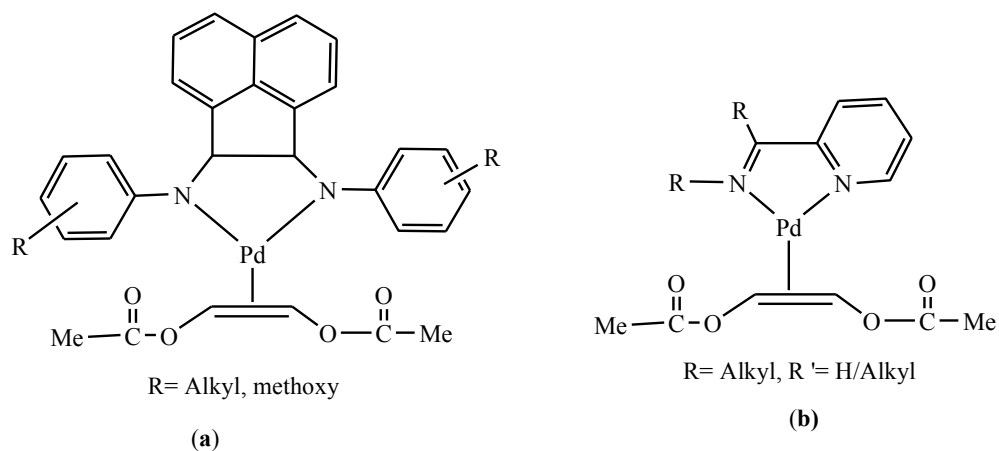


Figure 2.9: Bidentate nitrogen-donor Pd(0) complexes for partial homogeneous hydrogenation of alkynes<sup>61,139</sup>

These Pd(0) complexes are stable under hydrogen pressure and display excellent selectivities in the hydrogenation of a wide range of alkynes. Their selectivities depend on the nature of the substituents on the nitrogen-donor atoms and their stabilities increase with increase in the  $\sigma$ -donating ability of the respective substituent.<sup>139</sup> In 2000, Ruffo and co-workers also reported a water soluble bidentate nitrogen-donor Pd(0) complex (Figure 2.10) for the hydrogenation of olefins in water.<sup>140</sup>

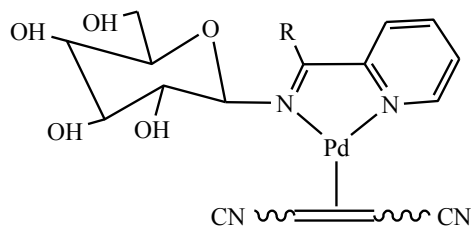
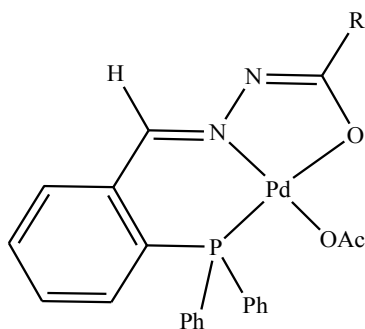


Figure 2.10: Water soluble bidentate nitrogen-donor Pd(0) complexes for the homogeneous hydrogenation of olefins<sup>140</sup>

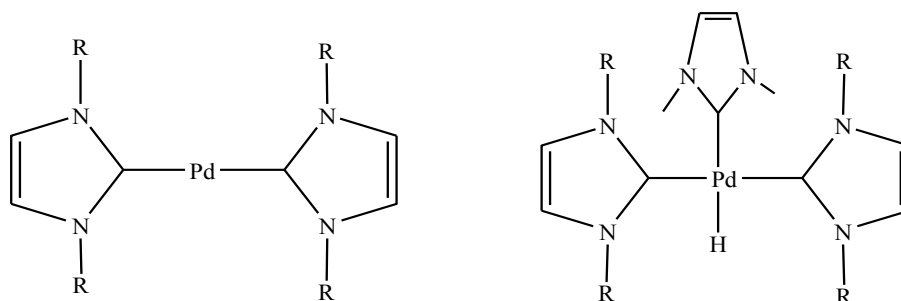
### 2.3.1.3 Mixed nitrogen-phosphine donor palladium complexes

Mixed donor atom ligands have also been used in designing homogeneous palladium catalysts for the hydrogenation of unsaturated hydrocarbons. For example, in 1994, Bacchi *et al.* synthesized palladium complexes bearing phosphine hydrazonic ligands which were active in the hydrogenation of styrene at room temperature under 1 atmosphere of H<sub>2</sub> pressure.<sup>141</sup> In a follow up study, they developed palladium complexes bearing tridentate and bidentate hydrozonic ligands with different donor atoms (Figure 2.11).<sup>142</sup> These new complexes showed improved activity in the hydrogenation of phenyl acetylene and styrene due to their hemilabile nature of the ligand. Generally, the catalytic activities of palladium complexes have been reported to highly dependent on the ligands. For example, the bulky aryl substituents on the carbene ligands of the tetradentate pyrrole Pd(II) and N-heterocyclic carbene palladium complexes (Figure 2.12) stabilize the metal centres, thereby enhancing their catalytic activities.<sup>143,144</sup>



R= Me, Me, PhMe, PhBr, PhNO<sub>2</sub>

Figure 2.11: Tridentate hydrozonic Pd(II) complexes for homogeneous hydrogenation of unsaturated carbon-carbon bonds.<sup>142</sup>



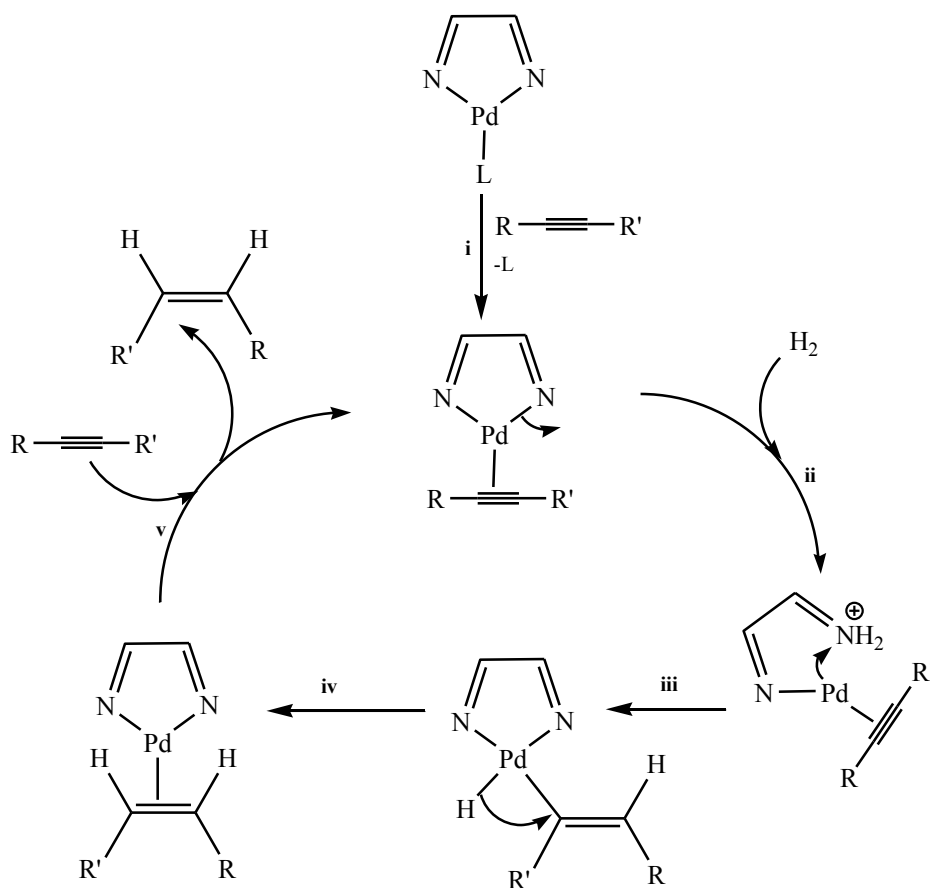
R= C<sub>9</sub>H<sub>11</sub> (**a**); C<sub>12</sub>H<sub>19</sub> (**b**); C<sub>7</sub>H<sub>6</sub> (**c**) and C<sub>10</sub>H<sub>13</sub> (**d**)

Figure 2.12: N-Heterocyclic carbene palladium complexes for semi hydrogenation of 1-phenyl-1-propyne.<sup>143,144</sup>

### 2.3.2 Mechanisms of high pressure semi-hydrogenation of alkynes with Pd(II) complexes

Metal complexes considered for hydrogenation catalysis should be able to heterolytically activate molecular hydrogen to form metal hydrides and transfer the hydride to the organic substrate.<sup>145</sup> The mechanism of hydrogenation of unsaturated hydrocarbons was first proposed in 1934. It has been established to proceed through several steps involving the formation of metal hydride, substrate adsorption, hydrogen transfer to the coordinated substrate and finally reductive elimination of the saturated product.<sup>146</sup>

In 2005, Kluwer *et al.* proposed a reaction mechanism for the semi-hydrogenation of 4-octyne (Scheme 2.5).<sup>147</sup> Their mechanism consists of five consecutive steps starting with alkyne coordination, step (i). The coordination of substrate leads to the weakening of the  $\pi$  bond of the substrate.<sup>148</sup> This is followed by heterolytic activation of dihydrogen which involves hydrogenolysis of one of the Pd-N bonds, step (ii). The hydro-palladation of the alkyne, addition of N-H to palladium, step (iii), and a reductive elimination of alkene hydride, step (iv). Step (v) involves catalyst regeneration to initiate a new cycle.



Scheme 2.5: Mechanism of semi-hydrogenation of 4-octyne<sup>61</sup>

### 2.3.3 High pressure hydrogenation of alkenes and alkynes using ruthenium complexes

#### 2.3.3.1 Homogeneous phosphine ruthenium complexes

Though palladium complexes have been known as suitable catalysts for hydrogenation of non-polar unsaturated hydrocarbons, other platinum group metal complexes are being considered. To date, ruthenium complexes are being studied in catalytic hydrogenation as possible replacements for the Pd and Rh, catalyst which are considered relatively expensive.<sup>149</sup>

Homogeneous ruthenium(II) complexes have been used to catalyse multiple organic transformation reactions. For example,  $[\text{RuCl}_2(\text{PPh}_3)_3]$ ,  $[\text{RuHCl}(\text{PPh}_3)_3]$  and  $[\text{RuH}_2(\text{PPh}_3)_4]$  have been reported as efficient precursors for hydrogenation of alkenes and alkynes.<sup>150</sup> Other neutral ruthenium complexes studied include ruthenium(II) carbonyl complexes  $[\text{RuHCl}(\text{CO})(\text{PPh}_3)_3]$ ,<sup>151</sup>  $\text{Ru}(\text{CO})_2(\text{OAc})_2(\text{P}^n\text{Bu}_3)(\text{PR}_3)$  ( $\text{R} = p\text{-XC}_6\text{H}_4$ ),  $\text{Ru}(\text{CO})_2(\text{OAc})_2(\text{PR}_3)_2$  ( $\text{R} = \text{Ph}, ^n\text{Bu}$ ) and  $[\text{RuH}(\text{dppb})_2]\text{PF}_6$  (Figure 2.13).<sup>152</sup>

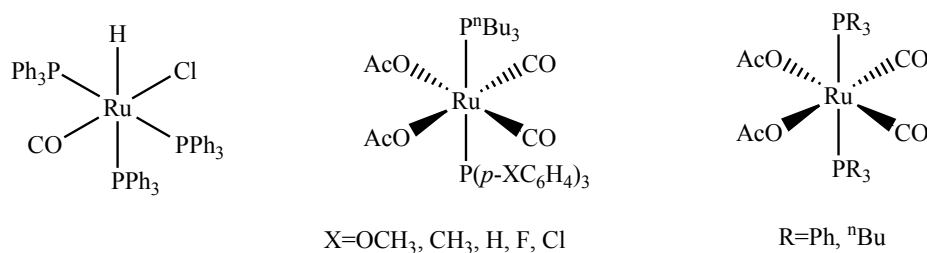
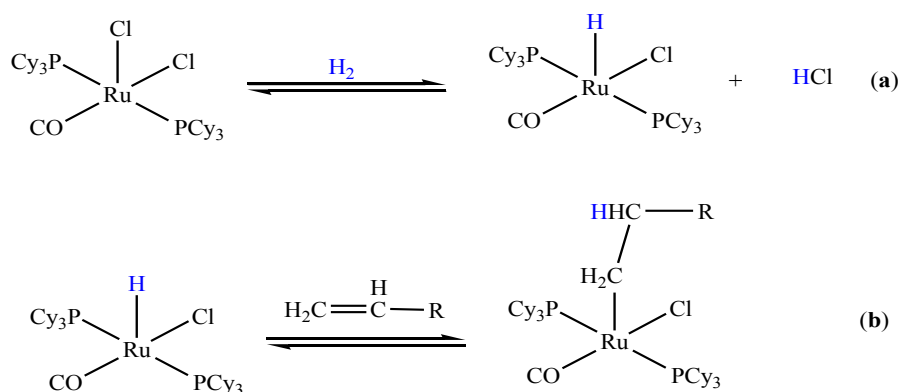


Figure 2.13: Neutral ruthenium complexes for high pressure hydrogenation<sup>152</sup>

These carbonyl complexes (Figure 2.13) have been reported to achieve conversions between 41.8%-97.8% after 3 h for the hydrogenation of 1-hexene to *n*-hexane.

However, they exhibit slow and incomplete conversion of terminal alkenes due to accompanying isomerization reactions.<sup>152</sup> Besides, the optimum reaction conditions for effective hydrogenation of 1-hexene to *n*-hexane are considerably severe: 100 bar hydrogen pressure and a temperature of 80 °C.<sup>152</sup> These neutral ruthenium complexes easily undergo substitution reactions to form the active hydride intermediates (Scheme 2.6a) and to bind the unsaturated substrates (Scheme 2.6a).<sup>153</sup>



Scheme 2.6: Substitution reactions of neutral ruthenium(II) complexes<sup>153</sup>

### 2.3.3.2 Cationic ruthenium complexes for homogeneous hydrogenation of alkenes and alkynes

Other than neutral ruthenium(II) complexes, cationic ruthenium complexes have also been applied in molecular hydrogenation of unsaturated hydrocarbons. For example, cationic NHC ruthenium(II) complexes and monohydride ruthenium(II) complexes (Figure 2.14) have been studied.<sup>154</sup> Despite the excellent conversions, ruthenium(II) complexes previously evaluated for hydrogenation of alkenes and alkynes still face some challenges. The cationic N-heterocyclic carbene ruthenium(II) complexes reported by Gandolfi *et al.* achieve only modest conversions under relatively harsh conditions of 80 °C and 60 bar of hydrogen pressure.<sup>155</sup>

Tremendous achievements have been made in developing catalysts for homogeneous, however, separation of catalysts from the product mixture remains an enormous task that must be addressed. There are different ways to achieve product and catalyst separation. The following section highlights one of the methods of enhancing catalyst-product separation currently drawing a lot of interest: biphasic catalytic hydrogenation.



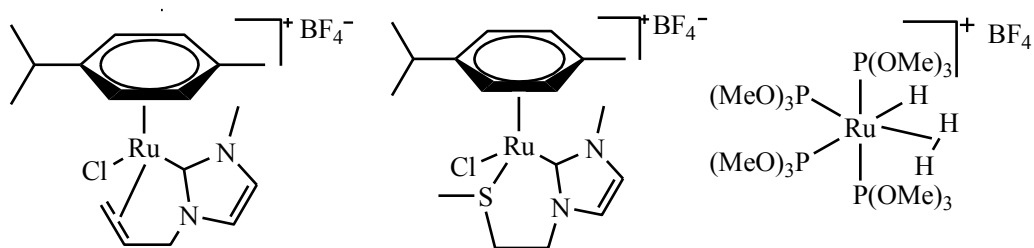


Figure 2.14: Cationic N-heterocyclic ruthenium(II) complexes for homogeneous hydrogenation<sup>154</sup>

#### 2.4 *Biphasic catalytic hydrogenation of unsaturated hydrocarbons*

Though catalytic hydrogenation reactions are commonly used in many industrial chemical processes, there is still a primary concern to improve catalysts selectivity and to address the environmental challenges resulting from catalyst use.<sup>4b</sup> While selectivity and the ability to operate under mild reaction conditions are some of the advantages of homogeneous catalysis, catalyst recovery, use of toxic organic solvents and contamination of the products are some of the challenges that needs to be addressed.<sup>156-158</sup> The inability to easily separate product from the catalyst-product mixtures in homogeneous catalysis greatly limits industrial applications.<sup>159</sup> These challenges can be effectively addressed by heterogenization of homogeneous catalytic systems.<sup>160,161</sup>

Significant progress has been made in developing heterogeneous systems, however, not without new challenges, the most pronounced being low selectivity.<sup>2</sup> To bridge between the advantages of homogenous and heterogeneous catalysis, various approaches of heterogenization of homogenous systems have emerged. They include, anchoring of single site catalysts on organic or inorganic supports and the use of multiphase operations (for example biphasic catalysis).<sup>162,163</sup>

Biphasic catalysis has attracted great attention since its successful industrial application in the Rhur Chemie-Rhone Poulenc hydroformylation reaction and is significantly gaining momentum for sustainability and environmental reasons.<sup>164- 167</sup> The other advantages of biphasic systems include recovery of catalysts and the possible use of 18-e complexes which are able to dissociate to give catalytically active ‘aqua’ species as intermediates.<sup>168</sup> To date, numerous water soluble transition meta- based catalysts have been applied in various biphasic hydrogenation reactions.<sup>169</sup> Examples of water soluble transition metal complexes include cationic 1’1-bisquinoline ruthenium complexes (Figure 2.15) and iridium, rhodium and ruthenium catalysts supported by water soluble ligands (Figure 2.16) among others.<sup>166a,169a</sup>

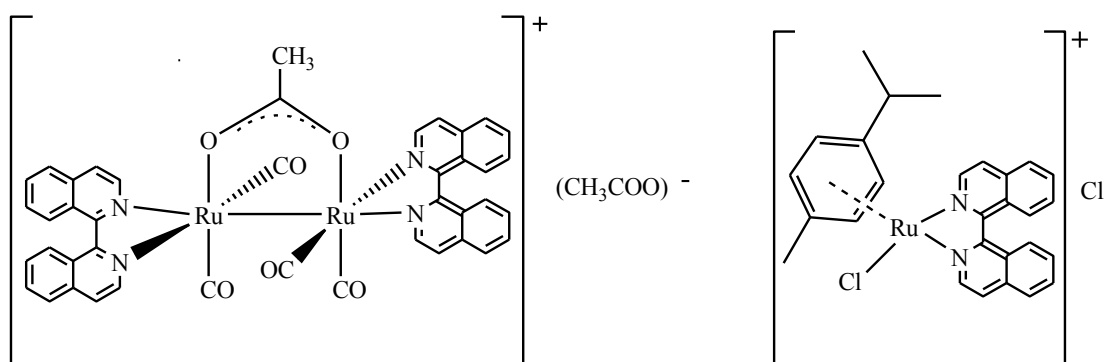


Figure 2.15: Cationic water-soluble transition metal complexes for hydrogenation reactions<sup>166a</sup>

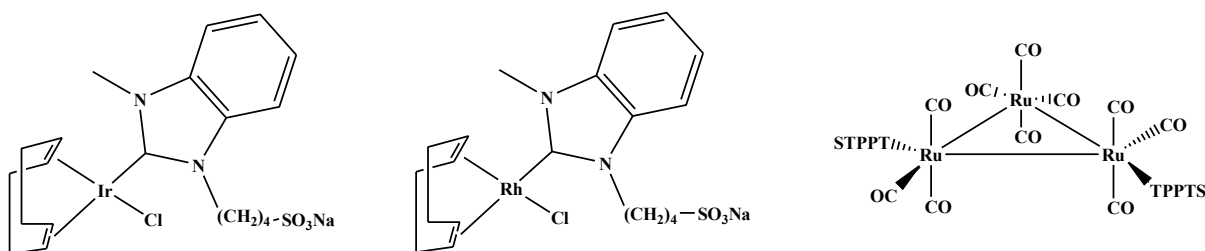


Figure 2.16: Water-soluble transition metal complexes for hydrogenation reactions<sup>169a</sup>

One great challenge facing biphasic catalysis is designing water soluble complexes and the decline in catalytic activity as a result of the partition coefficient when water is used as a solvent. To overcome the solubility challenges, the diffusion of the aqueous phase has been pursued by incorporating hydrophilic moieties in the ligand backbone (Figure 2.16).<sup>170</sup> On the other hand the catalytic activities of biphasic systems can be regulated by varying parameters such as pH and the ratio of solvents used to improve the interphase transfer during the reaction.<sup>171</sup>

## **2.5 Rationale of study**

Transition metal catalysed reactions have played significant roles in the petrochemical, fine chemical and pharmaceutical industries, as shown in Chapter 1. The search for highly active, selective and less expensive catalysts is a continuous process which has dominated the interest of many chemical scientists and engineers for decades. For example, one of the key areas of great interest is the use of inexpensive transition metal complexes to transform organic compounds to valuable starting materials or fine chemicals. Some of such transformations include hydrogenation of carbonyl compounds to alcohols, alkene and alkynes to saturated hydrocarbons.

Ruthenium and palladium complexes have dominated the field of catalytic hydrogenation reactions because of their favourable chemical properties. Their nitrogen-donor complexes are very reactive and easily prepared under mild reaction conditions.

The nitrogen-donor ligands also allow for the regulation of their steric and electronic properties thus improving their selectivity and solubility. Besides, phosphine-donor ligands stabilize these complexes in low oxidation states and can also be used to fine tune the steric properties of the complexes. However, some of the existing catalytic hydrogenation systems often suffer from lack of selectivity and instability due to isomerization in the case of hydrogenation of carbon-carbon multiple bonds. Thus, development of new systems to eliminate these challenges is a worthy endeavour. For these reasons, designing effective catalytic systems for the hydrogenation of unsaturated organic compounds presents a challenge for a good understanding of their operations at a molecular level and a study of their reaction mechanisms are of great importance. Thus, new, inexpensive and active catalytic systems for transfer and high pressure hydrogenation reactions are key to achieving effective beneficiation of a number of unsaturated compounds.

While homogeneous and heterogeneous catalytic methods are extensively used in industrial catalysis, they equally have various disadvantages that affect their active operations. Improving the selectivity, understanding the reaction mechanisms and striking a balance between the homogeneous and heterogeneous systems is therefore of interest to benefit from the advantages that come with developing new catalytic hydrogenation catalyst.

This project therefore aims to design active and stable catalysts of mixed nitrogen and phosphorous ruthenium and palladium complexes for effective hydrogenation of unsaturated compounds such as ketones, alkenes and alkynes. The bridge between homogeneous and heterogeneous catalysis has been attempted by designing single-site catalysts that are water soluble for biphasic catalysis.

## 2.6 Objectives

From the rationale above, the objectives of this study can be formulated as follows:

1. To synthesize and characterize new (pyridyl)benzoazoleruthenium(II) and ruthenium(III) complexes and to study them as catalysts for transfer hydrogenation (TH) of ketones. This was aimed at establishing the role of heteroatom and ancillary phosphine ligands in the reaction.
2. To synthesize and characterize neutral and cationic (pyridyl)benzoazole and pyrazolylpalladium(II) complexes, and to evaluate them as homogeneous catalysts for the high pressure hydrogenation of alkenes and alkynes.
3. To synthesize and characterize water soluble cationic (pyridyl)benzoazoleruthenium(II) complexes and to apply them in biphasic high pressure hydrogenation reaction of alkenes and alkynes.
4. To carry out kinetic and theoretical studies (DFT) in a bid to understand the mechanism and kinetics of these high pressure hydrogenation reactions using Pd(II) complexes.

The results of these studies are described in Chapters 3-5 and the key findings while the overall conclusions are summarized in Chapter 6.

## CHAPTER 3

### **(Pyridyl)benzoazoleruthenium(II) and ruthenium(III) complexes: Role of heteroatom and ancillary phosphine ligands in the transfer hydrogenation of ketones**

This chapter is adapted from the paper published in *Dalton Trans.* **43** (2014) 1228-1237 and is based on the experimental work of the first author, Aloice O. Ogwen. Copyright The Royal Society of Chemistry 2014. The contributions of the first author include: syntheses and characterization of the compounds, carrying out the catalytic reactions and drafting of the manuscript.

#### **3.1 Introduction**

There is rapid growth in transition metal chemistry especially in their synthesis and application as homogeneous catalysts in various organic transformation reactions.<sup>172</sup> Notably, nitrogen- and phosphine-donor complexes continue to receive significant attention due to their versatile coordination chemistry and propensity to form stable and active homogeneous catalysts.<sup>173-175</sup> Ruthenium complexes are classical examples of compounds that continue to attract a lot of attention due to their promising role in both catalytic and stoichiometric reactions.<sup>176-179</sup> One such reaction where ruthenium compounds have been widely applied is in the transfer hydrogenation of ketones. Transition metal-catalysed transfer hydrogenation of ketones is preferred to traditional high pressure hydrogenation reactions due to the mild conditions used.<sup>180</sup> Ruthenium complexes anchored on N- and P-donor ligands have been reported to form superior catalysts towards catalytic transfer hydrogenation of ketones.<sup>180</sup>

These mixed ligand complexes comprising of ‘hard’ N and ‘soft’ P ligands have the ability to stabilize the metal centre and fine-tune the electronic properties of the resultant catalysts.<sup>181</sup> So far, the most significant and active catalysts are ruthenium(II) complexes derived from monotosylated 1,2-diamine or amino-alcohols discovered by Noyori and co-workers.<sup>114</sup> These catalyst systems are highly active due to the presence of the N-H functionality. In this chapter, the synthesis and coordination chemistry of (pyridyl)benzoazoleruthenium(II) and ruthenium(III) complexes is reported. The role of the PPh<sub>3</sub> ancillary ligand in regulating the catalytic activities of these complexes in the transfer hydrogenation of ketones will also be discussed. The findings in this work demonstrate that the oxidation state of the metal centre, the nature of the ligand and the phosphine donor moiety control the activities of the complexes. We have also used density functional theory calculations to rationalize the catalytic trends obtained.

## 3.2 Experimental section

### 3.2.1 General methods and instrumentation

All manipulations were carried out under an inert atmosphere using standard Schlenk techniques unless stated otherwise. Starting materials, RuCl<sub>3</sub>·3H<sub>2</sub>O (99.98%), RuCl<sub>2</sub>(PPh<sub>3</sub>)<sub>3</sub> (97%), isopropanol (anhydrous, 99.5%), absolute ethanol and deuterated solvents were obtained from Sigma Aldrich and were used as received. 2-(2-pyridyl)benzimidazole (**L1**), 2-(2-pyridyl)bezothiazole (**L2**), 2-(2-pyridyl)bezoxazole (**L3**) were prepared following literature procedures.<sup>182</sup> Dichloromethane (ACS reagent, ≥99.8%) was dried over P<sub>2</sub>O<sub>5</sub> and distilled prior to use. NMR spectra were recorded on a Bruker 400 (<sup>1</sup>H, 400 MHz; <sup>13</sup>C, 100 MHz; <sup>31</sup>P, 162 MHz) Ultrashield instrument at room temperature in CDCl<sub>3</sub> and DMSO-d<sub>6</sub> solvents.

Chemical shifts are reported in  $\delta$  (ppm) and referenced to the residual proton in the solvents. All coupling constants are measured in hertz (Hz). Elemental analyses were performed on Thermal Scientific Flash 2000 instrument and mass spectra were recorded on an LC Premier micro-mass spectrometer.

### ***3.2.1.1 Synthesis of 1-propyl-2-(pyridin-2-yl)-1H-benzo[d]imidazole (L4)***

Dimethyl sulphoxide (15 mL) was added to ground KOH (1.14 g, 20.4 mmol). The mixture was stirred for 5 min and ligand **L1** (1 g, 5.10 mmol) was added. The mixture was further stirred for 1 h and 1-Bromopropane (1.26 g, 10.2 mmol) was then added and the resultant mixture stirred for 12 h. The solution was filtered and the solvent removed under vacuum to obtain ligand **L4** as orange oil. Yield = 0.65 g (53%).  $^1\text{H}$  NMR (400 MHz, DMSO- $d_6$ ):  $\delta$  0.96 (t, 3H, CH<sub>3</sub>,  $^3J_{\text{HH}}=8.0$  Hz); 1.93 (m, 2H, CH<sub>2</sub>-CH<sub>3</sub>); 4.81 (t, 2H, CH<sub>2</sub>-C<sub>2</sub>H<sub>5</sub>,  $^3J_{\text{HH}}=8.0$  Hz); 7.33 (m, 3H, bz<sub>im</sub>) 7.47 (d, 1H, py,  $^3J_{\text{HH}}=8.0$  Hz); 7.85 (d, 2H, bz<sub>im</sub>,  $^3J_{\text{HH}}=8.0$  Hz); 8.42 (t, 1H, py,  $^3J_{\text{HH}}=4.0$  Hz); 8.69 (d, 1H, py,  $^3J_{\text{HH}}=5.6$  Hz). Anal. Calcd For C<sub>15</sub>H<sub>15</sub>N<sub>3</sub>: C, 75.92; H, 6.37; N, 17.71%. Found: C, 75.81; H, 6.98; N, 17.37%.

### ***3.2.1.2 Synthesis of [2-(2-pyridyl)benzimidazole]RuCl<sub>3</sub> (1)***

A mixture of RuCl<sub>3</sub>·3H<sub>2</sub>O (0.10 g, 0.48 mmol) and ligand **L1** (0.09 g, 0.48 mmol) were refluxed in absolute EtOH (15 mL) for 4 h. A brown precipitate was collected by filtration, washed with excess EtOH and dried to afford analytically pure complex **1** as a brown solid. Single crystals suitable for X-ray analysis of complex **1** were grown by slow evaporation of acetonitrile-Et<sub>2</sub>O



solution. Yield = 0.06 g (40%). (ESI-MS)  $m/z$  (%) 402.89 ( $M^+$ ,100). Anal. Calcd. For  $C_{12}H_9Cl_3N_3Ru$ : C, 35.80; H, 2.25; N, 10.44%. Found: C, 35.98; H, 2.19; N, 10.66%.

### **3.2.1.3 Synthesis of $\{2-(2\text{-pyridyl})\text{benzothiazole}\}RuCl_3$ (2)**

The procedure used to prepare complex **1** was followed for the synthesis of complex **2**, using  $RuCl_3 \cdot 3H_2O$  (0.20 g, 0.98 mmol) and ligand **L2** (0.21 g, 0.98mmol) to afford complex **2** as a light brown solid. Single crystals suitable for X-ray analysis were grown by slow evaporation of an acetonitrile solution of complex **2**. Yield = 0.23 g (56%). (ESI-MS)  $m/z$  (%) 420.87 ( $M^+$ ,+H, 20). Anal. Calcd. For  $C_{12}H_8Cl_3N_2RuS$ : C, 34.44; H, 1.92; N, 6.67%. Found: C, 34.62; H, 2.08; N, 6.91%.

### **3.2.1.4 Synthesis of $\{2-(2\text{-pyridyl})\text{benzoxazole}\}RuCl_3$ (3)**

This complex was prepared following the procedure described for complex **1** using  $RuCl_3 \cdot 3H_2O$  (0.20 g, 0.98 mmol) and ligand **L3** (0.21 g, 0.98 mmol) to give complex **3** as a brown solid. Yield = 0.26 g (66%). (ESI-MS),  $m/z$  (%) 404.92 ( $M^+ + H$ , 20); 333.96 ( $M^+$ , -2Cl, 40). Anal. Calcd. For  $C_{12}H_8Cl_3N_2RuO$ : C, 35.71; H, 2.00; N, 6.94%. Found: C, 35.42; H, 1.83; N, 7.27%.

### **3.2.1.5 Synthesis of $\{2-(2\text{-pyridyl})\text{benzimidazole}\}RuCl_2(PPh_3)_2$ (4)**

*Method A:* To a solution of  $RuCl_2(PPh_3)_3$  (0.20 g, 0.21 mmol) in  $CH_2Cl_2$  (5 mL) was added ligand **L1** (0.04 g, 0.21 mmol) in  $CH_2Cl_2$  (5 mL). A light brown precipitate was formed immediately. The mixture was stirred at room temperature for 4 h and filtered to obtain a purple precipitate. The precipitate was washed with  $CH_2Cl_2$  (10 mL) to afford complex **4** as an analytically pure solid. Yield = 0.14 g (73%).

*Method B:* To a suspension of complex **1** (0.10 g, 0.25 mmol) in CH<sub>2</sub>Cl<sub>2</sub> (5 mL) was added PPh<sub>3</sub> (0.13 g, 0.50 mmol), and Et<sub>3</sub>N (1.00 mL, 7.16 mmol) and the mixture stirred at room temperature for 4 h. The solution was filtered and the filtrate concentrated to about 3 mL and hexane (5 mL) added to the concentrated solution. Slow evaporation of the mixture quantitatively afforded purple single crystals of complex **4** in quantitative amounts. Yield = 0.12 g (54%). <sup>1</sup>H NMR (400 MHz, DMSO-*d*<sub>6</sub>): δ 6.96 (t, 12H, PPh<sub>3</sub>, <sup>3</sup>*J*<sub>HH</sub> = 8.0 Hz); 7.08 (m, 2H, bz<sub>im</sub>); 7.23 (m, 6H, PPh<sub>3</sub>); 7.29 (t, 1H, py, <sup>3</sup>*J*<sub>HH</sub> = 6.4 Hz); 7.39 (m, 12H, PPh<sub>3</sub>); 7.77 (t, 1H, py, <sup>3</sup>*J*<sub>HH</sub> = 6.8 Hz); 7.99 (d, 2H, bz<sub>im</sub>, <sup>3</sup>*J*<sub>HH</sub> = 7.6 Hz); 8.52 (d, 1H, py, <sup>3</sup>*J*<sub>HH</sub> = 8.4 Hz); 8.91 (d, 1H, py, <sup>3</sup>*J*<sub>HH</sub> = 5.6 Hz). <sup>31</sup>P{H} NMR (DMSO-*d*<sub>6</sub>): δ 24.21 (s, PPh<sub>3</sub>). <sup>13</sup>C NMR (400 MHz, DMSO-*d*<sub>6</sub>): δ 137.15, 137.05, 133.80, 133.60, 129.46, 129.28, 129.21. <sup>31</sup>P{H} NMR (CDCl<sub>3</sub>): δ 28.18 (s, PPh<sub>3</sub>). (ESI-MS), *m/z* (%) 631.66 (M<sup>+</sup>, -PPh<sub>3</sub>, 20); 594.04 (M<sup>+</sup>, -ClPPh<sub>3</sub>, 20). Anal. Calcd. For C<sub>48</sub>H<sub>39</sub>Cl<sub>2</sub>N<sub>3</sub>P<sub>2</sub>Ru: C, 64.85; H, 4.41; N, 4.71%. Found: C, 65.19; H, 4.35; N, 4.35%.

The two synthetic procedures (methods A and B) described for complex **4** were employed in the synthesis of **5** and **6**.

### 3.2.1.6 Synthesis of [{2-(2-pyridyl)benzothiazole}RuCl<sub>2</sub>(PPh<sub>3</sub>)<sub>2</sub>] (**5**)

*Method A:* RuCl<sub>2</sub>(PPh<sub>3</sub>)<sub>3</sub> (0.10 g, 0.11 mmol) and ligand **L2** (0.02 g, 0.11 mmol) Yield = 0.06 g (58%). *Method B:* Complex **2** (0.10 g, 0.24 mmol), PPh<sub>3</sub> (0.13 g, 0.50 mmol) and Et<sub>3</sub>N (1.00 mL, 7.16 mmol). Recrystallization from CH<sub>2</sub>Cl<sub>2</sub>-hexane solution mixture afforded complex **5** as a purple solid. Yield = 0.08 g (53%). <sup>1</sup>H NMR (400 MHz, DMSO-*d*<sub>6</sub>): δ 7.00 (t, 3H, PPh<sub>3</sub>, <sup>3</sup>*J*<sub>HH</sub> = 7.6 Hz); 7.08 (t, 3H, PPh<sub>3</sub>, <sup>3</sup>*J*<sub>HH</sub> = 7.6 Hz); 7.24 (m, 12H, PPh<sub>3</sub>); 7.39 (m, 12H, PPh<sub>3</sub>); 7.46 (t, 1H, py, <sup>3</sup>*J*<sub>HH</sub> = 7.6 Hz); 7.64 (d, 2H, bz<sub>thio</sub>, <sup>3</sup>*J*<sub>HH</sub> = 11.6 Hz); 7.82 (t, 1H, py, <sup>3</sup>*J*<sub>HH</sub> = 7.2 Hz); 8.06 (d, 1H, py, <sup>3</sup>*J*<sub>HH</sub> = 7.2 Hz); 8.17 (d, 1H, bz<sub>thio</sub>, <sup>3</sup>*J*<sub>HH</sub> = 7.2 Hz); 9.17 (d, 1H, bz<sub>thio</sub>, <sup>3</sup>*J*<sub>HH</sub> = 5.6 Hz); 9.42

(d, 1H, py,  $^3J_{HH} = 8.4$  Hz).  $^{31}\text{P}\{\text{H}\}$  NMR (DMSO- $d_6$ ):  $\delta$  25.55 (s, PPh<sub>3</sub>).  $^{13}\text{C}$  NMR (400 MHz, DMSO- $d_6$ ):  $\delta$  137.16, 137.07, 133.78, 133.63, 129.45, 129.26, 129.21.  $^{31}\text{P}$  NMR (CDCl<sub>3</sub>):  $\delta$  26.16 (s, PPh<sub>3</sub>). Anal. Calcd. For C<sub>48</sub>H<sub>38</sub>Cl<sub>2</sub>N<sub>2</sub>P<sub>2</sub>RuS: C, 63.44; H, 4.21; N, 3.08%. Found: C, 63.14; H, 4.07; N, 3.12%.

### 3.2.1.7 Synthesis of $[\{2-(2\text{-pyridyl})\text{benzoxazoles}\}\text{RuCl}_2(\text{PPh}_3)_2]$ (6)

*Method A:* RuCl<sub>2</sub>(PPh<sub>3</sub>)<sub>3</sub> (0.10 g, 0.11 mmol) and ligand **L3** (0.02 g, 0.10 mmol). Yield = 0.08 g (86%). *Method B:* Complex **3** (0.10 g, 0.25 mmol), PPh<sub>3</sub> (0.13 g, 0.50 mmol) and Et<sub>3</sub>N (1.00 mL, 7.16 mmol). Purple solid. Yield = 0.12 g (77%).  $^1\text{H}$  NMR (400 MHz, DMSO- $d_6$ ):  $\delta$  7.03 (t, 2H, py,  $^3J_{HH} = 7.6$  Hz); 7.12 (t, 2H, bz<sub>ox</sub>,  $^3J_{HH} = 7.2$  Hz); 7.24 (m, 12H, PPh<sub>3</sub>); 7.39 (m, 12H, PPh<sub>3</sub>); 7.49 (t, 6H, PPh<sub>3</sub>,  $^3J_{HH} = 9.6$  Hz); 7.74 (d, 1H, py,  $^3J_{HH} = 8.4$  Hz); 7.89 (t, 1H, py,  $^3J_{HH} = 7.6$  Hz); 8.09 (d, 1H, bz<sub>ox</sub>,  $^3J_{HH} = 7.6$  Hz); 8.49 (d, 1H, bz<sub>ox</sub>,  $^3J_{HH} = 7.6$  Hz); 8.88 (d, 1H, py,  $^3J_{HH} = 5.6$  Hz).  $^{31}\text{P}\{\text{H}\}$  NMR (DMSO- $d_6$ ):  $\delta$  21.65 (s, PPh<sub>3</sub>).  $^{13}\text{C}$  NMR (400 MHz, DMSO- $d_6$ ):  $\delta$  137.14, 137.06, 133.77, 133.61, 129.44, 129.25, 129.20.  $^{31}\text{P}$  NMR (CDCl<sub>3</sub>):  $\delta$  29.93 (s, PPh<sub>3</sub>). (ESI-MS),  $m/z$  (%) 892.90 (M<sup>+</sup>, 42). Anal. Calcd. For C<sub>48</sub>H<sub>38</sub>Cl<sub>2</sub>N<sub>2</sub>OP<sub>2</sub>Ru: C, 64.58; H, 4.29; N, 3.14%. Found: C, 64.73; H, 4.31; N, 3.22%.

### 3.2.1.8 Synthesis of $[\{1\text{-propyl-2-(pyridin-2-yl)-1H-benzof[d]imidazole}\}\text{RuCl}_3]$ (7)

A mixture of RuCl<sub>3</sub>·3H<sub>2</sub>O (0.10 g, 0.48 mmol) and ligand **L4** (0.11 g, 0.48 mmol) were refluxed in absolute EtOH (20 mL) for 4 h. Yield = 0.12 g (56%). (ESI-MS)  $m/z$  (%) 408 (M<sup>+</sup>, -Cl 10). Anal. Calcd For C<sub>15</sub>H<sub>15</sub>Cl<sub>3</sub>N<sub>3</sub>Ru: C, 40.51; H, 3.40; N, 9.45%. Found: C, 40.42; H, 3.83; N, 9.27%.

### ***3.2.2 Transfer hydrogenation of ketones***

A typical procedure for the catalytic transfer hydrogenation of ketones was as follows: a mixture of acetophenone (0.23 mL, 2.0 mmol), KOH in isopropanol (100 mol%) and catalyst (0.02 mmol, 1 mol%) were introduced into a two-neck round-bottom flask fitted with a condenser under an inert atmosphere. The mixture was stirred at 82 °C and samples withdrawn at regular intervals. The percentage conversions were determined using <sup>1</sup>H NMR spectroscopy by comparing the intensities of the methyl signal of acetophenone (s, δ 2.59 ppm) and the methyl signal of 2-phenylethanol (d, δ 1.49 ppm) of the crude products. After the reaction period, the solvent was evaporated to dryness to afford a dark brown crude product which was isolated, recrystallized and characterized by <sup>1</sup>H NMR spectroscopy. The catalytic reactions were done in duplicate to ensure reproducibility of the results.

### ***3.2.3 Density functional theory (DFT) modelling***

DFT calculations were performed in the gas phase using a well-established approach for the third row transition metal complexes, to identify the energy-minimized structures based on B3LYP/LANL2DZ<sup>183,184</sup> (Los Alamos National Laboratory 2 double ζ) level theory, with inner core electrons of Ru atom replaced by a relativistic effective core potential (ECP). The singlet states were used due to the low electronic spin of Ru(II) complexes. The Gaussian09 suite of programs was used for all the computations.<sup>185</sup>

### ***3.2.4 X-ray crystallographic analyses***

X-ray data were recorded on a Bruker Apex Duo equipped with an Oxford Instruments Cryojet operating at 100(2) K and an Incoatec microsource operating at 30 W power. The data were collected with Mo Kα (λ = 0.71073 Å) radiation at a crystal-to-detector distance of 50 mm.

The following conditions were used for the data collection: omega and phi scans with exposures taken at 30 W X-ray power and 0.50° frame widths using APEX2.<sup>186</sup> The data were reduced with the programme SAINT<sup>187</sup> using outlier rejection, scan speed scaling, as well as standard Lorentz and polarisation correction factors. A SADABS semi-empirical multi-scan absorption correction was applied to the data. Direct methods, SHELXS-97 and WinGX<sup>188</sup> were used to solve all three structures. All non-hydrogen atoms were located in the difference density map and refined anisotropically with SHELXL-97. All hydrogen atoms were included as idealized contributors in the least squares process. Their positions were calculated using a standard riding model with C-H<sub>aromatic</sub> distances of 0.93 Å and  $U_{\text{iso}} = 1.2$  Ueq. The imidazole N-H were located in the difference density map, and refined isotropically.

### 3.3 Results and discussion

#### 3.3.1 Synthesis of 1-propyl-2-(pyridin-2-yl)-1H-benzo[d]imidazole (L4)

Alkylation of the (pyridyl)benzimidazole ligand **L1** with 1-bromopropane in the presence of KOH gave ligand **L4** as orange oil in moderate yield. Ligand **L4** was characterized by <sup>1</sup>H NMR spectroscopy (Figure 3.1) and elemental analyses.

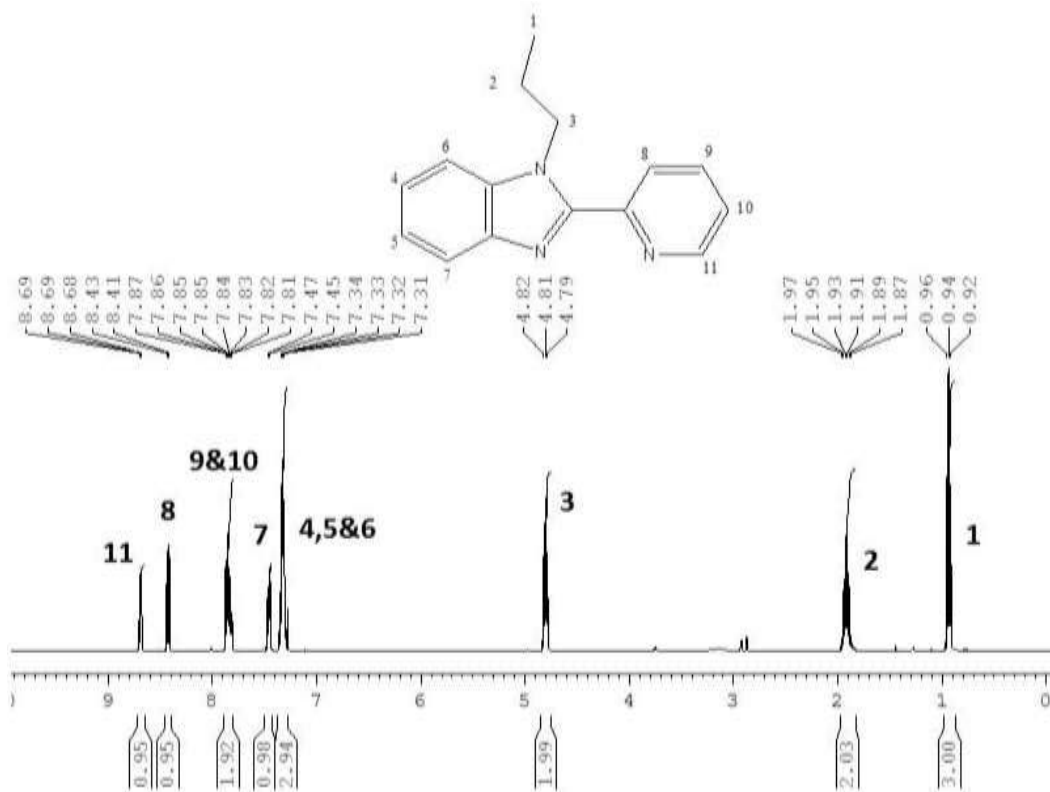
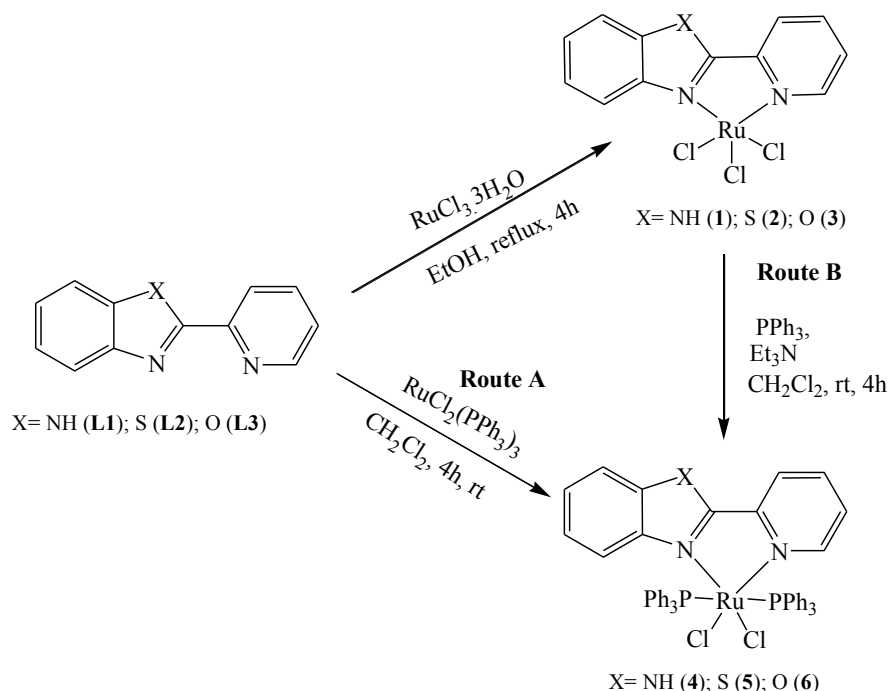


Figure 3.1: <sup>1</sup>H NMR spectrum of ligand 1-propyl-2-(pyridin-2-yl)-1H-benzo[*d*]imidazole (**L4**).

### 3.3.2 Synthesis of ruthenium complexes

Treatment of ligands **L1-L3** with RuCl<sub>3</sub>·3H<sub>2</sub>O produced the corresponding monometallic ruthenium complexes **1-3** in moderate yields (Scheme 3.1). On the other hand, reactions of ligands **L1-L3** with RuCl<sub>2</sub>(PPh<sub>3</sub>)<sub>3</sub> afforded the respective ruthenium(II) complexes **4-6** (Scheme 1, route A). In another synthetic protocol, reductions of ruthenium(III) complexes **1-3** with Et<sub>3</sub>N in the presence of two molar equivalents of PPh<sub>3</sub> also produced the corresponding ruthenium(II) complexes **4-6** (Scheme 3.2, route B). Route A gave complexes **4-6** in relatively higher yields (58% - 86%) compared to route B (53% -77%).



Scheme 3.1: Synthetic protocol for ruthenium(II) and ruthenium(III) compounds.

It is important to note that even the use of one equivalent of  $\text{PPh}_3$  in route B afforded the corresponding complexes **4-6**, though at reduced yields. The lower yields associated with route B could have emanated from partial reductions of complexes **1-3**. Complexes **1-3** were isolated as dark brown solids, while complexes **4-6** were obtained as purple solids.

Due to the paramagnetic nature of complexes **1-3**, NMR spectroscopy was not useful in their structural elucidation. Their identities were thus established by micro-analyses, mass spectrometry and single crystal X-ray analyses for complexes **1** and **2**. For example, the ESI-MS mass spectrum of complex **1** (Figure 3.2) showed  $m/z$  at 402.89 ( $\text{M}^+$ , +1) as the base peak corresponding to its molecular ion of 401.89.

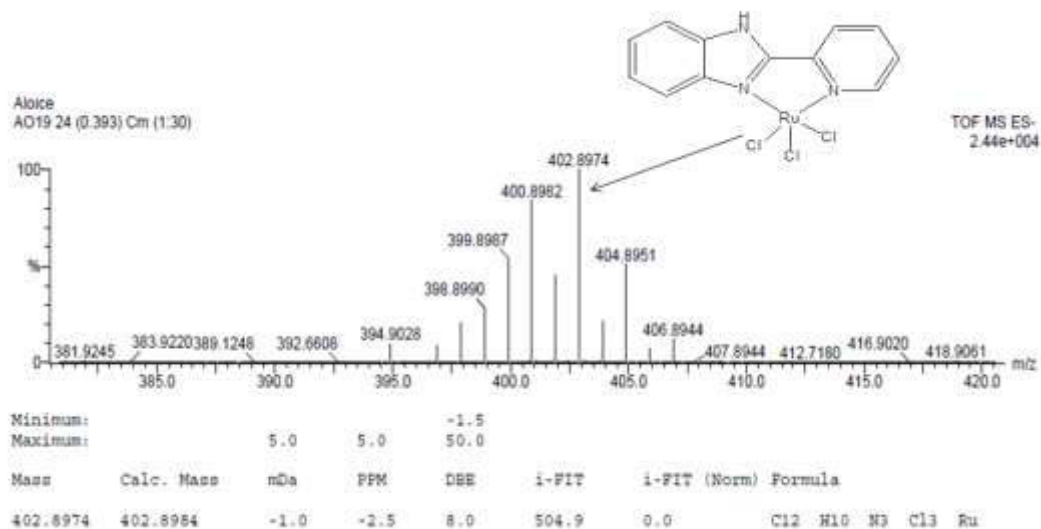


Figure 3.2: HR-MS spectrum of complex **1**.

Elemental analyses data of complexes **1-3** were consistent with the molecular formulae proposed structures in Scheme 3.1 and demonstrated their purity. Solid state structures of complexes **1** and **2** confirmed the bidentate coordination modes of ligands **L1** and **L2** to the ruthenium atom.

$^1\text{H}$ ,  $^{13}\text{C}$  NMR and  $^{31}\text{P}\{^1\text{H}\}$  NMR spectroscopy were also used in the structural elucidation of ruthenium(II) complexes **4-6**. For example, a broad signal at 13.07 ppm assigned to the N-H proton in ligand **L1** was recorded at 13.90 ppm in complex **4**. Similarly, the 6H-pyridyl protons recorded at 8.73 ppm in ligands **L1** and **L2** were observed downfield at 8.91 ppm and 9.42 ppm in complexes **4** and **5** respectively.



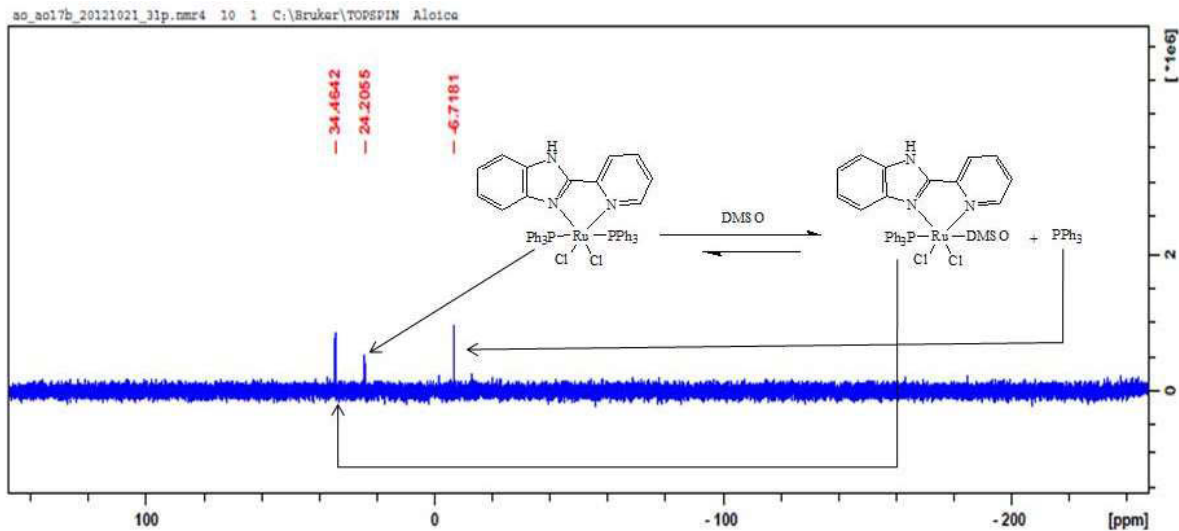
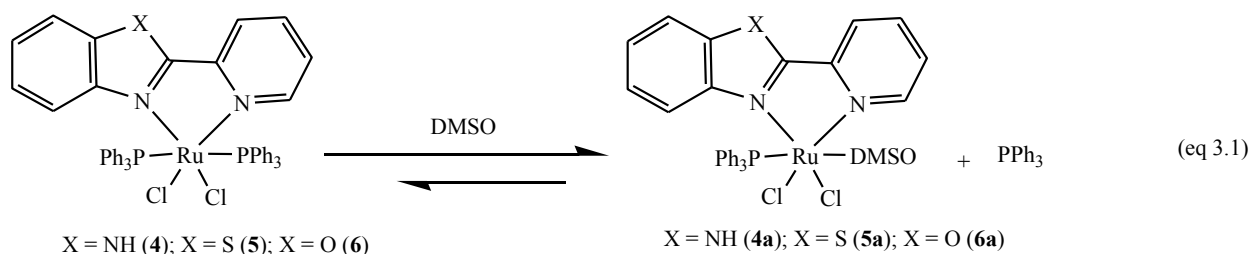


Figure 3.3:  $^{31}\text{P}\{^1\text{H}\}$  NMR spectra of complex  $[\text{Ru}(\text{L1})\text{PPh}_3)_2\text{Cl}_2](\mathbf{4})$  in DMSO. The signal at -6.72 ppm is assigned to free  $\text{PPh}_3$  and points to the dissociation of coordinated  $\text{PPh}_3$ .

$^{31}\text{P}\{^1\text{H}\}$  NMR spectroscopy was particularly useful in the characterization of complexes **4-6** in establishing the nature of coordination of the  $\text{PPh}_3$  ligand. Typical  $^{31}\text{P}\{^1\text{H}\}$  NMR spectra recorded in  $\text{DMSO-}d_6$  showed three signals (Figure 3.3a); one major peak at 34.46 ppm (**4**), 32.13 ppm (**5**); 32.48 ppm (**6**), a second minor signal between 25.55-21.64 ppm and a third peak at  $\approx -6.72$  ppm typical of free  $\text{PPh}_3$ . Our initial interpretation of the  $^{31}\text{P}$  NMR spectra pointed to the presence of free  $\text{PPh}_3$  and formation of other side products or existence of two different geometric isomers of complexes **4-6** (*trans*- and *cis*-dispositions of the two  $\text{PPh}_3$  ligands).<sup>101</sup> However, from the high purities of complexes **4-6** obtained from microanalyses data, the presence of impurities was ruled out. A closer inspection of the spectra and literature reports pointed to the displacement of one coordinated  $\text{PPh}_3$  by  $\text{DMSO-}d_6$  (eq.3.1) used to acquire the NMR spectra.<sup>189</sup>



The DMSO- $d_6$  coordinated ruthenium complexes (**4a-6a**) could thus be responsible for the peaks observed between 32.13-34.43 ppm. These values fall within the observed range of 31.4-33.8 ppm reported in mono-coordinated  $\text{PPh}_3$  compounds.<sup>189-192</sup> The signals at 24.20 ppm (**4**), 25.55 ppm (**5**) and, 21.64 ppm (**6**) were assigned to the *trans*- $\text{PPh}_3$  ligands.  $^{31}\text{P}\{\text{H}\}$  NMR signals for similar phosphine ruthenium compounds have been reported between 24.36-21.87 ppm.<sup>191,193</sup> This data therefore reveals the partial substitution of one coordinated  $\text{PPh}_3$  to establish an equilibrium mixture between complexes **4-6** and the corresponding DMSO- $d_6$  adducts **4a-6a**.

In order to confirm the displacement of one  $\text{PPh}_3$  by the DMSO- $d_6$  solvent, the  $^{31}\text{P}\{\text{H}\}$  NMR spectrum of **6** was acquired in non-coordinating  $\text{CDCl}_3$  NMR solvent (Figure 3.4). Indeed only one signal at *ca.* 29.9 ppm (Figure 3.4b) was observed. This is consistent with the *trans*-arrangement of the two  $\text{PPh}_3$  ligands and existence of one isomer in complexes **4-6**. Complexes **4** and **5** also showed similar spectra in DMSO- $d_6$  and  $\text{CDCl}_3$ .

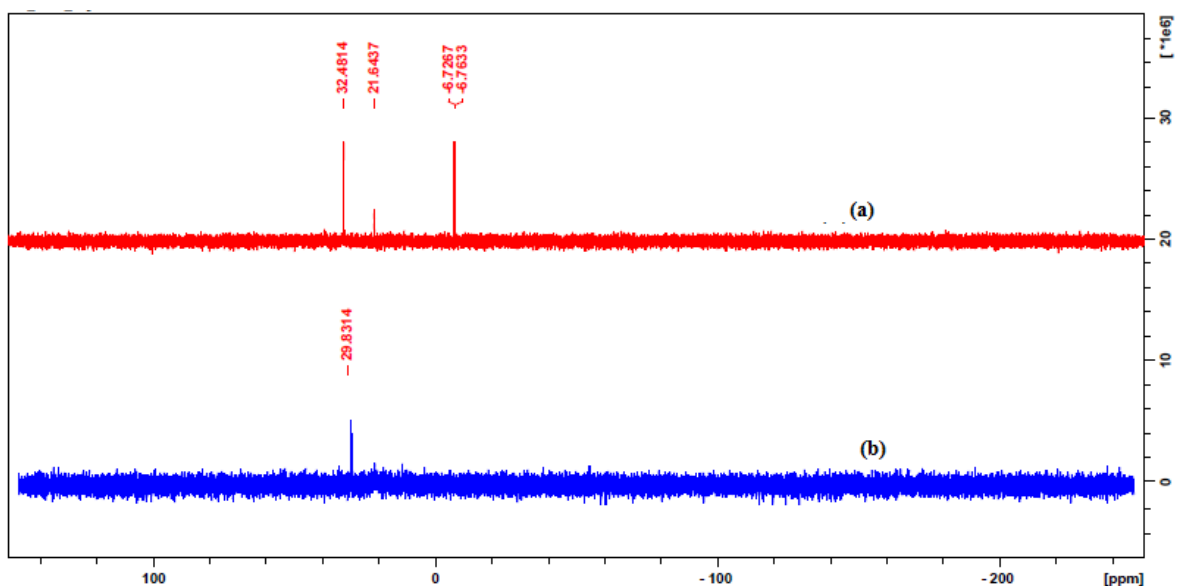


Figure 3.4:  $^{31}\text{P}\{^1\text{H}\}$  NMR spectra for complex **6** (a)  $\text{DMSO-}d_6$ , signal at 6.56 ppm reveals the generation of free  $\text{PPh}_3$  (b) in  $\text{CDCl}_3$ , one signal at 29.93 ppm indicates that the two *trans*- $\text{PPh}_3$  ligands are chemically equivalent.

### 3.3.3 Molecular structures of complexes **1** and **2**

Single crystals suitable for X-ray analyses of complexes **1** and **2** were grown by slow evaporation of their  $\text{MeCN-Et}_2\text{O}$  solutions at room temperature. Figures 3.5 and 3.6 show the molecular structures of complexes **1** and **2** respectively. Table 3.1 contains data collection and structural refinement parameters while selected bond lengths and angles of complexes **1** and **2** are given in Table 3.2. Complexes **1** and **2** both co-crystallized with one acetonitrile solvent. Both ligands **L1** and **L2** adopt bidentate coordination modes to ruthenium in complexes **1** and **2**.

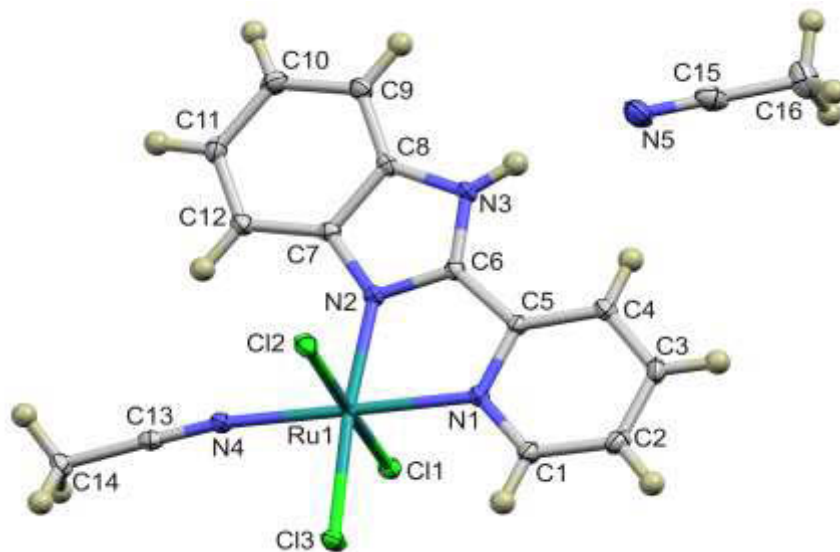


Figure 3.5: Molecular structure of complex **1** containing coordinated acetonitrile solvent drawn with 50% probability ellipsoids.

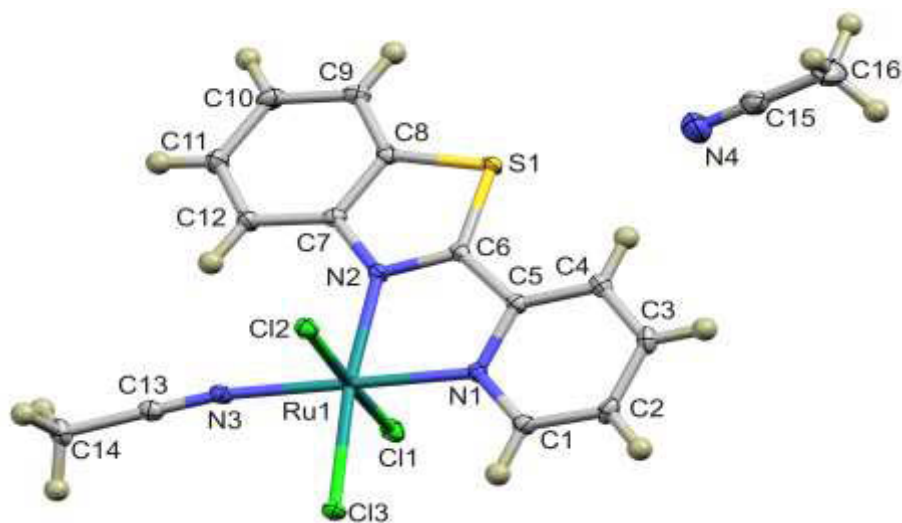


Figure 3.6: Molecular structure of complex **2** containing coordinated acetonitrile solvent drawn with 50% probability ellipsoids.

Table 3.1: Crystal data collection and structural refinement parameters for complexes **1** and **2**

Parameter	<b>1</b>	<b>2</b>
Empirical formula	C <sub>16</sub> H <sub>15</sub> Cl <sub>3</sub> N <sub>5</sub> Ru	C <sub>16</sub> H <sub>14</sub> Cl <sub>3</sub> N <sub>4</sub> RuS
Formula weight	484.75	501.79
Temperature(K)	100(2)	100(2)
Wavelength (Å)	0.71073	0.71073
Crystal system	Triclinic	Triclinic
Space group	P-1	P-1
<i>a</i> (Å)	8.6945(4)	8.5108(4)
<i>b</i> (Å)	9.5982(4)	9.7943(4)
<i>c</i> (Å)	11.3983(5)	11.4935(5)
$\alpha$ (°)	102.453 (2)	100.446 (2)
$\beta$ (°)	90.168 (2)	90.126(2)
$\gamma$ (°)	99.820 (2)	100.326(2)
Volume(Å <sup>3</sup> )	914.44 (7)	926.33(7)
Z	2	2
D <sub>calcd</sub> (mg/m <sup>3</sup> )	1.761	1.799
Absorption coefficient (mm <sup>-1</sup> )	1.310	1.398
F(000)	482	498
Theta range for data collection (°)	1.83 -26.56	1.80 -26.83
Reflections collected / unique	13981	13956
Completeness to theta (%)	97.3	96.5
Goodness-of-fit on F <sup>2</sup>	0.838	1.129
R indices (all data)	R <sub>1</sub> = 0.0208 wR <sub>2</sub> = 0.0929	R <sub>1</sub> = 0.0165 wR <sub>2</sub> = 0.0404
Largest diff. peak and hole (e Å <sup>-3</sup> )	0.673 and -0.367	0.417 and -0.349

Table 3.2: Selected bond lengths [ $\text{\AA}$ ] and bond angles [ $^\circ$ ] for complexes **1** and **2**

<b>Bond lengths [<math>\text{\AA}</math>]</b>		
	<b>1</b>	<b>2</b>
Ru(1)-N(1)	2.0630(16)	2.0536(12)
Ru(1)-N(2)	2.0471(15)	2.0769(12)
Ru(1)-N(4)/(N3)	2.0406(17)	2.0494(13)
Ru(1)-Cl(2)	2.3583(4)	2.3273(4)
Ru(1)-Cl(3)	2.3675(5)	2.3554(4)
<b>Bond Angles [<math>^\circ</math>]</b>		
N(1)-Ru(1)-N(2)	78.70(6)	79.15(5)
N(1)-Ru(1)-Cl(2)	91.34(4)	91.01(3)
N(1)-Ru(1)-N(4)	177.58(5)	179.32(5)
N(2)-Ru(1)-Cl(3)	173.80(5)	173.54(4)

The coordination environment around the ruthenium atom in complexes **1** and **2** consists of one ligand unit, three Cl ligands and one NCMe molecule in the sixth position to give a nominally octahedral coordination geometry. The bond angles for Cl(2)-Ru(1)-Cl(3) of  $92.47^\circ$  (**1**) and Cl(1)-Ru(1)-Cl(3) of  $91.43^\circ$  (**2**) deviate from  $90^\circ$ , typical of octahedral complexes. Thus the geometry around the ruthenium atoms in complexes **1** and **2** could be best described as a distorted octahedral. The Ru-N<sub>py</sub> bond lengths of 2.0630(16)  $\text{\AA}$  and 2.0536(12)  $\text{\AA}$  in complexes **1** and **2**, respectively, are statistically similar. However, the Ru-N<sub>bz</sub> bond distance of 2.0471(15)  $\text{\AA}$  in **1** is significantly shorter than the Ru-N<sub>bz</sub> bond distance of 2.0769(12)  $\text{\AA}$  in **2**, suggesting that ligand **L1** has less *trans*-effect than ligand **L2**.

In the structure of complex **1**, the Ru-Cl(1) and Ru-Cl(2) (*trans* to each other) bond distances of 2.3583(4) Å and 2.3305(4) Å, respectively, are shorter than the Ru-Cl(3) (Cl *trans* to N<sub>bz</sub>) bond length of 2.3675(5) Å. The elongation of the Ru-Cl(3) bond could be attributed to a stronger *trans* effect of the beizimidazole ring compared to the Cl ligand. A similar trend is observed in the Ru-Cl bond distances in complex **2**. The average Ru-Cl bond lengths of 2.3480(5) Å in complexes **1** and **2** are shorter than the average Ru-Cl bond distances of 2.430(4) Å reported for similar ruthenium complexes.<sup>176,194-196</sup>

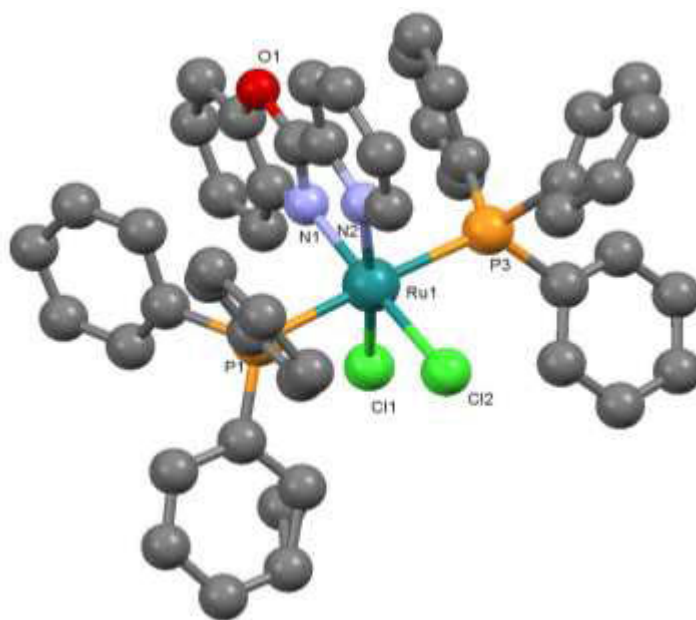
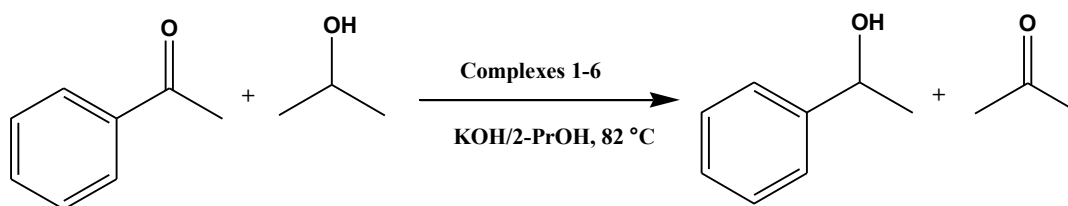


Figure 3.7: ORTEP view of complex **6** showing the atom labelling drawn at 50% probability ellipsoids (the structure could not be satisfactorily refined due to desolvation and the data obtained are not suitable for publication and discussion of bond parameters). Hydrogen atoms are omitted for clarity.

An interesting aspect in the solid state structures of complexes **1** and **2** is the coordination of one NCMe molecule to give an 18-electron metal centre. Thus, the expected 16-electron trichloride species are coordinatively unsaturated; a feature we have exploited in the use of complexes **1-3** as catalysts in the transfer hydrogenation of ketones. Solid state structure of complex **6** (Figure 3.7) confirmed the *trans*-disposition of the two PPh<sub>3</sub> ligands and the bidentate coordination mode of ligand **L3** to give a six-coordinate ruthenium centre. The structure could not be satisfactorily refined due to desolvation of the crystal; hence, the data obtained are not suitable for publication and discussion of bond parameters. However, the coordination chemistry and atom connectivity is not in doubt.

### 3.3.4 *Transfer hydrogenation of ketones catalysed by complexes 1-6*

Preliminary investigations of complexes **1-6** in the catalytic transfer hydrogenation of acetophenone as a model substrate were carried out using isopropanol and KOH at 82 °C (Scheme 2).



Scheme 3.2: Catalytic transfer hydrogenation of acetophenone by complexes **1-6**.



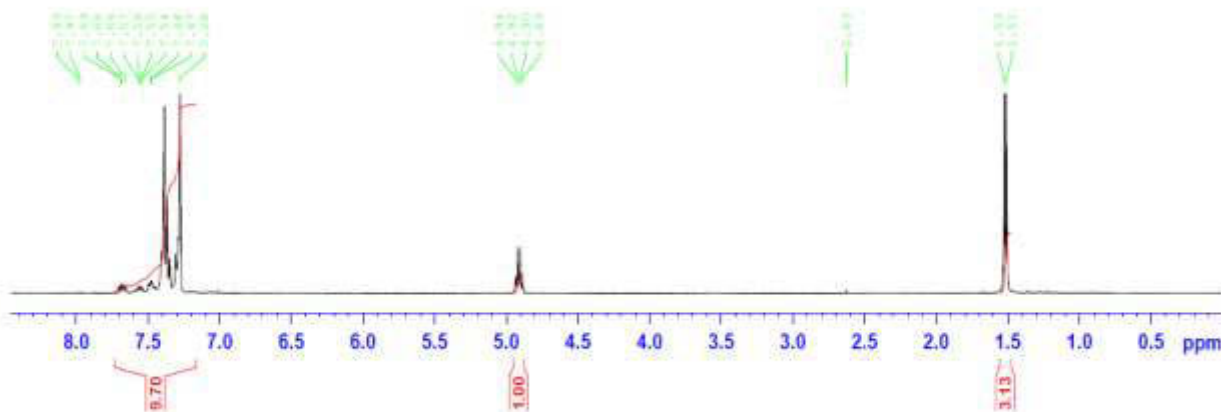


Figure 3.8: Typical  $^1\text{H}$  NMR spectrum of the 2-phenylethanol product obtained from the transfer hydrogenation reactions confirming the identity and purity of the product.

The catalytic reactions were performed using 2.0 mmol of acetophenone, 0.02 mmol of complexes **1-6** (1.0 mol%), KOH in isopropanol (100 mol%). The percentage conversions were determined by  $^1\text{H}$  NMR spectroscopy by comparing the intensity of the methyl signal of acetophenone (s,  $\delta$  2.59 ppm) and the methyl signal of 1-phenylethanol (d,  $\delta$  1.49 ppm) of the crude products (Figure 3.8).

All the complexes were found to form active catalysts affording conversions between 77% - 95% within 4 h at 82 °C (Table 3.3). A blank experiment without any ruthenium complex afforded only 17% conversion within 4 h under similar conditions. From Table 3.3, it is evident that both the identity of the ligand and the oxidation state of ruthenium metal determined the activities of the resultant catalysts. Catalysts derived from ruthenium(II) complexes (**4-6**) bearing  $\text{PPh}_3$  ligands were more active and exhibited shorter induction periods than the corresponding trichloride ruthenium(III) complexes **1-3** (Figure 3.9).

Table 3.3: Summary of transfer hydrogenation of acetophenone of complexes **1-6**<sup>a</sup>

Entry	Catalyst	Conversion [%] <sup>b</sup>	TOF <sup>c</sup>
1	<b>1</b>	91	23
2	<b>2</b>	77	19
3	<b>3</b>	88	22
4	<b>4</b>	95	24
5	<b>5</b>	92	23
6	<b>6</b>	93	23
7	<b>4</b>	59 <sup>d</sup>	30
8	<b>5</b>	79 <sup>d</sup>	40
9	<b>4</b>	59 <sup>e</sup>	59
10 <sup>f</sup>	<b>1</b>	92	23

<sup>a</sup>Conditions: acetophenone, 2.0 mmol; catalyst; 0.02 mmol (1.0 mol%); base, KOH in isopropanol (100 mol%); time, 4 h, temperature, 82 °C. <sup>b</sup>Determined by <sup>1</sup>H NMR spectroscopy; <sup>c</sup>TOF in mol substrate. mol<sup>-1</sup> catalyst.h<sup>-1</sup>; <sup>d</sup>0.01 mmol catalyst (0.5 mol%); <sup>e</sup>time, 1 h. <sup>f</sup>KOH, 25 mol%.

The active species in the transfer hydrogenation of ketones is known to contain low oxidation state ruthenium metal.<sup>174</sup> It is therefore conceivable that longer induction periods displayed by complexes **1-3** may be associated with reduction of ruthenium(III) to ruthenium(II)/ruthenium (I) species. Since complexes **4-6** already contain a ruthenium(II) metal centre, they are easily activated, consistent with the relatively shorter induction periods observed. In addition, the  $\pi$ -acceptor ability of the PPh<sub>3</sub> ligand in complexes **4-6** as opposed to the  $\sigma$ -donor Cl ligand in complexes **1-3** might play a crucial role in stabilization of low oxidation state ruthenium(II)/(I) species resulting in higher catalytic activities.<sup>198a</sup>

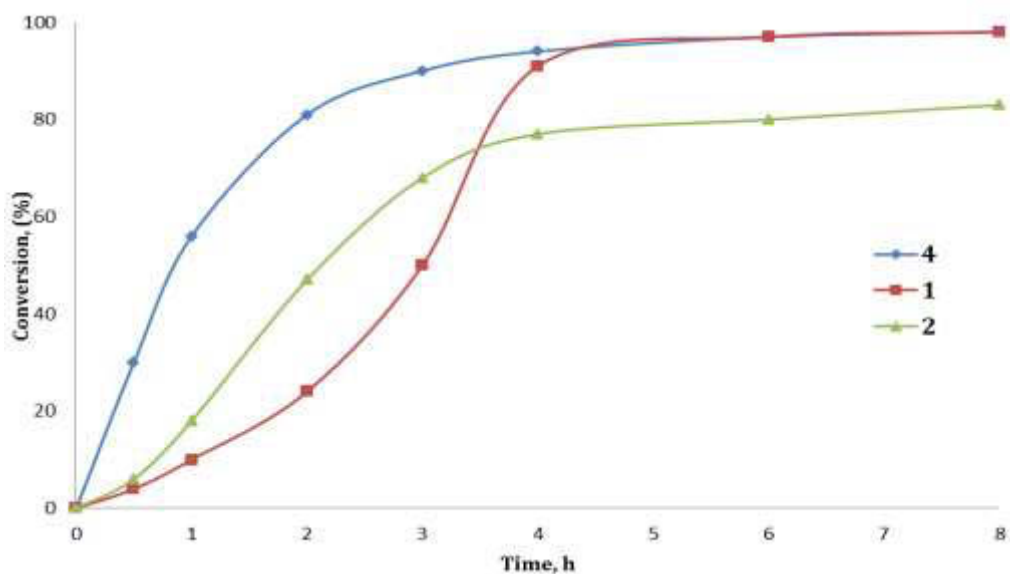


Figure 3.9: Time-dependence of transfer hydrogenation of acetophenone by complexes **1**, **2** and **4** showing a shorter induction period for **4**.

In fact, it is expected that reduction of ruthenium(III) complexes **1-3** to ruthenium(I) species would be energetically unfavourable. This is why the modest catalytic activities displayed by complexes **1-3** in this work are quite intriguing. An inspection of literature reveals no examples (to the best of our knowledge) where similar ruthenium(III) complexes have been used as catalysts in the transfer hydrogenation of ketones. We largely assign this behaviour to the coordinative unsaturated 16-electron ruthenium centres in complexes **1-3** which allows for ketone substrate coordination. The coordination of one NCMe solvent in the solid state structures of complexes **1** and **2** (Figures 3.6 and 3.7) further augments this hypothesis.

The catalyst concentration also influenced the catalytic transfer hydrogenation reactions (Table 3.3, entries 4 vs 7 and 5 vs 8). For example, reducing the catalyst loading of complex **4** from 1 mol% to 0.05 mol% was followed by a significant drop in activity from 95% to 59% (Table 3.3,

entries 4 and 7). The TOFs of complexes **1-6** of 22-60 h<sup>-1</sup> were lower compared to the pre-activated cationic bis-(pyrazolyl)pyridine and bis-(imidazolyl)pyridine ruthenium(II) complexes reported by Zeng *et al.*<sup>189</sup> which gave TOFs as high as 705 600 h<sup>-1</sup>. This difference could be largely attributed to the highly electrophilic metal centres in the Zheng catalysts compared to our catalysts **1-6**. However, complexes **1-6** gave relatively higher catalytic activities than the dinuclear phosphite ruthenium(II) complexes reported by Aydemir *et. al.* that gave TOF of 10-16 h<sup>-1</sup>.<sup>194</sup>

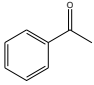
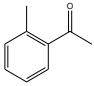
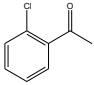
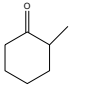
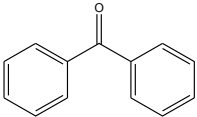
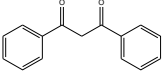
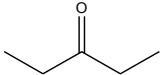
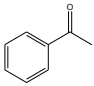
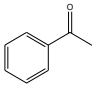
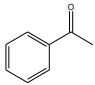
The identity of the heteroatom in the ligand architecture also affected the catalytic activities of complexes **1-6**. In general, complexes **1** and **4** bearing the (pyridyl)benzimidazole ligand **L1** were the most active, followed by the (pyridyl)benzoxazole complexes **3** and **6**. The (pyridyl)benzothiazole complexes **2** and **5** showed the lowest activities. From the basicity of ligands **L1-L3**, one would expect **3** and **6**, which contain the (pyridyl)benzoxazole ligand, to be the most active. Oxygen is more electronegative than N or S; hence, it would be expected to give a more electrophilic ruthenium centre.<sup>197</sup> Higher catalytic activities of complexes **3** and **6** (O-atom) in comparison to complexes **2** and **5** containing **L2** (S-atom) agrees with this argument. However, the greater activities observed for the (pyridyl)benzimidazole complexes **1** and **4** contradict this hypothesis. This may be attributed to the presence of the acidic amine proton which facilitates the “outer sphere” mechanism by enhancing deprotonation of the isopropanol as widely proposed in the literature.<sup>198-201</sup>

In order to establish the role of the N-H moiety, we synthesized the N-propyl protected ligand **L4** and the corresponding ruthenium trichloride complex **7**.

The percentage conversion of complex **7** of 57% was significantly lower compared to the 91% observed for the N-H complex **1** in the transfer hydrogen of acetophenone under similar conditions (Table 3.3, entries 1 and 7). This confirms the role of the N-H functional group in enhancing the activities of the resulting catalysts. Indeed, complex **7** displayed lower activity even in comparison to the S complex **2** (77%) and O complex **3** (88%).

Impressed by the catalytic activities of complexes **1-6** in the transfer hydrogenation of acetophenone, we explored the transfer hydrogenation of various ketones using catalyst **4** (Table 3.4, entries 1-4). Under similar conditions, complex **4** exhibited comparable catalytic activity with other ketones, achieving maximum conversions of 97% for cyclohexanone (Table 3.4, entry 4). It is important to note that even the presence of substituents in the *ortho* position in the phenyl ring as in 2-methylacetophenone did not significantly affect the reactions (Table 3.3, entry 1-4). Comparable conversions observed for acetophenone (95%), 2-methylacetophenone (91%) and 2-chloroacetophenone (95%), thus indicate less steric and electronic contributions in regulating the reactivities of ketone substrates.<sup>202</sup> High catalytic activity (98%) was also reported for the strained benzophenone. However, we observed a drastic drop in activities (50%) for 3-methylpentanone and 1, 3-dibenzolylmethane (64%), presumably due to the electronic rich alkyl groups and absence of  $\pi$ -delocalization in the substrate.

Table 3.4: Transfer hydrogenation of different ketones and bases using complex 4<sup>a</sup>

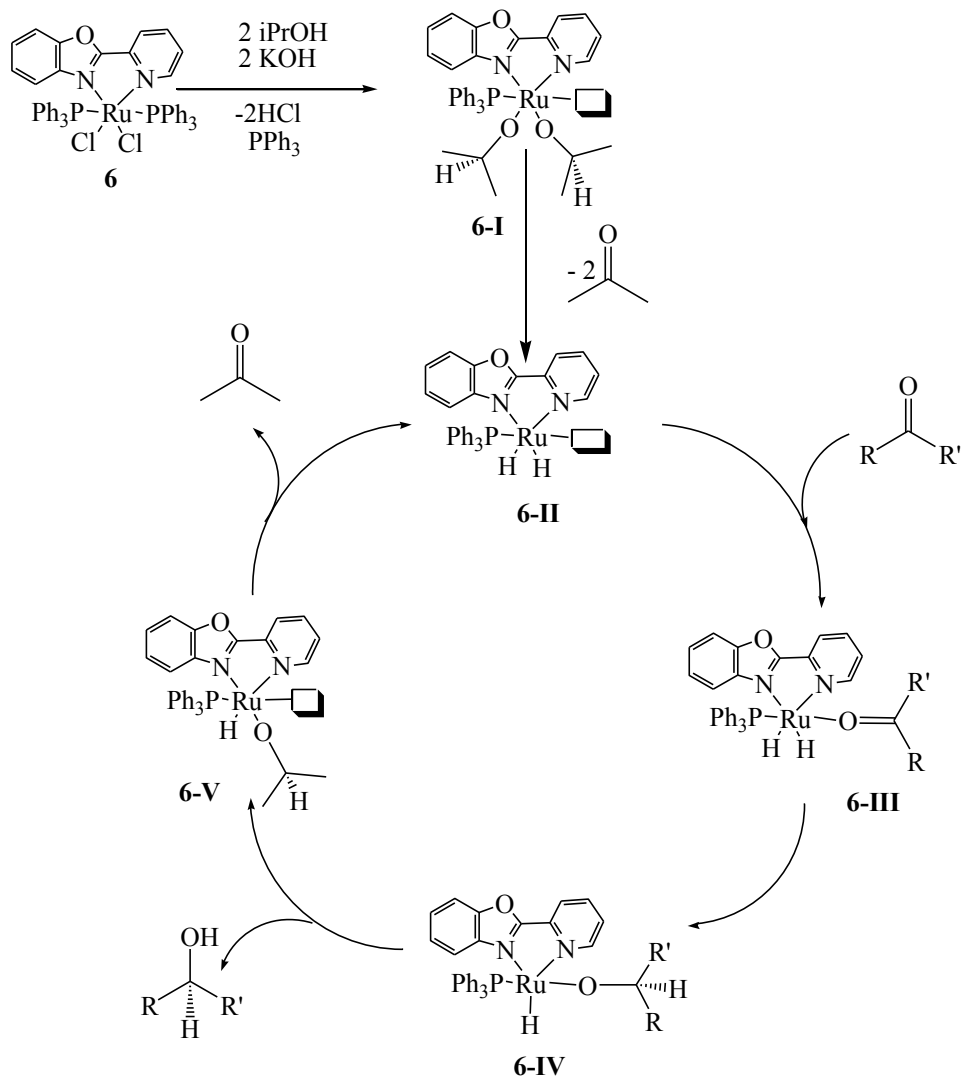
Entry	Substrate	Base	Conv [%] <sup>b</sup>	TOF (h <sup>-1</sup> )
1		KOH	95	24
2		KOH	91	23
3		KOH	95	24
4		KOH	97	24
5		KOH	98	25
6		KOH	64	16
7		KOH	78	20
8		NaOH	98	25
9		Na <sub>2</sub> CO <sub>3</sub>	73	18
10		<sup>t</sup> BuOK	97	24

<sup>a</sup>Conditions: ketone, 2 mmol; catalyst, 0.02 mmol (1 mol%); 0.4 M of base in isopropanol (5 mL), temperature 82 °C. <sup>b</sup>Determined by <sup>1</sup>H NMR spectroscopy after 4 h. <sup>c</sup>Conditions: ketone, 2 mmol; catalyst, 0.05 mol%; base, 0.4M in isopropanol (5 mL), temperature 82 °C (1 and 4)

The effect of the base used was also investigated using KOH, NaOH, Na<sub>2</sub>CO<sub>3</sub> and <sup>t</sup>BuOK (Table 3.4, entries 8-10). The activity trend was found to be in the order NaOH > <sup>t</sup>BuOK > KOH > Na<sub>2</sub>CO<sub>3</sub>, consistent with the relative strength of the bases (Table 3.4, entries 8-10).<sup>203</sup> Strong bases i.e. NaOH, <sup>t</sup>BuOK and KOH gave higher conversion compared to Na<sub>2</sub>CO<sub>3</sub> which is relatively weak. The slight differences in the activities of NaOH, <sup>t</sup>BuOK and KOH highlight their similar strengths in deprotonating isopropanol as previously observed by Aydemir *et. al.*<sup>194</sup>

### 3.3.5 Proposed transfer hydrogenation reaction mechanism

The Mechanism of transition metal catalysed transfer hydrogenation of a ketone has been proposed to involve formation of Ru(II) hydride species from a catalyst precursor followed by addition of a ketone to the coordinatively unsaturated Ru(II) hydride species.<sup>3,4</sup> Considering the lability of the PPh<sub>3</sub> ligand in complexes **4-6**, we propose dissociation of one PPh<sub>3</sub> group prior to the coordination of the ketone through an inner-sphere mechanism (Scheme 3.3). Using complex **6** as an illustration, the catalytic pathway would start by dissociation of one PPh<sub>3</sub> leading to formation of a metal alkoxide intermediate (**6-I**). Generation of a Ru-H intermediate **6-II** is followed by coordination of acetophenone substrate to produce the intermediate **6-III**. Subsequent insertion of the coordinated acetophenone into the Ru-H bond forms the Ru(II)-alkoxide **6-IV**. Protonation of the coordinated substrate by isopropanol affords 2-phenylethanol product and the alkoxide **6-V**. β-hydride elimination of the coordinated 2-propanal in **6-V** results in regeneration of the active catalyst **6-I**. Experimental evidence for the lability of PPh<sub>3</sub> is derived from the displacement of PPh<sub>3</sub> by DMSO-d<sub>6</sub> NMR solvent. To further support this assumption, we monitored the formation **6-I** from complex **6** in a iPrOH/KOH solution using <sup>31</sup>P NMR spectroscopy (Figure 3.10).



Scheme 3.3: Proposed catalytic cycle for the transfer hydrogenation of ketone by complex **6** in the presence of isopropanol and KOH.

Indeed, generation of a free PPh<sub>3</sub> was evident from the signal at -5.29 ppm. In addition, two signals for coordinated PPh<sub>3</sub> were recorded at 21.44 ppm and 29.38 ppm as opposed to one signal at 29.83 ppm in complex **6**. Similar displacement reactions of labile ligands to form coordinatively unsaturated intermediates in the transfer hydrogenation reactions have been reported in the literature.<sup>204, 205</sup>



Furthermore, dissociation of one PPh<sub>3</sub> is sterically acceptable since a six-coordinate species would be too saturated and sterically demanding to allow substrate coordination. Attempts to establish the formation of the Ru-H by <sup>1</sup>H NMR spectroscopy or stoichiometric reactions did not materialise as no signal was recorded near -10 ppm.<sup>206</sup> This is attributed to the likely instability of the intermediate Ru-hydride species formed.

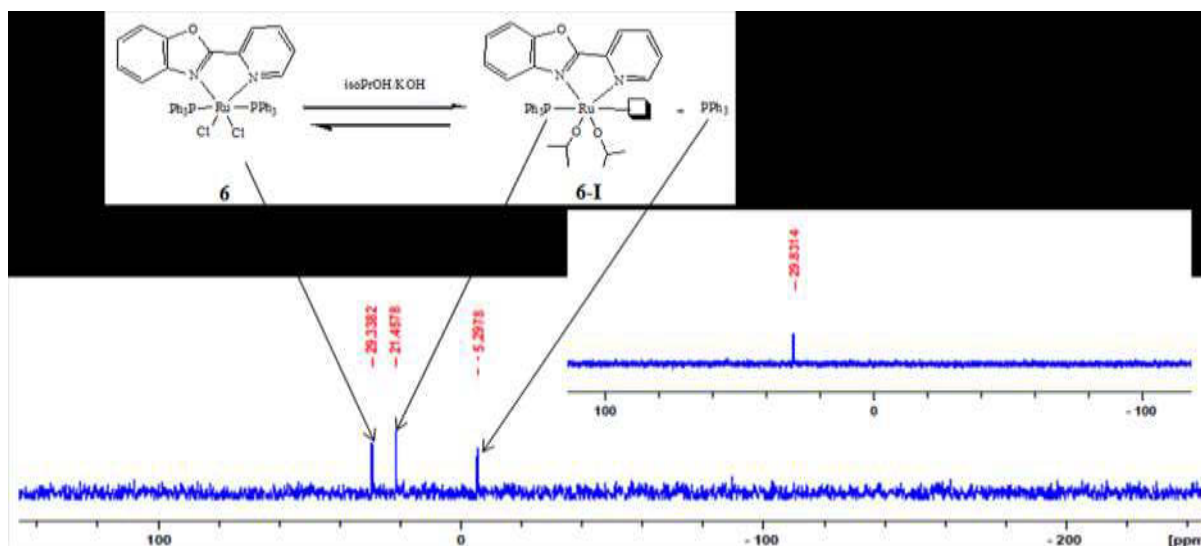


Figure 3.10: <sup>31</sup>P{<sup>1</sup>H} NMR spectra showing evidence of displacement of PPh<sub>3</sub> in *i*PrOH/KOH solution to form metal-alkoxide **6-I** from complex **6**. The signal at -5.29 ppm reveals the generation of free PPh<sub>3</sub> (inset; <sup>31</sup>P NMR spectrum of complex **6** in CDCl<sub>3</sub>, the signal at 29.83 ppm indicates that the two trans-PPh<sub>3</sub> ligands are chemically equivalent).

### 3.3.6 DFT calculations

To further understand the effect of ligand and catalyst structure on the catalytic activities of complexes **1-6**, density functional theory (DFT) calculations were performed on simplified ruthenium(II) analogues [RuCl<sub>2</sub>(**L1**)] **1a**, [RuCl<sub>2</sub>(**L2**)] **2a**, [RuCl<sub>2</sub>(**L3**)] **3a**. Frontier molecular orbitals of **1a-3a** calculated at B3LYP using the LANL2DZ basis set is shown in Figure 3.11. Table 3.5 contains a summary of charge distribution data of **1a-3a**. The benzimidazole complex **1a** showed the largest HOMO-LUMO gap while the benzothiazole and benzoxazole compounds **2a** and **3a** exhibited very similar energy gaps (Table 3.5). Since the HOMOs are predominantly occupied by ruthenium d-orbital electrons, it is expected that a smaller energy gap would facilitate  $\pi$ -back donation of electrons from ruthenium to the ligand thus creating an electrophilic metal centre. This should result in higher catalytic activities of complexes **2** and **3** compared to complex **1**.<sup>207</sup> The observation that complex **1** was more active than complexes **2** and **3** thus indicate that HOMO-LUMO gap does not control the activities of complexes **1-6**. This is supported by comparable Ru NBO of 0.344, 0.345 and 0.350 for **1a**, **2a** and **3a**, respectively. It is important to note that **1a** exhibited larger dipole moment of 12.41 compared to 9.36 (**2a**) and 95.2 (**3a**). This reflects that the N-H moiety in ligand **L1** increases the polarity of the respective ruthenium complex and thus accelerating its reactions with isopropanol to generate the active Ru-H species. This might explain the higher catalytic activities observed for the benzimidazole (**L1**) complexes **1** and **4** compared to the benzothiazole (**L2**) and benzoxazole (**L3**) complexes. The higher activities of benzoxazole complexes **3** and **6** than the benzothiazole analogues, complexes **2** and **5** are consistent with this argument.

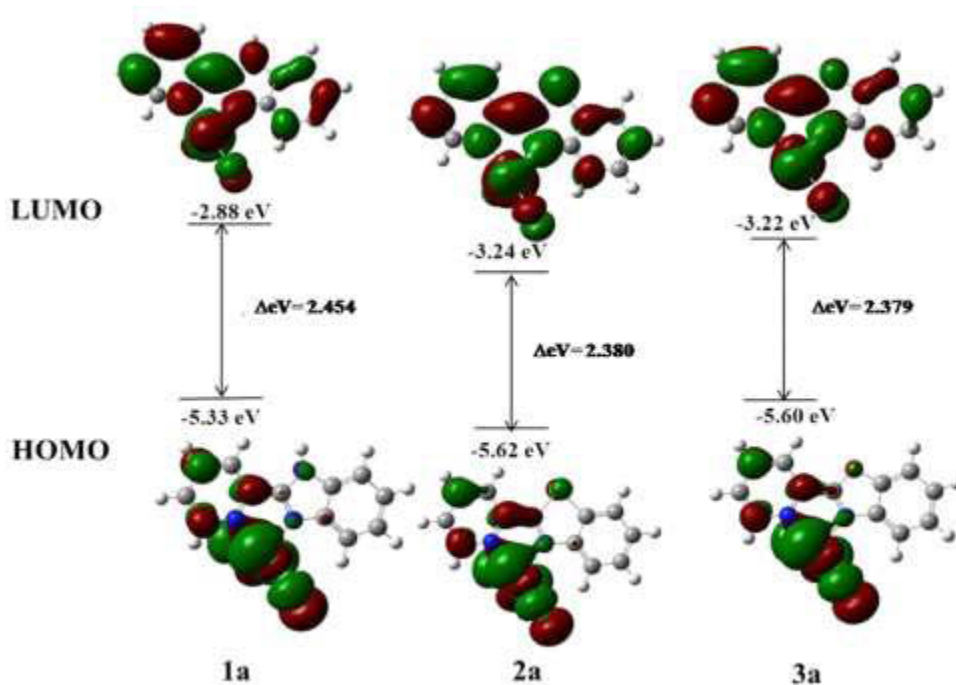


Figure 3.11: Frontier molecular orbitals of ruthenium(II) complexes  $[\text{RuCl}_2(\text{L1})]$  (**1a**)  $[\text{RuCl}_2(\text{L2})]$  (**2a**) and  $[\text{RuCl}_2(\text{L3})]$  (**3a**) as determined by Density Functional theory using B3LYP level of theory and LANL2DZ basis set (isovalue 0.02).

Table 3.5: Summary of the data obtained from DFT calculations of the Ru(II) complexes

Complex	Band Gap (eV)	NBO (Ru)	Charge on heteroatom	Dipole moment
<b>1a</b>	2.4540	0.344	-0.591	12.41
<b>2a</b>	2.3800	0.345	0.372	9.36
<b>3a</b>	2.3799	0.350	-0.496	9.52

### 3.3.7 *Conclusions*

Ruthenium(III) and ruthenium(II) complexes anchored on bidentate (pyridyl)benzoazole ligands have been prepared and structurally characterized. The coordinative unsaturation of the ruthenium(III) trichloride complexes and the high lability of the coordinated PPh<sub>3</sub> ligand are responsible for the catalytic activities of these compounds in the transfer hydrogenation of ketones. This work demonstrates examples of non-phosphine donor ruthenium(III) catalysts in transfer hydrogenation of ketones. Ruthenium(II) catalysts bearing the PPh<sub>3</sub> ancillary ligands form more active systems than the ruthenium(II) trichloride counterparts. The N-H moiety imparts higher catalytic performance in the complexes compared to O and S atoms. DFT studies show that a larger dipole moment induced by the N-H group enhances the activities of the resulting catalysts.

## **CHAPTER 4**

### **Cationic (pyridyl)benzazole and (pyrazo-1-ylmethyl)pyridinepalladium(II) complexes: Syntheses, characterization and kinetic studies in high pressure hydrogenation of alkenes and alkynes.**

#### **4.1 Introduction**

The varied structural properties and versatile nature of alkenes and alkynes makes them useful in a range of applications as building blocks or components of petrochemicals, fine chemicals, agrochemicals and pharmaceuticals.<sup>208</sup> As a result, syntheses of other organic compounds from this unsaturated carbon-carbon multiple bonds have become of enormous interest in both academic and industrial research.<sup>209-211</sup> One of the synthetic methods used to obtain other organic products is catalytic hydrogenation of unsaturated hydrocarbons such as alkenes and alkynes using molecular hydrogen in the presence of metal catalysts.<sup>212,213</sup> Several platinum group metal complexes have been extensively studied for hydrogenation of olefins and other unsaturated hydrocarbons under both heterogeneous and homogeneous reaction conditions.<sup>146,210b,214</sup> Palladium complexes, for example, the Lindlars' catalyst, is known to be an effective catalyst for the hydrogenation of unsaturated substrates in food industries.<sup>208,215</sup> These palladium complexes are preferred because they have a high surface-to-volume ratio compared to other platinum group metal complexes in most organic reactions.<sup>216</sup> However, few homogeneous palladium catalysts have been applied in high pressure hydrogenation reactions.<sup>217</sup>

Yilmaz *et al.* reported perfluoroalkylated S,O-chelated palladium acetate complexes which are homogeneous catalysts for high pressure hydrogenation of olefins using molecular hydrogen. The complexes were effective for the hydrogenation of styrene and 1-octene and their activity was found to be affected by the nature of the leaving group.<sup>218</sup>

Reactivity of metal complexes in catalytic hydrogenation also depends on the nature of the donor atoms of the ligand.<sup>219</sup> Palladium complexes bearing phosphine ligands are increasingly receiving attention due to their significant potential in enhancing various catalytic processes. In addition, cationic complexes bearing by weak coordinating counterions have been shown to be good catalyst precursors for hydrogenation reactions.<sup>220</sup> In this chapter, the syntheses and characterization of some cationic palladium(II) complexes bearing (pyridyl)benzoazole and (pyrazo-1-ylmethyl)pyridine ligands is reported. An extensive evaluation of the complexes in the high pressure catalytic hydrogenation of alkenes and alkynes and the investigations to establish the effect of ligands, ancillary phosphine ligands, reaction conditions and kinetic of the reactions are also discussed.

## 4.2 Experimental Section

### 4.2.1 Materials and instrumentation

All reactions were carried out under a nitrogen atmosphere using a dual vacuum/nitrogen line and standard Schlenk techniques unless stated otherwise. Dichloromethane (ACS reagent,  $\geq 99.8\%$ ), toluene (ACS reagent,  $\geq 99.5\%$ ), hexane (chromasolv®, 95%) and diethyl ether (ACS reagent,  $\geq 98\%$ ) were dried and distilled under nitrogen in the presence of suitable drying agents. PdCl<sub>2</sub> (anhydrous, 59%), PPh<sub>3</sub> (reagentplu®, 99%) and deuterated solvents were purchased from Sigma-Aldrich and used without any further purification. NaBAR<sub>4</sub> {Ar<sub>4</sub> = (3, 5-(CF<sub>3</sub>)<sub>2</sub>C<sub>6</sub>H<sub>3</sub>)<sub>4</sub>} (Selectophore™,  $\geq 98.0\%$ ) was obtained Boulder Scientific and used as received. Ligands, 2-(2-pyridyl)benzimidazole (**L1**), 2-(2-pyridyl)benzothiazole (**L2**), 2-(2-pyridyl)benzoxazole (**L3**), (2-(3,5-dimethylpyrazol-1-ylmethyl)pyridine (**L5**), 2-(3,5-diphenylpyrazol-1-ylmethyl)pyridine (**L6**) and complexes [Pd(**L1**)Cl<sub>2</sub>] (**8**), [Pd(**L2**)Cl<sub>2</sub>] (**9**), [Pd(**L3**)Cl<sub>2</sub>] (**10**), [Pd(**L1**)MeCl] (**11**), [Pd(**L5**)Cl<sub>2</sub>] (**14**), [Pd(**L6**)Cl<sub>2</sub>] (**15**) and [Pd(**L5**)MeCl] (**16**) were prepared according to the literature procedures.<sup>221-223</sup> NMR spectra were recorded on a Bruker 400 (<sup>1</sup>H, 400 MHz; <sup>13</sup>C, 100 MHz; <sup>31</sup>P, 162 MHz) Ultrashield instrument at room temperature in CDCl<sub>3</sub> and DMSO-*d*<sub>6</sub> solvents. The <sup>1</sup>H (400 MHz) and <sup>31</sup>P {<sup>1</sup>H} (162 MHz) chemical shifts are reported in  $\delta$  (ppm) and referenced to the residual proton in the solvents for <sup>1</sup>H and 85% H<sub>3</sub>PO<sub>4</sub> for <sup>31</sup>P nuclei. All coupling constants (*J*) are measured in hertz (Hz). Elemental analyses were performed on a Thermal scientific flash 2000 and mass spectra were recorded on a LC Premier micro-mass spectrometer. Electron microscopy analyses were done on JEOL JEM-1400X transmission electron microscope at the School of Life Sciences, University of KwaZulu-Natal.

## 4.2.2 Synthesis of cationic palladium(II) complexes

### 4.2.2.1 Synthesis of $\{[2-(2\text{-pyridyl})\text{benzimidazole}]\text{PdPPh}_3\text{Cl}\}\text{Cl}$ (**12**)

To a suspension of compound **8** (0.05 g, 0.13 mmol) in  $\text{CH}_2\text{Cl}_2$  (5 mL), was added a solution of  $\text{PPh}_3$  (0.04 g, 0.14 mmol) in  $\text{CH}_2\text{Cl}_2$  (5 mL) and the precipitate formed was stirred for 24 h. After the reaction period the mixture was filtered and the precipitate washed with  $\text{CH}_2\text{Cl}_2$  (10 mL) to afford complex **12** as a light yellow solid. Yield = 0.04 g (52%).  $^1\text{H}$  NMR ( $\text{DMSO}-d_6$ ):  $\delta$  7.39 (t, 1H, bz<sub>im</sub>,  $^3J_{\text{HH}} = 7.2$  Hz); 7.49 (t, 1H, py,  $^3J_{\text{HH}} = 14.0$  Hz); 7.68-7.44 (m, 15H, PPh<sub>3</sub>) 7.76 (d, 1H, bz<sub>im</sub>,  $^3J_{\text{HH}} = 8.0$  Hz); 7.82 (t, 2H, bz<sub>im</sub>,  $^3J_{\text{HH}} = 6.0$  Hz); 8.34 (d, 1H, bz<sub>im</sub>,  $^3J_{\text{HH}} = 7.2$  Hz); 8.42 (t, 1H, py,  $^3J_{\text{HH}} = 8.0$  Hz); 8.71 (d, 1H, py,  $^3J_{\text{HH}} = 8.4$  Hz); 9.11 (d, 1H, py,  $^3J_{\text{HH}} = 5.2$  Hz).  $^{13}\text{C}$  NMR (400 MHz,  $\text{DMSO}-d_6$ ):  $\delta$  129.17, 129.21, 129.26, 129.45, 131.90, 131.98, 133.63, 133.78, 137.07, 137.16  $^{31}\text{P}\{\text{H}\}$  NMR ( $\text{CDCl}_3$ ):  $\delta$  23.71 (s, 1P, PPh<sub>3</sub>). Anal. Calcd. For  $\text{C}_{30}\text{H}_{24}\text{Cl}_2\text{N}_3\text{PPd}$ : C, 56.76; H, 3.81; N, 6.62%. Found C, 56.68; H, 4.01; N, 1.71%. Positive mode (ESI-MS)  $m/z$  600.08 ( $\text{M}^+ + 1, 100$ ).

### 4.2.2.2 Synthesis of $\{[2-(2\text{-pyridyl})\text{benzimidazole}]\text{PdMePPh}_3\}\text{BAR}_4$ (**13**)

To a solution of complex **11** (0.03 g, 0.09 mmol) in  $\text{CH}_2\text{Cl}_2$  (5 mL), was added  $\text{NaBAR}_4$  (0.08 g, 0.09 mmol) and  $\text{PPh}_3$  (0.02 g, 0.09 mmol) in  $\text{CH}_2\text{Cl}_2$  (5 mL). The resultant clear orange solution was stirred for 12 h. The solution was filtered and concentrated *in vacuo* and hexane (15 mL) added to precipitate an orange solid. Yield = 0.09 g (75%).  $^1\text{H}$  NMR (400 MHz,  $\text{CDCl}_3$ ):  $\delta$  1.23 (s, 3H, Pd-Me); 7.02 (d, 1H, py,  $^3J_{\text{HH}} = 4.8$  Hz); 7.50 (s, 8H, BAR<sub>4</sub>); 7.88-7.41 (15H, PPh<sub>3</sub>); 7.73 (s, 4H, BAR<sub>4</sub>); 8.09 (d, 2H, bz<sub>im</sub>,  $^3J_{\text{HH}} = 8.0$  Hz); 8.72 (d, 2H, bz<sub>im</sub>,  $^3J_{\text{HH}} = 6.0$  Hz); 9.44 (d, 1H, py,  $^3J_{\text{HH}} = 4.4$  Hz); 10.72 (s, NH).  $^{13}\text{C}$  NMR (400 MHz,  $\text{CDCl}_3$ ):  $\delta$  121.54, 123.21, 123.67, 126.05, 128.19, 128.14, 132.36, 134.40, 134.77, 135.11, 149.94.  $^{31}\text{P}\{\text{H}\}$  NMR ( $\text{CDCl}_3$ ):  $\delta$  33.74



(s, 1P, PPh<sub>3</sub>). Anal. Calcd. For C<sub>63</sub>H<sub>40</sub>BF<sub>24</sub>N<sub>3</sub>PPd: C, 52.47; H, 2.73; N, 2.91%. Found C, 53.36; H, 2.91; N, 2.85%. A single crystal suitable for X-ray analysis was obtained by recrystallization of complex **13** from a CH<sub>2</sub>Cl<sub>2</sub>/hexane mixture.

#### 4.2.2.3 Synthesis of *{2-(3,5-dimethylpyrazol-1-ylmethyl)pyridine}PdPPh<sub>3</sub>Cl* (**17**)

To a suspension of complex **14** (0.09 g, 0.24 mmol) in CH<sub>2</sub>Cl<sub>2</sub> (5 mL), a solution of PPh<sub>3</sub> (0.07 g, 0.27 mmol) in CH<sub>2</sub>Cl<sub>2</sub> (5 mL) was added to give a light yellow precipitate. The mixture was stirred for 12 h and filtered to isolate complex **17** as light yellow solid. Yield = 0.10 g (62%). <sup>1</sup>H NMR (DMSO-*d*<sub>6</sub>): δ 2.40 (s, 3H, CH<sub>3</sub>, pz); 2.43 (s, 3H, CH<sub>3</sub>, pz); 5.79 (d, 2H, py-CH<sub>2</sub>-pz) 6.16 (d, 2H, pz, <sup>3</sup>*J*<sub>HH</sub> = 8.0 Hz); 7.66-7.61 (m, 15H, Ph); 7.94 (t, 1H, py, <sup>3</sup>*J*<sub>HH</sub> = 7.2 Hz); 8.12 (d, 1H, py, <sup>3</sup>*J*<sub>HH</sub> = 8.0 Hz); 8.79 (d, 1H, py, <sup>3</sup>*J*<sub>HH</sub> = 8.4 Hz. <sup>13</sup>C NMR (400 MHz, DMSO-*d*<sub>6</sub>): δ 10.60, 13.35, 52.90, 108.50, 116.85, 119.80, 122.53, 125.22, 125.64, 125.98, 126.56, 127.81, 127.94, 128.12, 128.43, 131.85, 133.86, 134.14, 140.60, 144.28, 151.67, 152.00, 160.30, 160.80, 161.30, 161.79 <sup>31</sup>P{H} NMR (DMSO-*d*<sub>6</sub>): δ 28.88 (s, 1P, PPh<sub>3</sub>). Anal. Calcd. For C<sub>29</sub>H<sub>28</sub>Cl<sub>2</sub>N<sub>3</sub>PPd: C, 55.56; H, 4.50; N, 6.70%. Found C, 55.71; H, 4.01; N, 5.34%. Positive mode (ESI-MS) *m/z* 525.94 (M<sup>+</sup>-ClMe<sub>2</sub>, 100).

#### 4.2.2.4 Synthesis of *{2-(3,5-dimethylpyrazol-1-ylmethyl)pyridine}PdClPPh<sub>3</sub>BAR<sub>4</sub>* (**18**)

To a suspension of complex **14** (0.10 g, 0.27 mmol) in CH<sub>2</sub>Cl<sub>2</sub> (10 mL), PPh<sub>3</sub> (0.08 g, 0.30 mmol) and NaBAR<sub>4</sub> (Ar<sub>4</sub> = 3,5-(CF<sub>3</sub>)<sub>2</sub>C<sub>6</sub>H<sub>3</sub>) (0.22 g, 0.27 mmol) were added and stirred under an inert atmosphere for 12 h. The solution mixture was filtered and concentrated to approximately 3 mL. Hexane (10 mL) was then added to precipitate complex **18** as a yellow crystalline solid. Recrystallization of complex **18** using CH<sub>2</sub>Cl<sub>2</sub>/Hexane solvent mixture afforded single crystals suitable for X-ray analysis. Yield = 0.26 g (65%). <sup>1</sup>H NMR (400 MHz, CDCl<sub>3</sub>): δ 2.21 (s, 3H,

CH<sub>3</sub>, pz); 2.28 (s, 3H, CH<sub>3</sub>, pz); 5.27 (d, 2H, py-CH<sub>2</sub>-pz) 6.06 (d, 2H, pz, <sup>3</sup>J<sub>HH</sub> = 8.0 Hz); 7.48-7.53 (m, Ph); 7.51 (s, 8H, BAr<sub>4</sub>) 7.71 (s, 4H, BAr<sub>4</sub>); 7.89 (t, 1H, py, <sup>3</sup>J<sub>HH</sub> = 7.2 Hz); 8.65 (d, 1H, py, <sup>3</sup>J<sub>HH</sub> = 8.0 Hz); 8.93 (d, 1H, py, <sup>3</sup>J<sub>HH</sub> = 8.4 Hz). <sup>13</sup>C NMR (400 MHz, CDCl<sub>3</sub>): δ 11.32, 14.08, 53.63, 109.22, 117.58, 120.55, 123.55, 125.96, 126.71, 127.29, 128.54, 128.67, 128.85, 129.16, 129.27, 129.46, 132.57, 134.48, 134.59, 134.87, 141.33, 145.00, 152.40, 152.73, 161.07, 161.53, 162.02, 162.52. <sup>31</sup>P{H} NMR (CDCl<sub>3</sub>): δ 27.85 (s, 1P, PPh<sub>3</sub>). Anal. Calcd. For C<sub>61</sub>H<sub>40</sub>ClF<sub>24</sub>N<sub>3</sub>PPd: C, 50.37; H, 2.77; N, 2.89%. Found: C, 50.35; H, 2.80; N, 3.12%. Positive mode (ESI-MS) *m/z* 555.36 (M<sup>+</sup>, -Cl, 40). Recrystallization of complex **18** from CH<sub>2</sub>Cl<sub>2</sub>/hexane gave a single crystal suitable for X-ray analysis.

#### 4.2.3 Density functional theory (DFT) modelling of 8-18

DFT calculations were performed in gas phase for benzoazole and pyrazolyl complexes **8-18** using a well-established approach for the third row transition metal complexes, to identify the energy-minimized structures based on B3LYP/LANL2DZ<sup>183,184</sup>(Los Alamos National Laboratory 2 double ζ) level theory, with inner core electrons of the Pd atom replaced by relativistic effective core potential (ECP). The Gaussian09 suite of program was used for all the computations.<sup>185</sup>

#### 4.2.4 X-ray crystallography

##### *Data collection*

X-ray data were recorded on a Bruker Apex Duo equipped with an Oxford instrument Cryojet operating at 100(2) K and an Incoatec microsource operating at 30 W. The data were collected with Mo Kα (λ = 0.71073 Å) radiation at a crystal-to-detector distance of 50 mm.

The following conditions were used for the data collection: omega and phi scans with exposures taken at 30 W X-ray power and 0.50° frame widths using APEX2.<sup>224</sup> The data were reduced with the programme SAINT<sup>225</sup> using outlier rejection, scan speed scaling, as well as standard Lorentz and polarisation correction factors. A SADABS semi-empirical multi-scan absorption correction was applied to the data.

### ***Structure solution and refinement***

Direct methods, SHELXS-97 and WinGX<sup>226</sup> were used to solve the structures at the University of KwaZulu-Natal, South Africa. All non-hydrogen atoms were located in the difference density map and refined anisotropically with SHELXL-97. All hydrogen atoms were included as idealised contributors in the least squares process. Their positions were calculated using a standard riding model with C-H<sub>aromatic</sub> distances of 0.93 Å and  $U_{\text{iso}} = 1.2$  Ueq. The imidazole N-H were located in the difference density map, and refined isotropically.

#### ***4.2.5 High pressure hydrogenation reactions of alkenes and alkynes***

In a typical experiment, styrene (0.73 mL, 8.00 mmol), catalyst **8** (6 mg, 0.02 mmol) substrate/catalyst (S/C) 400:1 and dry toluene (50 mL) were introduced into a stainless steel autoclave (Parr, 300 ml) fitted with internal stirring system. The solution mixture was purged with hydrogen (three times) before the autoclave was finally charged with hydrogen and the pressure and temperature adjusted to 5 bar and 30 °C, respectively. The stirring speed was set to 600 rpm and the stirring started when the temperature reached equilibrium. The mixture was stirred under constant hydrogen and the samples withdrawn at regular intervals, filtered using 0.45 µm micro filters and analysed by Varian CP-3800 GC (ZB-5HT column 30m×0.25 mm×0.10µm) to determine the consumption of styrene.

Ethylbenzene (anhydrous, 99.8%) from Sigma-Aldrich was used as an authentic standard to determine the percentage hydrogenation of styrene to ethylbenzene (analytical standard). Prior to conducting catalytic evaluation of complexes **8-18**, a blank experiment without the catalyst precursor was carried out.

#### **4.2.6 TEM analyses**

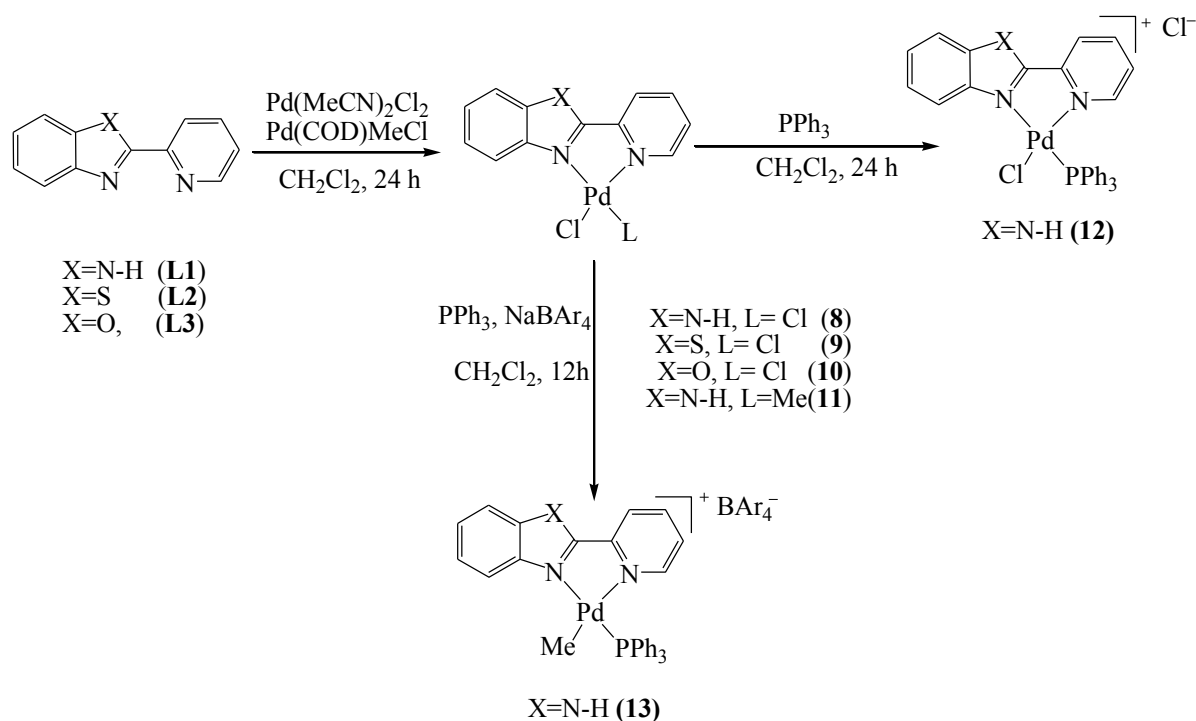
The solutions of palladium catalysts reaction mixtures were dried and the solids dispersed into suspension by sonicating in ethanol. A drop of suspension was placed on carbon grids and allowed to completely dry and thereafter mounted for TEM analyses.

### **4.3 Results and discussion**

#### **4.3.1 Synthesis and structural characterization of benzoazole and pyrazolyl Pd(II) complexes**

Ligands **L1-L3**, 2-(2-pyridyl)benzoimidazole (**L1**), 2-(2-pyridyl)benzothiazole (**L2**) and 2-(2-pyridyl)benzoxazole (**L3**), 2-(3,5-dimethylpyrazol-1-ylmethyl)pyridine (**L5**), 2-(3,5-diphenylpyrazol-1-ylmethyl)pyridine (**L6**) were prepared according to the literature procedures.<sup>227,228</sup> Likewise, neutral benzoazole Pd(II) complexes, [Pd(**L1**)Cl<sub>2</sub>] (**8**), [Pd(**L2**)Cl<sub>2</sub>] (**9**), [Pd(**L3**)Cl<sub>2</sub>] (**10**), [Pd(**L1**)MeCl] (**11**) and neutral pyrazolyl Pd(II) complexes [Pd(**L5**)Cl<sub>2</sub>] (**14**), [Pd(**L6**)Cl<sub>2</sub>] (**15**) and [Pd(**L5**)MeCl] (**16**) were synthesized following reported literature procedures.<sup>222,223</sup> The cationic Pd(II) complexes of ligands **L1** and **L5** were synthesized as summarized by Schemes 4.1a and 4.1b.

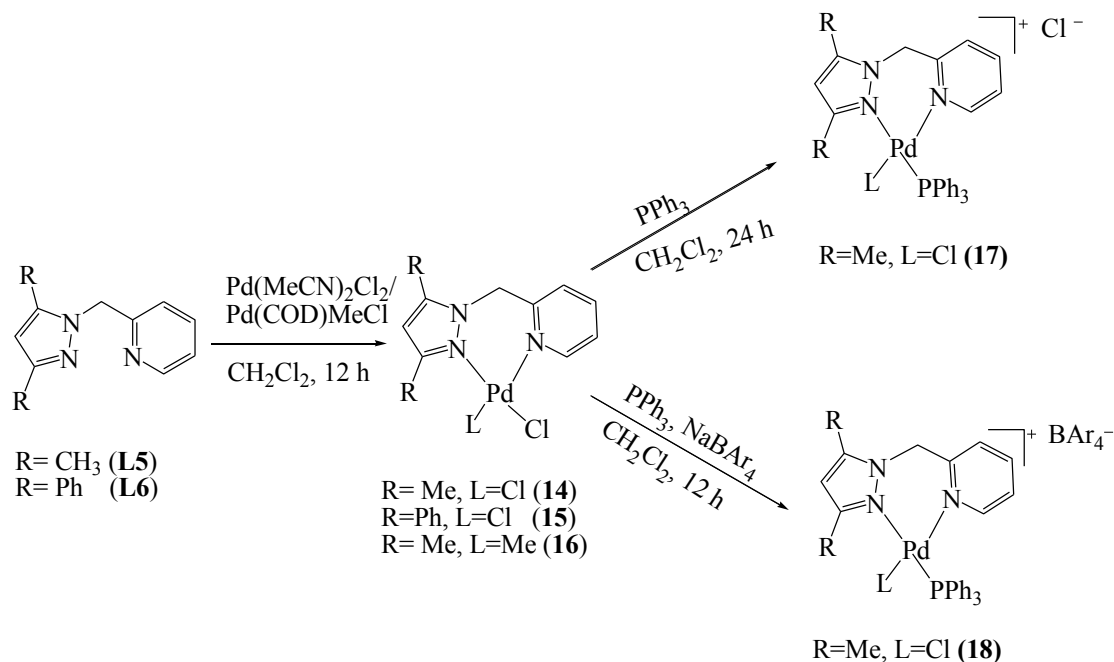
Treatment of suspensions of neutral complexes **8** and **11** with one molar equivalent of PPh<sub>3</sub> and PPh<sub>3</sub>/NaBAr<sub>4</sub>, respectively, gave the cationic complexes [Pd(L1)PPh<sub>3</sub>Cl]Cl (**12**) and [Pd(L1)PPh<sub>3</sub>Me]BAr<sub>4</sub> (**13**) (Scheme 4.1a). Similarly, the pyrazolyl complexes, [Pd(L5)PPh<sub>3</sub>Cl]Cl (**17**) and [Pd(L5)PPh<sub>3</sub>Cl]BAr<sub>4</sub> (**18**) were obtained by reacting the neutral pyrazolyl Pd(II) complex **14** with one molar equivalent of PPh<sub>3</sub> and PPh<sub>3</sub>/NaBAr<sub>4</sub>, respectively (Scheme 4.1b). All the complexes were isolated as yellow solids except for complexes **11** and **16** which were isolated as cream-white solids. Complexes **11**, **13**, **16** and **18** were highly soluble in chlorinated solvents probably due to the Me ligand and BAr<sub>4</sub><sup>-</sup> counter ions.



Scheme 4.1a: Synthesis of benzoazole palladium(II) complexes, **8-13**

The identities of the complexes were established by a combination of <sup>1</sup>H, <sup>13</sup>C, <sup>31</sup>P{H} NMR spectroscopy, micro-analyses, mass spectrometry and single crystal X-ray analysis for complexes **13** and **18**. From the <sup>1</sup>H NMR spectra obtained, significant downfield shifts of the pyridyl and benzoazole rings compared to the corresponding ligands were observed indicating ligand

coordination. For example, there were noticeable shifts on  $^1\text{H}$  NMR peaks for N-CH<sub>py</sub> (8.65 ppm); **L1**, N-CH<sub>py</sub>; (8.73 ppm); **L2** and N-CH<sub>py</sub>; (8.77 ppm); **L3** compared to the corresponding complexes **8** (9.10 ppm); **9** (9.13 ppm) and **10** (9.08 ppm).



Scheme 4.1b: Synthesis of pyrazolyl palladium(II) complexes, **14-18**.

Figure 4.1a and 4.1b show typical  $^1\text{H}$  NMR spectra of complexes **11** and **18**, respectively. In Figure 4.1b, the  $^1\text{H}$  NMR spectrum of **18** shows the pyridine (N-CH) peak at 8.93 ppm compared to 8.53 ppm for the ligand, **L5**. The appearance of the peaks at 0.97 ppm, 1.23 ppm and 0.99 ppm, which were attributed to the coordinated (Pd-Me) protons were also used to identify complexes **11**, **13** and **16**. These signals appeared in the range of -0.80 ppm to 0.69 ppm as reported by Nielsen *et al.*<sup>229</sup>  $^{13}\text{C}$  NMR spectra had fewer signals than the total number of carbon atoms in the compound possibly due to low solubility or overlaps of the carbon signals.  $^{31}\text{P}\{\text{H}\}$  NMR spectroscopy was particularly useful for determining the coordination of the PPh<sub>3</sub> ligand.

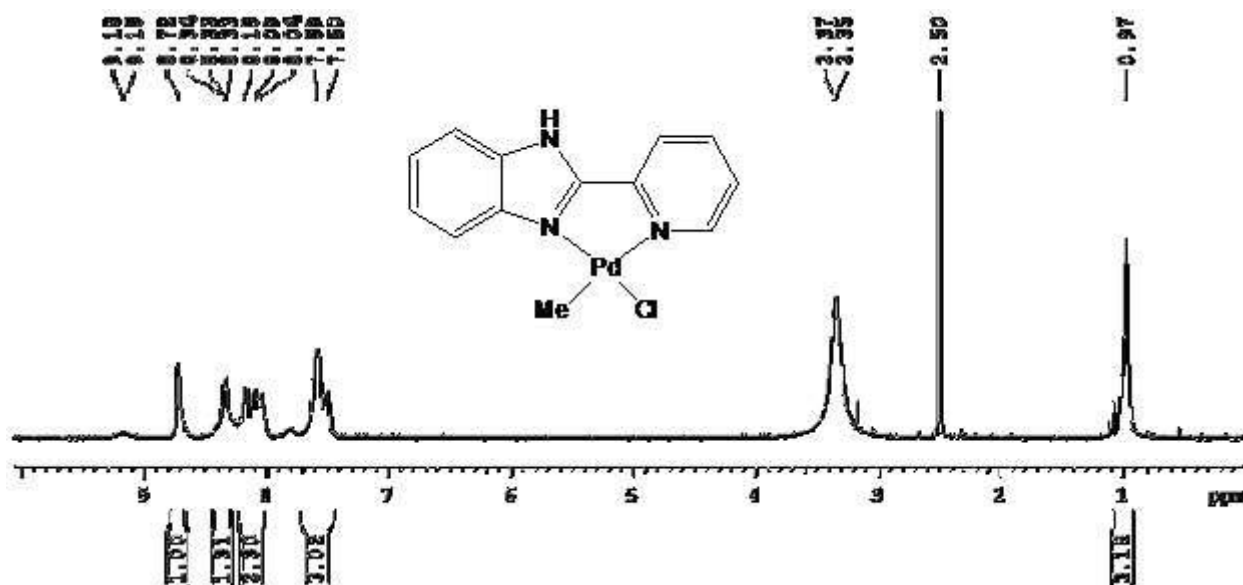


Figure 4.1a:  $^1\text{H}$  NMR spectrum for complex **11** showing coordinated Me ligand.

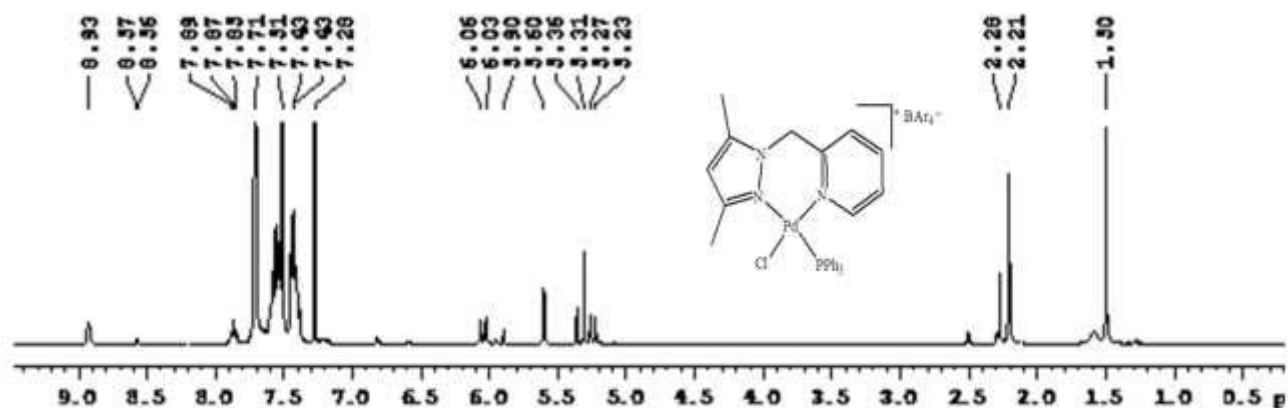


Figure 4.1b:  $^1\text{H}$  NMR spectrum for complex **18**.

Typical  $^{31}\text{P}$  NMR spectra of complexes **12** and **18** showed peaks at 28.89 ppm and 27.85 ppm respectively (Figure 4.2a and 4.2b) in comparison to the signal at 6.69 ppm usually observed for free  $\text{PPh}_3$ . The observed values are consistent with the range of 26.1-28.3 ppm reported by Aguirre *et. al.*<sup>230</sup> for the mono-coordinated Pd- $\text{PPh}_3$  complexes.

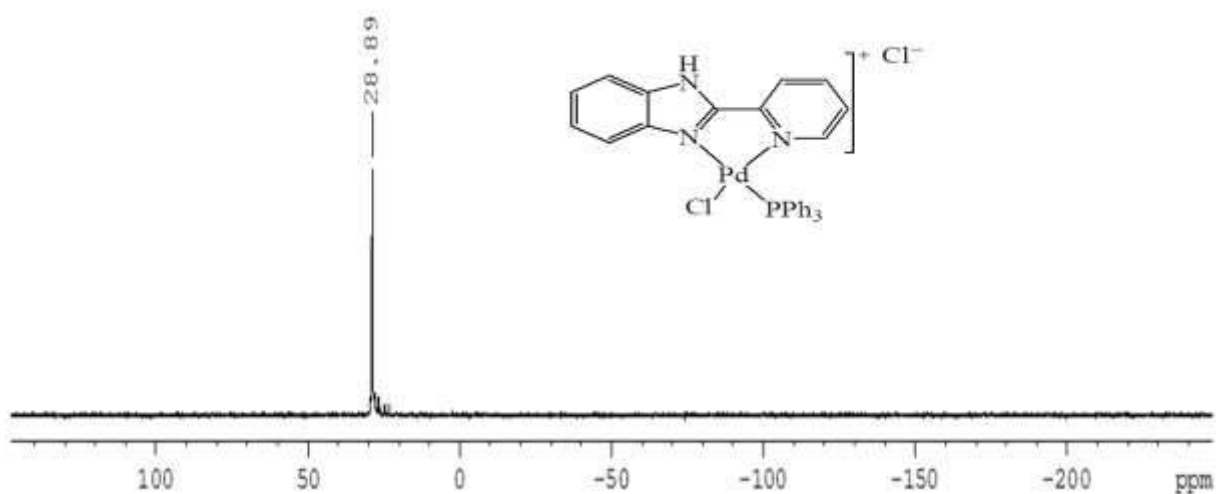


Figure 4.2a:  $^{31}\text{P}\{^1\text{H}\}$  NMR spectrum for complex **12** showing a peak for coordinated  $\text{PPh}_3$ .

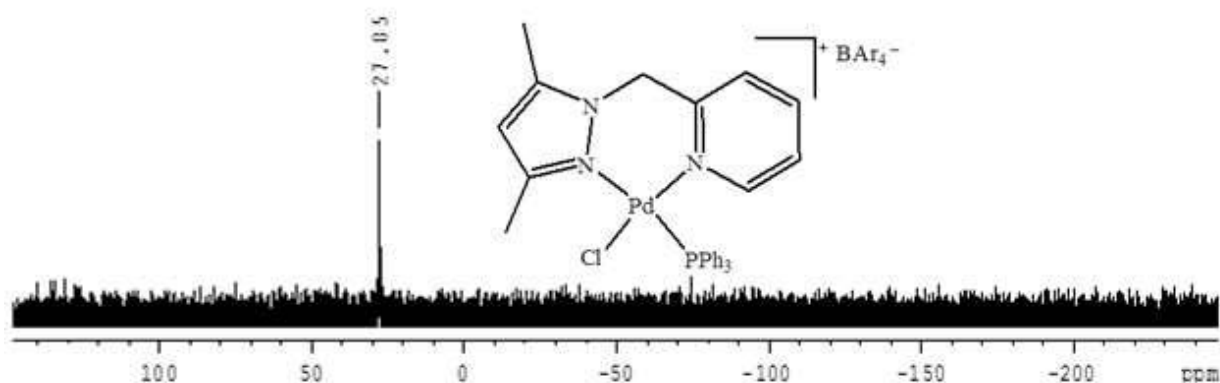


Figure 4.2b:  $^{31}\text{P}$  NMR spectrum for complex **18** showing a peak for coordinated  $\text{PPh}_3$

Mass spectral analyses of benzothiazole complex  $[\text{Pd}(\text{L}2)\text{Cl}_2]$  (**9**) and benzimidazole complex  $[\text{Pd}(\text{L}1)\text{MeCl}]$  (**11**) showed base peaks at  $m/z$  at 354.91 and 316.67 for monochloride coordinated fragments  $[\text{Pd}(\text{L}2)\text{Cl}]^+$  and  $[\text{Pd}(\text{L}1)\text{Cl}]^+$  having base peaks of  $m/z$  of 354.91 and 316.00, respectively (Figures 4.3 and 4.4). An electrospray ionization (ESI) mass spectrum of complex **12**, recorded in the positive ion mode, showed a base peak at  $m/z = 600.07$ , corresponding to  $[\text{Pd}(\text{L}1)\text{PPh}_3\text{Cl}]^+$  fragment (Figure 4.5).



Likewise, single mass analysis of complex **16** showed molecular ion at  $m/z$  of 308.03 corresponding to the  $[\text{Pd}(\text{L5})\text{Me}]^+$  fragment consistent with the loss of a chloride ligand (Figure 4.6).

The micro analyses data of the synthesized Pd(II) complexes were in good agreement with the empirical formulae of the compounds. However, it was observed that the micro-analyses data of cationic complexes **12** and **17**, bearing the chloride counter ions, showed consistently low percentage composition by nitrogen. Although, the analyses were carried in triplicate to establish reproducibility and instrument accuracy, the results did not improve. At this moment, we cannot unambiguously account for the lower percentages of the N element observed in compounds **12** and **17**.

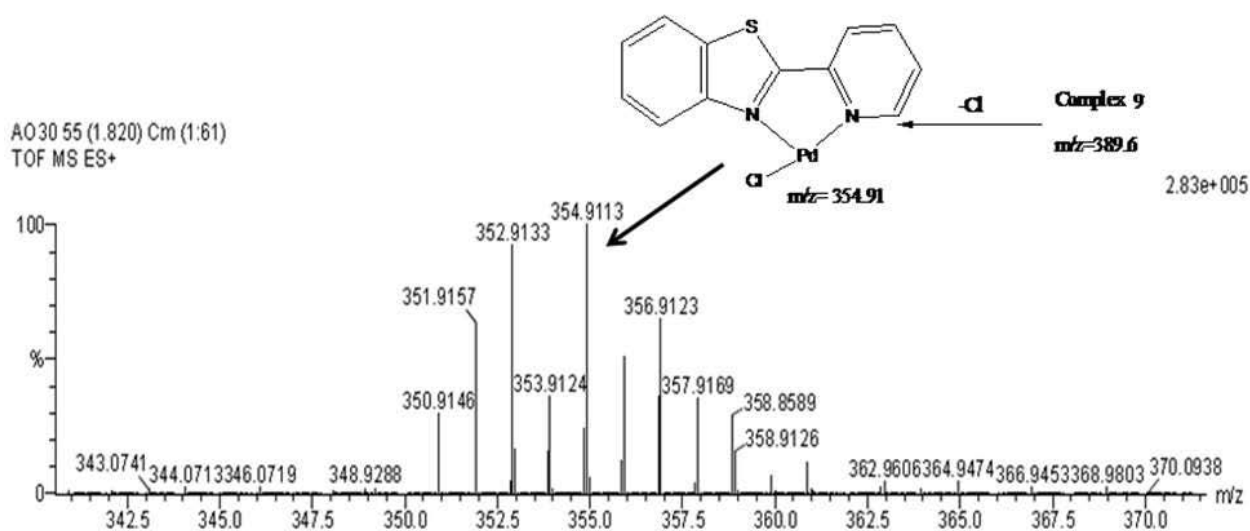


Figure 4.3: HR-MS showing a  $m/z$  peak of complex **9** fragment.

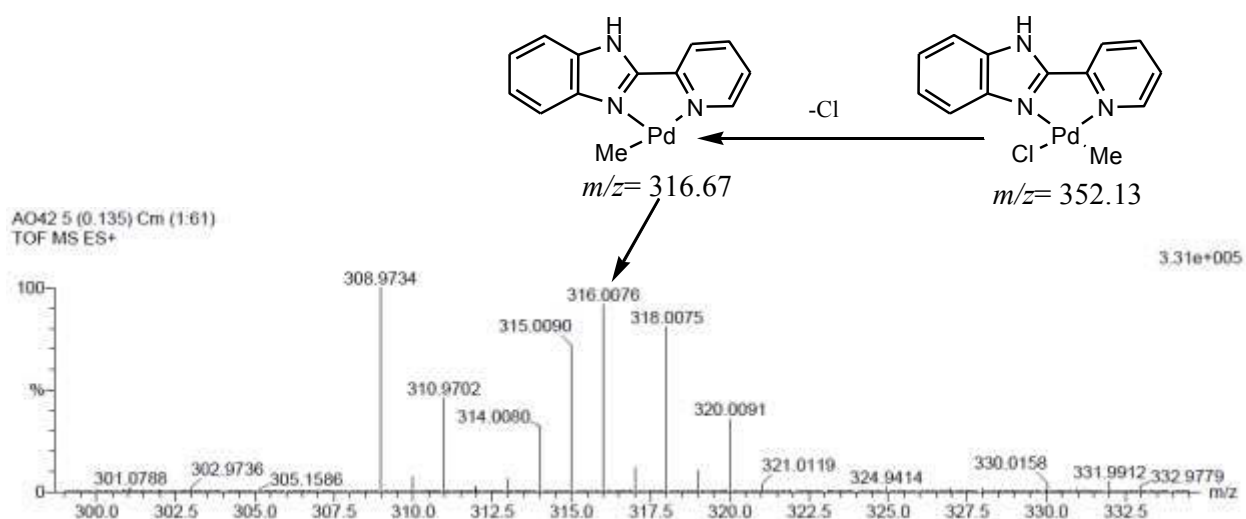


Figure 4.4: HR-MS of complex **11** showing the fragmentation pattern.

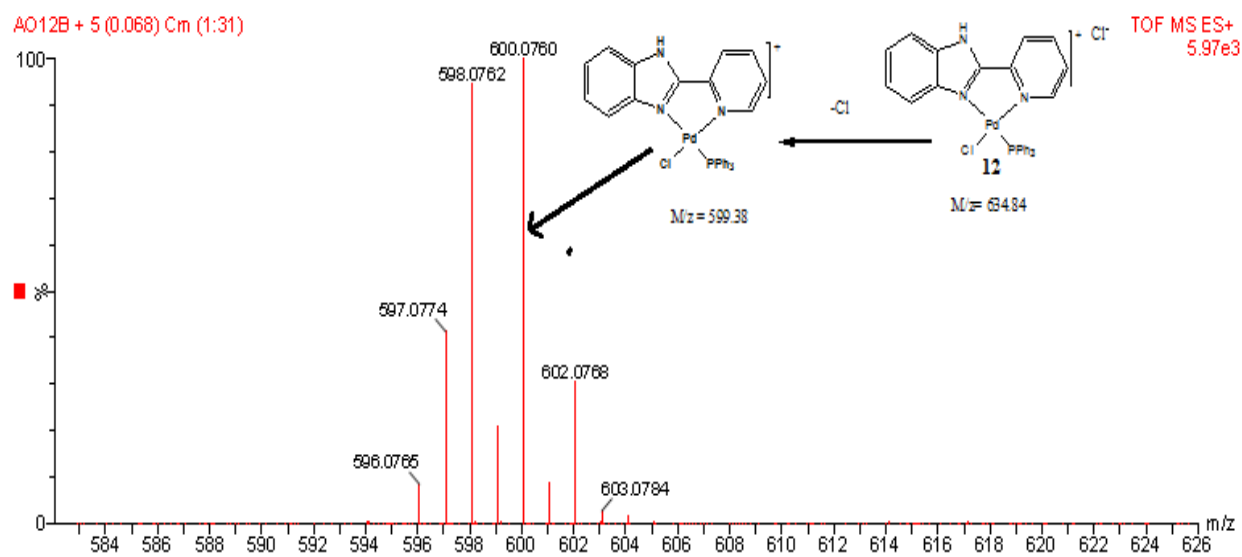


Figure 4.5: ESI mass spectrum showing  $m/z$  peak of molecular cation of complex **12**.

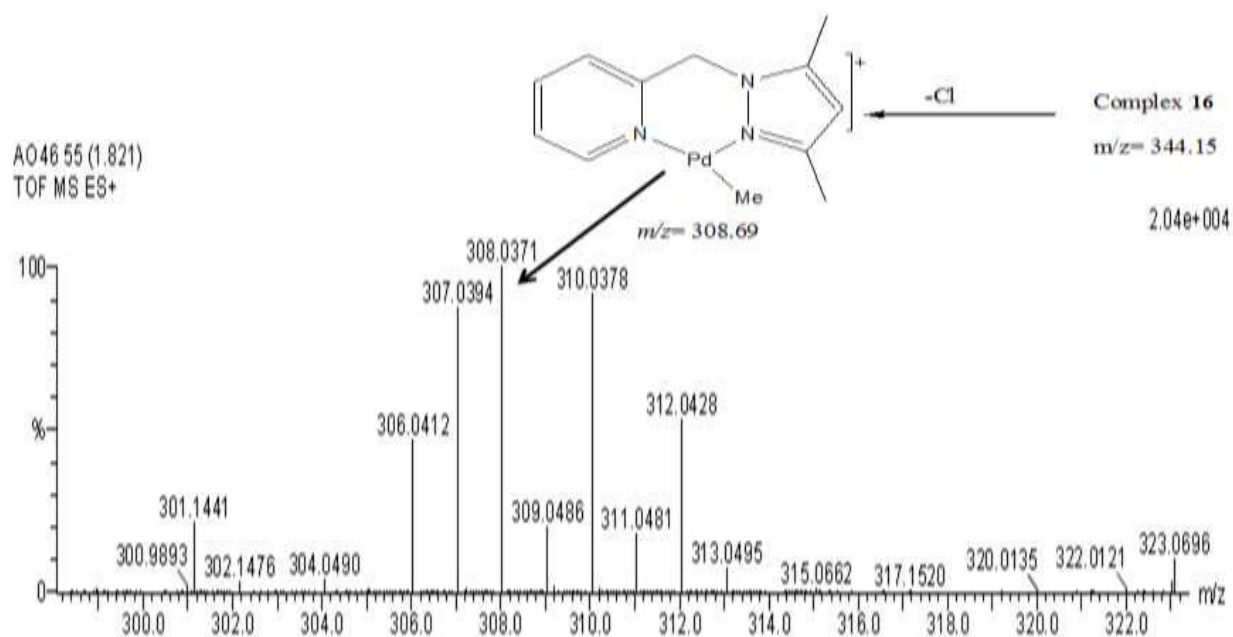


Figure 4.6: HR-MS of complex **16** showing m/z peak of  $[\text{Pd}(\text{L5})\text{Me}]^+$  fragment.

#### 4.3.2 Molecular structures of complexes **13** and **18**

Single crystals suitable for X-ray analyses for complexes **13** and **18** were grown by slow evaporation of their DCM/hexane solutions at room temperature. Figure 4.7 shows molecular structures of complexes **13** and **18**. Table 4.1 contain data collection and structural refinement parameters while Table 4.2 contain selected bond lengths (Å) and bond angles (°) for complexes **13** and **18** respectively. In the molecular structure of complex **13**, ligand **L1** adopts a bidentate coordination mode to the palladium metal centre (Figure 4.7). The bond angles N(2)-Pd(1)-C(14) of 93.29° and N(2)-Pd(1)-N(5) of 77.81° deviate from 90° typical of square-planar complexes. The bite angle P(1)-Pd-C(14) of 87.55° is larger than N(2)-Pd(1)-N(5) of 77.81° due to steric interaction between the PPh<sub>3</sub> and the methyl ligand.

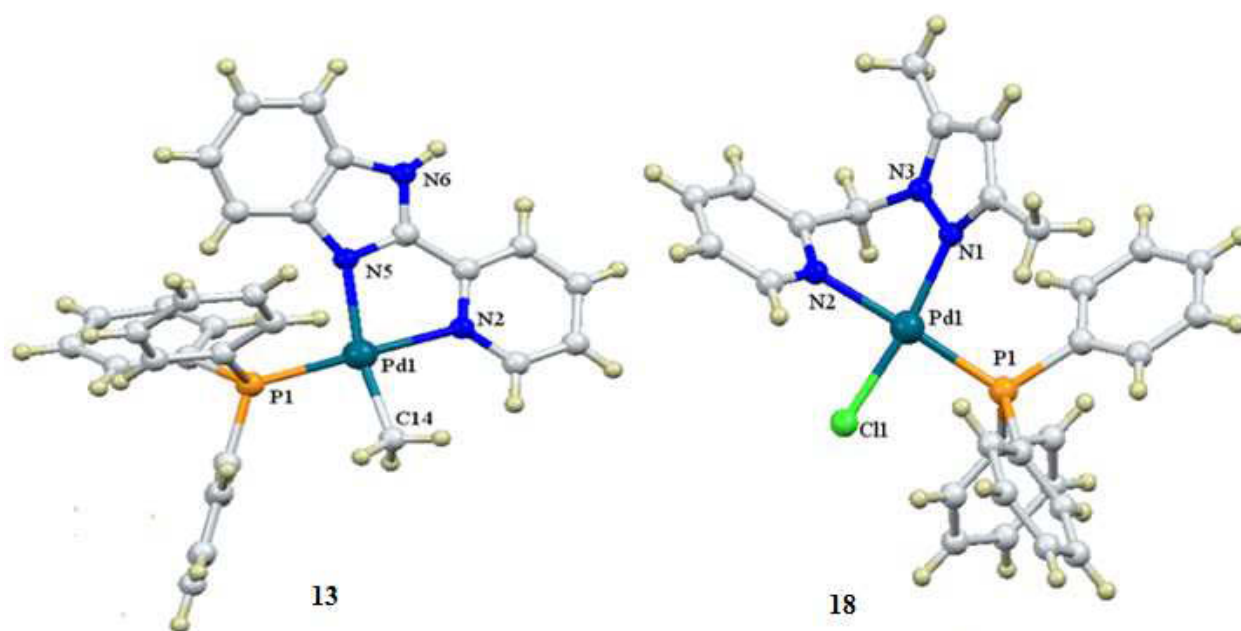


Figure 4.7: Molecular structures of complexes **13** and **18** drawn with 50% probability ellipsoids.

The Pd-N<sub>py</sub> bond length of 2.155(2) Å is longer than the average 2.0442 Å for similar Pd(II) complexes<sup>228</sup> and longer than those of 2-(2-pyridyl)benzoazole-PdCl<sub>2</sub> complexes reported by Haneda *et. al.*<sup>231</sup> Likewise, in the molecular structure of complex **18**, ligand **L5** binds to the metal centre in a bidentate manner (Figure 4.7). The bond angles for N(1)-Pd(1)-N(2) of 83.61° and N(1)-Pd(1)-P(1) of 98.34° deviate from 90° typical of square-planar complexes. Both the geometries around the Pd metal centres of complexes **13** and **18** can therefore be described as distorted square-planar structures. The Pd-N<sub>py</sub> bond length of 2.108(16) Å of complex **13** is longer than the average 2.0442 Å for similar Pd(II) complexes.<sup>228</sup>

Table 4.1: Data collection and structural refinement parameters of complexes **13** and **18**

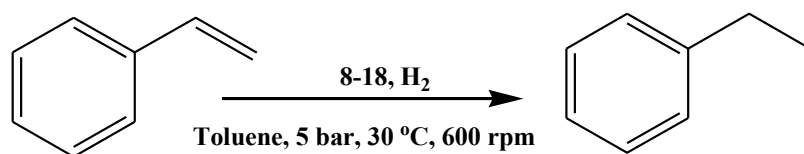
Parameter	<b>13</b>	<b>18</b>
Empirical formula	C <sub>63</sub> H <sub>39</sub> BF <sub>24</sub> N <sub>3</sub> PPd	C <sub>61</sub> H <sub>39</sub> BCIF <sub>24</sub> N <sub>3</sub> PPd
Formula weight	1442.15	1453.58
Temperature(K)	100(2)	100(2)
Wavelength (Å)	0.71073	0.71073
Crystal system	Triclinic	Triclinic
Space group	P-1	P2 <sub>1</sub> /c
<i>a</i> (Å)	12.7129(8)	13143(7)
<i>b</i> (Å)	13.3917(8)	16.791(9)
<i>c</i> (Å)	17.6166(11)	26.944(14)
$\alpha$ (°)	93.824 (3)	90.000 <sup>0</sup>
$\beta$ (°)	90.923 (2)	91.710 <sup>0</sup>
$\gamma$ (°)	93.204 (2)	90.000 <sup>0</sup>
Volume(A <sup>3</sup> )	2987.23 (3)	5943.77(5)
Z	2	4
D <sub>calcd</sub> (mg/m <sup>3</sup> )	1.603	1.624
Absorption coefficient (mm <sup>-1</sup> )	0.457	0.050
F(000)	1440	2900
Theta range for data collection (°)	1.50 -26.40	1.90 -30.10
Reflections collected / unique	13981	65303
Completeness to theta (%)	97.3	98.3
Goodness-of-fit on F <sup>2</sup>	0.838	1.116
R indices (all data)	R <sub>1</sub> = 0.0208 wR <sub>2</sub> = 0.0929	R <sub>1</sub> = 0.0477 wR <sub>2</sub> = 0.128
Largest diff. peak and hole (e Å <sup>-3</sup> )	1.69 and -0.96	1.48 and -1.09

Table 4.2: Selected bond lengths (Å) and bond angles (°) for complexes **13** and **18**.

<b>Bond Lengths [Å]</b>	<b>13</b>	<b>18</b>
Pd–N <sub>py</sub>	2.155(2)	2.108(16)
Pd–N <sub>bz/pz</sub>	2.174(2)	2.043(17)
Pd–Cl	-	2.277(5)
Pd–C	2.3554(3)	-
Pd–P	2.2441(6)	2.282(5)
<b>Bond Angles [°]</b>		
N <sub>py</sub> –Pd–N <sub>bz/pz</sub>	77.81(8)	83.61(6)
N <sub>py</sub> –Pd–Cl	-	88.05(5)
N <sub>py</sub> –Pd–C	93.29(10)	-
N <sub>py</sub> –Pd–P	172.44(6)	175.48(5)
P–Pd–C/Cl	87.55(8)	90.12(8)

### 4.3.3 Catalytic high pressure hydrogenation reactions of alkenes and alkynes

Preliminary investigations of the benzoazole and pyrazolyl Pd(II) complexes **8-18** as catalyst precursors for the high pressure hydrogenation were performed using styrene as a model substrate. In a typical reaction, styrene (0.74 mL, 8.00 mmol), complex **8** (0.02 mmol (0.31 mol%, substrate:catalyst ratio of 400:1) in toluene (50 mL) was reacted with H<sub>2</sub> (5 bar) at a stirring speed of 600 rpm (Scheme 4.2). Control experiments were conducted without any catalyst under similar reaction conditions and conversions of 3% and 6% were obtained after 1 h and 6 h, respectively.



Scheme 4.2: Catalytic hydrogenation of styrene using Pd(II) complexes, **8-18**.

These observations indicated that complexes **8-18** were responsible for the higher conversions of the alkenes in the hydrogenation than the reactions carried out without the catalysts. All the complexes showed significant catalytic activities in the hydrogenation of styrene to ethylbenzene giving conversions between 17%-98% within 1 h for the benzoazole Pd(II) complexes **8-13** and conversions of between 66%-99% after 2 h for the pyrazolyl Pd(II) complexes **14-18** (Figure 4.8).

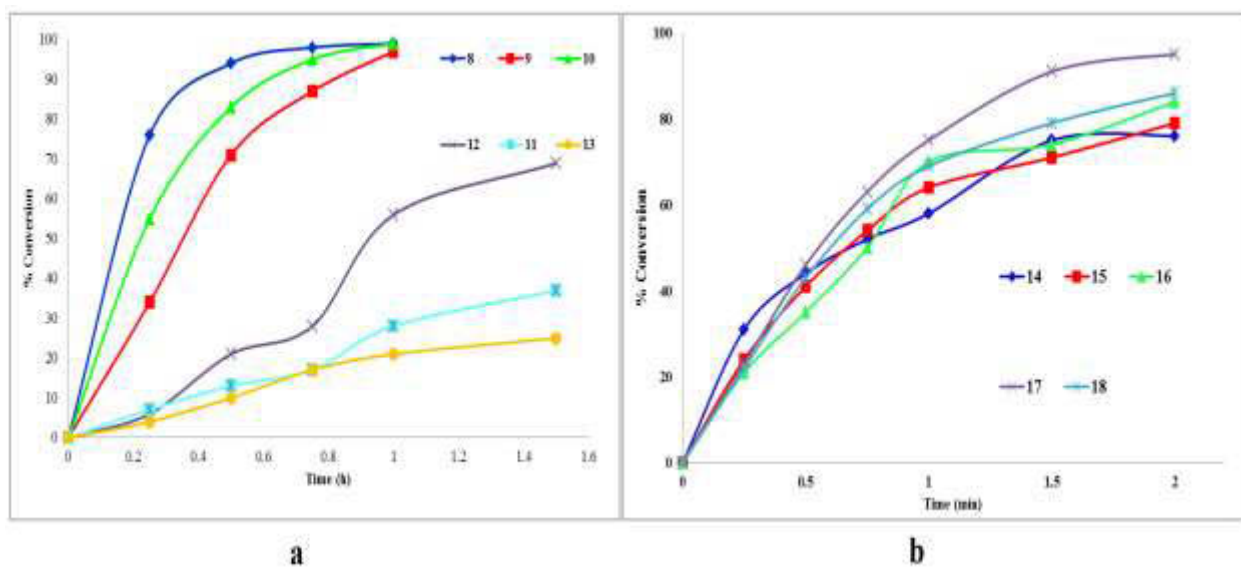


Figure 4.8: Time-dependence of high pressure hydrogenation of styrene by (a) benzoazole Pd(II) complexes **8-13** and (b) pyrazolyl Pd(II) complexes **14-18**.

After establishing that complexes **8-18** were effective catalysts, in-depth mechanistic, kinetic and theoretical studies were carried to evaluate the effect of catalyst structure and some reaction parameters. Parameters such as catalyst loading, hydrogen pressure, substrate and temperature were investigated using styrene as a model substrate. The chemo-selectivity of complexes **8** and **15** towards hydrogenation and isomerization products was also studied.

#### **4.3.4 Kinetic of hydrogenation reactions**

##### **4.3.4.1 Effect of catalyst structure on the hydrogenation of styrene**

In order to investigate the effect of the catalyst structure, hydrogenation reactions of styrene were carried out using (pyridyl)benzoazolepalladium(II) and (pyrazolyl)pyridinepalladium(II) complexes **8-18** as catalysts.

###### **4.3.4.1.1 (Pyridyl)benzoazolepalladium(II) complexes 8-13**

The data obtained for the hydrogenation of styrene to ethylbenzene using (pyridyl)benzoazolepalladium(II) complexes **8-13** are contained in Table 4.3a. The plot of  $\ln[\text{Sty}]_0/[\text{Sty}]_t$  versus time (Figure 4.9a) was used to compare the rates of hydrogenation using complexes **8-13**. From the results obtained, catalytic activities of complexes **8-13** were found to be dependent on the nature of the catalyst. It was observed that the identities of the ligands and the electrophilicity of the metal centre influenced the catalytic activities. For example, the neutral complex **8** bearing the 2-(2-pyridyl)beizimidazole ligand recorded the highest catalytic activity corresponding to an initial rate constant ( $k_{\text{obs}}$ ) of  $6.24 (\pm 0.055) \text{ h}^{-1}$  followed by analogous oxazole and thiazole complexes **10** ( $4.26 (\pm 0.021) \text{ h}^{-1}$ ) and **9** ( $3.02 (\pm 0.225) \text{ h}^{-1}$ ), respectively (Figure 4.9(a)). The activity trend observed for the benzoazole dichloride Pd(II) complexes **8-10** could be attributed to the presence of the heteroatom in the ligand.



The presence of the N-H moiety may have resulted to a more electrophilic metal centre, and hence the high reactivity observed. The ancillary ligands also affected the catalytic activities of the complexes. For example, complex [Pd(L1)MeCl] (**11**) was less active compared to the corresponding dichloride complex [Pd(L1)Cl<sub>2</sub>] (**8**) (0.30 (± 0.011) h<sup>-1</sup> vs 6.24 (± 0.055) h<sup>-1</sup>). This could be due to the difficulty in forming the palladium hydride species which is the catalytic active intermediate. This proposal is supported by the fragmentation pattern of complex **11**. The mass spectrum of complex **11** (Figure 4.4) shows a fragment of complex **11** with a coordinated Me ligand indicating that the Pd-Me bond is likely to be stronger than the Pd-Cl bond.

The cationic complexes [Pd(L1)PPh<sub>3</sub>Cl]Cl (**12**) and [Pd(L1)PPh<sub>3</sub>Me]BAR<sub>4</sub> (**13**) showed an initial rate constants of 0.72 (± 0.006) h<sup>-1</sup>, and 0.21(± 0.011) h<sup>-1</sup>, respectively, which were much lower than the neutral complex, **8** (6.24 (± 0.055) h<sup>-1</sup>) (Figure 4.9(a)). The low catalytic activities of complexes **12** and **13** could be attributed to the presence of the PPh<sub>3</sub> ligands. It was proposed that the formation of active Pd-hydride and or Pd-alkene/alkyl intermediates may be hindered due to the strong bond formed between palladium and PPh<sub>3</sub>.<sup>210b</sup> Besides, it has been reported that PPh<sub>3</sub> is a poor leaving group compared to Cl.<sup>232</sup> Salvi *et al.* reported a significant drop in the hydrogenation of 1-hexene from 54.5% to 2.5% using catalyst Ru(CO)<sub>2</sub>(OAc)<sub>2</sub>(P<sup>n</sup>Bu<sub>3</sub>)(PC<sub>6</sub>H<sub>5</sub>) and Ru(CO)<sub>2</sub>H<sub>2</sub>(P<sup>n</sup>Bu<sub>3</sub>)(PC<sub>6</sub>H<sub>5</sub>) catalysts, respectively.<sup>152</sup> In addition, the PPh<sub>3</sub> is likely to sterically hinder or limit substrate coordination to the metal centre.<sup>233</sup>

Table 4.3a: Effect of reaction parameters on the hydrogenation of styrene by benzoazole complexes **8-13**<sup>a</sup>

Entry	Catalyst	Sub/Cat	Time (h)	Conversion (mol%) <sup>b</sup>	Initial rates $k_{\text{obs}}(\text{h}^{-1})$ (error bar)	TOF( $\text{h}^{-1}$ ) <sup>c</sup>
1	<b>8</b>	400	0.75	98	6.24 ( $\pm 0.055$ )	523
2	<b>9</b>	400	0.75	73	3.02 ( $\pm 0.225$ )	389
3	<b>10</b>	400	0.75	87	4.26 ( $\pm 0.053$ )	464
4	<b>11</b>	400	0.75	17	0.30 ( $\pm 0.011$ )	91
5	<b>12</b>	400	0.75	28 (69) <sup>d</sup>	0.72 ( $\pm 0.068$ )	149(368)
6	<b>13</b>	400	0.75	17	0.21 ( $\pm 0.011$ )	91
7	<b>8</b>	400	0.5	71	-	1136
8	<b>8</b>	600	0.5	66	-	1584
9	<b>8</b>	800	0.5	53	-	1696
10	<b>8</b>	1200	0.5	15	-	720
11 <sup>e</sup>	<b>8</b>	400	6	06	-	4.8
12 <sup>f</sup>	<b>8</b>	400	0.5	85	-	680
13 <sup>g</sup>	<b>8</b>	400	0.25	81	-	1296
14 <sup>h</sup>	<b>8</b>	400	0.75	55	-	110

<sup>a</sup>Conditions: styrene, 8.00 mmol; catalyst, 0.02 mmol (0.31 mol%); 5 bar; toluene, temperature, 30 °C; time = 2 h

<sup>b</sup>Determined by GC. <sup>c</sup>TOF in mol substrate. mol<sup>-1</sup> catalyst.h<sup>-1</sup> <sup>d</sup>Time= 0.5 h

<sup>e</sup>25 °C, <sup>f</sup>50 °C, <sup>g</sup>60 °C

<sup>h</sup>Mercury drop test (5 drops of mercury added to the reaction mixture)

#### 4.3.4.1.2 (Pyrazolyl)pyridinepalladium(II) complexes 14-18

The data obtained for the hydrogenation of styrene using (pyrazolyl)pyridinepalladium(II) complexes **14-18** are recorded in Table 4.3b. Figure 4.9(b) shows the observed rate constants ( $k_{\text{obs}}$ ) for complexes **14-18**. From the rate constants of reactions of individual complexes, the order of activity was as follows;  $[\text{Pd}(\text{L5})\text{PPh}_3\text{Cl}]\text{BAr}_4$  (**18**)  $\gg$   $[\text{Pd}(\text{L5})\text{MeCl}]$  (**16**)  $>$   $[\text{Pd}(\text{L5})\text{PPh}_3\text{Cl}]\text{Cl}$  (**17**)  $>$   $[\text{Pd}(\text{L6})\text{Cl}_2]$  (**15**)  $>$   $[\text{Pd}(\text{L5})\text{Cl}_2]$  (**14**). The neutral complexes **14** and **15** displayed comparable rate constants of  $0.830 (\pm 0.053) \text{ h}^{-1}$  and  $0.851 (\pm 0.041) \text{ h}^{-1}$ , implying that their catalytic activities were not influenced by the aryl group on the pyrazole rings. As opposed to the results obtained for the benzoazole complexes **12** and **13** the methylated pyrazolyl Pd(II) complex (**16**) and the cationic complexes **17** and **18** were more active compared to the corresponding neutral pyrazolyl complex **14**. The significant high catalytic activity of complex **18** could be attributed to the non-coordinating  $\text{BAr}_4^-$  anions in comparison to the coordinating  $\text{Cl}^-$  anions. This results in an unsaturated Pd intermediate which is promotes substrate coordination to initiate the the hydrogenation process. The high solubility of the Pd-Me complex **16**, could explain its greater catalytic activity compared to complex **14**. Figure 4.9a shows that the  $k_{\text{obs}}$  of the benzoazole complexes **8-13** were approximately three times higher than those of pyrazolyl complexes **14-18** (Figure 4.9(b)). This was also evident on the time taken by the pyrazolyl complexes to achieve  $> 99\%$  conversion of the substrates. While it took approximately 45 min for benzoazole complexes **8-13** to achieve conversions of between 75-98%, pyrazolyl complexes **14-18** took a longer time (2 h) to obtain the same range of conversions. From kinetic studies, it was established that complexes **8-18** is a *pseudo-first* order reaction with respect to styrene. This can be represented as shown by the rate equation 4.1.

$$\text{Rate} = k[\text{Styrene}]^1 \dots\dots\dots \text{eq. 4.1}$$

Table 4.3b: Effect of reaction parameters on the hydrogenation of styrene complexes **14-18**<sup>a</sup>

Entry	Catalyst	Sub/Cat	Time (h)	Conversion (mol%) <sup>b</sup>	Initial rates $k_{\text{obs}}$ (h <sup>-1</sup> ) (error bar)	TOF(h <sup>-1</sup> ) <sup>c</sup>
1	<b>14</b>	400	2	76	0.83 (± 0.053)	152
2	<b>15</b>	400	2	87	0.85 (± 0.041)	174
3	<b>16</b>	400	2	86	1.04 (± 0.034)	172
4	<b>17</b>	400	2	84	0.94 (± 0.042)	168
5	<b>18</b>	400	2	95	1.49 (± 0.042)	190
6	<b>15</b>	600	2	84	-	252
7	<b>15</b>	800	2	78	-	312
8	<b>15</b>	1200	2	55	-	330
9 <sup>d</sup>	<b>18</b>	400	2	08	-	16

<sup>a</sup>Conditions: styrene, 8.00 mmol; catalyst, 0.02 mmol (0.31 mol%); 5 bar; toluene, temperature, 30 °C; <sup>b</sup>Determined by GC. <sup>c</sup>TOF in mol substrate. mol<sup>-1</sup> catalyst.h<sup>-1</sup>

<sup>d</sup>Mercury drop test (5 drops of mercury added to the reaction mixture)

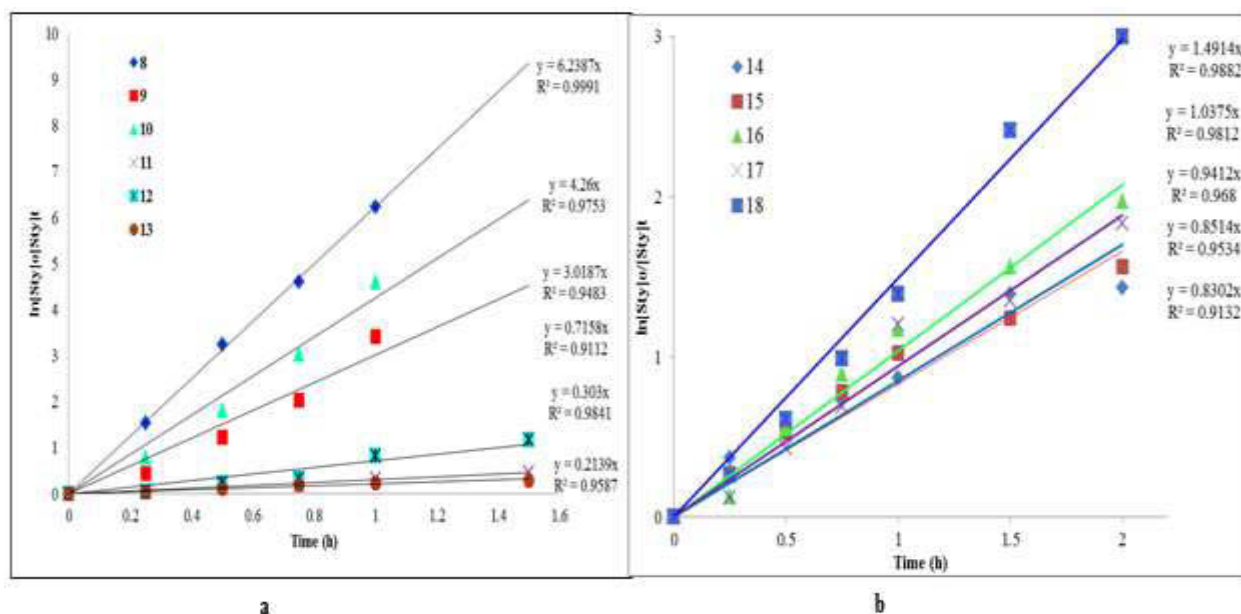


Figure 4.9: Plot of  $\ln[\text{Sty}]_0/[\text{Sty}]_t$  vs time for styrene hydrogenation with (a) **8-13** and (b) **14-18**

#### 4.3.4.2 Effect of catalyst concentration on the kinetic of reaction

Further kinetic experiments were performed to establish the effects of catalyst concentration on the hydrogenation using complexes **8** and **15**. The concentrations of complexes **8** and **15** were varied from  $1.0 \times 10^{-4}$  M to (1200:1) to  $3.0 \times 10^{-4}$  M (400:1). Plots of  $\ln[\text{Sty}]_0/[\text{Sty}]_t$  versus time (where  $[\text{Sty}]_0$  = initial concentration of styrene at time 0 and  $[\text{Sty}]_t$  = concentration of styrene at time t) gave a linear relationship (Figure 4.10). The initial rates constants ( $k_{\text{obs}}$ ) were determined for each reaction run and obtained from the slope of the graphs. The plots in Figure 4.10 show that the reaction rates were dependent on the substrate/catalyst (S/C) ratio concentration.

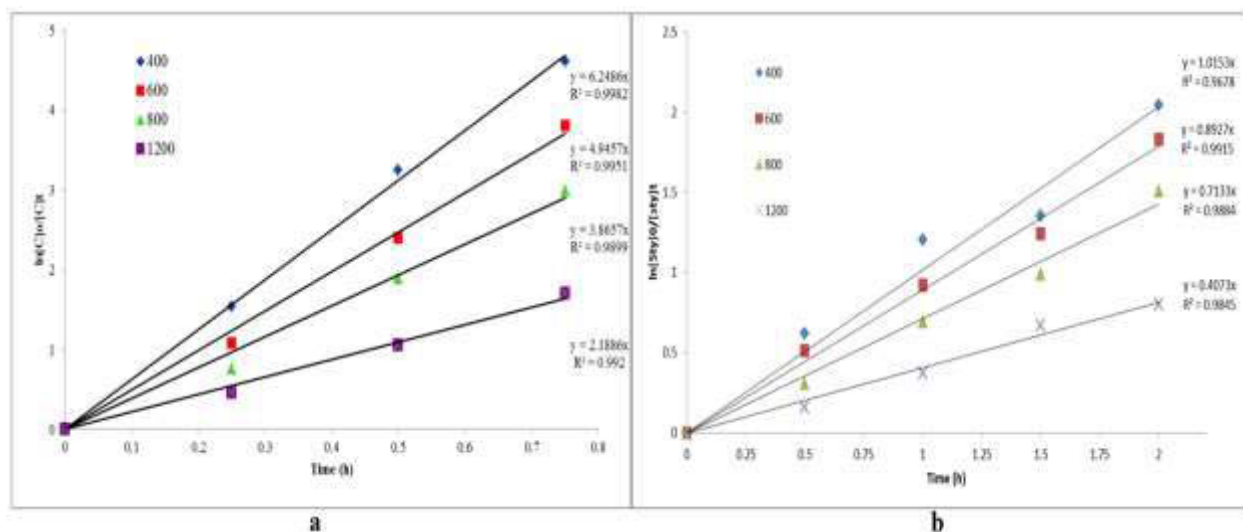


Figure 4.10: Effect of catalyst loading in hydrogenation of styrene using complexes (a) **8** and (b) **15**. Styrene, 8.00 mmol; pressure, 5 bar; temperature, 30 °C; solvent, toluene (50 mL); stirring speed, 600 rpm.

The rate constants of  $2.18 (\pm 0.011) \text{ h}^{-1}$  and  $6.24 (\pm 0.055) \text{ h}^{-1}$  were observed at S/C ratios of 1200 and 400, respectively (Figure 4.10a). Similarly, a higher a TOF of  $1696 \text{ h}^{-1}$  was reported for a S/C ratio of 800 compare to  $1136 \text{ h}^{-1}$  for 400 (Table 4.3a, entries 7 and 9). Further plots of  $-\ln(k_{\text{obs}})$  versus  $-\ln[\mathbf{8}]$  and  $-\ln[\mathbf{15}]$  were used to establish the orders of reactions with respect to catalysts **8** and **15** (Figure 4.11). The orders of reaction were obtained as  $0.94 (\pm 0.146) \text{ h}^{-1}$  and  $0.83 (\pm 0.187) \text{ h}^{-1}$  with respect to catalysts **8** and **15**, respectively (Figure 4.11). It could therefore be assumed that the hydrogenation reactions using catalyst **8** and **15** followed *pseudo-first* order kinetic (Figure 4.11). Thus the rate laws can be represented by equations 4.2 and 4.3.

$$\text{Rate} = k[\text{Styrene}]^1[\mathbf{8}]^{0.9} \dots\dots\dots \text{eq. 4.2}$$

$$\text{Rate} = k[\text{Styrene}]^1[\mathbf{15}]^{0.8} \dots\dots\dots \text{eq. 4.3}$$

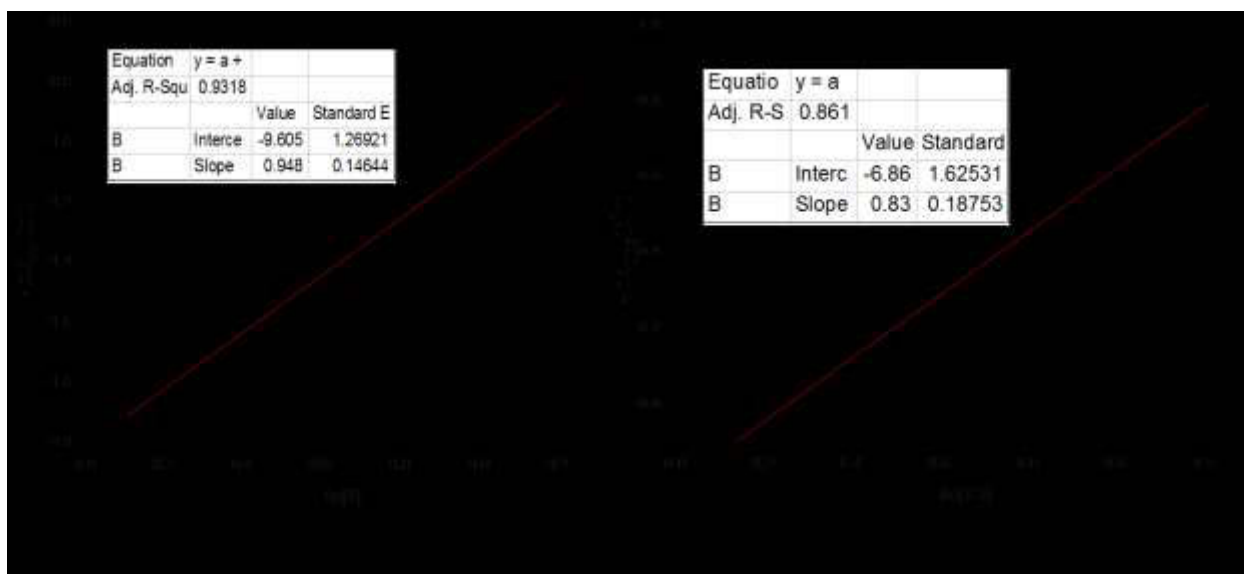


Figure 4.11: Plot of observed rate constants ( $k_{\text{obs}}$ ) versus catalyst concentration for complexes (a) **8** and (b) **15**

#### 4.3.4.3 Effect of hydrogen pressure on the kinetic of reactions

The influence of hydrogen pressure on the kinetic of the reaction was also investigated using complexes **8** and **15** by varying the pressure from 5 bar to 12.5 bar. Plots of  $\ln[\text{Sty}]_0/[\text{Sty}]_t$  versus partial pressures gave linear graphs (Figure 4.12). The observed rate constants ( $k_{\text{obs}}$ ) were obtained from the slopes of the graphs and were found to increase with increase in hydrogen pressure. For instance,  $k_{\text{obs}}$  of  $1.99 (\pm 0.041) \text{ h}^{-1}$  and  $3.13 (\pm 0.102) \text{ h}^{-1}$  were reported at  $p_{\text{H}_2}$  of 10 bar and 5 bar, respectively, using catalyst **15**. Plots of  $k_{\text{obs}}$  versus hydrogen pressures were used to determine the orders of reaction with respect to hydrogen pressure and were obtained as  $0.061 (\pm 0.009)$  and  $0.150 (\pm 0.036)$  for complexes **8** and **15**, respectively (Figure 4.13). Fractional and very low reaction orders with respect to hydrogen gas pressure as observed (Figure 4.13) are indicative of fast dissociative adsorption or dissociative desorption process. This is followed by surface reaction which is likely to be the rate determining step.<sup>234</sup>

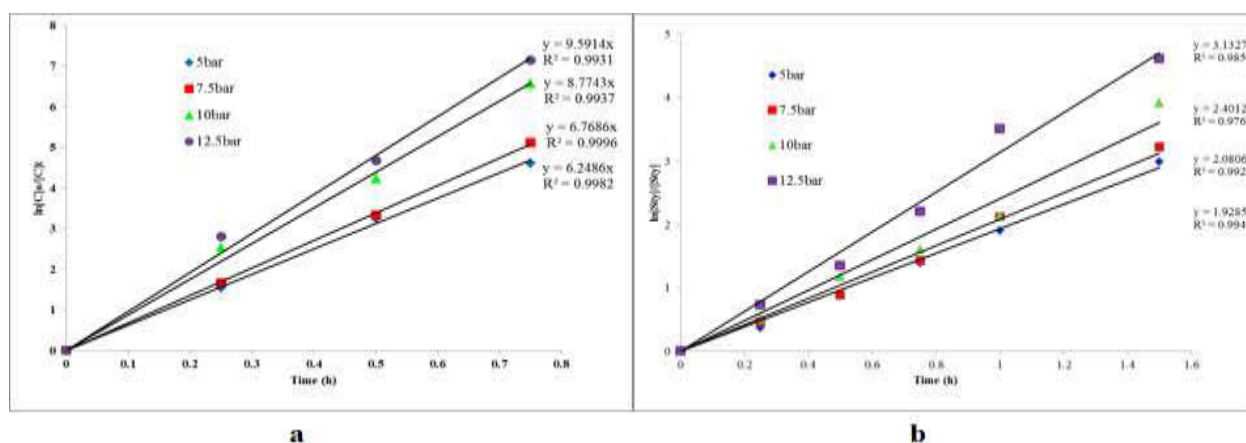


Figure 4.12: Effect of hydrogen pressure on hydrogenation of styrene using (a) complex **8** and (b) complex **15**. Styrene, 8.00 mmol. Pressure, 5 bar; temperature: 30 °C; solvent: toluene (50 mL); stirring speed, 600 rpm.

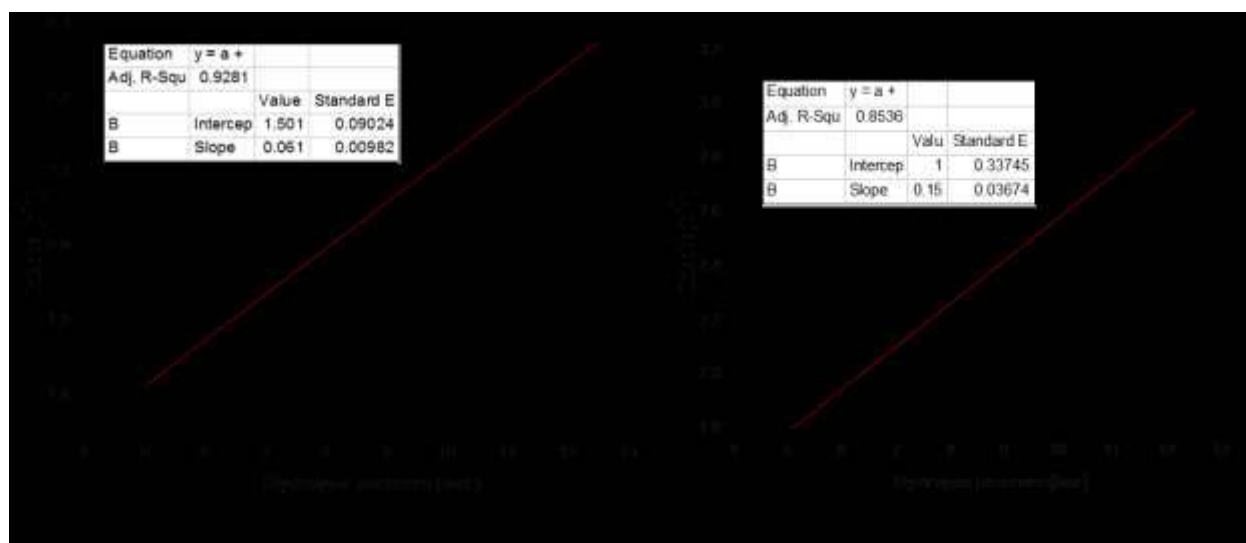


Figure 4.13: Plot of observed rate constants ( $k_{obs}$ ) versus hydrogen pressure (a) **8** and (b) **15**

Thus, the overall rate laws for styrene hydrogenation by complexes **8** and **15** can be represented by the equations 4.4 and 4.5 respectively.

$$Rate = k[styrene]^1[\mathbf{8}]^{0.9}[pH_2]^{0.06} \dots \dots \dots \text{eq. 4.4}$$



$$\text{Rate} = k[\text{styrene}]^1[\mathbf{15}]^{0.8}[\text{pH}_2]^{0.15} \dots \text{eq. 4.5}$$

#### 4.3.4.4 Effect of temperature on hydrogenation of styrene

The effect of temperature on the conversion of styrene was studied by varying the reaction temperature between 25 °C and 60 °C at S/C of 400 using complexes **8** and **15**. At 25 °C temperature only 6% (TOF = 4.8 h<sup>-1</sup>) molar conversion of styrene was obtained after 5 h while conversions of 81% (TOF = 1268 h<sup>-1</sup>) at 15 min was obtained at 60 °C. (Table 4.3a, entries 11 and 13). Generally, rate constants increased with increase in temperature. For example, while a rate constant of 3.58 (± 0.269) h<sup>-1</sup> was observed at 30 °C, a higher value of 5.34 (± 0.466) h<sup>-1</sup> was recorded at 60 °C. In both cases the formation of Pd black was not observed. This signifies the stability of the complexes at these reaction temperatures.

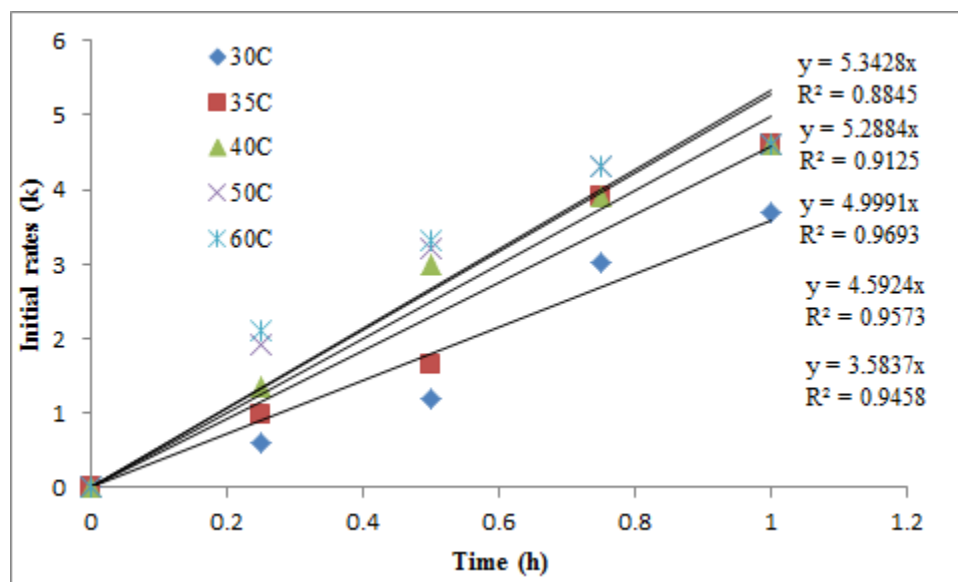


Figure 4.14: Effect of temperature on the kinetic of hydrogenation of styrene using complex **8**:

Substrate (8.00 mmol); Pressure: 5 bar; Solvent; toluene (50 mL); Stirring speed; 600 rpm.

#### 4.3.4.5 Effects of substrates on the kinetic of hydrogenation

The effect of different substrates on the hydrogenation behaviour of complexes **8** and **15** was also evaluated. The substrates, 1-hexene, 1-octene, 1-hexyne, 1-octyne and phenylacetylene were investigated under similar reaction conditions. It was observed that the catalytic activities of complexes **8** and **15** depended on the nature of substrate. Plots of  $\ln[\text{Substrate}]_0/[\text{Substrate}]_t$  versus time were used to determine the initial rate constants with respect to each substrate (Figure 4.15). From the data obtained, alkynes exhibited higher rate constants compared to the corresponding alkenes. For example, 1-hexyne showed a rate constant of  $6.38 (\pm 0.281) \text{ h}^{-1}$  while 1-hexene had a rate constant of  $0.49 (\pm 0.027) \text{ h}^{-1}$  (Figure 4.15a). This could be attributed to the high reactivity of alkynes compared to alkenes.<sup>235,236</sup> Another explanation to this observation would be the difference mode of hydrogenation of alkynes and alkenes. Teschner *et al.* reported that the hydrogenation of alkynes occur via surface hydrogen while that of alkenes occur by subsurface hydrogen.<sup>136</sup> This might further explain the observed higher reactivities of alkynes compared to alkenes towards hydrogenation.<sup>237</sup>

Furthermore, the catalytic activities were also found to be dependent on the alkyl chain length: the shorter the chain the higher the activity. For example, 1-hexene and 1-octene exhibited rate constants of  $1.63 (\pm 0.324) \text{ h}^{-1}$  and  $1.12 (\pm 0.197) \text{ h}^{-1}$ , respectively (Figure 4.15b). The same trend was observed in the activities of the 1-hexyne and 1-octyne exhibiting rate constants of  $6.38 (\pm 0.286) \text{ h}^{-1}$  and  $6.06 (\pm 0.249) \text{ h}^{-1}$  respectively (Figure 4.15a).

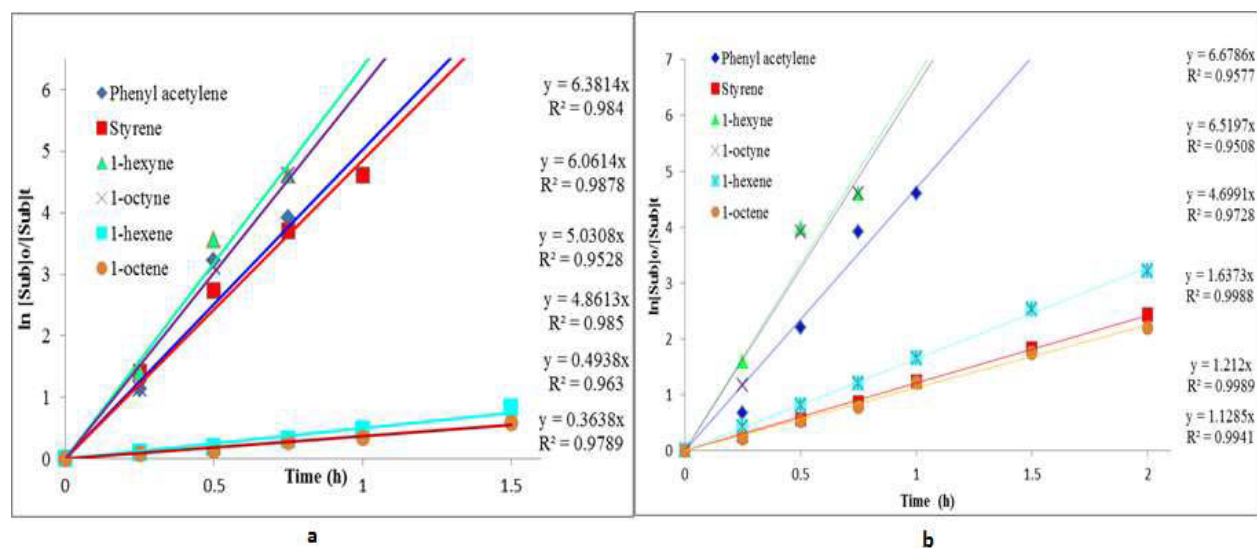


Figure 4.15: Effect of substrate on the kinetic of hydrogenation of alkenes and alkynes using complex **8** (a) and complex **15** (b). Substrate, 8.00 mmol; pressure, 5 bar; temperature, 30 °C; solvent, toluene (50 mL); stirring speed, 600 rpm.

### 4.3.5 Chemo- and regio-selectivity of hydrogenation reactions

#### 4.3.5.1 Isomerization of terminal alkenes and alkynes

The selectivity towards hydrogenation reactions was studied using benzoazole and pyrazolyl Pd(II) complexes **8** and **15**. The hydrogenation of the terminal alkenes and alkynes were observed to be accompanied by isomerization reactions. The linear  $\alpha$ -alkene and alkyne substrates were isomerized to their corresponding internal alkenes in addition to complete hydrogenation to respective alkanes (Figure 4.16). These observations are typical of palladium and other noble metal hydrogenation catalysts due to the existence of empty *d*-orbitals which interact with the  $\pi$ -orbitals of the alkenes and alkynes in the process of activating the adjacent C-H bonds.<sup>238</sup> The % catalytic activity and chemo- and regio-selectivities of the hydrogenation of 1-hexene and 1-octene are shown in Figure 4.17 (a) and Figure 4.17(b), respectively.

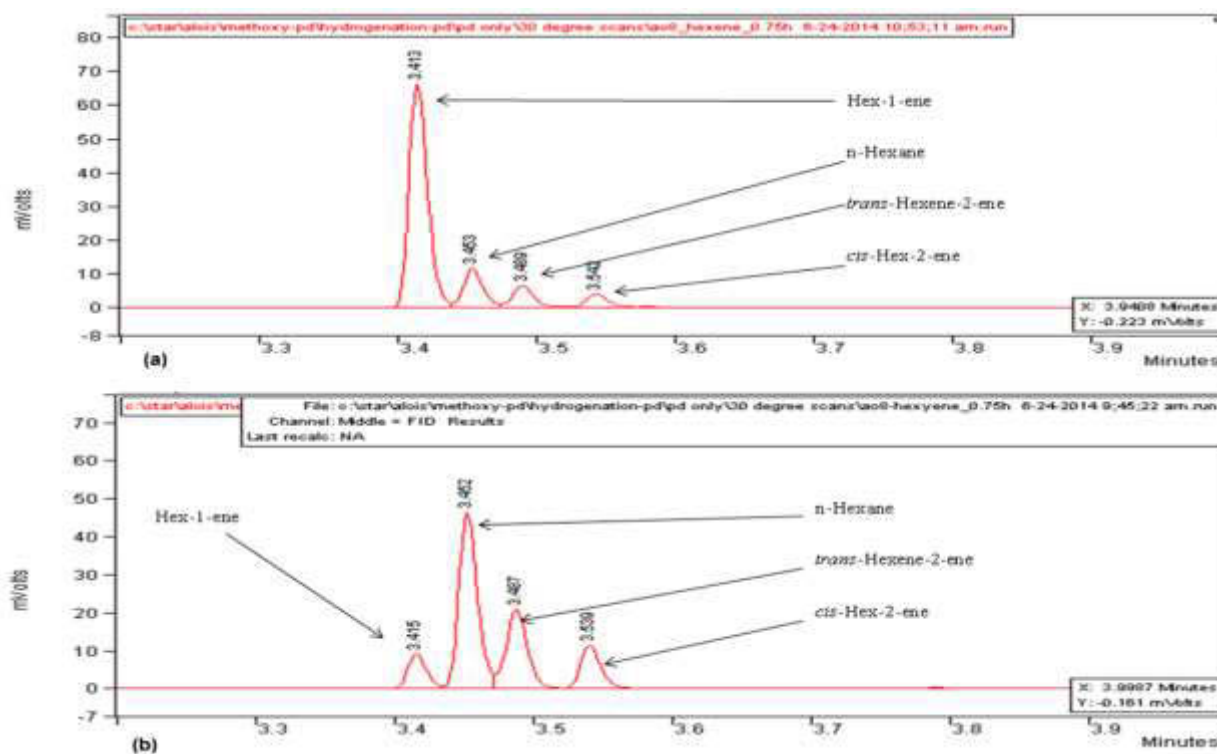


Figure 4.16: GC spectra showing isomerization of (a) 1-hexene and (b) 1-hexyne

It was observed that the isomerization of the alkenes led to reduction of catalytic activity. This could be attributed to the steric hindrance by the alkyl groups on both sides of the double bonds of the formed internal hexenes and octenes preventing further hydrogenation to corresponding alkanes.<sup>239,240</sup> The internal double bonds also exhibit a higher energy barrier to hydrogenation compared to terminal isomers.<sup>152</sup> Interestingly, this was not observed with the pyrazolyl complex **15** which recorded higher activities for 1-hexene and 1-octene compared to styrene. From Figure 4.17(a), out of the 27% conversion reached after 45 min reaction time, 49% of the products were n-hexane while 51% were internal hexenes (*cis*- and *trans*-2-hexene). The internal hexene products were generally distributed in the ratio of 2:3 for *cis*: *trans*- isomers. The larger composition of *trans*- 2-hexene could be due to reduced steric interactions of the alkyl substituents in the *trans*- isomer (Figure 4.17).<sup>241,242</sup>

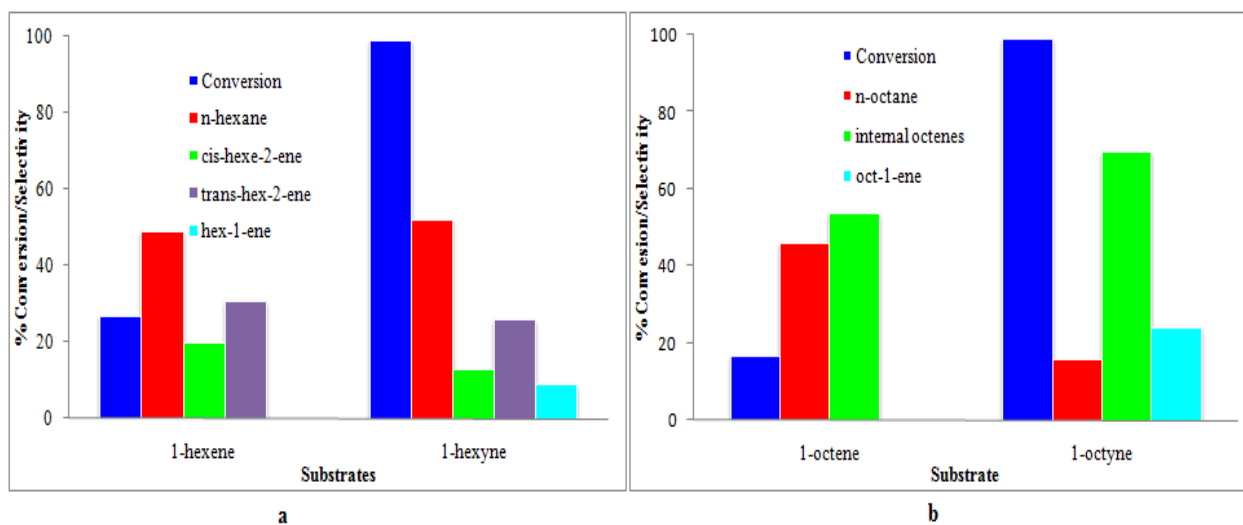


Figure 4.17a: Hydrogenation and isomerization of (a) 1-hexene and 1-hexyne; (b) 1-octene and 1-octyne using catalyst **8**. H<sub>2</sub> pressure; 5 bar; temperature; 30 °C; Solvent; toluene (50 mL); stirring speed; 600 rpm; time; 45 min.

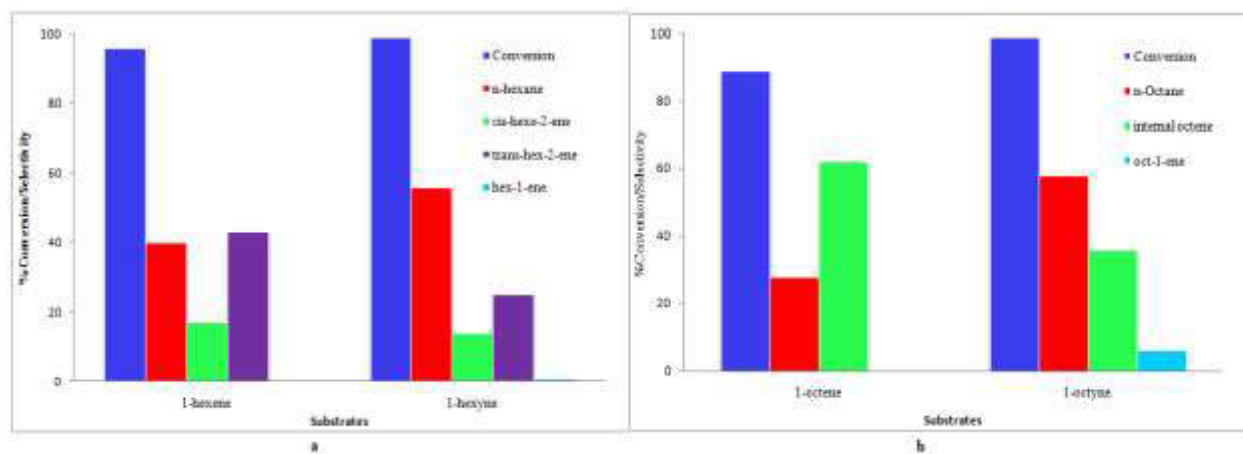


Figure 4.17b: Hydrogenation and isomerization of (a) 1-hexene and 1-hexyne, (b) 1-octene and 1-octyne, using catalyst **15**. H<sub>2</sub> pressure: 5 bar; temperature: 30 °C; Solvent: toluene (50 mL); Stirring speed: 600 rpm; Time: 45 min.

#### 4.3.5.2 Effect of time on chemo-selectivity of hydrogenation of 1-hexene

Further isomerization studies were performed using 1-hexene to establish the effect of time on chemo-selectivity. Figure 4.18 shows the product distribution with time for the hydrogenation of 1-hexene by complexes **8** and **15**. A high selectivity (61%) towards n-hexane compared to *cis*- and *trans*-hex-2-ene in the first 30 min of reaction was observed (Figure 4.18a).

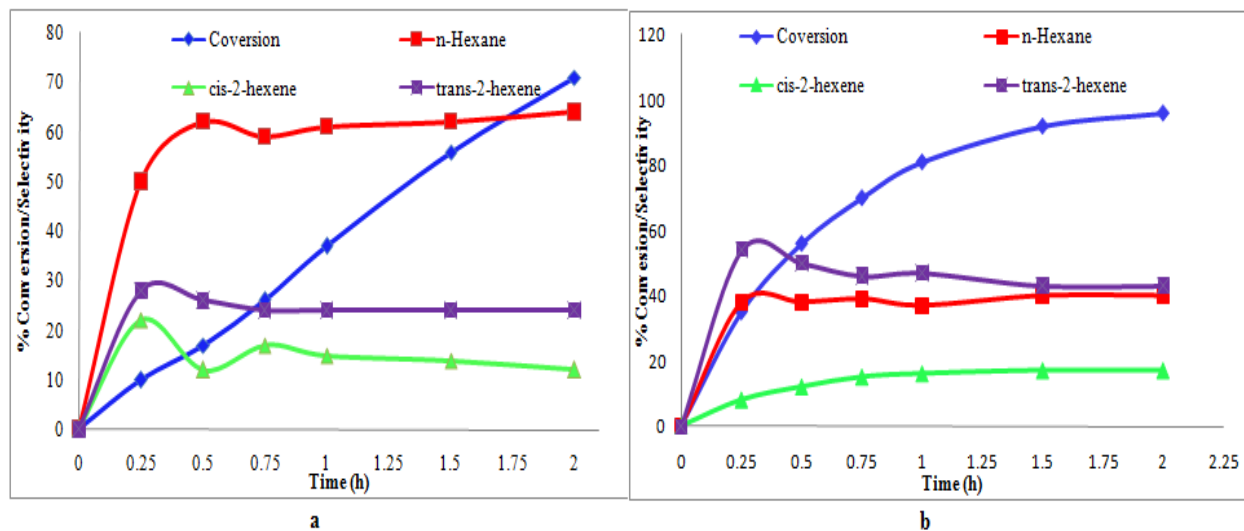
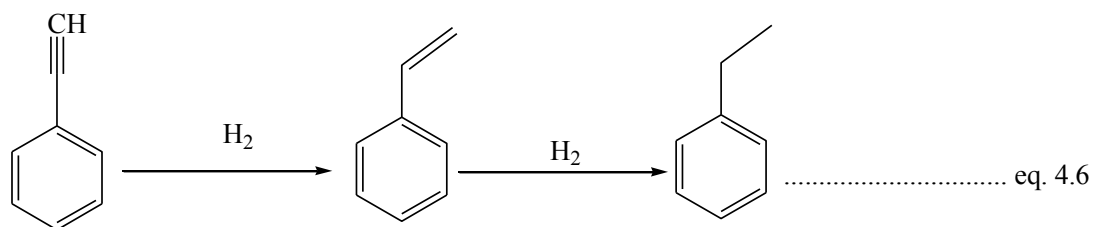


Figure 4.18: Conversion/selectivity vs. time profile for hydrogenation of 1-hexene using catalysts (a) **8** and (b) **15** H<sub>2</sub> pressure, 5 bar, temperature, 30 °C; solvent, toluene (50 mL); stirring speed, 600 rpm; time, 2 h.

The selectivity of complex **8** was not significantly affected with the increase in reaction time to 2 h. For example, after 30 min, 62% of the product mixture was n-hexane, 26% *trans* 2-hexene and 12% *cis*-2-hexene. After 2 h the percentage composition of the product mixture was n-hexane (64%), *trans*- 2-hexene (24%) and *cis*-2-hexene (12%). A fluctuation was observed in selectivities of the products (Figure 4.18a) at 0.75h and this may be attributed to analytical error. A similar trend was observed for the study conducted using pyrazoyl complex **15**.

However, the chemo-selectivity towards 2-hexene (55%) was higher than n-hexane (45%) indicating that complex **15** favoured an isomerization reaction over hydrogenation. This could explain the observed high conversion of terminal alkenes with pyrazolyl complex **15** compared to the benzoimidazole complex **8** (Figure 4.17(b) vs Figure 4.17(a)). The initial increase in the selectivity towards *cis*-hex-2-ene could be assigned to isomerization of 1-hexene to a mixture of *cis*- and *trans*-hex-2-ene. The selectivity was observed to decrease with time and this may be as a result of the *cis*-2-hexene adopting a more stable conformation (*trans*-hex-2-ene), hence reducing its composition.<sup>77</sup>

The study of alkyne product distribution was also performed using complexes **8** and **15** and phenylacetylene as a substrate. The choice of phenylacetylene was due to its inability to undergo isomerization unlike other aliphatic alkynes. The products of the hydrogenation process were mixtures of ethylbenzene and styrene (eq 4.6). Figure 4.19 shows conversion/selectivity verses time profiles for the hydrogenation of phenylacetylene using catalysts **8** and **15**.



From Figure 4.19, it is clear that the concentration of ethylbenzene in the reaction mixture was minimal until all the phenylacetylene was reduced to styrene. At the same time, the production of styrene increased correspondingly to a maximum of 92% and 86% for **8** and **15**, respectively.

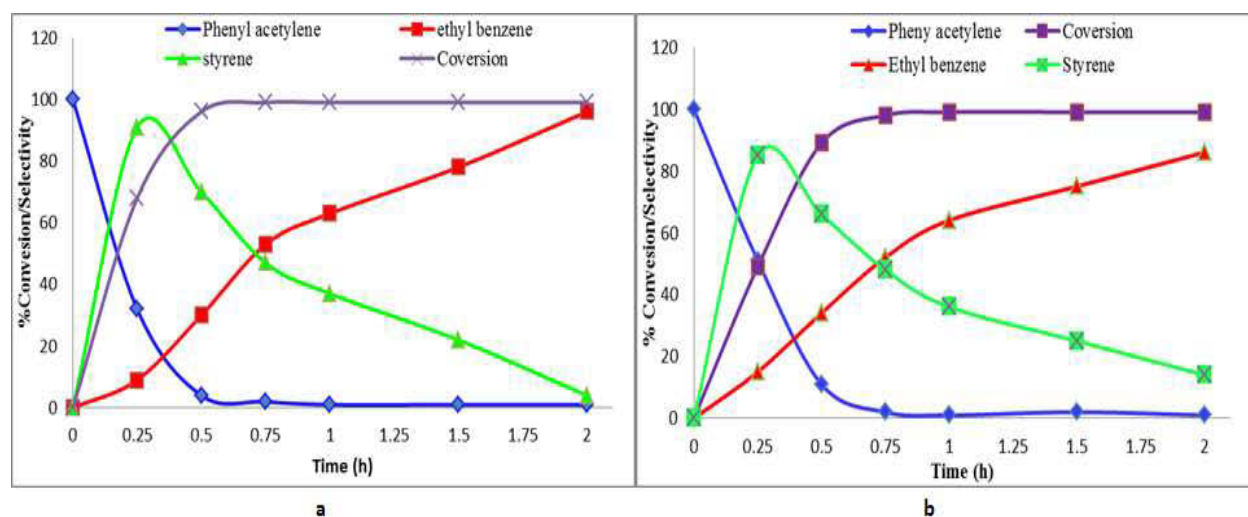


Figure 4.19: Conversion/ selectivity vs. time profile for hydrogenation of phenylacetylene using (a) **8** and (b) **15**. H<sub>2</sub> pressure: 5 bar; temperature, 30 °C; solvent, toluene (50 mL); stirring speed, 600 rpm; time, 2 h.

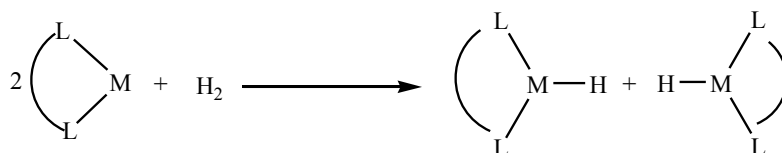
This suggested that the hydrogenation of phenylacetylene occurred in two steps; first hydrogenation to styrene followed by the hydrogenation of styrene to ethylbenzene.<sup>211b,243</sup> The graph in Figure 4.19(a) shows that after 15 min, there was 68% conversion of phenylacetylene of which 91% was styrene and 9% ethylbenzene. As the reaction time progressed, an increase in concentration of ethylbenzene followed by a concurrent decrease in the composition of styrene was observed.

At conversions above 99%, a continuous decrease of styrene substrate accompanied by the increase in the production of ethylbenzene was observed (Figure 4.19). This supported the proposed stepwise hydrogenation of alkynes which starts with conversion of alkynes (phenylacetylene) to alkenes (styrene) followed by hydrogenation of alkenes to the corresponding alkanes (ethylbenzene).<sup>244</sup>



### 4.3.6 Proposed mechanism of styrene hydrogenation

The mechanism of hydrogenation reaction catalysed by transition metal catalysts was first proposed in the early 1930s by Horiti and Polanyi to be initiated by molecular hydrogen cleavage by the metal complexes to form metal hydrides (Scheme 4.3).<sup>245,246</sup> This is followed by adsorption and subsequent addition of the hydrogen to the alkene and elimination of the alkane product completes the process resulting in catalyst regeneration.<sup>214</sup>



Scheme 4.3: Oxidative-addition of H<sub>2</sub> on a metal complex.

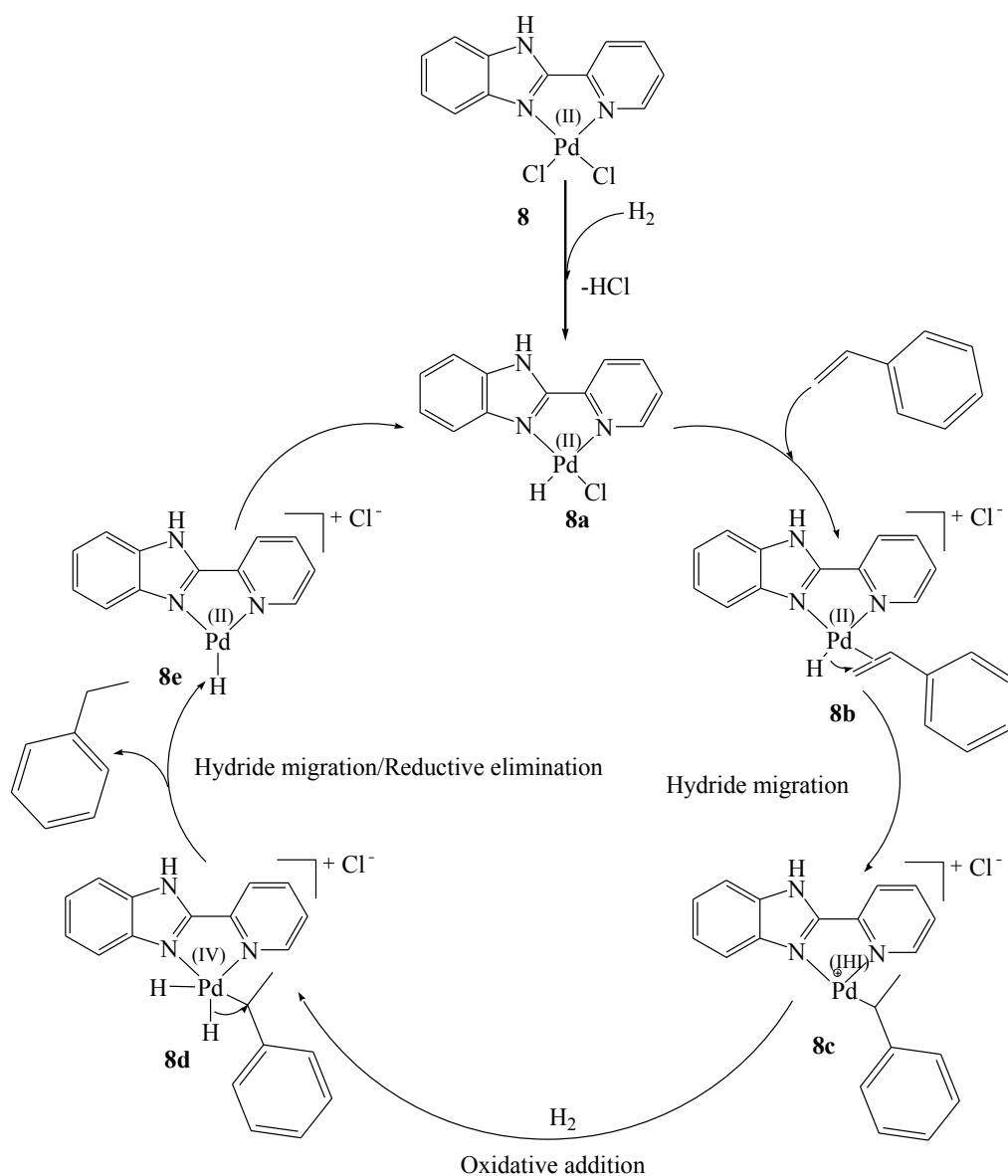
To understand the possible mechanism of alkene hydrogenation catalysed by complexes **8-18**, an experiment was conducted to first establish whether the active species were homogeneous or heterogeneous. Mercury poisoning tests<sup>247</sup> were conducted by adding 5 drops of mercury as a selective poison to the reaction mixtures using complexes **8** and **18**. The resulting conversions were significantly lower compared to those carried out in the absence of mercury. For example, the 98% (TOF = 523 h<sup>-1</sup>) conversions by complex **8** reduced to 55% (TOF = 110 h<sup>-1</sup>) (Table 4.3a, entries 1 and 14). Similarly, complex **18** showed a drastic decline from 95% (TOF = 190 h<sup>-1</sup>) to 8% (TOF = 16 h<sup>-1</sup>) (Table 4.3b, entries 5 and 9). This suggested that the active catalysts were either colloidal or made of nanoparticles.

Metal nanoparticles, when used as catalysts, are known to aggregate/agglomerate reducing the active surface of the catalyst and leading to loss of activity as observed in this experiment.<sup>248</sup>

The formation of these colloids/nanoparticles could be attributed to the presence of chloride ligands in the outer sphere of the complexes. Anionic ligands such as chlorides are known to stabilize colloids/nanocluster.<sup>247b,249</sup> Previous reports indicate that under an H<sub>2</sub> atmosphere soluble complexes can easily form nanoparticles.<sup>131,250</sup>

Since complexes **8-18** are coordinatively saturated, ligand dissociation would be necessary prior to the formation of Pd-hydride intermediate.<sup>210b</sup> The chloride ligand dissociates by heterolytic cleavage which leads to formation of the Pd-hydride. The dissociated chloride ion (Cl<sup>-</sup>) combines with hydrogen ion (H<sup>+</sup>) to form HCl.<sup>210b</sup> This is a significant step in the generation of the active hydrogenation intermediate<sup>251</sup> and depends on the relative strengths of metal-ligand bonds.<sup>210b</sup> In order to form Pd-hydride intermediates with complexes **8-18**, secondary ligands (chloride and PPh<sub>3</sub>) were proposed to dissociate from the Pd complexes **8-18**.<sup>252</sup>

The mono-hydride route is characterized by selectivity towards terminal unsaturated hydrocarbons and production of isomers.<sup>253</sup> Upon coordination of the alkene substrate, the coordinated hydride is transferred to form a Pd-alkyl intermediate.<sup>254</sup> Using complex **8**, a loss of one chloride ligand in the presence of hydrogen gas to form palladium monohydride is proposed, **8a**, accompanied by release of HCl (Scheme 4.4). The styrene substrate is then coordinated to the metal to form the cationic intermediate, **8b**. A Markovnikov migration of the hydride to the coordinated substrate leads to the formation of palladium alkyl intermediate **8c**. The intermediate **8c** undergo an oxidative addition in the presence of H<sub>2</sub> to give an alkyl Pd(IV) dihydride intermediate **8d**. Hydride migration to the coordinated alkyl ligand in **8d** followed by reductive elimination produces a monohydride Pd(II) intermediate **8e** and elimination of ethylbenzene product. The cycle is completed by the rearrangement of **8e** to form the neutral palladium hydride intermediated **8a**.



Scheme 4.4: Proposed mechanism for high pressure hydrogenation of styrene by complex **8**.

#### 4.3.7 TEM analysis

In order to ascertain if the palladium(II) complexes **8-18** indeed formed nanoparticles and thus were heterogeneous catalytic systems as suggested by the mercury poisoning test, a TEM analyses of the reaction mixtures after the end of the reaction were carried out. Figure 4.20 show TEM images of the benzoazole Pd(II) complexes.

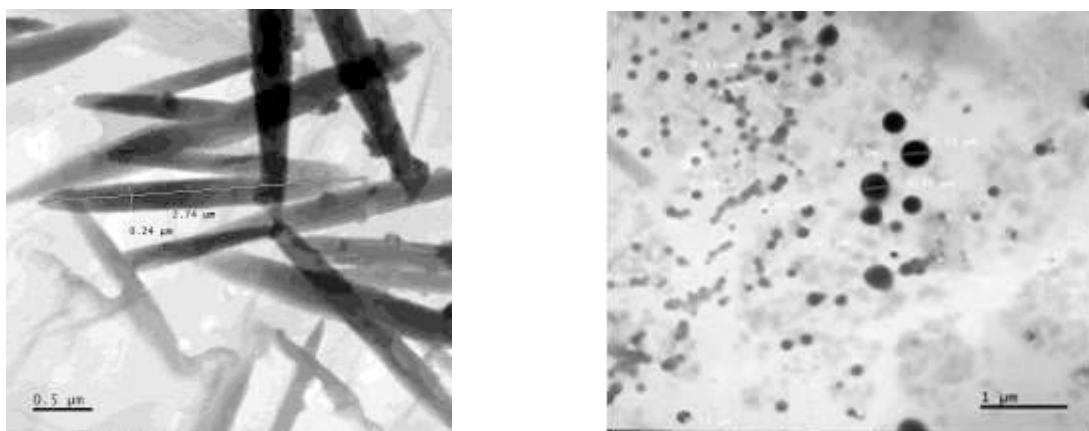


Figure 4.20: TEM image of complexes (a) **11** and (b) **12** isolated after catalytic reactions.

Figure 4.20 (b) is a TEM image showing particles for complex **12** after catalysis. These images indicate possible nanoparticle formation during the catalytic hydrogenation reactions. The particles were probably ligand stabilized as confirmed by the EDX analyses of the samples after the reaction. The particles size varied between 40-330 nm and could be attributed to the uncontrolled reaction conditions which are required to produce uniform nanoparticles.<sup>255</sup>

The formation of nanoparticles was not expected before the experiments and their formation took place in the process of catalytic reactions. The reaction conditions were probably not suitable for the formation of uniform size nanoparticles. The other possible reason for such wide variation and larger size particles could be due to particle aggregation which occurred during solvent evaporation.<sup>62,256</sup> The observed reduction in the catalytic activities of complexes **8** and **18** from TOF = 523 h<sup>-1</sup> to 55% (TOF = 110 h<sup>-1</sup>) and TOF = 190 h<sup>-1</sup> to 8% TOF = 16 h<sup>-1</sup>, respectively (Table 4.3a, entries 1 and 14) implies that the formed nanoparticles were possibly catalytic the active species in the hydrogenation reactions.

#### 4.3.8 DFT studies

Density functional theory calculations were performed on the palladium complexes **8-18** to further understand the effect of catalyst structure on catalytic activity. DFT calculations of complexes [Pd(**L1**)PPh<sub>3</sub>Cl]Cl (**12**), [Pd(**L1**)PPh<sub>3</sub>Me]BAr<sub>4</sub> (**13**), and [Pd(**L5**)PPh<sub>3</sub>Cl]Cl (**17**) were performed on their cations without their respective counterions. Frontier molecular orbitals of **8-17** calculated at B3LYP level using LANL2DZ basis set are shown in Figure 4.20. The highest occupied molecular orbitals, HOMOs of the Pd(II) complexes, **8-17** are predominantly occupied by the chloride ligand, Pd d-orbital electrons and one phenyl ring of the PPh<sub>3</sub> ligand while the lowest unoccupied molecular orbitals, LUMOs are occupied by Pd and benzoazole ligand d-orbitals for complexes **8-13** (Figure 4.21a) and Pd, pyridine moiety of the pyrazolyl ligand and PPh<sub>3</sub> for the complexes **14-17** (Figure 4.21b). From the DFT calculations, the activity trends of the benzoazole complexes **8-18** was observed to be dependent on the average of the bond lengths,  $\{(N_{Py} + N_{bz})/2\}$  and the HOMO-LUMO energy gap (eV).










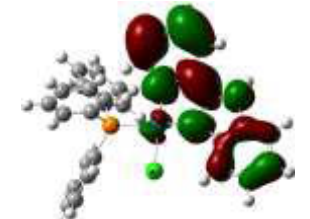


Complex	Homo	LUMO	Band Gap (eV)
8			2.8544
9			2.7334
10			2.7513
11			2.7304
12			2.4439
13			2.6096

Figure 4.21a: Frontier molecular orbitals of benzoazole Pd(II) complexes, **8-13** (as determined by density functional theory using B3LYP level of theory and LANL2DZ basis set (isovalue 0.02)).

The average bond lengths,  $\{(N_{py} + N_{bz})/2\}$ , were used to compare the relative stabilities of the complexes **8-18**. It was observed that the smaller the average bond length,  $\{(N_{py} + N_{bz})/2\}$ , the higher the HOMO-LUMO gap. The smallest average bond length for  $\{(N_{py} + N_{bz})/2\}$  of 2.0857 corresponded to the highest HOMO-LUMO gap energy of 2.854 (Table 4.4, entry 1). This was interpreted to mean that complex **8** was the most stable and was therefore less likely to decompose during the catalytic reaction. Indeed, complex **8** exhibited the highest initial rate constant of  $6.24 \text{ h}^{-1}$ . On the other hand complex **13** with the longest average bond distance,  $\{(N_{py} + N_{bz})/2\}$ , of 2.1953 Å and smallest energy gap of 2.360 eV was the least active exhibiting a rate constant of  $0.21 \text{ h}^{-1}$  (Table 4.4, entry 5). . Similarly, the pyrazolyl complex **17** which had the shortest average bond length,  $\{(N_{py} + N_{bz})/2\}$ , of 2.1003 Å and the highest HOMO-LUMO energy gap of 3.8169 eV was the most active compared to complex **15** which had the longest average bond length,  $\{(N_{py} + N_{bz})/2\}$ , of 2.1132 Å and the lowest energy gap of 3.5418 eV (Table 4.4, entries 7 and 8).

Table 4.4: Rate constants ( $k_{\text{obs}}$ ) dependence on the average Pd-N bond length and HOMO-LUMO gap for complexes, **8-17**

Entry	Complex	$k_{\text{obs}}$ ( $\text{h}^{-1}$ )	(Pd-N <sub>py</sub> + Pd-N <sub>bz</sub> )/2 (Å)	HOMO-LUMO GAP (ΔeV)
1	<b>8</b>	6.24 (± 0.055)	2.0857	2.854
2	<b>9</b>	3.02 (± 0.225)	2.1062	2.733
3	<b>10</b>	4.26 (± 0.053)	2.0914	2.751
4	<b>11</b>	0.30 (± 0.011)	2.1468	2.730
5	<b>13</b>	0.21(± 0.011)	2.1953	2.360
6	<b>14</b>	0.83 (± 0.053)	2.1081	3.8188
7	<b>15</b>	0.85 (± 0.041)	2.1132	3.5418
8	<b>17</b>	0.94 (± 0.042)	2.1003	3.8169

An exceptional observation was made for complex **12** which had a relatively lower HOMO-LUMO energy gap than complex **11** (2.443 eV vs 2730 eV) but was more active. Another exception was observed for complex **16**, among the pyrazolyl Pd complexes, which despite having both the longest average bond lengths and smallest energy gap compared to all other pyrazolyl complexes exhibited the higher rate constants than other pyrazolyl complexes. In general, The observed trend could be as a result of the relative stability of the two sets of Pd(II) complexes **8-18**. A similar trend where the activities of the benzoazole complexes **8-10** depended on the average  $\{(N_{\text{py}} + N_{\text{bz}})/2\}$  bond length was observed by Heneda *et al.* They observed that complex **8** was the most active followed by **10** and **9** giving conversions of 97%, 83% and 75% respectively in Mizoroki-Heck reactions and attributed this trend to the stability of the complexes as determined by the average bond lengths,  $\{(N_{\text{py}} + N_{\text{bz}})/2\}$ .<sup>257</sup>



Complex	Homo	LUMO	Band Gap (eV)
14			3.8188
15			3.5418
16			3.2460
18			3.8169

Figure 4.21b: Frontier molecular orbitals of pyrazolyl Pd(II) complexes **14-18** as determined by density functional theory using B3LYP level of theory and LANL2DZ basis set (isovalue 0.02).

The relative high reactivities of benzoazole Pd complexes **8-13** compared to pyrazolyl Pd complexes **13-18** were also in agreement with the corresponding low HOMO-LUMO gap energy. Generally, the benzoazole Pd complexes exhibited high gap energies of between 2.6096 eV and 2.8544 eV while the pyrazolyl Pd complexes have the energies of between 3.2460 eV and 3.8188 eV.

#### 4.4 Conclusions

Pd(II) complexes of (2-(2-pyridyl)benzoazole and (2-(3,5-dialkylpyrazol-1-ylmethyl)pyridine ligands have been successfully synthesized, structurally characterized and evaluated in high pressure hydrogenation reactions of alkenes and alkynes. Solid state structures of complexes **13** and **18** showed that both (pyridyl)benzoazole and (pyrazo-1-ylmethyl)pyridine ligands adopted bidentate coordination modes. All the complexes formed active catalysts for high pressure hydrogenation of alkenes and alkynes under mild conditions. Catalytic activities of the complexes were influenced by steric and electronic contributions of the ligands. The benzoazole complexes **8-13** were more active compared to the pyrazolyl complexes **14-18**. Styrene was more reactive than non-conjugated aliphatic alkenes and hydrogenation of terminal linear alkenes were accompanied by isomerization reactions to form internal alkenes. Isomerization of the terminal alkenes favoured *trans*-2-alkenes over *cis*-2-alkenes. Higher activities were reported in the hydrogenation of alkynes compared to the corresponding alkenes. Palladium nanoparticles were the active species in the catalytic hydrogenation reaction and this was confirmed by mercury poisoning test and TEM analysis.

The kinetic of hydrogenation indicated that the reactions were *pseudo* first order with respect to the catalyst and substrate. Catalyst loading, hydrogen pressure and temperature also influenced the activity of the catalysts. DFT studies further showed that the activity trend of complexes **8-18** are controlled by the stability of the respective complexes *i.e.* the higher the stability the more active the complex. In summary, electronic and steric properties of the catalysts and the identity of the substrate have been established to affect their overall activity in the high pressure

hydrogenation of alkenes and alkynes. Hydrogenation of terminal alkenes and alkynes are accompanied by isomerization reactions.

## CHAPTER 5

### **Cationic Pyridyl(benzoazole)ruthenium(II) complexes: Efficient and recyclable catalysts in biphasic hydrogenation of alkenes and alkynes**

This chapter is adapted from the paper published in *Appl. Catal. A: Gen.* **486** (2014) 250-258 and is based on the experimental work of the first author, Aloice O. Ogwen. Copyright 2014 Elsevier B.V. The contributions of the first author include synthesis and characterization of the ligands and complexes, catalysis experiments and drafting the manuscript.

#### **5.1 Introduction**

Catalysis is a major player in the manufacturing and processing industries with an estimated 85% of fine and bulk chemicals being produced through heterogeneous or homogenous processes.<sup>258,259</sup> Homogenous catalysis is preferred over heterogeneous systems mainly because of high activity and selectivity in addition to understanding of the mechanisms involved.<sup>260-263</sup> Despite these advantages, homogeneous catalysis is still facing several challenges. Most notable are limited catalyst recovery, use of toxic organic solvents and contamination of the products.<sup>264-266</sup> These setbacks have contributed to the limited industrial applications of homogenous catalysts, especially in the production of fine chemicals and pharmaceutical products. On the other hand, heterogeneous catalysis offers the possibility for catalyst recovery and recycling, use of less toxic solvents, and hence, greater purity of products.<sup>267,268</sup>

While significant progress has been made in developing heterogeneous systems, some drawbacks have been experienced over time. Low catalyst activities, poor selectivity and inability to establish their reaction mechanisms are some of the challenges which have undermined their

progress.<sup>259</sup> To overcome these drawbacks associated with both homogenous and heterogeneous processes, another approach of heterogenization of homogenous systems has emerged. This has been achieved by various methods such as anchoring of single site catalysts on organic or inorganic supports and the use of multiphase operations.<sup>269,270</sup> The overall aim of these strategies is to maximize the advantages of both homogenous and heterogeneous systems, which is to enhance catalyst separation from the reaction mixture while maintaining the selectivity and activity of the catalysts.

Biphasic catalysis employing water soluble complexes has attracted great attention since its successful industrial application in hydroformylation reactions.<sup>271,272</sup> Thus, the design of water-soluble catalysts in other organic transformations such as alkene hydrogenation is significantly gaining momentum.<sup>273</sup> To date, numerous water soluble transition metal based catalysts have been applied in various transition-metal catalysed reactions.<sup>274</sup> Notable examples include highly efficient and recyclable rhodium catalysts supported on TPPTS (TPPTS =  $P(C_6H_4-m-SO_3Na)_3$ ) for the hydrogenation of benzene to cyclohexane.<sup>216</sup> In another related work, Syska *et al.* reported the use of water-soluble rhodium complexes containing carbene ligands in the catalytic hydrogenation of acetophenone.<sup>275</sup> In this chapter the synthesis and characterization of cationic  $\eta^6$ -(2-phenoxyethanol) ruthenium complexes containing 2-(2-pyridyl)benzazole ligands and their successful application in the catalytic hydrogenation of styrene, 1-hexene, 1-octene, 1-decene, 1-hexyne and 1-octyne in methanol is reported.

Biphasic catalytic experiments were conducted using water and toluene medium to demonstrate the recyclability of these catalysts. The influence of reaction parameters, such as time, substrate/catalyst ratio, temperature, aqueous/organic phase ratio and pressure have been investigated and are herein discussed.

## 5.2 Experimental

### 5.2.1 Materials and instrumentation

All reactions were carried out under a nitrogen atmosphere using a dual vacuum/nitrogen line and standard Schlenk techniques unless stated otherwise. Dichloromethane (ACS reagent,  $\geq 99.8\%$ ) was distilled from  $P_2O_5$  prior to use. The Ru(II) starting material,  $[\eta^6\text{-}(2\text{-phenoxyethanol})RuCl_2]_2$  was prepared according to literature procedures.<sup>276,277</sup> The ligands, 2-(2-pyridyl)benzimidazole (**L1**), 2-(2-pyridyl)bezothiazole (**L2**), 2-(2-pyridyl)bezoxazole (**L3**) were also prepared according to previous literature methods.<sup>278</sup> NMR spectra were recorded on a Bruker 400 Ultrashield instrument at room temperature in DMSO- $d_6$  solvent. The  $^1H$  (400 MHz) and  $^{13}C$  (100 MHz) chemical shifts are reported in  $\delta$  (ppm) and referenced to the residual proton in the solvents for  $^1H$  and to solvent signals for  $^{13}C$ . Coupling constants ( $J$ ) are measured in hertz (Hz). Elemental analyses were performed on Thermal scientific flash 2000 and mass spectra were recorded on a LC Premier micro-mass spectrometer in the micro-analysis laboratory at the University of KwaZulu-Natal, South Africa. GC analyses were carried out on a Varian CP-3800 GC (ZB-5HT column 30 m $\times$ 0.25 mm $\times$ 0.10  $\mu$ m) instrument.

## 5.2.2 Syntheses of cationic Ru(II) complexes

### 5.2.2.1 Synthesis of $[\eta^6\text{-(2-phenoxyethanol)RuCl}_2\text{L1}]\text{Cl}$ (**19**)

To a suspension of  $[\eta^6\text{-(2-phenoxyethanol)RuCl}_2\text{]}_2$  (0.10 g, 0.16 mmol) in  $\text{CH}_2\text{Cl}_2$  (10 mL) was added a solution of ligand **L1** (0.06 g, 0.31 mmol) in  $\text{CH}_2\text{Cl}_2$  (5 mL) and the mixture was stirred for 24 h. A yellow precipitate formed which was isolated by filtration and washed with  $\text{CH}_2\text{Cl}_2$  (15 mL) to give complex **19** as a yellow solid. Recrystallization by slow evaporation of a methanol solution of complex **19** at room temperature afforded single crystals suitable for X-ray analysis. Yield = 0.14 g (88%).  $^1\text{H}$  NMR ( $\text{DMSO-d}_6$ ):  $\delta$  3.64 (t, 2H, C-OH,  $^3J_{\text{HH}} = 4.8$  Hz); 4.14 (m, 2H, C-O-Ph); 5.56 (t, 1H, Ph,  $^3J_{\text{HH}} = 5.2$  Hz); 5.94 (d, 1H, Ph,  $^3J_{\text{HH}} = 5.2$  Hz); 6.13 (d, 1H, Ph,  $^3J_{\text{HH}} = 6.4$  Hz); 6.49 (m, 2H, ph); 7.57 (m, 2H, bz<sub>im</sub>); 7.82 (d, 2H, bz<sub>im</sub>,  $^3J_{\text{HH}} = 6.4$  Hz); 8.15 (d, 1H, py,  $^3J_{\text{HH}} = 6.8$  Hz); 8.36 (t, 1H, py,  $^3J_{\text{HH}} = 8.0$  Hz); 8.64 (d, 1H, py,  $^3J_{\text{HH}} = 8.0$  Hz); 9.61 (d, 1H, py,  $^3J_{\text{HH}} = 5.2$  Hz); 15.33 (s, 1H, N-H).  $^{13}\text{C}$  NMR (400 MHz,  $\text{DMSO-d}_6$ ):  $\delta$  59.31, 62.84, 64.59, 71.88, 72.15, 85.60, 91.49, 93.20, 118.71, 123.73, 125.18, 126.43, 127.47, 134.44, 138.66, 140.43, 141.45, 146.94, 150.53, 156.65. MS (ESI)  $m/z$  (%) 470.02( $\text{M}^+$ , 100). Anal. Calcd. For  $\text{C}_{20}\text{H}_{19}\text{Cl}_2\text{N}_3\text{O}_2\text{Ru} \cdot 0.5\text{CH}_2\text{Cl}_2$ : C, 44.94; H, 3.68; N, 7.67%. Found C, 44.58; H, 4.24; N, 7.77%.

The procedure used to prepare complex **19** was followed to synthesize complexes **20** and **21**.

### 5.2.2.2 Synthesis of $[\eta^6\text{-(2-phenoxyethanol)RuCl}_2\text{L2}]\text{Cl}$ (**20**)

To a suspension of  $[\eta^6\text{-(2-phenoxyethanol)RuCl}_2\text{]}_2$  (0.20 g, 0.32 mmol) was added ligand **L2** (0.14 g, 0.64 mmol). Yellow solid. Yield = 0.26 g (78%).  $^1\text{H}$  NMR ( $\text{DMSO-d}_6$ ):  $\delta$  3.66 (t, 1H, C-OH,  $^3J_{\text{HH}} = 4.8$  Hz); 4.21-4.12 (m, 2H, C-O-Ph); 5.66 (t, 1H, Ph,  $^3J_{\text{HH}} = 5.2$  Hz); 5.99 (d, 1H, Ph,  $^3J_{\text{HH}} = 5.2$  Hz); 6.30 (d, 1H, Ph,  $^3J_{\text{HH}} = 6.4$  Hz); 6.53 (m, 2H, Ph); 7.84 (t, 1H, py,  $^3J_{\text{HH}} = 7.2$  Hz); 7.91 (t, 2H, bz<sub>thio</sub>,  $^3J_{\text{HH}} = 7.6$  Hz); 8.35 (t, 1H, py,  $^3J_{\text{HH}} = 8.0$  Hz); 8.49 (m, 2H, bz<sub>thio</sub>); 8.63 (d,

1H, py,  $^3J_{HH} = 7.6$  Hz); 9.70 (d, 1H, py,  $^3J_{HH} = 5.2$  Hz).  $^{13}\text{C}$  NMR (400 MHz, DMSO- $d_6$ ):  $\delta$  59.27, 64.10, 64.32, 72.18, 73.05, 86.60, 92.67, 94.54, 123.69, 124.97, 126.11, 128.77, 129.62, 133.28, 139.88, 140.76, 150.38, 150.69, 156.57, 166.25. MS (ESI)  $m/z$  (%) 486.98 ( $\text{M}^+$ , 100). Anal. Calcd. For  $\text{C}_{20}\text{H}_{18}\text{Cl}_2\text{N}_2\text{O}_2\text{RuS}$ .  $\text{CH}_2\text{Cl}_2$ : C, 41.53; H, 3.32; N, 4.61%. Found C, 41.96; H, 3.53; N, 4.87%.

### 5.2.2.3 Synthesis of $[\eta^6\text{-(2-phenoxyethanol)RuCl L3}]Cl$ (21)

$[\eta^6\text{-(2-phenoxyethanol)RuCl}_2]_2$  (0.10 g, 0.16 mmol) and ligand **L3** (0.06 g, 0.32 mmol). Greenish-yellow solid. Yield = 0.13 g (87%).  $^1\text{H}$  NMR (DMSO- $d_6$ ):  $\delta$  3.63 (t, 1H, C-OH,  $^3J_{HH} = 4.8$  Hz); 4.21-4.10 (m, 2H, C-O-Ph); 5.67 (t, 1H, Ph,  $^3J_{HH} = 5.2$  Hz); 6.02 (d, 1H, Ph,  $^3J_{HH} = 5.2$  Hz); 6.18 (d, 1H, ph,  $^3J_{HH} = 6.4$  Hz); 6.58 (m, 2H, Ph); 7.80 (m, 2H,  $\text{bz}_{\text{ox}}$ ); 7.98 (t, 1H, py,  $^3J_{HH} = 7.2$  Hz); 8.13 (d, 1H, py,  $^3J_{HH} = 8.0$  Hz); 8.41 (t, 2H,  $\text{bz}_{\text{ox}}$ ,  $^3J_{HH} = 7.6$  Hz); 8.50 (d, 1H, py,  $^3J_{HH} = 7.2$  Hz); 9.69 (d, 1H, py,  $^3J_{HH} = 5.2$  Hz).  $^{13}\text{C}$  NMR (400 MHz, DMSO- $d_6$ ):  $\delta$  59.27, 63.14, 64.55, 72.15, 73.24, 85.95, 91.74, 93.54, 119.95, 125.57, 127.91, 129.47, 129.57, 138.53, 139.14, 140.89, 143.05, 150.73, 157.38, 162.07. MS (ESI)  $m/z$  (%) 471.00 ( $\text{M}^+$ , 100). Anal. Calcd. For  $\text{C}_{20}\text{H}_{18}\text{Cl}_2\text{N}_2\text{O}_3\text{Ru}$ .  $0.5\text{CH}_2\text{Cl}_2$ : C, 44.86; H, 3.49; N, 5.52%. Found C, 45.27; H, 3.79; N, 5.52%.

### 5.2.3 X-ray crystallography analyses of complexes 19-21

The X-ray data were recorded on a Bruker Apex Duo diffractometer equipped with an Oxford Instruments Cryojet operating at 100(2) K and an Incoatec micro-source operating at 30 W power. The data were collected with Mo  $K\alpha$  ( $\lambda = 0.71073$  Å) radiation at a crystal-to-detector distance of 50 mm. The data collections were performed using omega and phi scans with exposures taken at 30 W X-ray power and  $0.50^\circ$  frame widths using APEX2.<sup>279</sup>



The data were reduced with the programme SAINT<sup>279</sup> using outlier rejection, scan speed scaling, as well as standard Lorentz and polarisation correction factors. A SADABS semi-empirical multi-scan absorption correction<sup>279</sup> was applied to the data. Direct methods, SHELXS-97<sup>280</sup> and WinGX<sup>281</sup> were used to solve both structures. All non-hydrogen atoms were located in the difference density map and refined anisotropically with SHELXL-97.<sup>279</sup> All hydrogen atoms were included as idealized contributors in the least squares process. Their positions were calculated using a standard riding model with C–H<sub>aromatic</sub> distances of 0.95 Å and  $U_{\text{iso}} = 1.2 U_{\text{eq}}$  and C–H<sub>methylene</sub> distances of 0.99 Å and  $U_{\text{iso}} = 1.2 U_{\text{eq}}$ . The positions of the hydroxyl O–H of complexes **19** and **21** were constrained using O–H distances of 0.84 Å and  $U_{\text{iso}} = 1.5 U_{\text{eq}}$ . The hydroxyl O–H of **20**, all hydrogen atoms of the water solvate molecules and the imidazole N–H of complex **19** were located in the difference density map, and refined isotropically. Disordered solvent molecules were removed from the lattices of complexes **19** and **21**, using Platon SQUEEZE.<sup>282</sup> This leaves solvent accessible voids of 46 and 65 Å<sup>3</sup> in the lattices of complexes **19** and **21**, respectively.

## 5.2.4 Hydrogenation reactions

### 5.2.4.1 Homogenous experiments

A typical procedure for the catalytic hydrogenation of alkenes was as follows. The reactor was charged with styrene (0.56 mL, 5.00 mmol), catalyst (5 mg, 0.01 mmol) and methanol (50 mL) and sealed. It was then evacuated, flushed with H<sub>2</sub> three times and the pressure adjusted to 10 bar. The mixture was stirred under constant hydrogen pressure for the duration of the reaction period. After the reaction time, the autoclave was vented and samples drawn for GC analyses.

The samples were filtered using 0.45  $\mu\text{m}$  micro filters and the solutions analysed by Varian CP-3800 GC (ZB-5HT column 30 m $\times$ 0.25 mm $\times$ 0.10  $\mu\text{m}$ ). Commercial ethylbenzene (99%) was used as an authentic standard to determine the percentage hydrogenation of styrene to ethylbenzene.

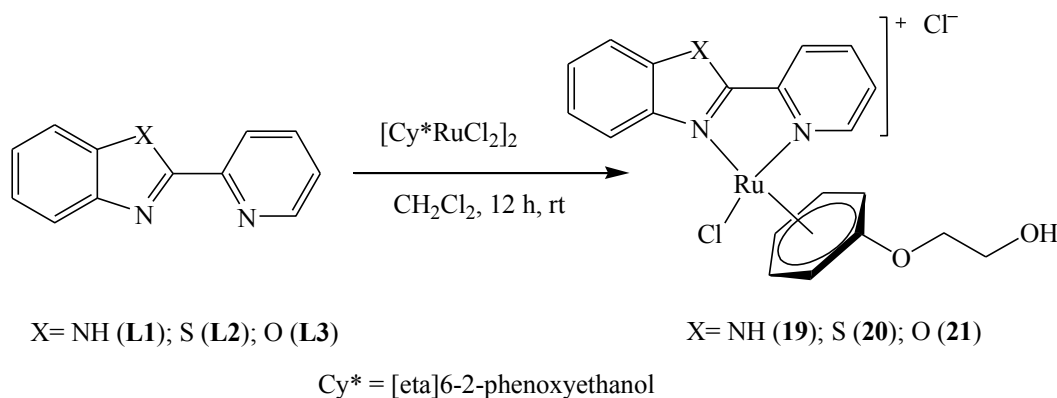
#### ***5.2.4.2 Biphasic hydrogenation experiments***

These reactions were carried in a biphasic system consisting of a mixture of water and toluene. In a typical experiment, complex **19** (5 mg, 0.01 mmol, equivalent to a substrate/catalyst ratio of 500) was weighed and dissolved in water (25 mL) in a two-neck round-bottom flask. A solution of styrene 0.56 mL (5.00 mmol) in toluene (25 mL) was added and the mixture transferred to the reactor *via* cannula and sealed. The autoclave was evacuated and flushed with H<sub>2</sub> three times, filled with H<sub>2</sub> and the pressure adjusted to 10 bar. After the reaction period, the autoclave was depressurized and the mixture allowed to settle for approximately 5 min. The aqueous layer was then separated from the organic layer using a separatory funnel. The organic layer was filtered and analysed by GC to determine the percentage conversion of the substrate to the products. In the recycling experiments, a fresh solution of styrene (0.56 mL, 5.00 mmol) in toluene (25 mL) was added without addition of the catalyst in the aqueous phase. This experiment was repeated for six consecutive cycles.

## 5.3 Results and discussion

### 5.3.1 Synthesis of cationic ruthenium(II) complexes

Compounds 2-(2-pyridyl)benzimidazole (**L1**), 2-(2-pyridyl)benzothiazole (**L2**) and 2-(2-pyridyl)benzoxazole (**L3**) were synthesized according to literature procedures.<sup>278</sup> Treatment of  $[\eta^6\text{-(2-phenoxyethanol)RuCl}_2]_2$  dimer with two molar equivalents of ligands **L1-L3** in  $\text{CH}_2\text{Cl}_2$  gave the corresponding monometallic complexes ruthenium(II)  $[\eta^6\text{-(2-phenoxyethanol)RuCl(L1)Cl}]^+\text{Cl}^-$  (**19**),  $[\eta^6\text{-(2-phenoxyethanol)RuCl(L2)Cl}]^+\text{Cl}^-$  (**20**) and  $[\eta^6\text{-(2-phenoxyethanol)RuCl(L3)Cl}]^+\text{Cl}^-$  (**21**) as yellow solids in high yields of 78-88% (Scheme 5.1). All the complexes were insoluble in chlorinated solvents but were highly soluble in methanol, ethanol and water.



Scheme 5.1: Synthesis of Ru(II) complexes **19-21**.

Complexes **19-21** were characterized by  $^1\text{H}$  and  $^{13}\text{C}$ -NMR spectroscopy, micro-analyses, mass spectrometry and single crystal X-ray analyses. As an illustration, the  $^1\text{H}$  NMR spectrum of complex **19** showed a broad signal at 15.53 ppm assigned to the N-H proton recorded at 13.07 ppm in the corresponding ligand, **L1**.

The 6H-pyridyl protons were observed downfield at 9.61, 9.70 and 9.69 ppm in complexes **19**, **20** and **21**, respectively in comparison to 8.66 ppm, 8.73 ppm and 8.84 ppm in ligands, **L1**, **L2** and ligand **L3** indicating coordination to the ruthenium metal. In general, downfield shifts of the proton signals in ligands **L1-L3** were observed in their corresponding complexes **19-21**. Figure 5.1 shows an overlay of spectra of ligand **L1** and complex **19** depicting the downfield shifts on peaks.

ESI-MS of complexes **19**, **20** and **21** showed  $m/z$  base peaks at 470.02 (Figure 5.2), 486.98 and 471.00 corresponding to the molecular masses of 470.02, 486.98 and 471.00 g/mol of the respective molecular cations. Elemental analyses data of complexes **19-21** were consistent with the empirical formulae of the proposed structures in Scheme 5.1 and confirmed their purity. The  $^1\text{H}$  NMR spectra of complexes **19-21** were initially interpreted to conform to the change of hapticity of the cymene ring from  $\eta^6$ - $\eta^1$  upon coordination of **L1-L3**.

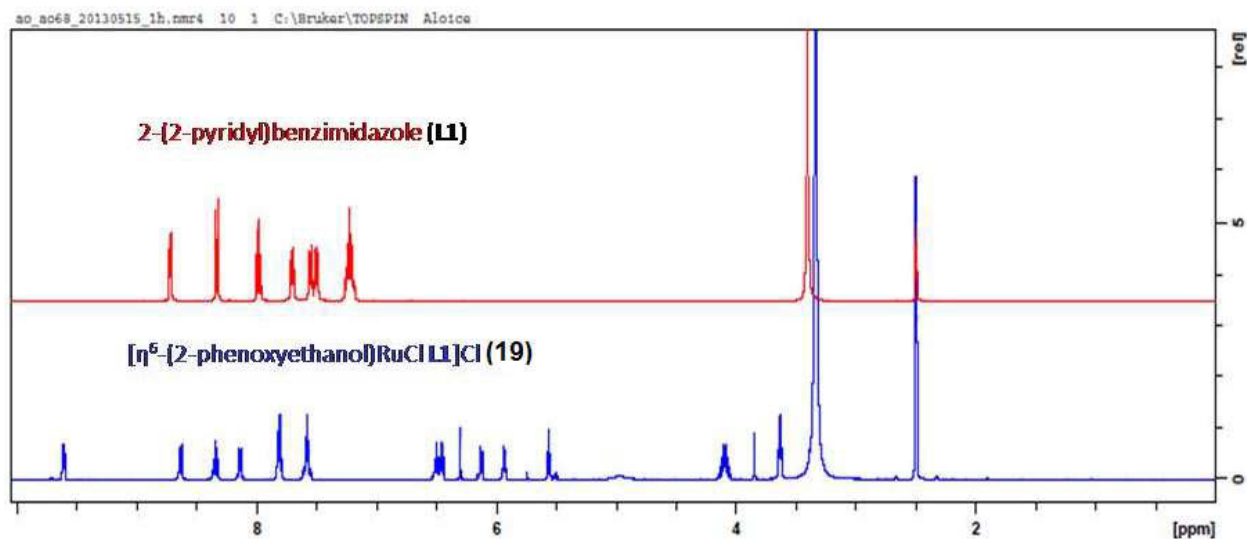


Figure 5.1: An overlay of  $^1\text{H}$  NMR spectra for ligand, **L1**, and complex **19**.

Five signals of the cymene protons were recorded in the  $^1\text{H}$  NMR spectra of complexes **19-21** in comparison to three peaks recorded in the Ru starting material (Figure 5.3). This indicated that all the protons in the cymene ring in complexes **19-21** are inequivalent.

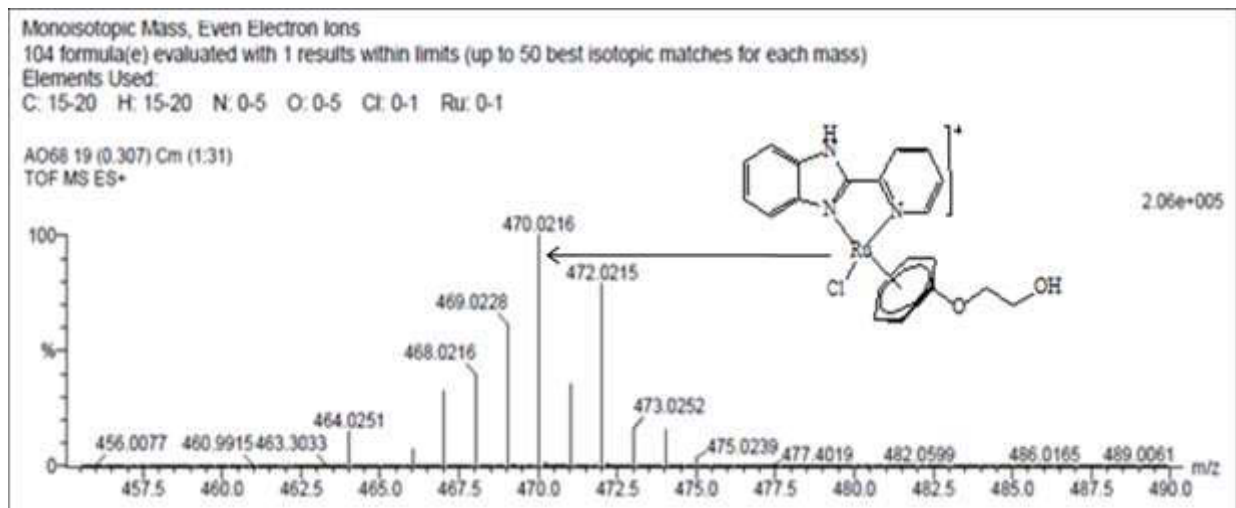


Figure 5.2: ES-MS spectrum of complex **19** showing m/z signal at 470.02 (100%) corresponding to the molecular ion,  $\text{M}^+-\text{Cl}$  of **19**.

This observation is proposed to be as a result of the chirality induced on the cymene ring by the benzoazole ligands, **L1-L3**. In addition, a high resolution mass spectral data obtained for complexes **19-21** pointed to the formation of cationic species with the chloride counter anions in the outer sphere. Likewise, solid state structures of complexes **19-21** (*vide infra*) confirmed the  $\eta^6$ -coordination of the cymene ring.

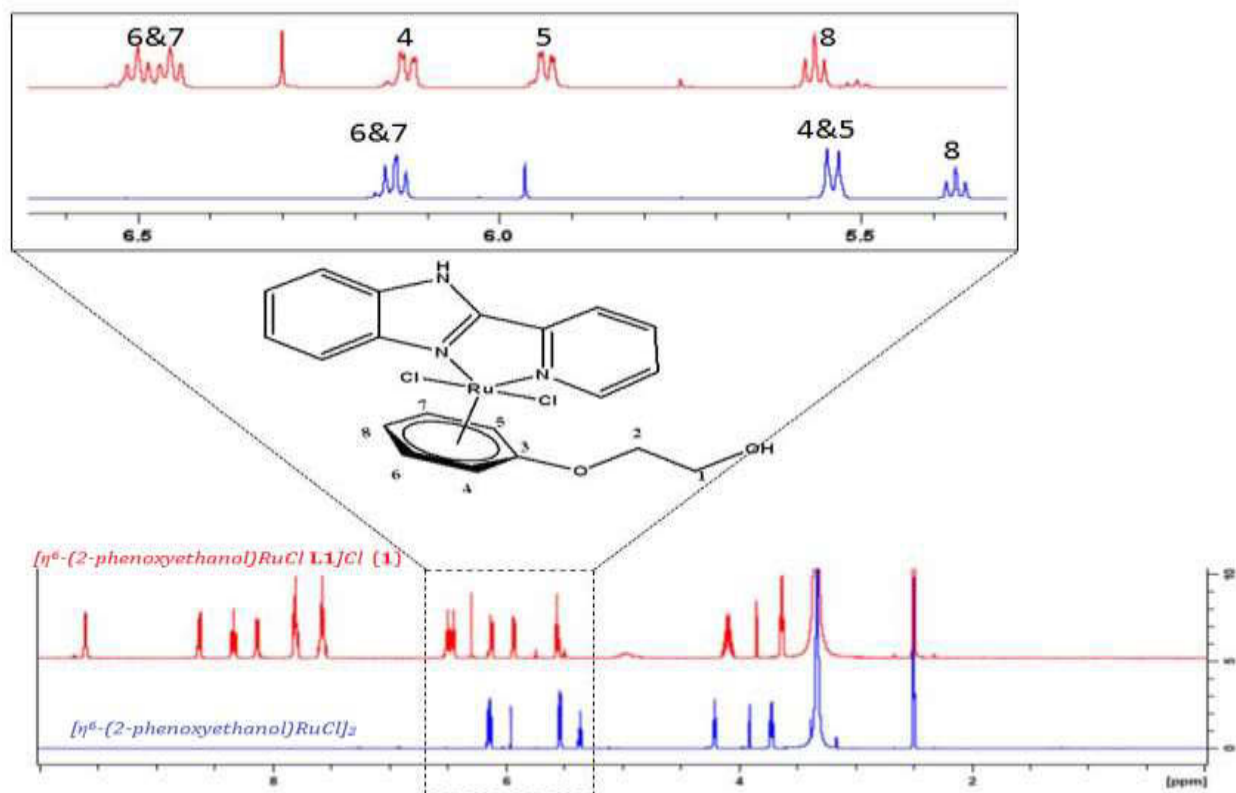


Figure 5.3: An overlay of  $^1\text{H}$  NMR spectra for complex **19** and  $[\eta^6\text{-(2-phenoxyethanol)RuCl}_2]_2$  dimer.

### 5.3.2 Molecular structures of complexes 19-21

The solid state structures of complexes **19-21** were elucidated using single crystal X-ray crystallography (Figure 5.4). Table 5.1 contains data collection and structural refinement parameters while selected bond lengths and angles of complexes **19-21** are given in Table 5.2. While complexes **19** and **21** crystallized in the  $P2_1/c$  space group with a single ruthenium cation and associated chloride counter anion in the asymmetric unit ( $Z = 4$ ), complex **20** crystallized in the  $P2_1/n$  space group as the dihydrate with a single cation and anion as well as two water molecules in the asymmetric unit. The coordination geometry of complexes **19-21** could best be described as a three-legged piano stool.

The Ru–Cl bond lengths measure 2.398(2), 2.389(1) and 2.393(1) Å in complexes **19–21**, respectively. A Mogul structural search<sup>283</sup> showed these values to be typical for this class of compounds. The influence of the heteroatom on the Ru–N<sub>bz</sub> (where N<sub>bz</sub> is the nitrogen atom of the heterocyclic rings: imidazole, thiazole or oxazole) bond length is evident. Complex **20** with the sulphur atom has the longest Ru–N<sub>bz</sub> bond length of 2.100(2) Å, while the oxazole complex **21** has the shortest Ru–N<sub>bz</sub> bond length, 2.078(2) Å.

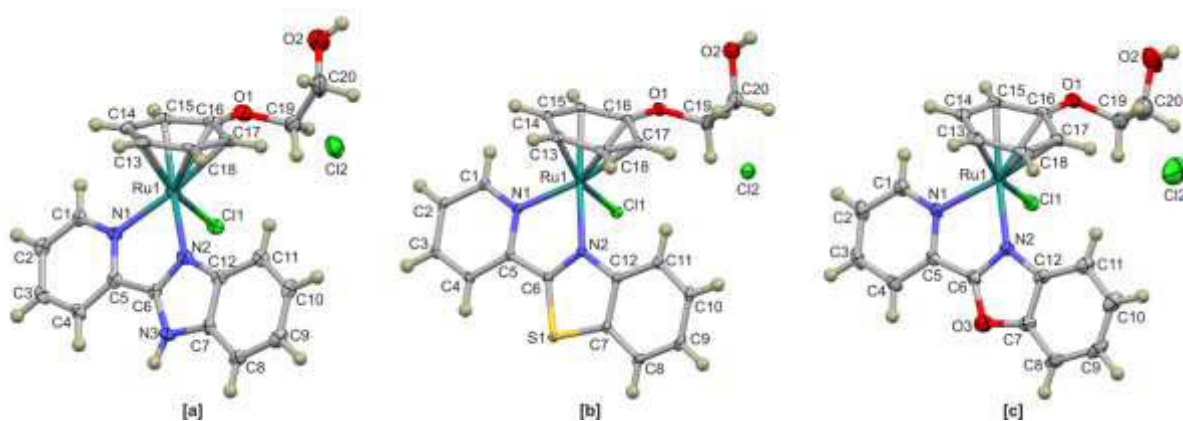


Figure 5.4: Thermal ellipsoid plots (50% probability surfaces) showing the atom numbering schemes of complexes (a) **19**, (b) **20** and (c) **21**. Hydrogen atoms have been rendered as spheres of arbitrary radius.

A similar trend is evident when this series of ligands is coordinated to other metal ions, in all cases the M–N<sub>thiazole</sub> bond length is longer than either the M–N<sub>imidazole</sub> or M–N<sub>oxazole</sub> bond length (where M is either Pd(II) or Pt(II)).<sup>284–286</sup> The Ru–N<sub>py</sub> bond lengths measure 2.107(5), 2.090(2) and 2.103(2) Å for complexes **19–21**, respectively, and are this statistically similar, presumably due to the remote proximity of the heteroatoms to the Ru atom.

Table 5.1: Crystal data and structure refinement details for complexes **19-21**

<b>Crystal Data</b>	<b>(19)</b>	<b>(20)</b>	<b>(21)</b>
Chemical formula	C <sub>20</sub> H <sub>19</sub> Cl <sub>2</sub> N <sub>3</sub> O <sub>2</sub> Ru	C <sub>20</sub> H <sub>18</sub> Cl <sub>2</sub> N <sub>2</sub> O <sub>2</sub> RuS·2H <sub>2</sub> O	C <sub>20</sub> H <sub>18</sub> Cl <sub>2</sub> N <sub>2</sub> O <sub>3</sub> Ru
Molar Mass (g mol <sup>-1</sup> )	505.35	558.43	506.33
Crystal system, space group	Monoclinic, <i>P2<sub>1</sub>/c</i>	Monoclinic, <i>P2<sub>1</sub>/n</i>	Monoclinic, <i>P2<sub>1</sub>/c</i>
Temperature (K)	100(2)	100(2)	100(2)
<i>a</i> , <i>b</i> , <i>c</i> (Å)	7.1035(5), 26.058(), 11.748(1)	6.6907(4), 12.2281(6)	26.329(2), 7.1859(4), 25.965(2), 11.9779(6)
$\alpha$ , $\beta$ , $\gamma$ (°)	$\alpha = \gamma = 90$ , $\beta = 103.511(3)$	$\alpha = \gamma = 90$ , $\beta = 105.842(2)$	$\alpha = \gamma = 90$ , $\beta = 105.193(2)$
<i>V</i> (Å <sup>3</sup> )	2114.4(3)	2155.9(2)	2156.71(6)
<i>Z</i>	4	4	4
Radiation type	Mo <i>K</i> $\alpha$	Mo <i>K</i> $\alpha$	Mo <i>K</i> $\alpha$
$\mu$ (mm <sup>-1</sup> )	1.01	1.10	1.00
Crystal size (mm)	0.39 × 0.15 × 0.10	0.16 × 0.11 × 0.09	0.18 × 0.18 × 0.08
<b>Data collection</b>			
Diffractometer	Bruker Apex Duo CCD diffractometer		
Absorption correction	Multi-scan, <i>SADABS</i> , Bruker 2012		
<i>T</i> <sub>min</sub> , <i>T</i> <sub>max</sub>	0.693, 0.905	0.843, 0.907	0.841, 0.925
No. of Measured, independent and observed [ <i>I</i> > 2 $\sigma$ ( <i>I</i> )] reflections	16799, 3955, 3695	18423, 4227, 3950	20146, 4221, 3888
<i>R</i> <sub>int</sub>	0.025	0.028	0.022
<b>Refinement</b>			
<i>R</i> [ <i>F</i> <sup>2</sup> > 2 $\sigma$ ( <i>F</i> <sup>2</sup> )], <i>wR</i> ( <i>F</i> <sup>2</sup> ), <i>S</i>	0.069, 0.157, 1.21	0.026, 0.063, 1.09	0.029, 0.072, 1.03
No. of reflections	3955	4227	4221
No. of parameters	258	291	254
No. of restraints	0	1	2
H-atom treatment	H atoms treated by a mixture of independent and constrained refinement.		
$\Delta\rho_{\max}$ , $\Delta\rho_{\min}$ (e Å <sup>-3</sup> )	2.26, -2.22	0.74, -0.48	0.85, -0.80



Table 5.2: Selected bond lengths (Å) and bond angles (°) for complexes **19**, **20** and **21**

<b>Bond lengths</b>	<b>19</b>	<b>20</b>	<b>21</b>
Ru–N <sub>py</sub>	2.101(5)	2.090(2)	2.103(2)
Ru–N <sub>bz</sub> <sup>a</sup>	2.088(5)	2.100(2)	2.078(2)
Ru–Cl	2.398(2)	2.389(1)	2.393(1)
Ru–C <sub>p</sub> <sup>b</sup>	1.686(2)	1.696(1)	1.690(1)
<b>Bond angles</b>			
N <sub>py</sub> –Ru–N <sub>bz</sub>	76.6(2)	76.87(8)	76.61(8)
N <sub>py</sub> –Ru–Cl	85.2(2)	87.47(6)	84.79(6)
N <sub>bz</sub> –Ru–Cl	85.3(2)	82.87(6)	85.05(6)

However, these bond lengths are longer than those previously reported for related Ru(II) complexes of pyridyl ligands, which range from 2.063 to 2.102 Å averaging 2.084 Å.<sup>288</sup> The distances from the centroids of the phenyl rings to the coordinated Ru(II) ions are all statistically comparable for complexes **19-21** ranging from 1.685(2) to 1.696(1) Å.

The absence of hydrogen bonding in solvent molecules in the lattices of complexes **19** and **21** contributes to the insignificant hydrogen bonding interactions in these structures. Both exhibit similar intermolecular hydrogen bonding between the hydroxyl group of the cation and the chloride counter ion. This interaction, however, does not lead to any extended supramolecular network. The addition of two water molecules in the lattice of complex **20** leads to a more complex three-dimensional hydrogen-bonded network. The cations of complex **20** pack such that there are channels which run co-linear with the a-axis.

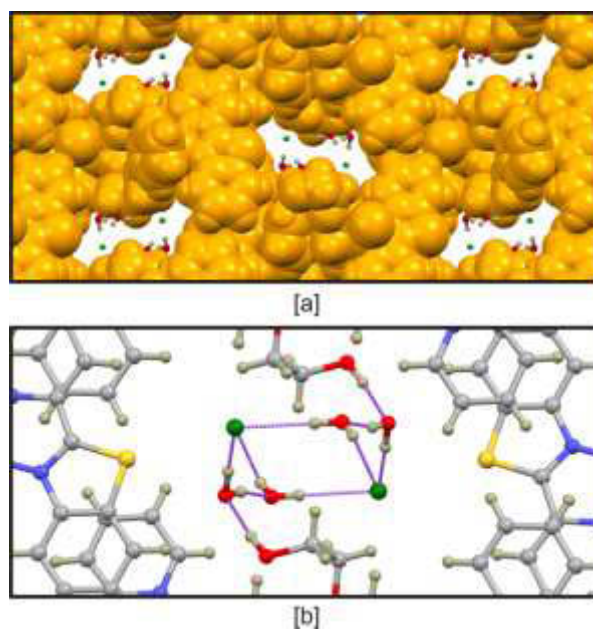


Figure 5.5: [a] Partial space-filling model illustrating the solvent and anion-filled channels of complex **20**. The channels are co-linear with the  $a$ -axis. [b] Hydrogen bonding interactions between the hydroxyl groups of the cations, the water molecules and the chloride anions of complex **20** (viewed down the  $a$ -axis). These interactions lock the solvent molecules and chloride anions in the channels.

These channels are occupied by water molecules and chloride anions which are linked through extensive hydrogen bonding (Figure 5.5). The hydrogen bond lengths and bond angles of complexes **19-21** are summarized in Table 5.3. The hydrogen bond lengths are all significantly shorter than the sum of the van der Waals radii of the interacting atoms. Although bond distance do not necessarily correlate linearly to bond strength due to packing constraints in the lattice,<sup>287</sup> it is likely that these bonds are strength due to packing constraints in the lattice,<sup>287</sup> it is likely that these bonds are relatively stronger. The minimal deviation of the hydrogen bond angles from the ideal bond angle, particularly in complex **20**, further augments this argument.

Table 5.3: Summary of hydrogen bond lengths (Å) and bond angles (°) of complexes **19-21**.

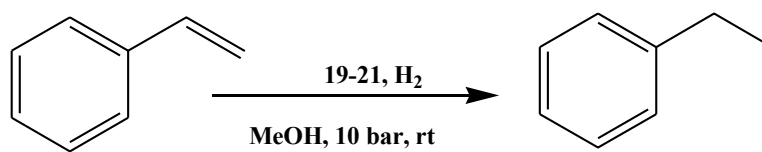
	<b>D-H</b>	<b>D···A</b>	<b>H···A</b>	<b>D-H···A</b>
<b>(19)</b>				
O2–H101···Cl2	0.841 <sup>a</sup>	3.158(9)	2.590	126.0
<b>(20)</b>				
O2–H101···O1w	0.97(5)	2.713(4)	1.75(5)	174(4)
O1w–H3w···Cl2	0.96(5)	3.117(2)	2.17(5)	169(5)
O1w–H4w···O2w	0.86(4)	2.742(4)	1.89(4)	167(4)
O2w–H1w···Cl2	0.79(5)	3.224(3)	2.45(5)	169(4)
O2w–H2W···Cl2	0.83(4)	3.199(3)	2.37(4)	180(3)
<b>(21)</b>				
O2–H101···Cl2	0.840 <sup>a</sup>	3.070(2)	2.274	158.2

<sup>a</sup>Hydrogen atom in calculated position hence no standard deviation for the measurement

### 5.3.3 High pressure catalytic hydrogenation of olefins

#### 5.3.3.1 Effect of catalyst structure on hydrogenation of styrene

Preliminary investigations of complexes **19-21** in high pressure catalytic hydrogenation of alkenes were performed using styrene as a model substrate. In a typical reaction, 4.90 mmol of styrene and 0.01 mmol (0.2 mol%, substrate/catalyst ratio of 500) of complexes **19-21** under H<sub>2</sub> pressure (10 bar) in MeOH (50 mL) were employed (Scheme 5.2). Table 5.4 contains a summary of hydrogenation data of styrene to ethylbenzene.



Scheme 5.2: Catalytic hydrogenation of styrene by benzoazole Ru(II) complexes, **19-21**.

From Table 5.4, it is evident that all the complexes formed efficient catalysts in the homogeneous catalytic hydrogenation of styrene to ethylbenzene giving conversions of 86% to > 99% within 1 h corresponding to TOFs of up to 430 h<sup>-1</sup> to 495 h<sup>-1</sup>. The identity of the ligand was found to have a profound effect on the catalytic activities of these complexes. For instance, complex **19** bearing the 2-(2-pyridyl)benzimidazole ligand recorded the highest activity giving conversions of 89% within 0.5 h (TOF = 890 h<sup>-1</sup>) compared to 42% (TOF = 420 h<sup>-1</sup>) and 64% (TOF = 640 h<sup>-1</sup>) for the analogous thiazole and oxazole complexes **20** and **21**, respectively. This trend is in good agreement with the acidity trends of **L1-L3**.

Ligand **L1** is the most acidic while ligand **L2**, containing the S atom, is the least acidic,<sup>288</sup> It is therefore apparent that increased acidity of the ligands promotes substrate coordination. A more acidic ligand would therefore increase the electrophilicity of the metal centre and facilitate substrate coordination. This might account for the higher catalytic activities observed in catalyst **19** compared to complexes **20** and **21**. This data agrees with our earlier reports in which the Ru(II) complex of ligand **L1** gave a more active catalyst in the transfer hydrogenation of ketones than the corresponding complexes of ligands **L2** and **L3**.<sup>289</sup>

Table 5.4: Effect of reaction parameters on the hydrogenation of styrene to ethylbenzene by complexes **19-21**

Entry	Catalyst	Cat/Sub	Time (h)	Conversion (%) <sup>a</sup>	Selectivity (%ethylbenzene)	TOF(h <sup>-1</sup> ) <sup>d</sup>
1	<b>19</b>	500	1	>99 (89) <sup>b</sup>	100	495(890)
2	<b>20</b>	500	1	86	100	430
3	<b>21</b>	500	1	90(64) <sup>b</sup>	100	450 (640)
4	<b>20</b>	500	1.5	>99	100	330
5	<b>20</b>	500	0.5	42	100	420
6	<b>20</b>	500	0.25	20	100	400
7 <sup>c</sup>	<b>20</b>	200	0.25	>99	100	792
8 <sup>c</sup>	<b>20</b>	500	0.25	49	100	980
9 <sup>c</sup>	<b>20</b>	500	0.5	>99	100	990
10 <sup>e</sup>	<b>21</b>	500	1	32	100	160
11 <sup>f</sup>	<b>21</b>	500	1	29	100	145
12 <sup>g</sup>	<b>19</b>	500	1	99	100	495

<sup>a</sup>Conditions: styrene, 4.9 mmol; catalyst; 0.01 mmol (0.2 mol%); 10 bar; MeOH, temperature, 25 °C; . Determined by GC.

<sup>b</sup>Time, 0.5h; <sup>c</sup>Temperature, 50 °C

<sup>d</sup>TOF in mol substrate. mol<sup>-1</sup> catalyst.h<sup>-1</sup>

<sup>e</sup>Pressure = bar

<sup>f</sup>Pressure = 1bar

<sup>g</sup>Mercury drop test (5 drops of mercury added to the reaction mixture)

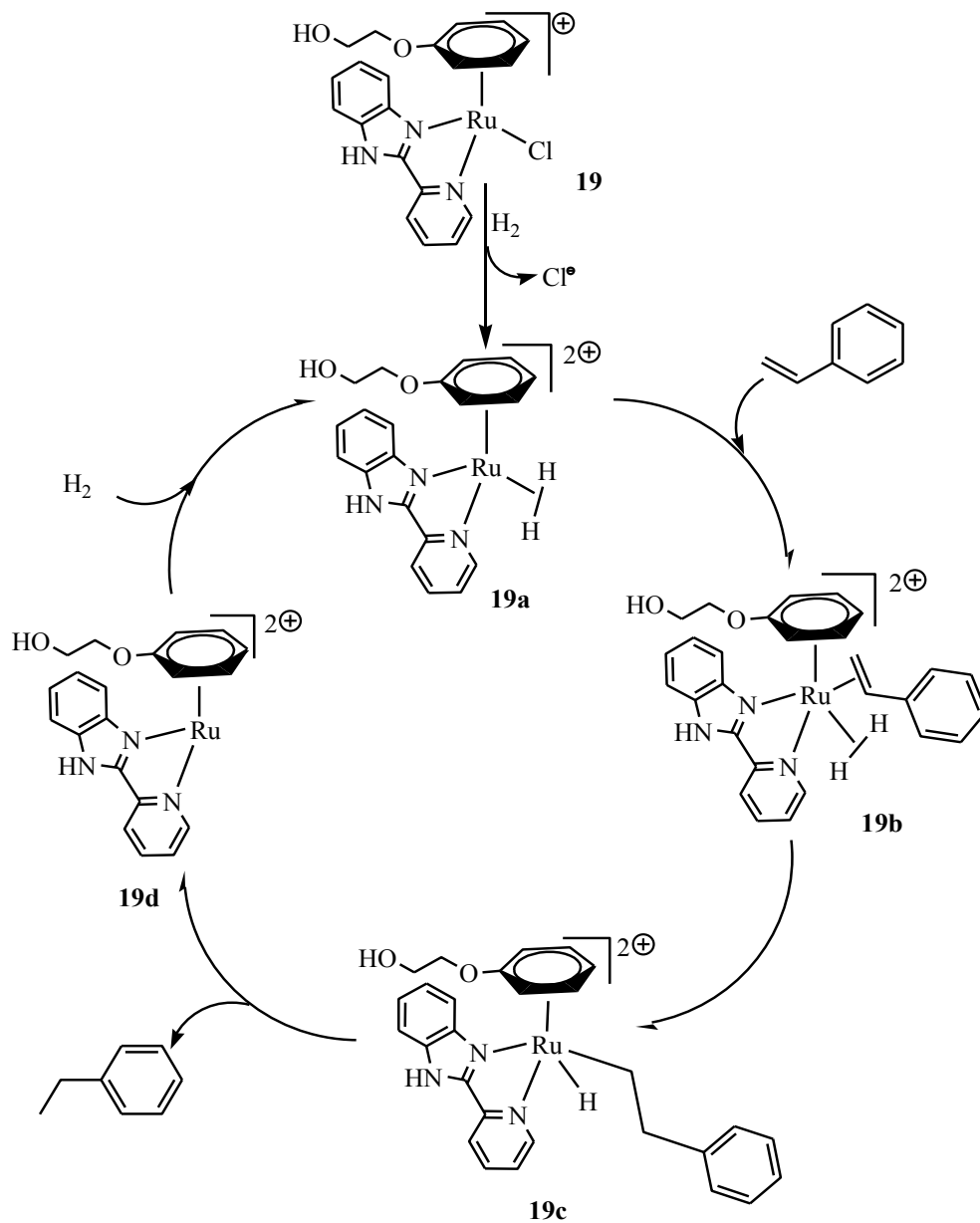
### 5.3.3.2 Proposed mechanism for hydrogenation of styrene

In order to try and understand the mechanism of hydrogenation reactions catalysed by complexes **19-21**, attempt was made to establish the homogeneity of the active species. A mercury drop experiment<sup>290</sup> was conducted using complex **19** to establish the homogeneity of the active Ru species or formation of ruthenium colloids/nanoparticles (Table 5.3, entry 12). No significant decrease in the catalytic activity of complex **19** (99%) was observed when five drops of mercury were added to the reaction mixture (Table 5.3, entries 1 and 12). This confirmed that no heterogeneous ruthenium colloids/nanoparticles were involved and that the hydrogenation reactions were predominantly homogeneous in nature.<sup>291,292</sup>

Ruthenium(II)-arene type complexes have been proposed to catalyse the hydrogenation of alkenes through a dihydrogen intermediate, since oxidation to Ru(IV) species would be energetically disfavoured.<sup>293</sup> Considering that complexes **19-21** are saturated 18-electron systems, a dissociative process would be preferred in order to generate an active dihydrogen intermediate.<sup>294</sup> To allow for substrate coordination, a change of hapticity of the  $\eta^6$ -arene group ring from  $\eta^6$  to  $\eta^4$  is most likely since ligands **L1-L3** are expected to be too strongly coordinated to act as hemi-labile ligands.<sup>293</sup> In addition, the dependence of the hydrogenation reaction on the identity of the ligands (**L1-L3**) implicates their involvement in the catalytic cycles. <sup>1</sup>H-NMR spectra of complexes **19-21** (*vide supra*) further supports this hypotheses, since a change of hapticity of the arene ring was evident (Figures. 5.1 and 5.3).

Starting with complex **19**, a dissociation of the chloride ligand leading to the formation of dihydrogen intermediate **19a** is postulated (Scheme 5.3). Coordination of the substrate is simultaneously accompanied with a change in hapticity of the arene group from  $\eta^6$  -  $\eta^4$  to give **19b**.

Hydride addition to the coordinated styrene substrate by the dihydrogen ligand leads to the formation of hydride and alkyl ligands and an increase in hapticity from  $\eta^4$  to  $\eta^6$  to form ruthenium(IV) intermediate **19c**. Reduction elimination in **19c** leads to the formation and elimination of ethylbenzene product and the hydride complex **19d**. Reactions of **19d** with  $H_2$  results in regeneration of the active species **19a** and initiates another catalytic cycle.



Scheme 5. 3: Proposed mechanism for the high pressure hydrogenation of styrene by complex **19**.

### 5.3.3.3 Optimization of hydrogenation reaction conditions

Upon establishing that complexes **19–21** form effective catalysts for the hydrogenation of styrene, the optimization of the reaction conditions were carried out. This was accomplished by varying the reaction time, substrate/catalyst ratio, temperature and hydrogen pressure (Table 5.4). From Table 5.4, it is evident that an increase in reaction time resulted in a slight increase in percentage conversions for catalysts **19–21** (Table 5.3, entries 1,3,4,5 and 6). For example, using catalyst **20**, increasing the reaction time from 0.5 h to 1 h was marked by an increase in percentage conversion from 42% to 86%. However, there was a general drop in TOFs of all the catalysts with time. For instance, the TOF of complex **19** dropped from 890 h<sup>-1</sup> within 0.5 h to 495 h<sup>-1</sup> after 1 h.

This trend is consistent with some degree of catalyst degradation with time hence, loss of efficiency. It is also worthy to note that complex **20**, containing the benzothiazole ligand **L2**, showed a longer induction period than catalyst **19** or **21** (Table 5.4, entries 4 and 6).

This feature is likely to originate from the lower electrophilicity of the Ru(II) metal due to the electron rich ligand **L2**. Increased in catalytic activity with an increase in reaction temperature was also observed. Increasing the reaction temperature from 25 °C to 50 °C resulted in an increase in TOF of complex **2** from 420 h<sup>-1</sup> to 990 h<sup>-1</sup>, respectively, (Table 5.4, entries 5 and 9). Similar trends have been reported in literature where Yilmaz *et al.* observed an increase in TOF from 8 h<sup>-1</sup> to 38 h<sup>-1</sup> when the reaction temperature was increased from 27 °C to 80 °C.<sup>218</sup> As expected, increasing the hydrogen pressure from 1 bar to 10 bar was also followed by a concurrent increase in TOF of complex **21** from 145 h<sup>-1</sup> to 450 h<sup>-1</sup> respectively (Table 5.4, entries 3 and 11).



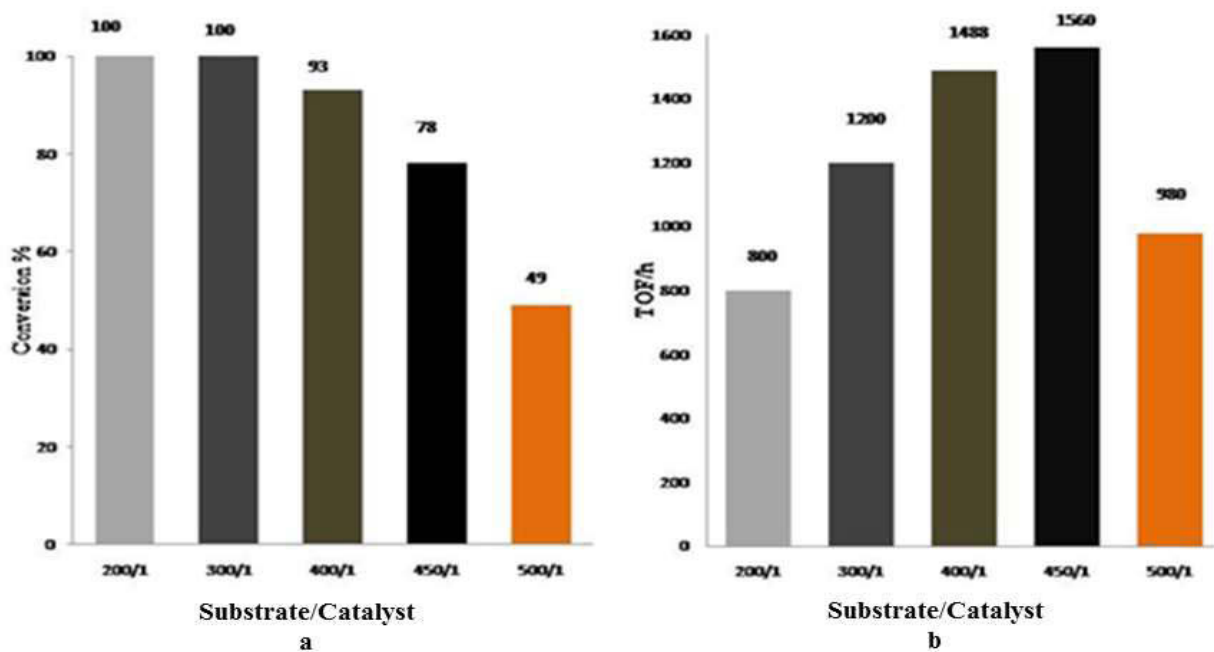


Figure 5.6: Effect of substrate/catalyst molar ratio on (a) conversion (b) TOF of complex **20** on hydrogenation of styrene.

To examine the effect of substrate/catalyst ratio on the hydrogenation of styrene by complex **20**, a variation of the styrene/catalyst ratio from 200 to 500 at room temperature and 10 bar at constant styrene concentration of 5.00 mmol was done (Figure 5.6). The conversion of styrene was observed to decrease with increase in substrate to catalyst ratio. While a 100% conversion was obtained within 15 min at 200/1 ratio, only 49% conversion was achieved at the higher substrate/catalyst ratio of 500. However, it is important to take cognizance of the higher TOF of 980 h<sup>-1</sup> obtained at catalyst/substrate of 500 compared to TOF of 800 h<sup>-1</sup> recorded at substrate/catalyst ratio of 200 (Figure 2b). The highest TOF of 1560 h<sup>-1</sup> was obtained at substrate/catalyst ratio of 450 (78%). Thus, a catalyst/substrate ratio of 450 could be taken as the optimum catalyst loading in the hydrogenation of styrene using complex **20** (Figure 5.6b).

#### 5.3.3.4 Substrate scope

Upon optimization of the reaction conditions using styrene as the model substrate, the versatility of these complexes in the catalytic hydrogenation of a range of alkene and alkyl substrates were investigated using catalyst complex **21**. The substrates studied were 1-hexene, 1-octene, 1-decene, 1-hexyne and 1-octyne. The results obtained clearly reflect a significant effect of the substrate identity on the catalytic performance of complex **21** (Figure 5.7). Generally, higher catalytic activities were reported for the alkene substrates compared to the corresponding alkynes. For example, percentage conversions of 100% (TOF = 800 h<sup>-1</sup>) and 42% (TOF = 336 h<sup>-1</sup>) were obtained in the hydrogenation of 1-hexene and 1-hexyne respectively (Figure 5.7). A reasonable explanation for this occurrence could be the stepwise hydrogenation of 1-hexyne to 1-hexene and then to the hexane product. Costa and co-workers reported a similar trend in which the activities of (pyridyl)iminopalladium complexes were lower in the hydrogenation of phenylacetylene than in styrene.<sup>294</sup>

The selectivities in the hydrogenation of 1-hexyne and 1-octyne were biased towards the corresponding alkanes giving 65% and 52% for hexane and octane, respectively (Figure 5.7). This indicates some degree of catalyst poisoning, which is synonymous with partial hydrogenation of alkynes to the respective alkenes.<sup>295</sup> Increase in chain length of the terminal alkenes from C<sub>14</sub> to C<sub>18</sub> resulted in a slight drop in percentage conversions of complex **21** from 99% to 89%, respectively, while the activities observed for C<sub>6</sub>-C<sub>10</sub> alkenes were comparable.

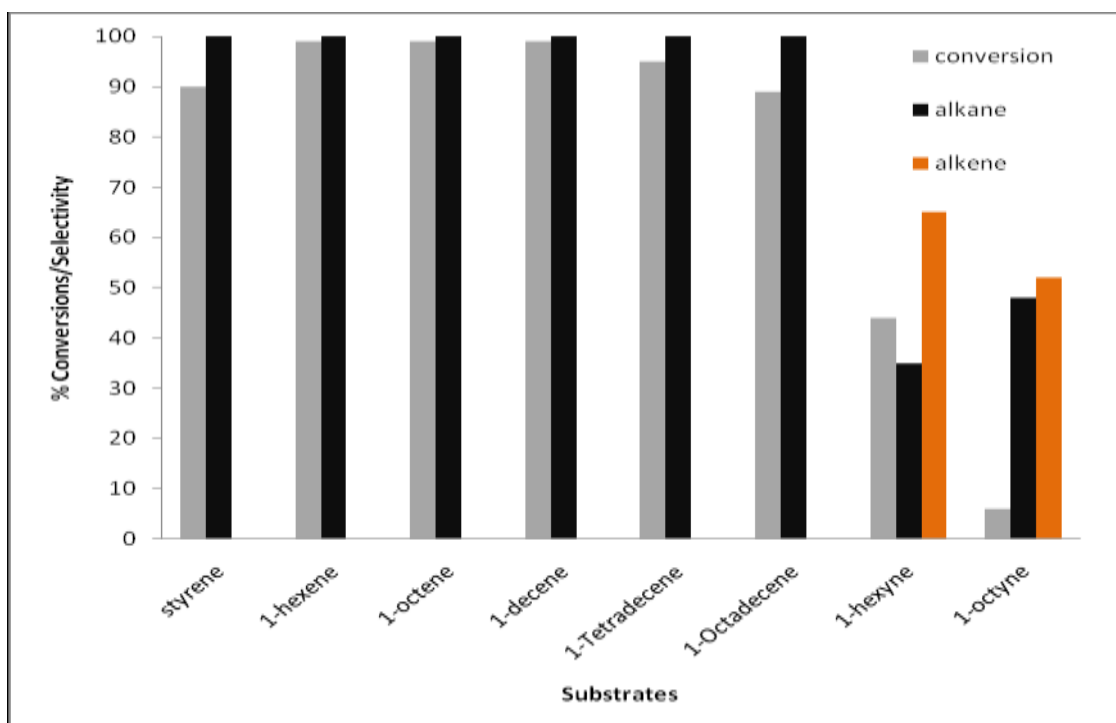


Figure 5.7: Catalytic activity and selectivity of complex **21** in the hydrogenation of various substrates. Reaction conditions: substrate, 4.9 mmol; catalyst; 0.01 mmol (0.2 mol%); 10 bar; MeOH (50 mL), temperature, 25 °C; time, 1 h.

Another interesting observation was the higher catalytic activities of complex **21** reported in the hydrogenation of unsubstituted alkenes compared to styrene reactions. For example, complete conversions of 1-hexene, 1-octene and 1-decene to the corresponding alkanes were realized within 1 h compared to 90% conversion of styrene to ethylbenzene (Figure 5.7). These could be attributed to the reduced activities in styrene reactions to the  $\pi$ -delocalization of electrons in the phenyl ring, thus reducing the electron density of the double bond.

This has the overall effect of limiting styrene substrate coordination to the Ru metal resulting in lower activities. This trend is consistent with reports by Frediani *et. al.* using  $[\text{Ru}(\eta^6\text{-p-cymene})(\text{Cl})(\text{biisoq})](\text{Cl})$  in which they obtained 52.3% (TOF = 85.1 h<sup>-1</sup>) conversion in the hydrogenation of styrene compared to 99.1% (TOF = 161.1 h<sup>-1</sup>) in 1-hexene reactions.<sup>77</sup> Indeed, attempts to use complexes **19-21** in the catalytic hydrogenation of benzene to cyclohexane did not result in any activity.<sup>296</sup> The catalytic activities of complexes **19-21** in the homogeneous hydrogenation of alkenes compare favourably with related non-phosphine complexes reported in the literature.<sup>297</sup> For example, Ellis *et. al.* reported TOFs of 490 h<sup>-1</sup>, 76 h<sup>-1</sup> and 32 h<sup>-1</sup> in the hydrogenation of styrene, 1-octene and 1-decene respectively at 60 bar and 60 °C using ruthenium cluster complexes  $[\text{Ru}_3(\text{CO})_{10}(\text{TPPTN})]$ ,  $[\text{Ru}_3(\text{CO})_9(\text{TPPTN})]$  and  $[\text{Ru}_4(\text{CO})_{11}(\text{TPPTN})]$ , where TPPTN = tris 3-sulfonatophenyl phosphine trisodium salt.<sup>297a</sup> Comparatively, our ruthenium catalysts displayed TOFs of up to 1560 h<sup>-1</sup> in these reactions at milder conditions of 10 bar and at room temperature. In another report, Caballero *et. al.* reported TOFs of 1.9 h<sup>-1</sup> and 32 h<sup>-1</sup> in styrene and 1-hexene reactions respectively using immobilized  $\text{RuCl}_2(\text{bpea})\text{PPh}_3$ , (bpea=N,N-bis(2-pyridylmethyl)ethylamine) at 5 bar and 50 °C.<sup>297b</sup>

### 5.3.3.5 Biphasic catalysis and catalyst recycling

One of the major challenges hindering industrial applications of homogenous catalysts is the difficulty in product separation from the reaction mixture, in addition to lack of catalyst recycling.<sup>262-265</sup> Various technologies have been employed to improve catalyst recovery and product separation.<sup>264</sup> The water soluble properties of complexes **19-21** were exploited to investigate their catalytic activities and recovery in biphasic medium.

In a typical experiment, 0.20 mol% (substrate/catalyst ratio = 500) of the complex was dissolved in water (25 mL) to form the aqueous phase and the alkene substrate (5.00 mmol) dissolved in toluene (25 mL) to give the organic phase. Catalyst recovery experiments were done by carefully decanting the aqueous phase containing the catalyst followed by addition of an equivalent amount of substrate in toluene without catalyst addition for six cycles (Figure 5.8).

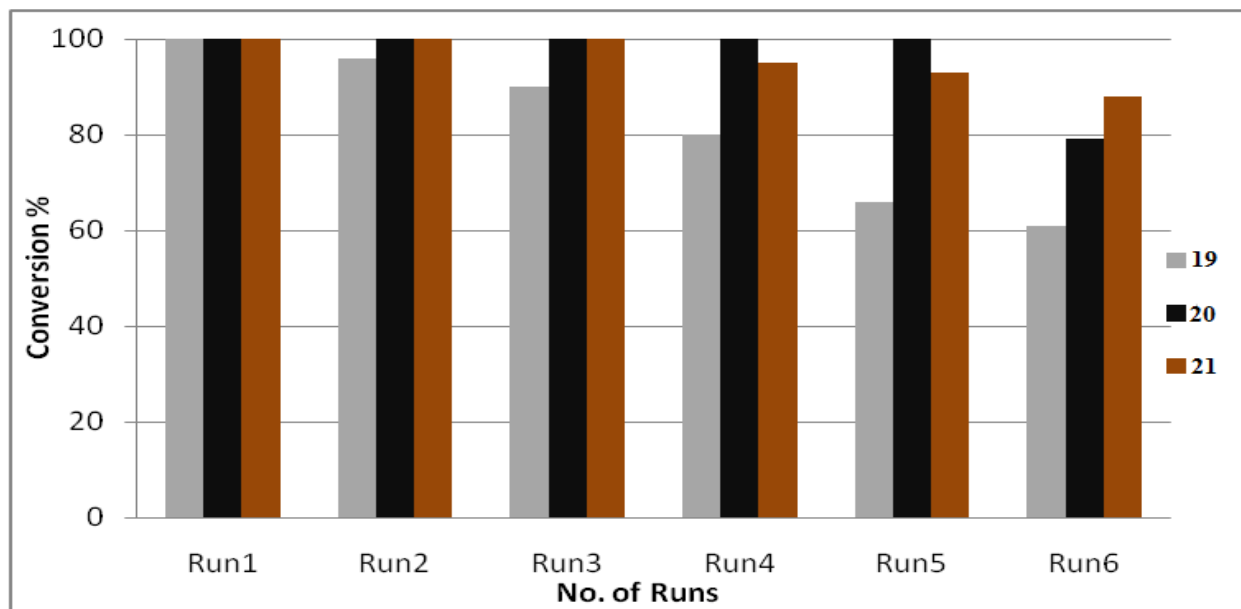


Figure 5.8: Conversion of styrene as a function of cycles by complexes **19-21**. Reaction conditions: styrene, 4.9 mmol; catalyst; 0.01 mmol (0.2 mol%); 10 bar; H<sub>2</sub>O:Toluene (1:1, total volume, 50 mL), temperature, 25 °C, time, 1 h.

The catalytic activities of complexes **19-21** were comparable to the single phase reactions performed in toluene giving complete conversions within 1 h. Most important was the retention of appreciable activities even in the sixth cycle giving conversions of 60%, 79% and 88% for complexes **19**, **20** and **21**, respectively (Figure 5.8). Table 5.5 shows the comparative TOF values obtained for complexes **19-21** in the first and sixth runs and corresponding percentage drops in their catalytic activities.

Complex **20** achieved 100% conversion in five consecutive runs, translating to a cumulative TON of 289.5. These results mirror those obtained for related single-site water soluble catalysts and heterogeneous systems. For example, using Rh/TPPTS (TPPTS =  $[P(C_6H_4-m-SO_3Na)_3]$ ), Vangelis and co-workers reported 95% conversion in the hydrogenation of benzene in the fifth cycle.<sup>298</sup> Using heterogeneous palladium nanoparticles supported on polyethylene glycol, Harraz *et al.* observed 78% conversion of styrene to ethylbenzene in the 10<sup>th</sup> cycle.<sup>216</sup> Comparatively, complex **19** was the least stable displaying 39% drop in activity in the sixth run compared to reductions of 21% and 12% reported for complexes **20** and **21**, respectively (Table 5.5, entries 1-3). The low stability of complex **19** could originate from the weaker donor-ability of the benzimidazole ligand **L1** leading to a relatively unstable complex and is consistent with its observed higher catalytic activity in the homogenous experiments (Table 5.4, entries 2 and 3). This observation demonstrates one of the major challenges in catalyst design of balancing catalyst activity and stability. Another possible reason for reduced catalytic activities in subsequent recycled catalysts could emanate from catalyst leaching into the organic phase, thereby reducing the concentration of the active species in subsequent experiments.<sup>274b</sup>

The distribution co-efficient of the substrate and catalyst between the solvent systems employed greatly affects catalysts' performance in biphasic reactions.<sup>274b</sup> The effect of aqueous/organic volume ratios on the biphasic hydrogenation of styrene was investigated using catalyst **21**. Figure 5.8 and Table 5.5 provide a summary of the data obtained in the six consecutive runs. The greatest activity was observed using aqueous/organic ratio of 1:1. Increasing the aqueous/organic ratio to 2:1 resulted in a drop in activity from > 99% to 86%. A more drastic decline in activity to 70% was observed when higher volumes of the organic phase were employed (aqueous/organic of 1:2).

It is therefore conceivable that greater volumes of aqueous phase might limit the diffusion of the catalyst to the interphase. The same argument might apply for the alkene substrate when a large volume of the organic phase is employed. Vangelis *et al.*<sup>298</sup> reported higher catalytic activities when higher volumes of organic phase were used in the biphasic hydrogenation of benzene. However, in their design, they used neat benzene in the hydrogenation reaction.

Table 5.5: Comparison of the TOFs catalysts **19-21** in the first and sixth cycle experiments

Entry	Catalyst	H <sub>2</sub> O/toluene	TOF <sup>b</sup> h <sup>-1</sup> (Run 1)	TOF <sup>b</sup> h <sup>-1</sup> (Run 6)	% Drop
1	1	1:1	333	203	39
2	2	1:1	333	263	21
3	3	1:1	333	293	12
4	3	2:1	430	320	26
5	3	1:2	350	290	17
6 <sup>c</sup>	3	1:1	500	400	20

<sup>a</sup>Conditions: styrene, 4.9 mmol; catalyst; 0.01 mmol (0.2 mol%); 10 bar; rt. Determined by GC.

<sup>b</sup>TOF in mol substrate. mol<sup>-1</sup> catalyst.h<sup>-1</sup> <sup>c</sup>Temperature = 50 °C

Thermal stability is another important feature in catalyst recycling as it leads to catalyst deactivation and loss of activity in subsequent experiments.<sup>274c</sup> The thermal stability of catalyst **21** was studied by comparison of the recycling efficiencies at room temperature and at 50 °C (Figure 5.9).

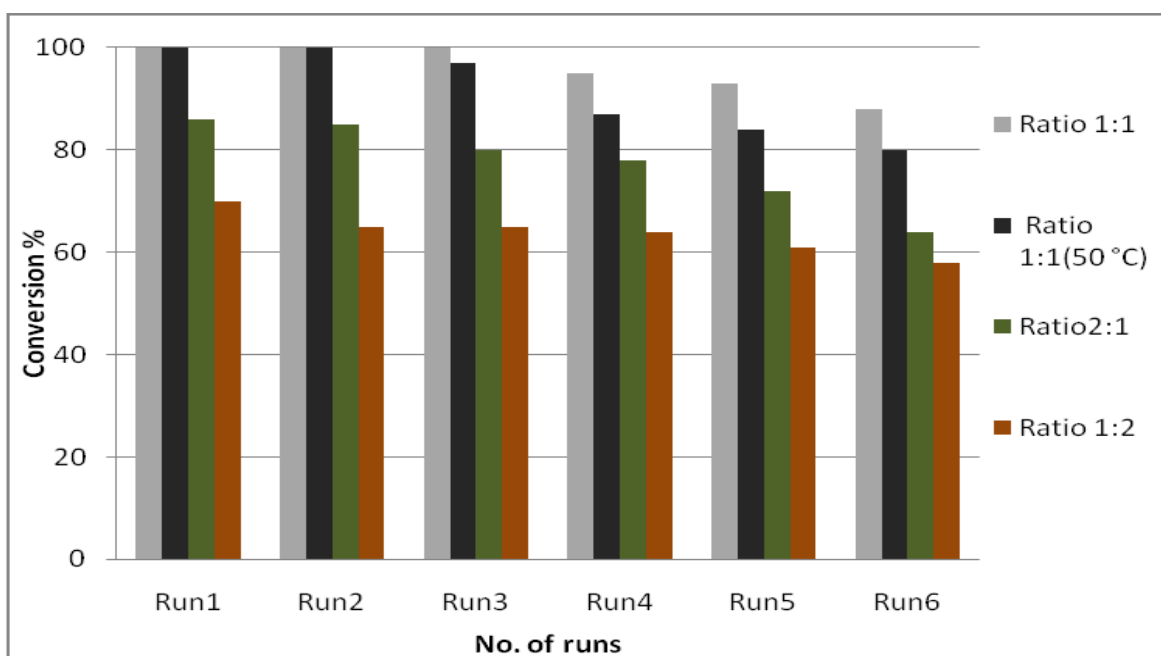


Figure 5.9: Influence of aqueous: organic volume ratio and temperature on catalyst regeneration using complex **21**.

From the results, it is evident that catalyst **21** exhibited a rapid loss in activity at 50 °C compared to the room temperature reactions. This is demonstrated by a drop of 12% and 20% in the sixth run at room temperature and at 50 °C reactions, respectively (Table 5.5, entries, 3 vs 6). It is however, worth noting that catalyst **21** retains significant catalytic activity in the recycling experiments; hence, these systems can be said to portray some degree of thermal stability.



## 5.4 Conclusions

Three new cationic (pyridyl)benzoazoleruthenium(II) complexes have been successfully isolated and structurally characterized and extensively studied their applications in homogeneous and biphasic hydrogenation of alkenes and alkynes. Solid state structures of the ruthenium complexes **19-21** support the bidentate coordination mode of the ligands and formation of cationic species with a chloride as a counter anion. All the complexes form highly active catalysts for high pressure hydrogenation of olefins under mild conditions. The electronic contributions of the ligand motif influenced the catalytic activities of the resultant complexes. Higher activities were reported in the hydrogenation of alkenes compared to the corresponding alkynes. The complexes were found to be stable and recyclable in biphasic reactions retaining significant catalytic activities in six consecutive cycles. The aqueous/organic volume ratio and temperature influenced the catalytic activities and recovery of these complexes in biphasic medium. In summary, a simple synthetic protocol to the design of effective and recoverable water soluble catalysts in biphasic hydrogenation of alkenes has been demonstrated.

## CHAPTER 6

### General concluding remarks and future prospects

#### *6.1 General conclusions*

In conclusion, this thesis presents the findings of a systematic investigation of pyridyl(benzoazole)ruthenium(II/III), pyridyl(benzoazole) and (pyrazol-1-ylmethyl)pyridinepalladium(II) and water soluble cationic pyridyl(benzoazole)ruthenium(II) complexes as hydrogenation catalysts. The benzoazole ligands (**L1-L3**) and the pyrazolyl ligand (**L5**) coordinate to the ruthenium and palladium metal centres in a bidentate manner giving rise to mononuclear complexes.

(Pyridyl)benzoazoleruthenium(II) and ruthenium(III) complexes, **1-7**, form active catalysts for the transfer hydrogenation of ketones. The catalytic activity of the (pyridyl)benzoazoleruthenium(III) complexes **1-3** and **7** is due to their coordinative unsaturation while the presence and the lability of the ancillary PPh<sub>3</sub> ligands on the benzoazole Ru(II) complexes **4-6** enhance their catalytic activities above the corresponding Ru(III) complexes **1-3**. The N-H moiety of ligand **L1** fosters the outer-sphere mechanism of transfer hydrogenation leading to consistent by higher activity for complexes **1** and **4**.

In Chapter 4 the catalytic activities of complexes **8-18** in high pressure hydrogenation were found to be influenced by steric and electronic contributions of the ligands. The benzoazole Pd(II) complexes **8-13** were generally more active than (pyrazolylmethyl)pyridinepalladium(II) complexes **14-18**.

From the DFT results, the activities of **8-18** are generally controlled by the relative stabilities of the complexes as depicted by the average  $\{(N_{\text{py}} + N_{\text{bz/pz}})/2\}$  bond lengths and the HOMO-LUMO energy gaps. The rate of hydrogenation of alkynes was higher than the corresponding rates for alkenes. Hydrogenation of aliphatic alkynes and alkenes is accompanied by isomerization of the terminal alkenes and alkynes to internal alkenes. Kinetic studies of the hydrogenation reactions indicate that they are *pseudo* first order with respect to the substrate and catalyst.

Chapter 5 presents a discussion on water soluble cationic ruthenium(II) complexes **19-21** and their applications in biphasic high pressure hydrogenation. The complexes are highly active catalysts for the high pressure hydrogenation of alkenes and alkynes under mild conditions. The catalytic activities of the complexes are influenced by the electronic properties contributed by the (pyridyl)benzoazole ligands **L1-L3**. Unlike the palladium complexes (Chapter 4), higher catalytic activities were observed in the hydrogenation of alkenes compared to the corresponding alkynes for these water soluble cationic ruthenium complexes. This suggests that the mechanism of hydrogenation of alkenes and alkynes by palladium complexes and ruthenium complexes probably follow different pathways.

The complexes were recycled up to six times without significant loss in activity under biphasic conditions. In general, catalyst loading, temperature, hydrogen pressures and reaction time influenced the activity of the complexes **8-21** in the high pressure hydrogenation of alkenes and alkynes. The water soluble cationic complexes (Chapter 5) also provide an effective method for bridging between homogeneous and heterogeneous catalysis.

## 6.2 *Future prospects*

The results and findings of this study have significantly contributed towards the design and synthesis of active hydrogenation catalysts. One such finding from Chapter 3 is the role of a vacant coordinative site and phosphine ligands in developing highly active transfer hydrogenation catalysts. While the Ru(III) complexes were active due to the presence of a labile solvent ligand, the triphenylphosphine coordinated Ru(II) complexes were much more active due to the stability and the enhanced electronic properties of the metal centre imparted by the phosphine ligands. The benzimidazole complexes were also more active due to the presence of the “NH” moiety. However, the activities of these complexes were relatively low compared to some reported tridentate ruthenium complexes. This may be due to the process of reducing Ru(III) to the active Ru(II) and the relative difficulty in labilization of PPh<sub>3</sub> ligands. From the study, it was observed that the lability and electrophilicity are significant in controlling the reactivity of the complexes. We therefore propose studies to explain the roles of tridentate complexes bearing N<sup>^</sup>P donor ligands with a hemilabile arm (Figure 6.1a). The potential hemilability due to the weakly coordinating N-donor provides the coordinative flexibility to respond to changes on the metal during the catalytic cycle. The phosphine-donor stabilizes the complex and provides electrophilicity to the metal centre. Since the process of transfer hydrogenation involves the formation of metal hydride intermediate, [HRuCl(PPh<sub>3</sub>)<sub>3</sub>], metal precursor are thus proposed as starting material to synthesize the hydride complexes (Figure 6.1b)

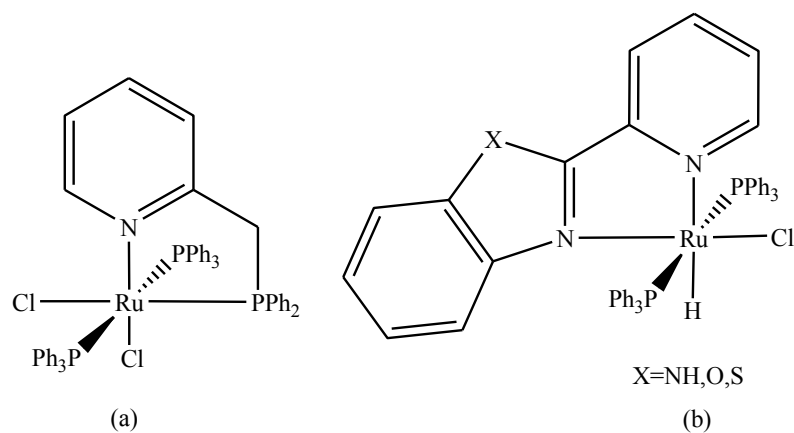


Figure 6. 1: General structures of the proposed  $N^1P$  (a) and monohydride  $N^1N$  ruthenium(II) complexes (b)

From Chapter 4, the benzoazole and the pyrazolyl palladium complexes are relatively active towards hydrogenation of the alkenes and alkynes. We observed that their activities were controlled by the strength of the metal-ancillary ligand bonds. The palladium hydride intermediate formation step and availability of a site for substrate coordination are dependent on the ease of labilization of the ligands coordinated onto the metal centre. For example, the dichloride palladium complexes were more active compared to the corresponding triphenylphosphine coordinated analogues due to the ease of labilization of chloride ligands as opposed to phosphine ligands. We envisage developing new cationic bidentate palladium(II) complexes which are hemilabile and are able to easily create a vacant site for substrate coordination (Figure 6.2).

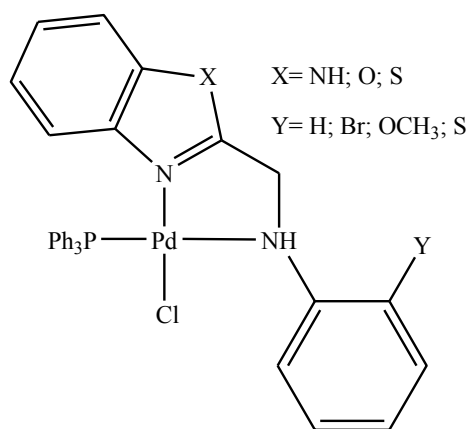


Figure 6.2: General structure of the proposed hemilabile palladium(II) complexes.

The significance of water soluble complexes in developing biphasic catalytic systems was highlighted in Chapter 5. The complexes enabled the recyclability of the complexes in hydrogenation and the ease product-catalyst separation in biphasic media. To further enhance the separation of product from the catalyst-product mixture, anchored water soluble complexes are proposed (Figure 6.3).

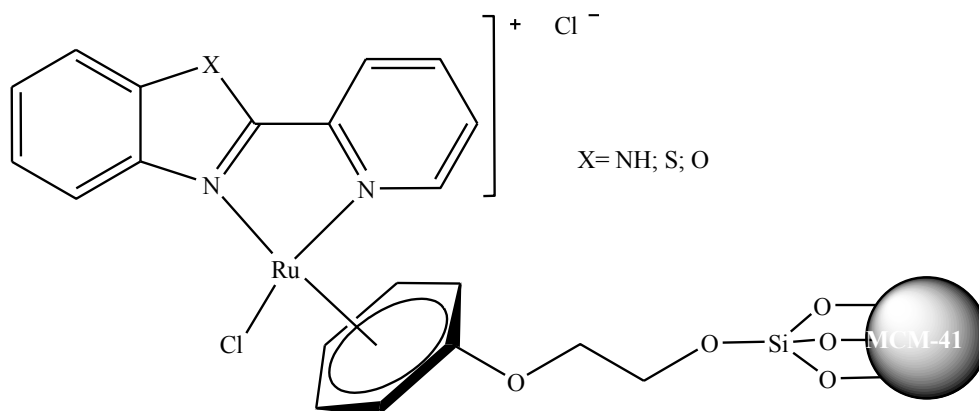


Figure 6.3: Possible structures of anchored cationic benzazole Ru(II) complexes

Finally, the importance of asymmetric catalytic hydrogenation is emphasized by the quantity of literature available and the increase in demand for chiral organic products. For these reasons we development of new chiral ruthenium complexes bearing N<sup>^</sup>N<sup>^</sup>P donor atoms (Figure 6.4) for asymmetric hydrogenation reactions is proposed.

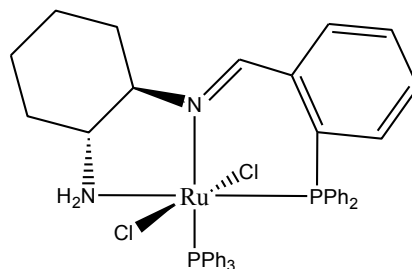


Figure 6.4: Proposed structure of asymmetric Ru(II) complexes

## References

---

1. N. S. Goncalves, M. A. S. Rios, G. Mele, I. C. G. Vasconcellos, S. E. Mazzetto, *J. Photoch Photobio. A* **184** (2006) 265-272.
2. (a) B. Cornils, W. A. Herrmann, *J. Catal.* **216** (2003) 23-31; (b) J. Hagen, *Industrial Catalysis: A Practical Approach*; Wiley-VCH: Weinheim, Germany (2006) 1-14.
3. R. Noyori, T. Ohkuma, *Angew. Chem. Int. Ed.* **40** (2001) 40-73.
4. R. A. W. Johnstone, A. H. Wilby, I. D. Entwistle, *Chem. Rev.* **85** (1985) 129-170.
5. B. Cornils, W. A. Herrmann, (Eds) Hagen, *Applied Homogeneous Catalysis with Organometallic Compounds*; VCH: Weinheim, Germany (1996) pp 22-24.
6. B. Breit, *Angew. Chem. Int. Ed.* **44** (2005) 6816-6825.
7. R. Raja, T. Khimiyak, J. M. Thomas, S. Hermans, B. F. G. Johnson, *Angew. Chem.* **113** (2001) 4774-4778.
8. (a) S. Diez-Gonzalez, N. Marion, S. P. Nolan, *Chem. Rev.* **109** (2009) 3612-3676; (b) R. H. Morris, *Chem. Soc. Rev.* **38** (2009) 2282-2291.
9. N. Meyer, A.J. Lough, R.H. Morris, *Chem. Eur. J.* **15** (2009) 5605-5610.
10. T. Liu, Y. Yang, T. Wang, H. Wang, H. Zhang, Y. Su, Z. Jiang, *Polym. Eng. Sci.* **54** (2014) 1695-1703.
11. L. Zeng, F. Wu, Y.-Y. Li, Z.-R. Dong, J.-X. Gao, *J. Organomet. Chem.* **762** (2014) 34-39.
12. Z. E. Clarke, P. T. Maragh, T. P. Dasgupta, D. G. Gusev, A. J. Lough, K. Abdur-Rashid, *Organometallics* **25** (2006) 4113-4117.
13. F. Dumur, C. R. Mayer, E. Dumas, F. Miomandre, M. Frigoli, F. Secheresse, *Org. Lett.* **10** (2008) 321-324.
14. R. Malacea, R. Poli, E. Manoury, *Coord. Chem. Rev.* **254** (2010) 729-752.



- 
15. M. C. Carrion, F. Sepulveda, F. A. Jalon, B. R. Man, A. M. Rodriguez, *Organometallics* **28** (2009) 3822-3833.
  16. D. Elma, F. Durap, M. Aydemir, A. Baysal, N. Meric, B. Ak, Y. Turgut, B. Gumgum, *J. Organomet. Chem.* **729** (2013) 46-52.
  17. L. G. Wade, *Organic Chemistry*. 8<sup>th</sup> Ed. Pearson Education Ltd; (2014) pp 442.
  18. S. Gomez, J. A. Peters, T. Maschmeyer, *Adv. Synth. Catal.* **344** (2002) 1037-1057.
  19. A. Grabulosa, A. Mannu, E. Alberico, S. Denurra, S. Gladiali, G. Muller, *J. Mol. Catal. A. Chem.* **363** (2012) 49-57.
  20. (a) M. R. Johnson, B. Rickborn, *J. Org. Chem.*, **36** (1976) 1041-1045 (b) S. W. Chaikin, W. G. Brown, *J. Am. Chem. Soc.* **71** (1949) 122-125 (c) Zassinovich, G. Mestroni, S. Gladiali, *Chem. Rev.* **92** (1992)1051-1069.
  21. (a) S. Gladiali, E. Alberico, *Chem. Soc. Rev.* **35** (2006) 226-236; (b) F. Saleem, G. K. Rao, A. Kumar, G. Mukherjee, A. K. Singh, *Organometallics* **33** (2014) 2341-2351 and the references therein.
  22. J.-E. Backvall, *J. Organomet. Chem.* **652** (2002) 105-111.
  23. W. Ponndorf, *Angew. Chem.* **39** (1926) 138-146.
  24. S. Chakraborty, H. Guan, *Dalton Trans.* **39** (2010) 7427-7436.
  25. M. Aydemir, A. Baysal, S. Ozkar, L. T. Yildirim, *Inorg. Chim. Acta.* **367** (2011) 166-172.
  26. H. Meerwein, R. Schmidt, *Liebigs Ann. Chem.* **444** (1925) 221-238.
  27. P. S. Kumbhar, J. Sanchez-Valente, J. Lopez, F. Figueras, *Chem. Commun.* (1998) 535-536.
  28. B.T. Cho, S. K. Kang, M. S. Kim, S. R. Ryub, D. K. An, *Tetrahedron* **62** (2006) 8164-8168; (b) H. C. Brown, S. Krishnamurthy, *Tetrahedron* **35** (1979) 567-607.
  29. R. V. Oppenauer, *Recl. Trav. Chim. Pays-Bas.* **56** (1937) 137-144.

- 
30. (a) P. Hauwert, G. Meastri, J. W. Sprengers, M. Catellani, C. J. Elsevier, *Angew. Chem. Int. Ed.* **47** (2008) 3223-3226; (b) G. Zassinovich, G. Mestroni, S. Gladiali, *Chem. Rev.* **92** (1992) 1051-1069; (c) X.-H. Zhu, L.-H. Cai, C.-X. Wang, Y.-N. Wang, X.-Q. Guo, X.-F. Hou, *J. Mol. Catal. A: Chem.* **393** (2014) 134-141.
31. G. Brieger, T. J. Nestruck, *Chem. Rev.* **74** (1974) 567-580.
32. M. Zhu, *Applied Catal. A: Gen.* **479** (2014) 45-48.
33. (a) C. P. Casey, S. W. Singer, D. R. Powell, R. K. Hayashi, M. Kavana, *J. Am. Chem. Soc.* **123** (2001) 1090-1100; (b) S. Horn, C. Gandolfi, M. Albrecht, *Eur. J. Inorg. Chem.* (2011) 2863-2868.
34. N. Raja, R. Ramesh. *Tetrahedron Lett.* **53** (2012) 4770-4774.
35. (a) A. C. Hillier, H. M. Lee, E. D. Stevens, S. P. Nolan, *Organometallics* **20** (2001) 4246-4252; (b) R. A. W. Johnstone, A. H. Wilby, I. D. Entwistle, *Chem. Rev.* **85** (1985) 129-170.
36. G. Zassinovich, G. Mestroni, S. Gladiali, *Chem. Rev.* **92** (1992) 1051-1089.
37. (a) N. B. Jokic, M. Z.-Presse, S. L. M. Goh, C. S. Straubinger, B. Bechlars, W. A. Herrmann, F. Khun, *J. Organomet. Chem.* **696** (2011) 3900-3905; (b) P. K. Mandal, J. S. McMurray, *J. Org. Chem.* **72** (2007) 6599-6601.
38. (a) R. H. Morris, *Chem. Soc. Rev.* **38** (2009) 2282-2291; (b) X. Wu, J. Xiao, *Chem. Commun.* (2007) 2449-2466; (d) V. Rautenstrauch, X. Hoang-Cong, R. Churlaud, K. Abdur-Rashid, R. H. Morris, *Chem. Eur. J.* **9** (2003) 4954-4967.
39. S. Ozkar, R. G. Finke, *J. Am. Chem. Soc.* **127** (2005) 4800-4808.
40. J. Li, R. Hua, *Chem. Eur. J.* **17** (2011) 8462-8465.
41. L. G. Wade, *Organic chemistry*. 6<sup>th</sup> Ed. New Jersey: Prentice Hall; (2005) pp 523.

- 
42. (a) M. K. Masato, W. Yang, *J. Am. Chem. Soc.* **11** (1994) 10793-10784; (b) Edgren, R. A. *Steroids* **59** (1994) 58-59.
43. S. K. Bhattacharyya, A. K. Sen, *Ind. Eng. Chem. Process Des. Dev.* **3** (1964) 169-176.
44. W. Reppe, W. Schweckendiek, *Liebigs Ann. Chem.* **560** (1948) 104-116.
45. (a) D. Hoegaerts, B. F. Sels, E. Dirk, D. E. De Vos, F. Verpoort, P. A. Jacobs, *Catal. Today*, **60** (2000) 209-218; (b) J. Genet, *Acc. Chem. Res.* **36** (2003) 908-918; (c) V. Touloupides, V. Kanellopoulos, P. Pladis, C. Kiparissides, D. Mignon, P. Van-Grambezen, *Chem. Eng. Sci.* **65** (2010) 3208-3222; (d) S. Oi, N. Nomura, T. Aiko, Y. Inoue, Y. *J. Mol. Catal. A Chem.* **115** (1997) 289-295; (e) A. Seayad, S. Jayasree, K. Damodaran, L. Toniolo, R. V. Chaudhari, *J. Organomet. Chem.* **601** (2000) 100-107; (f) E. Drent, P. H. M. Budzelaar, *Chem. Rev.* **96** (1996) 663-681.
46. R. Faiz, K. Li, *Chem. Eng. Sci.* **73** (2012) 261-284.
47. X. Li, B. Shen, Q. Guo, J. Gao, *Catal. Today* **125** (2007) 270-277.
48. (a) H. Kurokawa, K. Miura, K. Yamamoto, T. Sakuragi, T. Sugiyama, M. Ohshima, H. Miura, *Catalysis*, **3** (2013) 125-136; (b) S. Mizuta, S. Verhoog, K. M. Engle, T. Khotavivattana, M. O'Duill, K. Wheelhouse, G. Rassias, M. Medebielle, V. Gouverneur, *J. Am. Chem. Soc.* **135** (2013) 2505-2508; (c) R. B. Seymour, *J. Chem. Edu.* **66** (1989) 670-672.
49. B. B. H. Doreswamy, M. Mahendra, K. Mantelingu, M. A. Sridhar, J. Shashidhara, P. K. S. Rangappa, *Indian J. Chem. B* **44** (2005) 148-151.
50. M. Berthelot, *Bull. Soc. Chim. Fr.* **11** (1869) 278-286.
51. P. Sabatier, *J. Am. Chem. Soc.* **66** (1944) 1615-1617.

- 
52. (a) H. L. Poh, F. Sanek, Z. Sofer, M. Pumera, *Nanoscale* **4** (2012) 7006-7011; (b) A. J. McCue, C. J. McRitchie, A. M. Shepherd, J. A. Anderson, *J. Catal.* **319** (2014) 127-135; (c) M. Krajcia, J. Hafner, *J. Catal.* **312** (2014) 232-248.
53. (a) M. Zengin, H. Genc, T. Demirci, M. Arslan, M. Kucukislamoglu, *Tetrahedron Lett.* **52** (2011) 2333-2335; (b) J. R. Shapley, R. R. Schrock, J. A. Osborn, *J. Am. Chem. Soc.* **91** (1969) 2816-2817; (c) V. Pandarus, G. Gingras, F. Béland, R. Ciriminna, M. Pagliaro, *Org. Process Res. Dev.* **16** (2012) 1230-1234; (d) S. Monfette, Z. R. Turner, S. P. Semproni, P. J. Chirik, *J. Am. Chem. Soc.* **134** (2012) 4561-4564.
54. Q.-A. Chen, Z.-S. Ye, Y. Duan, Y.-G. Zhou, *Chem. Soc. Rev.* **42** (2013) 497-511.
55. F. Nerozzi, *Platin Met. Rev.* **56** (2012) 236-241.
56. (a) J.-J. Brunet, P. Caubere, *J. Org. Chem.* **49** (1984) 4058-4060; (b) J. Choi, N. M. Yoon, *Tetrahedron Lett.* **37** (1996) 1057-1060.
57. G. Ertl, H. Knozinger, J. Weitkamp, *Preparation of Solid Catalysts*. WILEY-VCH Verlag GmbH, D-69469 Weinheim, Germany (1999) pp 567.
58. S. Nishimura, *Bull. Chem. Soc. Jpn.* **32** (1959) 61-64.
59. U.S Patent 1.628.190: filed May 14. 1926: issued May 10. 1927 to Murray Raney. of Chattanooga, Tennessee
60. H. Adkins, Harry R. Billic, *J. Am. Chem. Soc.* **70** (1948) 695-698.
61. M. W. van Laren, C. J. Elsevier, *Angew. Chem. Int. Ed.* **38** (1999) 3715-3717.
62. J. G. Ulan, E. Kuo, W. F. Maier, R. S. Rai, G. Thomas, *J. Org. Chem.* **52** (1987) 3126-3132.
63. J. Rajaram, A. P. S. Narula, H.P.S. Chawla, S. Dev, *Tetrahedron* **39** (1983) 2315-2322.
64. K. Šiška, J. Ilavský, D. Mravec, *Chem. Pap.* **45** (1991) 541-545.
65. Y. Jiang, Q. Gao, *J. Am. Chem. Soc.* **128** (2006) 716-717.

- 
66. S. Ikeda, S. Ishino, T. Harada, N. Okamoto, T. Sakata, H. Mori, S. Kuwabata, T. Torimoto, M. Matura, *Angew. Chem.* **118** (2006) 7221-7224.
67. R. D. Adams, E. Trufan, *Phil. Trans. R. Soc. A* **368** (2010) 1473-1493
68. P.G. Jessop, T. Ikariya, R. Noyori, *Chem. Rev.* **99** (1999) 475-493
69. P. J. Dyson, D. J. Ellis, D. G. Parker, T. Welton, *Chem. Commun.* (1999) 25-26.
70. J. A. Osborn, F. H. Jardine, J. F. Young, G. Wilkinson, *J. Chem. Soc. A*, (1966) 1711-1732.
71. (a) L. Vaska, J. W. DiLuzio *J. Am. Chem. Soc.* **83** (1961) 2784-2785; (b) J. Kovacs, T. D. Todd, J. H. Reibenspies, F. Joo, D. J. Darensbourg, *Organometallics* **19** (2000) 3963-3969.
72. (a) J. Halpern, T. Okamoto, A. Zakhariyev, *J. Mol. Catal.* **2** (1976) 65-68; (b) S. B. Duckett, C. L. Newell, R. Eisenberg, *J. Am. Chem. Soc.* **116** (1994) 10548-10556.
73. W. S. Knowles, *Acc. Chem. Res.* **16** (1983)106-112.
74. (a) W. S. Knowles, *Angew. Chem. Int. Ed.* **41** (2002) 1998-2007; (b) W. S. Knowles, *Adv. Synth. Catal.* **345** (2003) 3-13.
75. J. Halpern , D. P. Riley , A. S. C. Chan , J. J. Pluth, *J. Am. Chem. Soc.* **99** (1977) 8055-8057.
76. A. H. Hoveyda, D. A. Evans , G.C. Fu, *Chem. Rev.* **93** (1993) 1307-1370.
77. P. Frediani, C. Giannelli, A. Salvini, S. Ianelli, *J. Organomet. Chem.* **667** (2003)197-208.
78. H. Sajiki, S. Mori, T. Ohkubo, T. Ikawa, A. Kume, T. Maegawa, Y. Monguchi, *Chem. Eur. J.* **14** (2008) 5109-5111.
79. T. Yuan, H. Gong, K. Kailasam, Y. Zhao, A. Thomas, J. Zhu, *J. Catal.* **326** (2015) 38-42.
80. (a) E. Peris, R. H. Crabtree, *Coord. Chem. Rev.* **248** (2004) 2239-2246; (b) L. S. Hegedus, *Transition metals in the synthesis of complex organic molecules, University science books: 2<sup>nd</sup> Ed.* Sausalito, CA, (1999) pp4.

- 
81. K. -T. Chan, Y. -H. Tsai, W. -S. Lin, J. -R. Wu, S. -J. Chen, F. -X. Liao, C.-H. Hu, H. M. Lee, *Organometallics* **29** (2010) 463-472.
82. P. Frediani, L. Rosi, L. Cetarini, M. Frediani, *Inorg. Chim. Acta* **359** (2006) 2560-2657.
83. J. I. van der Vlugt, J. N. H. Reek, *Angew. Chem. Int. Ed.* **48** (2009) 8832-8846.
84. D. Wang, D. Astruc, *Chem. Rev.* **115** (2015) 6621-6686.
85. J. Trocha-Grimshaw, H. B. Henbest, *Chem. Commun. (London)* (1967) 544-544.
86. G. Kang, S. Lin, A. Shiwakoti, B. Ni, *Catal. Commun.* **57** (2014) 111-114.
87. W. Baratta, S. Baldino, M. J. Calhorda, P. J. Costa, G. Esposito, E. Herdtweck, S. Magnolia, C. Mealli, A. Messaoudi, S. A. Mason, L. F. Veiros, *Chem. Eur. J.* **20** (2014) 13603-13617.
88. J. Moritani, Y. Kayaki, T. Ikariya, *RSC Adv.* **4** (2014) 61001-61004.
89. W. Zuo, S. Tauer, D. E. Prokopchuk, R. H. Morris, *Organometallics* **33** (2014) 5791-5801.
90. (a) P. Gamez, F. Fache, M. Lemaire, *Tetrahedron Asymmetr.* **6** (1995) 705-718; (b) R. H. Morris, *Chem. Soc. Rev.* **38** (2009) 2282-2291.
91. (a) M. Aydemir, N. Meric, A. Baysal, Y. Turgut, C. Kayan, S. Seker, M. Togrul, B. Gümgüm, *J. Organomet. Chem.* **696** (2011) 1541-1546; (b) E. P. Kelson, P.P. Phengsy, *J. Chem. Soc. Dalton Trans.* (2000) 4023-4024; (c) T. Ikariya, A. J. Blacker, *Acc. Chem. Res.* **40** (2007) 1300-1308; (d) D. Pandiarajan, R. Ramesh, *J. Organomet. Chem.* **723** (2013) 26-35.
92. Y. Sasson, J. Blum, *Tetrahedron Lett.* (1971) 2167-2170.
93. R. L. Chowdhury, J.-E. Backvall, *J. Chem. Soc. Chem. Commun.* (1991) 1063-1064.
94. Y. Sasson, J. Blum, *J. Org. Chem.* **40** (1975) 1887-1896.
95. M. Aydemir, N. Meric, F. Durap, A. Baysal, M. Togrul, *J. Organomet. Chem.* **695** (2010) 1392-1398.

- 
96. (a) S. E. Clapham, A. Hadzovic and R. H. Morris, *Coord. Chem. Rev.* **248** (2004) 2201-2237;  
(b) A. E. Braude, R. P. Linstead, *J. Chem. Soc.* (1954) 3544-3547.
97. L. Wang, Q. Yang, H.-Y. Fu, H. Chen, M.-L. Yuan, R.-X. Li, *Appl. Organometal. Chem.* **25**  
(2011) 626-631.
98. F. Zeng, Z. Yu, *Organometallics* **27** (2008) 6025-6028.
99. Z. K. Yu, F. L. Zeng, X. J. Sun, H. X. Deng, J. H. Dong, J. Z. Chen, H. M. Wang, C. X. Pei,  
*J. Organomet. Chem.* **692** (2007) 2306-2313.
100. F. L. Zeng, Z. K. Yu, *Organometallics* **27** (2008) 2898-2901.
101. (a) N. J. Beach, G. J. Spivak, *Inorg. Chim. Acta* **343** (2003) 244-252. (b) S. Gulcemel, A.  
G. Gokce, B. Cetinkaya, *Dalton Trans.* **42** (2013) 7305-7311.
102. T. Chen, L.-P. He, D. Gong, L. Yang, X. Miao, J. Eppinger, K. -W. Haung, *Tetrahedron  
Lett.* **53** (2012) 4409-4412.
103. O. Dayan, S. Demirmen, N. Özdemir, *Polyhedron* **85** (2015) 926-932.
104. (a) S. Dayan, F. Arslan, N. K. Ozpozan, *Appl Catal. B: Environ.* **164** (2015) 305-315; (b) S.  
Gulcemel, A. G. Gokce, B. Cetinkaya, *Dalton Trans.* **42** (2013) 7305-7311.
105. (a) J. Takehara, S. Hashiguchi, A. Fujii, S. Inoue, T. Ikariya, R. Noyori, *J. Chem.  
Soc. Chem. Commun.* (1996) 233-234; (b) S. Hashiguchi, A. Fujii, J. Takehara, T. Ikariya, R.  
Noyori, *J. Am. Chem. Soc.* **117** (1995) 7562-7563.
106. K. Matsumura, S. Hashiguchi, T. Ikariya, R. Noyori, *J. Am. Chem. Soc.* **119** (1997) 8738-  
8739.
107. R. G. Guo, R. H. Morris, D. Song, *J. Chem. Soc.* **127** (2005) 516-517.
108. W. Baratta, G. Chelucci, S. Gladioli, K. Siega, M. Toniutti, M. Zanette, E. Zangrando, P.  
Rigo, *Angew. Chem. Int. Ed.* **44** (2005) 6214-6219.

- 
109. D. J. Morris, A.M. Hayes, M. Wills, *J. Org. Chem.* **71** (2006) 7035-7044.
110. (a) S. Karabuga, S. Bars, I. Karakaya, S. Gumus, *Tetrahedron Lett.* **56** (2015) 101-104; (b) Z. R. Dong, Y. Y. Li, S. L. Yu, G. S. Sun, J. X. Gao, *Chinese Chem. Lett.* **23** (2012) 533-536
111. (a) A. Togni, L. M. Venanzi, *Angew. Chem. Int. ed. Engl.* **33** (1994) 497- 526; (b) M. Zhao, Z. Yu, S. Yan, Y. Li, *J. Organomet. Chem.* **694** (2009) 3068-3075; (c) J. G. Malecki, T. Gron, H. Duda, *Polyhedron* **31** (2012) 319-331.
112. T. Ohkuma, H. Ooka, S. Hashiguchi, T. Ikariya, R. Noyori, *J. Am. Chem. Soc.* **117** (1995) 2675-2676.
113. D.A. Cavarzan, F. D. Fagundes, O. Fuganti, C. W.P. da Silva, C. B. Pinheiro, D. F. Back, A. Barison , A. L. Bogado, M. P. de Araujo, *Polyhedron* **62** (2013) 75-82.
114. C. A. Sandoval, T. Ohkuma, K. Muniz, R. Noyori, *J. Amer. Chem. Soc.* **125** (2003) 13490-13503.
115. H. Kumobayashi, *Recl. Trav. Chim. Pays-Bas* **115** (1996) 201-210.
116. O. Pamies, J.-E. Backvall, *Chem. Eur. J.* **7** (2001) 5052-5058.
117. W. Ponndorf, *Angew. Chemie*, **39** (1926) 138-143
118. Y. R. S. Laxmi, J. -E. Bäckvall, *Chem. Comm.* (2000) 611-612.
119. (a) J. S. M. Samec, J. -E. Backvall, P. G. Andersson, P. Brandt, *Chem. Soc. Rev.* **35** (2006) 237-248 (b) W. Baratta, M. Ballico, G. Esposito, P. Rigo, *Chem. Eur. J.* **14** (2008) 5588-5595 (c) S. Bi, Q. Xie, X. Zhao, Y. Zhao, X. Kong, *J. Organomet. Chem.* **693** (2008) 633-638 (d) H. A. McManus, S. M. Barry, P. G. Anderson, P. J. Guiry, *Tetrahedron* **60** (2004) 3405-3416.
120. T. Privalov, J. S. M. Samec, J. -E. Backvall, *Organometallics* **26** (2007) 2840-2848.
121. A. Aranyos, G. Csjernyk, K. J. Szabo, J.-E. Backvall, *Chem. Commun.* (1999) 351-352.



- 
122. H. D. Kaesz, R. B. Saillant, *Chem. Rev.* **72** (1972) 231-281.
123. S. Gladiali, L. Pinna, G. Delogu, S. De Martin, G. Zassinovich, G. Mestroni, *Tetrahedron Asymmetr.* **1** (1990) 635-648.
124. R. Hudson, A. Rivie`re, C. M. Cirtiu, K. L. Luska, A. Moores, *Chem. Commun.* **48** (2012) 3360-3362.
125. C. S. Yi, D. W. Lee, *Organometallics* **18** (1999) 5152-5156.
126. K. H. Hopmann, A. Bayer, *Organometallics* **30** (2011) 2483-2497.
127. D. Chatterjee, H. C. Bajaj, A. Das, K. Bhatt, *J. Mol. Catal.* **92** (1994) L235-L238.
128. T. Zhang, B. Li, X. Zhang, J. Qiu, W. Han, K. Lun Yeung, *Micropor. Mesopor. Mat.* **197** (2014) 324-330.
129. R. A.W. Johnstone, J.-Y. Liu, L. Lu, D. Whittaker, *J. Mol. Catal. A: Chem.* **191** (2003) 289-294.
130. (a) J. J. Verendel, O. Pamies, M. Dieguez, P. G. Anderson, *Chem. Rev.* **114** (2014) 2130-2169; (b) J. P. Collman, W. R. Roper, *J. Am. Chem. Soc.* **87** (1965) 4008-4009.
131. W. M. Mo, B. S. Wan, S. J. Liao, *Chinese Chem. Lett.* **12** (2001) 817-820.
132. C. K. Lambert, R. D. Gonzalez, *Catal. Lett.* **57** (1999)1-7.
133. (a) T. Naota, H. Takaya, S.-I. Murahashi, *Chem. Rev.* **98** (1998) 2599-2660; (b) A. M. Lozano-Vila, S. Monsaert, A. Bajek, F. Verpoort, *Chem. Rev.* **110** (2010) 4865-4909; (c) C. Gunanathan, D. Milstein, *Chem. Rev.* **114** (2014) 12024-12087.
134. (a) W. T. Tysoe, G. L. Nyberg, R. M. Lambert, *J. Phys. Chem.* **88** (1984) 1960-1963; (b) P.-H. Phua, L. Lefort, J. A. F. Boogers, M. Tristany, J. G. de Vries, *Chem. Commun.* (2009) 3747-3749.
135. N. Yan, C.X. Xiao, Y. Kou, *Coord. Chem. Rev.* **254** (2010) 1179-1218.

- 
136. (a) T. T. Pham, L. L. Lobban, D. E. Resasco, R. G. Mallinson, *J. Catal.* **266** (2009) 9-14;  
(b) D. Teschner, Z. Rvay, J. Borsodi, M. Havecker, A. Knop-Gericke, R. Schlogl, D. Milroy, S. D. Jackson, D. Torres, P. Sautet, *Angew. Chem. Int. Ed.* **47** (2008) 9274-9278.
137. P. W. N. M. van Leeuwen, J. C. Chadwick, *Homogeneous Catalysis, Activity-Stability-Deactivation*, Wiley-VCH, Weinheim, Germany, (2005)
138. D. Drago, P. S. Pregosin, *Organometallics* **21** (2002) 1208-1215.
139. M. W. van Laren, M. A. Duin, C. Klerk, M. Naglia, D. Rogolino, P. Pelagatti, A. Bacchi, C. Pelizzi, C. J. Elsevier, *Organometallics* **21** (2002) 1546-1553.
140. C. Borriello, M. L. Ferrara, I. Orabona, A. Panunzi, F. Ruffo, *J. Chem. Soc. Dalton Trans.* (2000) 2545-2550.
141. A. Bacchi, M. Carcelli, M. Costa, P. Pelagatti, C. Pelizzi and G. Pelizzi, *Gazz. Chim. Ital.*, **124** (1994) 429-434.
142. (a) A. Bacchi, M. Carcelli, M. Costa, A. Leporati, P. Pelagatti, C. Pelizzi, G. Pelizzi, *J. Organomet. Chem.* **535** (1997) 107-120; (b) P. Pelagatti, A. Bacchi, M. Carcelli, M. Costa, A. Fochi, P. Ghidini, E. Leporati, M. Masi, C. Pelizzi, G. Pelizzi, *J. Organomet. Chem.* **583** (1999) 94-105.
143. A. Bacchi, M. Carcelli, L. Gabba, S. Ianelli, P. Pelagatti, G. Pelizzi, D. Rogolino, *Inorg. Chim. Acta* **342** (2003) 229-235.
144. J. W. Prengers, J. Wassenaar, N. D. Clement, K. J. Cavell, C. J. Elsevier, *Angew. Chem. Int. Ed.* **44** (2005) 2026-2029.
145. W.S. Mahoney, J.M. Stryker, *J. Am. Chem. Soc.* **111** (1989) 8818-8823.
146. A. M. Doyle, S. K. Shaikhutdinov, S. D. Jackson, H. -J. Freud, *Angew. Chem. Int. Ed.* **42** (2003) 5240-5243.

- 
147. A. M. Kluwer, T. S. Koblenz, T. Jonischkeit, K. Woelk, C. J. Elsevier, *J. Am. Chem. Soc.* **127** (2005) 15470-15480.
148. (a) J. Halpern, C. S. Won, *Chem. Commun.* (1973) 629-630; (b) J. Halpern, T. Okamoto, A. Zakhariiev, *J. Mol. Catal.* **2** (1976) 65-68.
149. D. Chandrika Mudalige, G. L. Rempel, *J. Mol. Catal. A: Chem.* **123** (1997) 15-20.
150. K. Sung, S. Huh, M. Jun, *Polyhedron* **18** (1999) 469-474.
151. S. Huh, Y. Cho, M.-J. Jun, D. Whang, K. Kim, *Polyhedron* **13** (1994) 1887-1894.
152. (a) L. Salvi, A. Salvini, F. Micoli, C. Bianchini, W. Oberhauser, *J. Organomet. Chem.* **692** (2007) 1442-1450; (b) M. O. Albers, E. Singleton, M. M. Viney, *J. Mol. Catal* **33** (1985) 77-89.
153. (a) C. S. Yi, D. W. Lee, *Organometallics* **18** (1999) 5152-5156; (b) C. S. Yi, D. W. Lee, Y. Chen, *Organometallics* **18** (1999) 2043-2045.
154. (a) C. Gandolfi, M. Heckenroth, A. Neels, G. Laurency, M. Albrecht, *Organometallics*, **28** (2009) 5112-5113; (b) G. Albettin, P. Amendok, S. Antoniutti, S. Ianelli, G. Pelizzi, E. Bordigno, *Organometallics* **10** (1991) 2876-2883.
155. C. Gandolfi, M. Heckenroth, A. Neels, G. Laurency, M. Albrecht, *Organometallics* **28** (2009) 5112-5121.
156. I. W. Davies, L. Matty, D. L. Hughes, P. J. Reider, *J. Am. Chem. Soc.* **123** (2001) 10139-10140.
157. N. Ren, Y. Yang, Y. Zhang, Q. Wang, Y. Tang, *J. Catal.* **246** (2007) 215-222.
158. C. de Bellefon, N. Tanchoux, S. Caravieilhès, *J. Organomet. Chem.* **567** (1998) 143-150.
159. C. Stangel, G. Charalambidis, V. Varda, A. G. Coutsolelos, I. D. Kostas, *Eur. J. Inorg. Chem.* (2011) 4709-4716.

- 
160. S. Alexander, V. Udayakumar, V. Gayathri, *J. Mol. Catal. A. Chem.* **314** (2009) 21-27
161. V. Caballero, F. M. Bautista, J. M. Campelo, D. Luna, R. Luque, J. M. Marinas, A. A. Romero, I. Romero, M. Rodrigues, I. Serrano, J. M. Hidalgo, A. Llobet, *J. Mol. Catal., A. Chem.* **308** (2009) 41-45.
162. (a) T. J. Geldbach, P. J. Dyson, *J. Am. Chem. Soc.* **126** (2004) 8114-8115; (b) B. Cornils, W. A. Herrmann, I. T. Horvath, W. Leitner, S. Mecking, H. Olivier-Bourbigou, D. Vogt (Eds) *Multiphase Homogeneous Catalysis*, Wiley-VCH, Weinheim, Germany, (2005)
163. P. Wasserscheid, H. Waffenschmidt, P. Machnitzki, K. W. Kottsieper, O. Stelzer, *Chem. Comm.* **5** (2001) 451-452.
164. (a) B. Cornils, *J. Mol. Catal. A: Chem.* **143** (1999) 1-10; (b) A. Bouriazos, S. Sotiriou, P. Stathis, G. Papadogianakis, *Appl Catal. B: Environ.* **150-151** (2014) 345-353.
165. A. A. Dabbawala, H. C. Bajaj, H. Bricout, E. Monflier, *Catal. Sci. Technol.* **2** (2012) 2273-2278.
166. (a) H. Syska, W.A. Herrmann, F. E. Kuhn, *J. Organomet. Chem.* **703** (2012) 56-62; (b) S. Ogo, T. Abura, Y. Watanabe, *Organometallics* **21** (2002) 2964-2969.
167. (a) Y. Wang, X. Wu, F. Cheng, Z. Jin, *J. Mol. Catal. A. Chem.* **195** (2003) 133-137; (b) B. Richter, A. L. Spek, G. van Koten, B. Deelman, *J. Am. Chem. Soc.* **122** (2000) 3945-3951.
168. A. Andriollo, A. Bolivar, F.A. Lopez, D.E. Paez, *Inorganica Chimica Acta.* **238** (1995) 187-192.
169. (a) P. J. Dyson, D. J. Ellis, T. Welton, *Platin. Met. Rev.* **42**(1998) 135-140; (b) F. Joó , *Aqueous Organometallic Catalysis* Kluwer Academic Publishers, Dordrecht, Netherlands (2002).
170. H. B. Zang, L. lui, Y. J. Chen, D. Wang, C. J. Li, *Eur. J. Org. Chem.* (2006) 869-873.

- 
171. C. A. Mebi, B. J. Frost, *Organometallics* **24** (2005) 2339-2346.
172. N. S. Goncalves, M. A. S. Rios, G. Mele, I. C. G. Vasconcellos, S. E. Mazzetto, *J. Photoch Photobio. A* **184** (2006) 265-272.
173. H. Deng, Z. Yu, J. Dong, S. Wu, *Organometallics* **24** (2005) 4110-4112.
174. G. Zassinovich, G. Mestroni, S. Gladiali, *Chem. Rev.* **9** (1992) 1051-1069.
175. S. L. Yu, Y. Y. Li, Z. R. Dong, J. X. Gao, *Chinese Chem. Lett.* **23** (2012) 395-398.
176. I. Moldes, E. de la Encarnacion, J. Ros, A. Alvarez-Larena, J. F. Piniella, *J. Organomet. Chem.* **566** (1998) 165-178.
177. R. A. Krause, *Inorg. Chim. Acta* **22** (1977) 209-213.
178. Y. Jiang, J. Qiongzong, X. Zhang, *J. Am. Chem. Soc.* **120** (1998) 3817-3818.
179. M. P. Araujo, A. T. Figueiredo, A. L. Bogado, G. V. Poelhsitz, J. Ellena, E. E. Castellano, C. L. Donnici, J. V. Comasseto, A. A. Batista, *Organometallics* **24** (2005) 6159-6168.
180. D. Elma, F. Durap, M. Aydemir, A. Baysal, N. Meric, B. Ak, Y. Turgut, B. Gumgum, *J. Organomet. Chem.* **729** (2013) 46-55.
181. (a) S. Enthaler, R. Jackstell, B. Hagemann, K. Junge, G. Erre, M. Beller, *J. Organomet. Chem.* **691** (2006) 4652-4659; (b) Z. R. Dong, Y. Y. Li, S. L. Yu, G. S. Sun, J. X. Gao, *Chinese Chem. Lett.* **23** (2012) 533-535.
182. N. Park, Y. Heo, M. R. Kumar, Y. Kim, K. H. Song, S. Lee, *Eur. J. Org. Chem.* (2012) 1984-1993.
183. (a) A. D. Becke, *Chem. Phys.* **98** (1993) 5648-5652; (b) C. T. Lee, W. T. Yang, R. G. Parr, *Phys. Rev. B.* **37** (1988) 785-789.
184. P. J. Hay, W. R. Wadt, *Chem. Phys.* **82** (1985) 270-283.

- 
185. Gaussian 09, Revision *A.1*, M. J. Frisch, G. W. Trucks, H. B. Schlegel, G. E. Scuseria, M. A. Robb, J. R. Cheeseman, G. Scalmani, V. Barone, B. Mennucci, G. A. Petersson, H. Nakatsuji, M. Caricato, X. Li, H. P. Hratchian, A. F. Izmaylov, J. Bloino, G. Zheng, J. L. Sonnenberg, M. Hada, M. Ehara, K. Toyota, R. Fukuda, J. Hasegawa, M. Ishida, T. Nakajima, Y. Honda, O. Kitao, H. Nakai, T. Vreven, J. A. Montgomery, Jr., J. E. Peralta, F. Ogliaro, M. Bearpark, J. J. Heyd, E. Brothers, K. N. Kudin, V. N. Staroverov, R. Kobayashi, J. Normand, K. Raghavachari, A. Rendell, J. C. Burant, S. S. Iyengar, J. Tomasi, M. Cossi, N. Rega, J. M. Millam, M. Klene, J. E. Knox, J. B. Cross, V. Bakken, C. Adamo, J. Jaramillo, R. Gomperts, R. E. Stratmann, O. Yazyev, A. J. Austin, R. Cammi, C. Pomelli, J. W. Ochterski, R. L. Martin, K. Morokuma, V. G. Zakrzewski, G. A. Voth, P. Salvador, J. J. Dannenberg, S. Dapprich, A. D. Daniels, O. Farkas, J. B. Foresman, J. V. Ortiz, J. Cioslowski, and D. J. Fox, Gaussian, Inc., Wallingford CT, (2009).
186. Bruker (2010). APEX2, SAINT and SADABS. Bruker AXS Inc., Madison, Wisconsin, USA.
187. G. M. Sheldrick, *Acta Cryst.* **A64** (2008) 112-122.
188. L. J. Farrugia, *J. Appl. Cryst.* **32** (1999) 837-838.
189. F. Zeng, Z. Yu, *Organometallics* **28** (2009)1855-1862.
190. M. Serratrice, M. A. Cinellu, L. Maiore, M. Pilo, A. Zucca, C. Gabbiani, A. Guerri, I. Landini, S. Nobili, E. Mini, L. Messori, *Inorg. Chem.* **51** (2012) 3161-3171.
191. A. Valore, M. Balordi, A. Colombo, C. Dragonetti, S. Righetto, D. Roberto, R. Ugo, T. Benincori, G. Rampinini, F. Sannicol'o, F. Demartine, *Dalton Trans.* **39** (2010) 10314-10318.
192. J. Weiwei, W. Laindi, Y. Zhengkun, *Organometallics* **31** (2012) 5664-5672.

- 
193. A. A. Batista, M. O. Santiago, C. L. Donnici, I. S. Moreira, P. C. Healy, S. J. Berners-Price, S. L. Queiroz, *Polyhedron* **20** (2001) 2123-2128.
194. M. Aydemir, N. Meric, A. Baysal, *J. Organomet. Chem.* **72** (2012) 38-45.
195. Y. Cheng, X. Lu, H. Xu, Y. Li, X. Chen, Z. Xue, *Inorg. Chim. Acta* **363** (2010) 430-437.
196. S. J. La-Placa, J. A. Ibers, *Inorg. Chem.* **4** (1965) 778-783.
197. S. P. Baran, J. M. Ritcher, *Heterocyclic Chemistry*, Lecture Notes. Retrieved from <http://www.scripps.edu/baran/heterocycles/>
198. S. E. Clapham, A. Hadzovic, R. H. Morris, *Coord. Chem. Rev.* **248** (2004) 2201-2237.
199. Y. Jiang, Q. Jiang, X. Zhang, *J. Am. Chem. Soc.* **120** (1998) 3817-3818.
200. L. J. Hounjet, M. J. Ferguson, M. Cowie, *Organometallics* **30** (2011) 4108-4114.
201. K. A. Rashid, A. J. Lough, R. H. Morris, *Organometallics* **19** (2000) 2655-2657.
202. J. W. Faller, A. R. Lavoie, *Organometallics* **20** (2001) 5245-5247.
203. M. C. Carrion, F. Sepulveda, F. A. Jalon, B. R. Manzano, *Organometallics* **28** (2009) 3822-3833.
204. A. Grabulosa, A. Mannu, A. Mezzetti, G. Muller, *J. Organomet. Chem.* **696** (2012) 4221-4228.
205. V. Cadierno, P. Crochet, J. Diez, S. E. Garcia-Garrido, J. Gimeno, *Organometallics* **23** (2004) 4836-4845.
206. (a) A. Arnayos, G. Csjernyik, K. J. Szabo, J. -E. Backvall, *Chem. Comm.* (1999) 351-352; (b) D. E. Linn, J. Halpern, *J. Am. Chem. Soc.* **109** (1987) 2969-2974; (c) L. S. Van Der Sluys, G. J. Kubas, K. G. Caultaon, *Organometallics* **10** (1991) 1033-1038.
207. R. G. Pearson, *J. Chem. Educ.* **64** (1987) 561-567.

- 
208. F. Corvaisier, Y. Schurman, A. Fecant, C. Thomazeau, P. Raybaud, H. Toulhoat, D. Farrusseng, *J. Catal.* **307** (2013) 352-361.
209. (a) K. A. Vallianatou, D. J. Frank, G. Antonopoulou, S. Georgakopoulos, E. Siapi, M. Zervou, I. D. Kostas, *Tetrahedron Lett.* **54** (2013) 397-401; (b) D.-S. Wang, Q.-A. Chen, S.-M. Lu, Y.-G. Zhou, *Chem. Rev.* **112** (2012) 2557-2590.
210. (a) H. E. Hoelscher, W. G. Poynter, E. Weger, *Chem. Rev.* **54** (1954) 575-592; (b) R. Harmon, S. K. Gupta, D. J. Brown, *Chem. Rev.* **73** (1973) 21-52.
211. O. Schmidt, *Chem. Rev.* **12** (1933) 363-417; (b) S.D. Jackson, L. A. Shaw, *Appl. Catal. A: Gen.* **134** (1996) 91-99.
212. A. M. Doyle, S. K. Shaikhutdinov, H. -J. Freund, *J. Catal.* **223** (2004) 444-453
213. J. Halpern, J. F. Harrod, B. R. James, *J. Amer. Chem. Soc.* **88** (1966) 5150-5155.
214. J. L. Zuffa, M. L. Blohm, W. L. Gladfelter, *J. Am. Chem. Soc.* **108** (1986) 552-553
215. (a) Y. Zhang, S. Liao, Y. Xu, D. Yu, *Appl. Catal. A: Gen.* **192** (2000) 247-251; (b) Q.-A. Chen, Z. -S. Ye, Y. Duan, Y. -G. Zhou, *Chem. Soc. Rev.* **42** (2013) 497-511.
216. F. A. Harraz, S. E. El-Hout, H. M. Killa, I. A. Ibrahim, *J. Catal.* **286** (2012) 184-192
217. (a) J. G. Ulan, W. F. Maier, *J. Org. Chem.* **52** (1987) 3132-3142; (b) R. -J. Liua, P.A. Croziera, C. M. Smith, D.A. Huculc, J. Blacksond, G. Salaita, *Appl. Catal. A: Gen.* **282** (2005) 111-121; (c) M. A. Aramend'ia, V. Borau, C. Jim'enez, J. M. Marinas, A. Porras, F. J. Urbano, *J. Catal.* **172** (1997) 46-54.
218. F. Yilmaz, A. Mutlu, H. Unver, M. Kurtca, I. Kani, *J. Supercrit. Fluids* **54** (2010) 202-209.
219. J. P. Collman, L. Zeng, John I. Brauman, *Inorg. Chem.* **43** (2004) 2672-2679.
220. B. Munoz, A. Marinetti, A. Ruiz, S. Castillon, C. Claver, *Inorg. Chem. Comm.* **8** (2005) 1113-1115.



- 
221. D.W. Hein, R.J. Alheim, J. J. Leavit, *J. Am. Chem. Soc.* **79** (1957) 427-429.
- 222 S. O. Ojwach, I. A. Guzei, J. Darkwa, *J. Organomet. Chem.* **694** (2009) 1393-1399.
223. (a) S. O. Ojwach, G. Westman, J. Darkwa, *Polyhedron* **26** (2007) 5544-5552; (b) W. Chen, C. Xi, Y. Wu, *J. Organomet. Chem.* **692** (2007) 4381-4388.
224. Bruker (2010). APEX2, SAINT and SADABS. Bruker AXS Inc., Madison, Wisconsin, USA.
225. G. M. Sheldrick, *Acta Cryst.* **A64** (2008) 112-122.
226. L. J. Farrugia, *J. Appl. Cryst.* **32** (1999) 837-854.
227. D. W. Hein, R. J. Alheim, J. J. Leavitt, *J. Am. Chem. Soc.* **79** (1957) 427-429.
- 228 S. O. Ojwach, I. A. Guzei, J. Darkwa, *J. Organomet. Chem.* **694** (2009) 1393-1399.
229. D. J. Nielsen, K. J. Cavell, B. W. Skelton, A. H. White, *Inorg. Chim Acta.* **359** (2006) 1855-1869.
230. (a) P.A. Aguirre, C. A. Lagos, S. A. Moya, C. Zuninga, C. Vera-Oyarce, E. Sola, G. Peris, J. C. Bayon *Dalton Trans.* (2007) 5419-5426; (b) K. R. Reddy, K. Surekha. G. -H. Lee, S. -M. Peng, J. -T. Chen, S.-T. Liu, *Organometallics* **20** (2001) 1292-1299.
231. S. Haneda, Z. Gan, K. Eda, M. Hayashi, *Organometallics* **26** (2007) 6551-6555.
232. L. S. Hegedus, *Transition metals in the synthesis of complex organic molecules*, University science books: Sausalito, CA, (1999) pp15.
233. D. J. M. Snelders, N. Yan, W. Gan, G. Laurenczy, P. J. Dyson, *ACS Catal.* **2** (2012) 201-207.
234. (a) P. J. Rheinlander, J. Herranz, J. Durst, H. A. Gasteiger, *J. Electrochem. Soc.* **161** (2014) F1448-F1457; (b) M. H. Kima, E. K. Leea, J. H. Juna, S. J. Konga, G. Y. Hana, B. K. Leeb, T.-J. Leec, K. J. Yoona, *Int. J. Hydrogen Energ.* **29** (2004) 187-193

- 
235. D. Teschner, Z. Revay, J. Borsodi, M. Havecker, A. Knop-Gericke, R. Schlogl, D. Milroys, S. D. Jackson, D. Torres, P. Sautet, *Angew. Chem. Int. Ed.* **47** (2008) 9274-9248.
236. (a) H. Yoshida, T. Zama, S. Fujita, J. Panpranot, M. Arai, *RSC Adv.* **4** (2014) 24922-24928; (b) M. Costa, P. Pelagatti, C. Pelizzi, D. Rogolino, *J. Mol. Catal. A. Chem.* **178** (2002) 21-26; (c) G. C. Bond, *Disc. Faraday Soc.* **41**(1966) 200-214.
237. G. Schmid, S. Emde, V. Maihack, W. Meyer-Zaika, S. Peschel, *J. Mol. Catal. A: Chem.* **107** (1996) 95-104.
238. A. Bernas, N. Kumar, P. Mäki-Arvela, N.V. Kul'kova, B. Holmbom, T. Salmi, D. Y. Murzin, *Appl. Catal. A: Gen.* **245** (2003) 257-275
239. K. Okitsu, A. Yue, S. Tanabe, H. Matsumoto, *Chem. Mater.* **12** (2000) 3006-3011
240. P.S. Hallman, B. R. McGavey. G. Wilkinson, *J. Chem. Soc. A*, (1968) 3143-3150.
241. J. March, *Advanced Organic Chemistry: Reactions, Mechanisms, and Structure*, Wiley: New York, NY, (1992) pp111.
242. P. Frediani, C. Giannelli, A. Salvini, S. Ianelli, *J. Organomet. Chem.* **667** (2003) 197-208.
243. (a) S. Kamiguchi, S. Takaku, M. Kodomari, T. Chihara, *J. Mol. Catal., A: Chem.* **260** (2006) 43-48; (b) W. Carruther, I. Coldham, *Modern methods of organic synthesis, 4<sup>th</sup> Ed*, Cambridge University Press, Cambridge, UK (2004) pp 34.
244. Z. Dobrovolna, P. Kacer, L. Cerveny, *J. Mol. Catal. A. Chem.* **130** (1998) 279-284.
245. R. Flores, Z. K. Lopez-Castillo, I. Kani, J. P. Fackler, Jr., *Ind. Eng. Chem. Res.* **42** (2003) 6720-6729.
246. K. Abdur-Rashid, T. Fedorkiw, A. J. Lough, R. H. Morris, *Organometallics* **23** (2004) 86-94
247. J. A. Widegren, R. G. Finke, *J. Mol. Catal. A. Chem.* **198** (2003) 317-341

- 
248. (a) E. A. Karakhanov, A. L. Maksimova, E. M. Zakhariana, Y. S. Kardashevaa, S. V. Savilov, N. I. Truhmanova, A.O. Ivanov, V. A. Vinokurov, *J. Mol. Catal. A: Chem.* **397** (2015) 1-18; (b) X. Liu, Z. Zhang, Y. Yang, D. Yin, S. Su, D. Lei, J. Yang, *Chem. Eng. J.* **263** (2015) 290-298.
249. (a) K. S. Weddle, J. D. Aiken III, R. G. Finke, *J. Chem. Soc.* **120** (1998) 5683-5666 (b) Y. Wang, Y. Denga, F. Shi, *J. Mol. Catal. A: Chem.* **395** (2014) 195-201.
250. (a) G. Schmid, V. Maihack, F. Lanternmann, S. Peschel, *J. Chem. Soc., Dalton Trans.* (1996) 589-595 (b) G. Schmid, *Chem. Rev.* **92** (1992) 1709-1727.
251. S. P. Smidt, N. Zimmermann, M. Studer, A. Pfaltz, *Chem. Eur. J.* **10** (2004) 4685-4693.
252. P. Pelagatti, A. Venturini, A. Leporati, M. Carcelli, M. Costa, A. Bacchi, G. Pelizzi, C. Pelizzi, *J. Chem. Soc., Dalton Trans.* (1998) 2715-2721.
253. C.S. Yi, D. W. Lee, *Organometallics* **18** (1999) 5152-5156.
254. J. Gaube, H.-F. Klein, *Appl. Catal. A: Gen.* **470** (2014) 361-368.
255. J. P. Rao, K. E. Geckeler, *Prog. Polym. Sci.* **36** (2011) 887-913.
256. K. Naka, Y. Chujo, *Nanohybridization of Organic-Inorganic Materials, Advances in Materials Research*, **13** (2009) 3-40.
257. S. Haneda, Z. Gan, K. Eda, M. Hayashi, *Organometallics* **26** (2007) 6551-6555.
258. B. Cornils W. A. Herrman, *J. Catal.* **216** (2003) 23-31.
259. J. Hagen, *Industrial Catalysis: A Practical Approach*, Wiley-VCH: Weinheim, Germany (2006) 1-14.
260. E. L. V. Goetheer, A. W. Verkerk, L. J. P. van den Broeke, E. de Wolf, B. Deelman, G. van Koten, J. T. F. Keurentjes, *J. Catal.* **219** (2003) 126-133.
261. P.G. Jessop, T. Ikariya, R. Noyori, *Chem. Rev.* **99** (1999) 475-493.

- 
262. M. Heitbaum, F. Glorius, I. Escher, *Angew. Chem. Int. Ed.* **45** (2006) 4732-4762.
263. K. De Smet, S. Aerts, E. Ceulemans, I. F. J. Vankelecom, P. A. Jacobs, *Chem. Comm.* (2001) 597-598.
264. I. W. Davies, L. Matty, D. L. Hughes, P. J. Reider, *J. Am. Chem. Soc.* **123** (2001) 10139-10140.
265. N. Ren, Y. Yang, Y. Zhang, Q. Wang, Y. Tang, *J. Catal.* **246** (2007) 215-222.
266. C. de Bellefon, N. Tanchoux, S. Caravieilhès, *J. Organomet. Chem.* **567** (1998) 143-150.
267. S. Alexander, V. Udayakumar, V. Gayathri, *J. Mol. Catal., A. Chem.* **314** (2009) 21-27.
268. V. Caballero, F. M. Bautista, J. M. Campelo, D. Luna, R. Luque, J. M. Marinas, A. A. Romero, I. Romero, M. Rodrigues, I. Serrano, J. M. Hidalgo, A. Llobet, *J. Mol. Catal., A. Chem.* **308** (2009) 41-45.
269. T. J. Geldbach, P. J. Dyson, *J. Am. Chem. Soc.* **126** (2004) 8114-8115.
270. P. Wasserscheid, H. Waffenschmidt, P. Machnitzki, K. W. Kottsieper, O. Stelzer, *Chem. Comm.* **5** (2001) 451-452.
271. C. Stangel, G. Charalambidis, V. Varda, A. G. Coutsolelos, I. D. Kostas, *Eur. J. Inorg. Chem.* (2011) 4709-4716.
272. Y. Wang, X. Wu, F. Cheng, Z. Jin, *J. Mol. Catal. A. Chem.* **195** (2003) 133-137.
273. B. Cornils, *J. Mol. Catal. A: Chem.* **143** (1999) 1-10.
274. (a) P. J. Dyson, D. J. Ellis, T. Welton, *Platin. Met. Rev.* **42** (1998) 135-140; (b) F. Joó, *Aqueous Organometallic Catalysis*, Kluwer Academic Publishers, Dordrecht, Netherlands (2002); (c) B. Cornils, W. A. Herrmann, *Aqueous-Phase Organometallic Catalysis: Concepts and Applications*, 2<sup>nd</sup> Ed. Wiley-Vch Verlag GmbH and Co. KGaA, Weinheim, Germany, (2004).

- 
275. H. Syska, W.A. Herrmann, F. E. Kuhn, *J. Organomet. Chem.* **703** (2012) 56-62.
276. J. Soleimannedjad, C. White, *Organometallics* **24** (2005) 2538-2541.
277. J. Soleimannedjad, A. Sisson, C. White, *Inorg. Chimica Acta.* **352** (2003) 121-128.
278. D. W. Hein, R. J. Alheim, J. J. Leavitt, *J. Am. Chem. Soc.* **79** (1957) 427-429.
279. Bruker APEX2, SAINT and SADABS, Bruker AXS Inc., Madison, Wisconsin, USA (2012).
280. G. M. Sheldrick, *Acta Cryst.* **A64** (2008) 112-122.
281. L. J. Farrugia, *J. Appl. Cryst.* **45** (2012) 849-854.
282. A. L. Spek, *Acta Cryst.* **D65** (2009) 148-155.
283. I. J. Bruno, J. C. Cole, M. Kessler, J. Luo, W. D. S. Motherwell, L. H. Purkiss, B. R. Smith, R. Taylor, R. I. Cooper, S. E. Harris, A. G. Orpen, *J. Chem. Inf. Comput. Sci.* **44** (2004) 2133-2144.
284. S. Haneda, Z. Gan, K. Eda, M. Hayashi, *Organometallics* **26** (2007) 6551-6555.
285. X. F. He, C. M. Vogels, A. Decken, S. A. Wescott, *Polyhedron* **23** (2004) 155-160.
286. J. S. Casas, A. Castineiras, E. Garcia-Martinez, Y. Parajo, M. L. Perez-Paralle, A. Sanchez-Gonzalez, J. Sordo, *Z. Anorg. Allg. Chem.* **631** (2005) 2258-2264.
287. T. Steiner, *Chem. Comm.* **8** (1997) 727-734.
288. J. M. Abboud, C. Roussel, E. Gentric, K. Sraidi, J. Lauransan, G. Guiheneuf, M. J. Kamlet, R. W. Taft, *J. Org. Chem.* **53** (1988) 1545-1550.
289. A. O. Ogwenio, S. O. Ojwach, M. P. Akerman, *Dalton Trans.* **43** (2014) 1228-1237.
290. P. Foley, R. DiCosimo, G.M. Whitesides, *J. Am. Chem. Soc.* **102** (1980) 6713-6725.

- 
291. O. Prakash, K.N. Sharma, H. Joshi, P.L. Gupta, A.K. Singh, *Organometallics* **33** (2014) 2535-2543.
- 292 (a) Y. Lin, R.G. Finke, *Inorg. Chem.* **33** (1994) 4891-4910 (b) R. Crabtree, D. R. Anton, *Organometallics* **2** (1983) 855-859.
- 293 C. Dagueuet, R. Scopelliti, P. J. Dyson, *Organometallics* **23** (2004) 4849-4857.
294. M. Costa, P. Pelagatti, C. Pelizzi, D. Rogolino, *J. Mol. Catal. A. Chem.* **178** (2002) 21-26.
295. (a) H. Lindlar, R. Dubuis, *Org. Syn. Coll.* **50** (1973) 880 (b) L. E. Overman, M. J. Brown, S. F. McCann, *Org. Syn. Coll.* **8** (1993) 609 (c) M. Garacia-Mota, J. Gomez-Diaz, G. Novell-Leruth, C. Vargas-Fuentes, L. Bellarosa, B. Bridier, J. Perez-Ramirez, N. Lopez, *Theor. Chem. Acc.* **128** (2010) 663-673.
296. Complex **21** (5 mg, 0.01 mmol) in methanol (50 mL) and benzene (0.44 mL, 4.9 mmol) H<sub>2</sub> pressure, 10 bar, time 1 h. No catalytic activity was observed.
297. (a) D. J. Ellis, P. J. Dyson, D.G. Parker, T. Welton, *J. Mol. Catal. A. Chem.* **150** (1999) 71-75; (b) V. Caballero, F.M. Bautista, J. M. Campelo, D. Luna, R. Luque, J. M. Marinas, A. A. Romero, I. Romero, M. Rodriguez, I. Serrano, J. M. Hidalgo, A. Llobet, *J. Mol. Catal. A. Chem.* **308** (2009) 41-45 V. J. Catalano, T. J. Craig, *Polyhedron*, **19** (2000) 475-485; (c) C. Aliende, M. P. Manrique, F. A. Jalon, B. R. Manzano, A. M. Rodriguez, G. Espino, *Organometallics* **31** (2012) 6106-6123; (d) M. Heckenroth, V. Khlebnikov, A. Neels, P. Schrtenberger, M. Albrecht, *Chem. Cat. Chem.* **3** (2011) 167-173.
298. C. Vangelis, A. Bouriazos, S. Sotiriou, M. Samorski, B. Gutsche, G. Papadogianakis, *J. Catal.* **274** (2010) 21-28.